UNIVERSITY OF CALIFORNIA
RIVERSIDE

Dipole Mediated Charge Transfer in Molecular Electrets

A Dissertation submitted in partial satisfaction
of the requirements for the degree of

Doctor of Philosophy

in

Biochemistry and Molecular Biology

by

James Bennett Derr

September 2021

Dissertation Committee:
Dr. Valentine I. Vullev, Chairperson
Dr. Russ Hille
Dr. William Grover

The Dissertation James Bennett Derr is approved:

_____

_____

_____

Committee Chairperson

University of California, Riverside

Acknowledgements:

First and foremost, I want to thank Dr. Vullev for taking me in as a graduate student back in 2016, which feels like a lifetime ago. He truly saw my potential and pushed my education further with his years of intellect both in chemistry and other topics like history and how to make the coffee. His devotion as a mentor helped me achieve my goals and turned me into the chemist I am today. Not only am I grateful for his vast intellect but his understanding and welcoming personality. Thank you for accepting me into your lab!

I'm thankful to my committee members: Dr. Russ Hille and Dr. William Grover for their constructive criticism leading to my growth as a chemist. I would like to thank Dr. Hille for giving me the opportunity to work in his lab the summer before starting graduate school and taking me in for rotations. I would also like the Biochemistry Department for giving me Teaching Assistant positions to help fund my education and enrich the lives of future scientists.

I'm appreciative for Dr. Daniel Gryko for giving me the privilege to work in his lab in Poland for the summer and help hone in on my synthetic abilities. Also, I would like to thank everyone in the Gryko lab for all their knowledge and support that summer.

I couldn't have been more graced with my current and previous lab partners. John Clark for helping me with all the spectroscopy, data analysis and most importantly spending the past 5 years in lab together. I am thankful to Dr. Eli Espinoza for helping me adjust to the

lab when I first joined by taking the time to explain the reactions we were doing and the rationality behind it. I would like to thank Dr. Katarzyna Rybicka-Jasinska for being an amazing lab partner and friend thoughout my PhD in California and Poland. I would like to thank Max Mayther for introducing me into the lab and some of the weekends we spent in the lab together. I would like to thank Jesse Tamayo for being a great partner to work with on our review papers and for having such a great sense of humor. I am grateful to have worked with all my undergrads. Maryann Morales has grown so much as a chemist since she first joined the lab. Mimi Billones spent the last year of my PhD learning and applying her synthetic knowledge to the laboratory. Ahmed Srass has certainly excelled since the day he joined and has a positive future ahead of him. I would also like to thank Sandra Vadin for helping me early on in my PhD with my first author paper.

Finally, I want to thank my family and friends because I would have never made it here without them. I want to thank my mother and step-father for raising me to pursue my dreams. My mother definetly went the extra mile because she cared for her children. My older brother Matt motivated me to apply myself in college so I can have a promising career in the future. I lastly want to thank all of the friends I have made over the years in Riverside and West Chester.

ABSTRACT OF THE DISSERTATION

Dipole Mediated Charge Transfer in Molecular Electrets

by

James Bennett Derr

Doctor of Philosophy, Graduate Program in Biochemistry and Molecular Biology
University of California, Riverside, September 2021
Dr. Valentine I. Vullev, Chairperson

Accounting for the best features of biological electrets and biomolecular charge transfer (CT) systems, we design bioinspired molecular electrets based on anthranilamide (Aa) motifs. Similar to protein helices, ordered amide bonds generate a macromolecular dipole. The hydrogen-bonding network not only supports the extended Aa conformation, but also provides a polarization that enhances the total dipole of these molecular electrets. Unlike the protein helices, the aromatic Aa moieties and the extended π-conjugation along the Aa backbone provide pathways for efficient long-range CT. These structures illustrate the unexplored potentials of bioinspired approaches to design and development of electronic and energy-conversion systems.

Despite all the advances in solid phase peptide synthesis, none of these synthetic protocols are applicable for making Aa oligomers. First, the anthranilic residues are considerably less reactive than aliphatic amino acids. The carbonyls at the ortho-position decrease the nucleophilicity of the free amines. Similarly, the protected ortho-amines decrease the electrophilicity of the carbonyl carbons of the activated carboxylates. Second

and most important, activation of carboxyl groups at the ortho position to amides or protected amines leads to the formation of stable cyclic structures that cannot react with the aromatic free amines on the oligomer termini and suppress any further coupling all together. Introducing each of the Aa residues as its 2-nitrobenzoic acid analogue addresses both issues. The strongly electron-withdrawing nitro group increases the electrophilicity of the carbonyl carbon. In addition, the nitro group does not react with the neighboring activated carboxylates to form stable structures that terminate the coupling step. Therefore, I spent my early research synthesizing Aa oligomers from their C- to N-termini via a sequence of various amide coupling and nitro-group-reduction steps.

For long-range CT in organic materials, it is important to attain a hopping (or incoherent) mechanism, for which the kinetics exhibits negligible distance dependence beyond about 1 nm. In order to prevent oxidative degradation of electrets mediating such hole hopping, it is crucial for the comprising Aa residues to form stable radical cations, $Aa^{\bullet+}$. For attaining such stability, we have determined that: (1) the spin density distribution (SDD) of $Aa^{\bullet+}$ should not extend over its C-terminal amide; and (2) the reduction potentials for oxidizing Aa, should not be too large, *i.e.*, $E_{Aa^{\bullet+}|Aa} < 1.5$ V *vs.* SCE, to prevent the inherent oxidative degradation of the amides. The latter places a limit on how oxidizing the transferred holes can be. Hole hopping along moieties with as positive $E_{Aa^{\bullet+}|Aa}$ as possible ensures the potency of the holes for attaining large open-circuit voltages and for driving chemical transformations. Therefore, a significant amount of my studies involved placing alkoxy side chains on Aa residues brings the reduction potentials of their radical cations, $Aa^{\bullet+}$, to the limit of 1.5 V *vs.* SCE, such ether conjugates present a

key paradigm in the pursuit of organic derivatives that can transduce strongly oxidizing charge carriers.

Overall, the most significant contributions to my doctoral research are: (1) developing a variety of nitro reduction and amide coupling methods to suit both solution-phase and solid-phase peptide synthesis; (2) designing alkoxy anthranilamides to positively shift the reduction potential and still be chemical reversible; and (3) designing the ether synthesis protocols that selectively lead to etherification, without esterification via solvent selection and microwave chemistry.

Table of Contents

List of Figures

Chapter 1

Chapter 2

Chapter 3

Chapter 4

List of Schemes

Chapter 2

Chapter 3

Chapter 4

List of Tables

Chapter 2

Chapter 3

Chapter 4

List of Charts

Chapter 3

List of Abbreviations

Aa: Anthranilamide

$CHCl_{3:}$ Chloroform

C_{el}: Electrolyte Concentration

CT: Charge Transfer

CV: Cyclic VOltammetry

D: Debye

DCM: Dichloromethane

DFNBA: 4,5-difluoro-2-nitrobenzoic acid

DFT: Density Functional Theory

DNA: Deoxyribonucleic acid

E_{00}: zero-to-zero energies

$E^{(0)}$: Electrode Potential

$E^{(1/2)}$: Half-wave Potential

E_a: Anodic Peak

E_c: Cathodic Peak

E_{CO}: Cutoff Reduction Potential

ET: Electron Transfer

eV: Electron Volt

EDG: Electron Donating Group

ε : Dielectric Constant

^{19}F NMR: Fluorine Nuclear Magnetic Resonance

Fmoc: Fluorenylmethyloxycarbonyl

h^+: Hole

HOMO: Highest Molecular Orbital

LE: Locally Excited

LUMO: Lowest Molecular Orbital

MeCN: Acetonitrile

M: Molarity

NOESY: Nuclear Overhauser Effect Spectroscopy (2D NMR)

NMR: Nuclear Magnetic Resonance

NPy: Nitropyrene

PC: Propylene Carbonate

PhCN: Benzonitrile

Pip: Piperidine

PNA: Peptide Nucleic Acid

Py: Pyrene

SCE: Standard Calomel electrode

SDD: Spin-Density Distribution

tBoc: *tert*-butyloxycarbonyl

UV: Ultraviolet

V: Volt

Chapter 1

Introduction

What defines biomimetic and bioinspired science and engineering?

Need for alternative energy

Our planet currently struggles to cope with destructive forces of environmental pollution, waste and increasing amounts of greenhouse gases in the atmosphere. Projections show 6% rise in CO_2 emissions from energy production in the period between 2015 and 2050, should the current policies be in place. To meet the goals set by the Paris agreement, the world has to reduce the release of CO_2 by more than than 29% [1].

The ever-increasing human population places growing demands for energy, thus, cornering us to expediently make choices for alternative carbon-neutral sources of energy. Current social movements, such as the international school strike for climate (Youth for Climate), bring rising awareness of the challenges for the 21st century. Worldwide news of dramatic natural disasters has led to discussions about climate change and the urgent need for action.

While the timely importance of these efforts is paramount, in their extremes they set environmental safety against technological progress. Such ways of thinking do not necessarily lead to constructive discussions and feasible solutions for long-term sustainability. Nature with all living systems represents forms of “technologies" that have evolved for a few billion years. Spinning out of them, human ingenuity has led the development of tools and industries that made us the first living species who have the power to affect the planet, and we did in many different ways. Hence, we do have the knowhow for putting the brakes on environmental pollution and climate change in order to ensure our survival not only as a species but also as a civilization.

Nature offers paradigms for sustainability. Understanding and mimicking the

natural systems and the structure-function relationships that governs them is crucial for building a scientific foundation for a sustainable future (Figure 1-1). Taking ideas from biology to employ them in bioinspired ways allows for achieving functionalities that are beyond what nature can offer (Figure 1-1). Such biological inspiration paves the paths

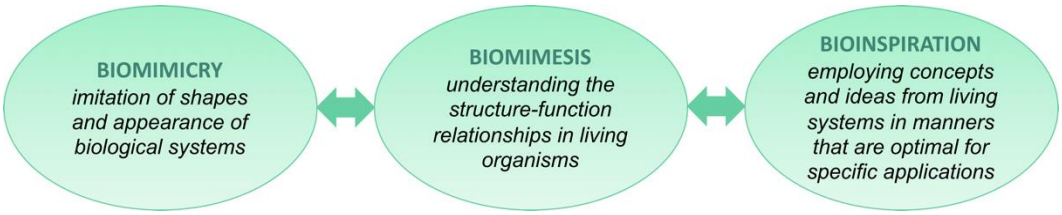

Fig. 1-1: Evolution of biomimetic to bioinspired approaches

forward to powerful technologies that can meet the growing socio-economic demands of humanity in environmentally benign manners.

Although coal powered the Industrial Revolution in a cost-efficient manner, its use, along with that of other fossil fuels, has led to an exponential increase in CO_2 emissions [2]. The recent emergence of renewable energy technologies, such as solar, hydro, geothermal and wind, offers access to electricity in unprecedented environmentally safe manners [3]. (Strictly speaking, nothing is "renewable", and this term has erroneous denotation in this case. The entropy increase defines the direction of time and turning back to restore states of the Universe the way they were is impossible. Hence, "sustainable energy" is the scientifically correct term, instead.) Among the carbon-neutral energy sources, solar has the incomparable capability to meet our global energy needs. The solar light radiation brings energy to the Earth's surface at rates of 1.76×10^5 TW, and about 1.2×10^5 TW get absorbed when accounting for the global albedo [4]. Utilizing only 0.5% of this abundant energy source, i.e., at rates of 600 TW, will still meet our global demands

for centuries to come. While photothermal energy has been utilized for centuries by using solar light to heat water and other materials, photovoltaics (PV) provides a means to incorporate directly the produced electrical energy into most of our current infrastructures. After the discovery of the PV effect in the 19th century by Edmond Becquerel [5], it took about 100 years before PVs was used for powering not only small electronic devices, but also space stations and satellites.

Considering the abundance of solar light, one of the "greenest" ways for driving modern science and engineering is to use photochemistry. Solar energy offers the greatest opportunity to harvest the energy over any other renewable energy. With advancing light-harvesting research, solar energy can replace coal and fossil fuels entirely [6].

The events in the recent decades have given a bad reputation to atmospheric CO_2. Nevertheless, in abundance of about 200 ppm, CO_2 is vital for maintaining the climate in which human civilizations flourished. The lack of green-house gases in the atmosphere is as bad as having too much of them. Depleting the carbon dioxide from the atmosphere increases the rates of planetary heat loss and will turn Earth into an ice block [7-9].

Atmospheric carbon dioxide also is crucially important for sustaining life on Earth and solar energy makes it possible. By reducing CO_2 to carbohydrates, photosynthesis stores light energy in the form of biological fuels. Biological respiration provides the vital energy for living organisms by "burning" these fuels and releasing CO_2 back in the atmosphere. Therefore, CO_2 is a key part of the shuttling that brings the energy from the photosynthetic sites to all organisms in the biosphere. Fossil fuels represent photosynthetically stored energy in the form of reduced carbon [10]. Humans have

developed and perfected technologies for releasing this stored energy, along with CO_2, from fossil fuels. Unfortunately, no technology exists for taking carbon dioxide from the atmosphere and reducing it to store energy. Such a bioinspired solar-fuel industry will be most beneficial not only for human civilization, but also for the planet.

Herein, we introduce the evolution from biomimetic concepts to bioinspired approaches (Figure 1-1). To illustrate their impacts, we focus on solar-energy science and engineering.

BIOMIMICRY, BIOMIMETICS and BIOINSPIRATION

Biomimicry

Biomimicry involves imitation of shapes and appearance of biological systems (Figure 1-1) [11]. The amazing diversity of natural occurrences in living organisms, which took millions of years to evolve, have greatly fascinated humans since the down of mankind. Animals and plants have been intricate components of art ever since the Cognitive Revolution (about 70,000 BCE). Agricultural Revolution (about 10,000 BCE) drove the human unification and the rise of civilizations (starting with Sumer about 4,000 BCE), which provided avant-garde tools and immense resources for people to express their observations and imagination. Elements of the flora and the fauna became a part of everyday life. For example, the colonnade motifs of ancient Greece have been the backbone of European and world architecture for centuries. The straight-forward Doric order from the western (mainland) Greece, along with its cotemporary Ionic order adopting thin-looking tall shapes from the eastern regions, shaped the images of this ancient civilization. It was the Corinthian order, however, with its characteristic acanthus leaves and other plant

and flower motifs at the capitals of the columns that brought the aesthetics of architecture to a completely new level. In his writings from 30 BCE, the Roman architect Vitruvius ascribes the origin of Corinthian style to an Athenian sculptor Callimachus who was inspired by the shapes of tree branches grown through a hanging basket over the grave of a young maiden from Corinth. As a corollary, in the 5th century BCE, Callimachus merged the strengths of the Doric and Ionic orders with biomimicry to create one of the most elegant and beautiful styles of architecture in the ancient world.

While it is common to ascribe the emergence of biomimicry to human ingenuity of mankind, the tendencies for imitating shapes and colors of living organism are not limited to Homo sapiens. In order to deter predators, in Batesian mimicry, a benign organism adopts the colors of another organism that is dangerous and threatening. Batesian mimicry in a sense takes advantage of Müllerian mimicry, in which several poisonous, venomous, or foul-tasting organisms imitate from one another patterns of vibrant colors to display distinct warnings to common predators [12]. On the other side of the spectrum, blending with the environment, i.e., camouflage, drastically improves the chances of animals to survive. Camouflage mimicking colored patterns and odors not only keeps vulnerable species hidden from potential predators in their ecosystems, but also provides predators with capabilities to remain undetected as they approach potential prey. Animals, such as moths, octopi, sharks, tigers, chameleons, and many others, illustrate countless examples of importance of camouflage for their survival. For millennia, humans have adopted the biomimicry of camouflage for hunting and military tactics, and overall, for gaining favorable advantages in a wide range of compromising situations.

Biomimesis

Biomimesis represents the next level of adopting the lessons from nature by understanding the structure-function relationships in living organisms (Figure 1-1) [11]. Since the commencement of the Scientific Revolution about 500 years ago, following the flourishment of Renaissance, the strives for deep understanding how things truly function have sent the humanity on an exponential trajectory of developments leading to the Industrial Revolution and the Anthropocene. Despite his perfect biomimicry of bird wings, Leonardo da Vinci could not help humans take flight. About a century later, it took Hezârfen Ahmed Çelebi deep understanding of structure-function relationships to be able to take numerous gliding flights from Europe to Asia over the Bosporus. Understanding the effects of the ratios between the wing area and bird weight helped Çelebi succeed where others had failed before him.

The multiscale complexity of structure-function relationships in living organisms leads to emergence of unique properties. Beavers are semiaquatic warm-blooded animals that do not possess thick blubbers, i.e., insulating adipose tissue under their skin, to keep them warm. Nevertheless, they survive in freezing water. The mesoscale structures of their fur, with hydrophobic surfaces, dynamically lock small pockets of air that serve as heat insulators. An international research team from the Massachusetts Institute of Technology and École Polytechnique studied this structure-function relationship and built biomimetics comprising pilli of polydimethylsiloxane that manifest the functionality of the natural systems. The pilli with hydrophobic surface of the artificial systems efficiently trap air [13]. The practicality of advanced “beaver-inspired” diving suits is indisputable. This

discovery, however, illustrate the broad scientific impacts of biomimesis. Imitating biological structures allow us to test how well we understand the parameters responsible for their functionality. That is, biomimesis deepens our understanding of how natural systems work.

Bioinspiration

Bioinspiration involves employing concepts and ideas from living systems in manners that are optimal for specific applications (Figure 1-1) [11,14]. Bioinspired structures do not need to resemble their natural counterparts. Most robots, which replaced human labor, do not look like two-legged humanoids. Millions of years of divergent and convergent evolution have produced an amazing variety of organisms with multiscale complexity of perfectly tuned structures and functionalities. Most biological structures become less than useless when taken out of the living organisms. Globular proteins are susceptible to denaturation and self-assembled structures – to degradation. Even if photosynthetic reaction centers within the whole assemblies of thylakoid membranes are wired to electrode surfaces, solar cells containing such biological structures will not operate for long. The lack of self-repairing in manmade devices sets requirements for photostability and durability that is beyond what photosynthetic protein assemblies can offer.

Bioinspiration represents the top level of employing our understanding of living systems for advancing engineering and developing technologies. An impressive but less known example involves the use of a countercurrent multiplier for bioinspired separation of CO_2 and O_2 from other gases. Deepsea fish utilize countercurrent amplification for attaining neutral buoyancy by increasing the partial pressure of O_2 in their swim bladders.

It involves loops of blood vessels where oxygen can diffuse from the blood exiting the loops into the blood entering the loops. As oxygenated blood enters such capillary loops, situated around the bladder, a change in pH triggers hemoglobin to release O_2 around the midpoints of the paths along these loops. Some of the freed oxygen diffuses into the bladder, but much of it diffuses into the incoming oxygenated blood flow in the neighboring capillary. That is, the oxygenated blood gets further saturated with O_2 prior to reaching oxygen-release triggering point. This countercurrent amplification results in four orders of magnitude increase in the concertation of oxygen in the swim bladder. Bioinspired microfluidic devices, employing the same countercurrent amplification principles with thermal and photothermal release triggering, demonstrate 2.4-fold enrichment of gas mixtures with CO_2 [15]. The impact of such a bioinspired approach fills a key void in the solar-fuel engineering. Electrotechnical and photoelectrochemical reduction of CO_2 is achievable. Nevertheless, capturing the diluted atmospheric CO_2 to bring it to the reducing catalytic sites at feasible concentrations is still a formidable challenge.

Effects of permanent electric dipoles on charge transfer

Electric dipoles generate localized fields that can reach GV m^{-1} in their proximity, but rapidly fall off with distance, especially in polar media. For non-polar solvents, therefore, the effects of permanently oriented dipoles on CT are enormous when they are located near the donors and acceptors or incorporated in one of them [20,21]. Protein interior, comprising a huge number of polar groups, such as the amides of the backbones, in a relatively non-polar surrounding of mostly aliphatic chains, represents the situation

where dipole-generated fields form complex networks of potentials that can govern CT. Such biomolecular systems triggered the interest in dipole effects on CT in the mid-20th century [22,23].

The accepted notion for dipole effects on CT focusses on the driving force. The potentials from the dipole-generated fields exerted on the donor and the acceptor, i.e., $\phi\mu^{(D)}$ and $\phi\mu^{(A)}$, respectively, modulate their reduction potentials and the overall the CT driving force [19,20]:

$$\Delta G_{CT}^{(0)} = F\,((E_{D^{\bullet+}|D} + \phi_{\boldsymbol{\mu}}^{(D)}) - (E_{A|A^{\bullet-}} + \phi_{\boldsymbol{\mu}}^{(A)})) - \mathscr{E}_{00} + \Delta G_S + W \qquad (2)$$

When CT affects the dipoles generating the external potentials, it is important to consider this change in $\phi_{\boldsymbol{\mu}}$ and how it affects the reduction potentials, as we showed in the quantification of these effects using eq. 2 [20].

In living systems, dipole effects on CT and ion transport are vital [24-26]. The complexity of such systems, however, warrants challenging analysis to relate the observed CT kinetics with the dipolar structural features. Therefore, biomimetic electrets emerged as principal tool for furthering the field. With ordered electric dipole moments, electrets are the electrostatic analogues of magnets.

Biomimetic molecular electrets

While the ideas for dipole effects on CT emerged in the 1960s, it was the 1990s when Galoppini and Fox demonstrated experimentally dipole-induced rectification of long-range CT employing polypeptide helices as macromolecular electrets [16,17,18].

Using a polypeptide as a bridge in donor-bridge-acceptor systems, the analysis revealed that CT is much faster when electrons move along the dipole rather than against it [16].

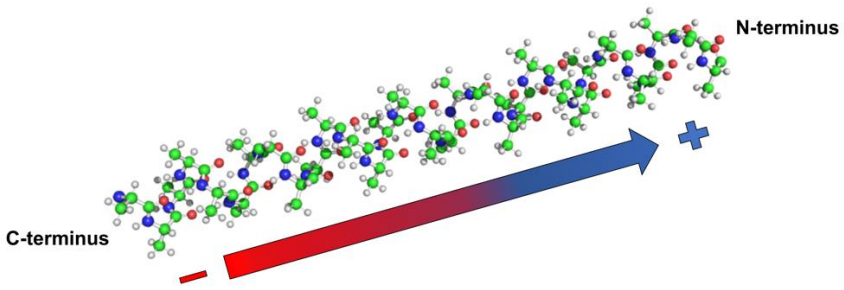

Fig. 1-2: Balls-and-sticks model of a polypeptide α-helix composed of alanine residues, representing one of the best known molecular electrets as indicated by its permanent electric macrodipole.

Protein helices are some of the best molecular electrets. For example, α-helices have permanent dipole moments oriented from their N- to their C-termini (Figure 1-2), originating from the codirectional hydrogen-bonding polarization and the ordered amides on the backbone, and amounting to about 5 Debyes per residue [24,27]. The 3_{10}-helices are more tightly strained than the α-helices. As the name suggests, these conformers contain 3 residues per turn and 10-bond loops between neighboring hydrogen bonds that hold the structure together. Following this nomenclature, α-helices are in fact 3.6_{13}-helices [28]. Each residue contributes about 4.6 Debyes to the overall dipole moment of 3_{10}-helices [27]. While α-helices have slightly larger macrodipoles than the 3_{10} conformers, the tight 3_{10}-helix structures are more stable folds than the α-helices for short polypeptides, i.e., shorter than 20 amino-acid residues. On the other side of the spectrum, with 4.1 residues per turn, π-helices are more loosely folded than α-helices [29-31]. Despite their abundance in nature, π-helices predominantly exist as single-loop folds of short segments of about seven residues.

Containing only tertiary amides along their backbones, polyproline (PP) assumes helical conformations without hydrogen bonding networks. Therefore, the PP macrodipoles originate only from the ordered amides and are smaller than those of the other protein helices [27]. The different conformations of the peptide bonds results in two types of PP helices: polyproline I (PPI) and polyproline II (PPII). In PPI helices, the backbone amides assume Z conformation with their dipole orientated from the N- to C-termini, contributing about 4.1 D per residue to the macrodipole [27]. The PPII helices contain E-conformers of the amides resulting in macrodipoles of about 1.5 D (or less) per residue, oriented from their C- to their N-termini [27], i.e., in same direction as that of the α-helix and 3_{10}-helix dipoles (Figure 1-2). A change in solvent polarity induces a switch between PPI and PPII conformations. The amide bond planes of PPII are near orthogonal to the principal helix axis. Therefore, relatively small structural changes, often induced by the solvent media, induce sizable variations of the PPII macrodipole from about 0 to 1.5 D per residue.

This wealth of electronic features of polypeptide helices made these structures the preferred choice for biomimetic electrets to unravel the dipole effects on CT in the first decades of the 21st century. The use of polypeptide conformers for CT scaffolds, however, poses some challenging limitations: (1) the conformational integrity of polypeptide α-helices is often compromised when taken out of their natural environment, thus limiting the scopes of their applications, and (2) injection of electrons or holes in polypeptides composed of natural α-amino acids leads to their reductive or oxidative degradation, respectively, preventing them from mediating long-range CT via hopping. Along their

backbones, therefore, polypeptides mediate CT only via quantum mechanical tunneling, or super-exchange mechanism, the rates of which exponentially decrease with distance. Such rates become unfeasibly small for attaining efficient CT (initiated by excited states with nanosecond lifetimes) at distances exceeding about 2 nm. Conversely, incoherent charge hopping along (1) protein cofactors, (2) redox-active amino-acid side chains, and (3) π-stacked base pairs in polynucleotides, allows biomolecules and their assemblies to efficiently mediate CT at impressively long ranges. These inherent limitations of biomimetic electrets warrant the implementation of bioinspired approaches to further the advances of the field [11,14].

Bioinspired molecular electrets

While biomimetics play a crucial role in exploratory research and in basic science, their technological implementations are somewhat limited. The translation from basic to applied science and from exploratory to developmental research is where bioinspiration takes over. In addition to driving the scientific discoveries to applied engineering, biological inspirations open unprecedented fields for exploration of new properties and phenomena that cannot emerge from natural systems.

Combining the structural motifs of protein helices, responsible for the intrinsic macrodipoles, with the concepts of biological arrays that mediate long-range CT, we developed bioinspired molecular electrets based on anthranilamide (Aa) structures (Figure 1-3) [32-34]. The Aa bioinspired electrets are aromatic oligo-ortho-amides with their

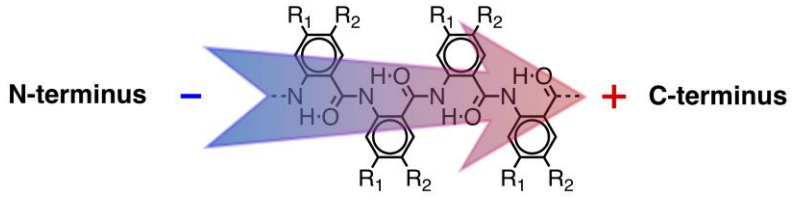

Fig. 1-3: Bioinspired molecular electret composed of anthranilamide (Aa) residues and its permanent electric dipole moment.

extended structures supported by a hydrogen-bond network (Figure 1-3). Similar to protein helices, ordered amide and hydrogen bonds generate macrodipoles along the backbones of the Aa oligomers amounting to about 3 D per residue [32,33]. Unlike proteins and synthetic polypeptide helices, aromatic moieties, directly linked with amide bonds, provide sites for electron or hole hopping that are essential for attaining long-range CT. The electric fields resultant from such ordered dipoles can visibly affect the CT processes they mediate (eq. 2). That is, the dipole-generated local electric fields can serve as important tools for accelerating desired CT processes, while suppressing undesired ones [20,21], which is paramount not only for conversion and storage of harvested solar energy, but also for organic and molecular electronics. Similar to other polypeptides, the chemical synthesis of Aa electret proceeds from their C- to their N-termini. Despite all the advances in peptide chemistry, none of the established synthetic protocols is applicable for the synthesis of Aa oligomers because of key structural differences between anthranilic-acid derivatives and the analogues of the native α-amino acids [35]. Instead of using anthranilic acids with protected β-amines, introducing each residue as the corresponding derivative of the 2-nitrobenozic acid addresses the grave inherent challenges for making polypeptides based on Aa structures [32,35]. The building of Aa molecular electrets involves a series of amide-coupling and selective nitro-group-reduction steps [32-36]. Adopting this approach, we

have developed robust methodologies for reliable synthesis of Aa oligomers [35,36].

To determine the extent at which Aa dipoles affect CT, we compare the rates of ET towards the C-termini versus the N-termini of an electron-rich Aa residue, defining CT rectification as $R = \lg(k_{N\rightarrow C} / k_{C\rightarrow N})$ [21]. Specifically, we construct dyads comprising Aa as an electron donor and 1-alkylpyrene (Py) as an electron acceptor (Figure 1-4). These donor-acceptor dyads distinctly rectify not only the forward photoinduced ET, but also the subsequent CR [21], which was a key step forward in the field of dipole-modulated CT. Our findings show that charge separation (CS) is faster when the electron moves along the dipole than when it moves against it, which perfectly agrees with the accepted notion for the dipole effects on the CT driving forces, $-\Delta G^{(0)}$. The observed rectification of CS decreases with an increase in medium polarity, which is consistent with screening of the dipole-generated localized electric field [21]. The charge-recombination (CR) rates are also larger when the electron moved along the dipole than against it [21]. Because of the large $-\Delta G_{CR}^{(0)}$, CR operates in the Marcus inverted region and the observed dipole effect on CR appears to contradict the transition-state theory. An increase in solvent polarity, however, which screens the dipole field, leads to a slight increase in the CR rectification [21]. These

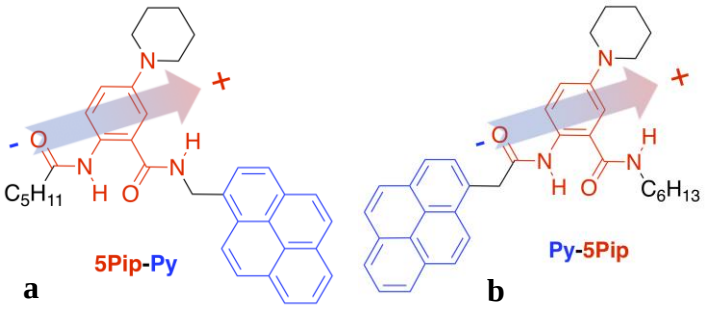

Fig. 1-4: Donor-acceptor dyads composed of an electron-rich Aa residue (5Pip) as a donor and pyrene (Py) as an acceptor. The Aa residue also bears a permanent electric dipole moment of about 6 D. (a) 5Pip-Py that mediates photoinduced CS involving ET along the dipole and CR – ET against the dipole. (a) Py-5Pip that mediates photoinduced CS involving ET against the dipole and CR – ET along the Aa dipolemoment.

findings indicate that the donor-acceptor electronic-coupling, in addition to the Franck-Condon factors (via the thermodynamic driving forces), govern the CR kinetics [21]. This first demonstration of an interplay between the dipole effect on $\Delta G_{CR}^{(0)}$ and the donor-acceptor electronic coupling illustrates the power of biological inspiration for the discovery of new emerging properties and phenomena. These immensely encouraging results set the foundation for developing a broad variety of Aa residues with diverse electronic and optical features (Figure 1-5).

Each of the Aa residues can have two side chains (R_1 and R_2, Figure 1-3). These side chains are essential for controlling the solubility and aggregation propensities of the Aa structures [37]. In addition, varying the Aa side chains provides an important handle for modifying the electronic and optical properties of these conjugates [38-41]. That is, a library of Aa residues with different R_1 and R_2 represents a synthetic proteome for structures with countless electronic and photonic functionalities [14,39,42]. Our initial focus has been on hole-transfer Aa residues with electron-donating side chains. Varying the electron-donating strength of the R_1 and R_2 groups from amines to alkyls, adjusts the reduction potentials of Aa oxidation over a range of 1 V [37-40]. For pursuing CT via hole hopping mechanism, it is essential for the oxidized residues, $Aa^{\bullet+}$, to manifest reasonable stability [38,43]. Aliphatic and aromatic amides have notorious propensity for degradation when oxidized at potentials exceeding about 1.4 – 1.5 V vs. SCE, which is an underlying reason why proteins cannot sustainably mediate hole hopping along their backbones. Recently, we discovered that using ether substituents for R_2 can stabilize the $Aa^{\bullet+}$ oxidized species at potentials exceeding 1.5 V vs. SCE (Box, Hox, Fox and Dmx, Figure 1-5), as

evident from the reversibility of their electrochemical oxidation [44]. Making Aa oligomers of such residues with ether side chains provides paths toward attaining amide electrets that can transfer strongly oxidizing holes [36]. The diversity of electronic structures that Aa bioinspired molecular electrets offer (Figure 1-5), makes them a perfect platform for exploring dipole effects not only on CT, but also on electronic and photonic dynamics at different scales. Local electric fields, originating from molecular dipoles, have profound effects on the electronic properties of the microenvironment. Overall, local electric fields from molecular dipoles affect ET and HT, providing a promising means for increasing the efficiency of the desired CT processes while suppressing the undesired ones.

In summary, the most important contributions from my doctoral work are: (1) building a library of ether anthranilamide residues that have a positive shift in the reduction

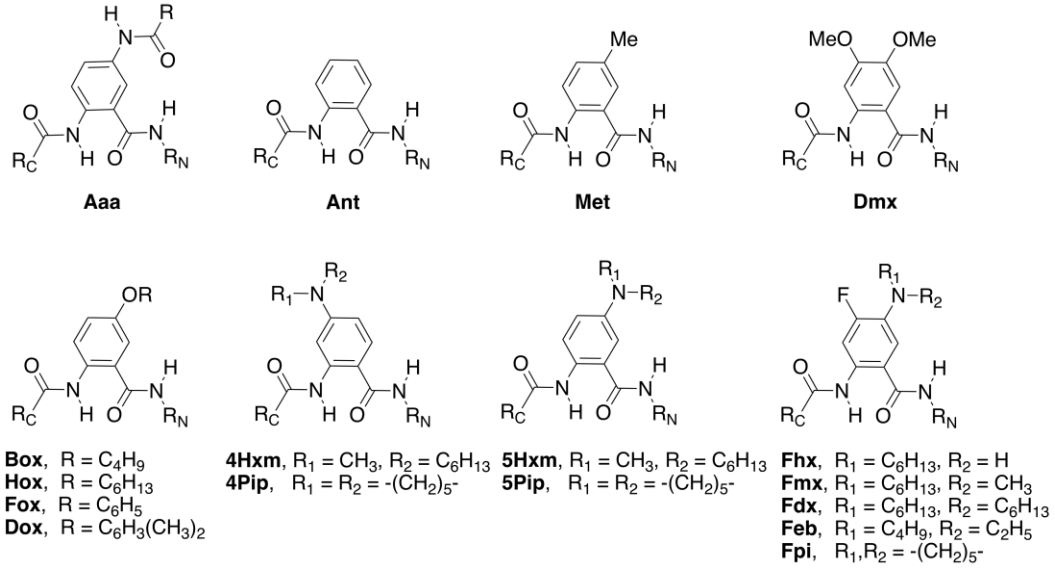

Fig. 1-5: Anthranilamide (Aa) residues with electron-donating side chains (R_1 and R_2, Figure 1-4) for building hole-transfer (p-type) bioinspired molecular electrets.

potential to employ them as molecular electrets (2) Using Purdie-Irvine Alkylation with Ag_2O to build ether residues without their adjacent ester sideproduct forming only their

free carboxylic acid derivatives (3) developing alternative amide coupling and nitro reduction procedures to build polyanthranilamide oligomers used for X-ray studies.

References

[1] D. Gielen, F. Boshell, D. Saygin, M. D. Bazilian, N. Wagner, R. Gorini. *Energy Strateg. Rev.* **24**, 38 (2019).

[2] P. A. Owusu, S. Asumadu-Sarkodie. *Cogent Eng.* **3**, 1167990 (2016).

[3] A. Demirbas. *Energy Sources Part A* **28**, 779 (2006).

[4] A. Henderson-Sellers, M. F. Wilson. *Phil. Trans. R. Soc. Lond. A* **309**, 285 (1983).

[5] A.-E. Becquerel. *Compt. Rend.* **9**, 561 (1839).

[6] V. Kumar, R. L. Shrivastava, S. P. Untawale. *Aquat. Pr.* **4**, 473 (2015).

[7] A. A. Lacis, G. A. Schmidt, D. Rind, R. A. Ruedy. *Science* **330**, 356 (2010).

[8] W. Steffen, K. Richardson, J. Rockström, S. E. Cornell, I. Fetzer, E. M. Bennett, R. Biggs, S. R. Carpenter, W. de Vries, C. A. de Wit, C. Folke, D. Gerten, J. Heinke, G. M. Mace, L. M. Persson, V. Ramanathan, B. Reyers, S. Sörlin. *Science* **347** (2015).

[9] A. Indermuhle, T. F. Stocker, F. Joos, H. Fischer, H. J. Smith, M. Wahlen, B. Deck, D. Mastroianni, J. Tschumi, T. Blunier, R. Meyer, B. Stauffer. *Nature* **398**, 121 (1999).

[10] G. Ciamician. *Science* **36**, 385 (1912).

[11] V. I. Vullev. *J. Phys. Chem. Lett.* **2**, 503 (2011).

[12] S. Lev-Yadun. *Plant Signal. Behav.* **13** (2018).

[13] A. Nasto, M. Regli, P. T. Brun, J. Alvarado, C. Clanet, A. E. Hosoi. *Phys. Rev. Fluids* **1** (2016).

[14] E. M. Espinoza, J. M. Larsen-Clinton, M. Krzeszewski, N. Darabedian, G. D. T., V. I. Vullev. *Pure Appl. Chem.* **89**, 1777 (2017).

[15] K. Brubaker, A. Garewal, R. C. Steinhardt, A. P. Esser-Kahn. *Nat. Commun.* **9** (2018).

[16] E. Galoppini, M. A. Fox. *J. Am. Chem. Soc.* **118**, 2299 (1996).

[17] M. A. Fox, E. Galoppini. *J. Am. Chem. Soc.* **119**, 5277 (1997).

[18] A. Knorr, E. Galoppini, M. A. Fox. *J. Phys. Org. Chem.* **10**, 484 (1997).

[19] J. B. Derr, J. Tamayo, J. A. Clark, M. Morales, M. F. Mayther, E. M. Espinoza, K. Rybicka-Jasinska, V. I. Vullev. *Phys. Chem. Chem. Phys.* **22**, 21583 (2020). Fleming. *J. Am. Chem. Soc.* **143**, 3104 (2021).

[20] M. Krzeszewski, E. M. Espinoza, C. Cervinka, J. B. Derr, J. A. Clark, D. Borchardt, G. J. O. Beran, D. T. Gryko, V. I. Vullev. *Angew. Chem., Int. Ed.* **57**, 12365 (2018).

[21] D. Bao, S. Upadhyayula, J. M. Larsen, B. Xia, B. Georgieva, V. Nunez, E. M. Espinoza, J. D. Hartman, M. Wurch, A. Chang, C.-K. Lin, J. Larkin, K. Vasquez, G. J. O. Beran, V. I. Vullev. *J. Am. Chem. Soc.* **136**, 12966 (2014).

[22] R. A. Marcus. *Discuss. Faraday Soc.*, 21 (1960).

[23] S. Yomosa. *Sup. Prog. Theor. Phys.*, 249 (1967).

[24] J. B. Derr, J. Tamayo, E. M. Espinoza, J. A. Clark, V. I. Vullev. *Can. J. Chem.* **96**, 843 (2018).

[25] D. A. Doyle, J. M. Cabral, R. A. Pfuetzner, A. Kuo, J. M. Gulbis, S. L. Cohen, B. T. Chait, R. MacKinnon. *Science* **280**, 69 (1998).

[26] R. Dutzler, E. B. Campbell, M. Cadene, B. T. Chait, R. MacKinnon. *Nature* **415**, 287 (2002).

[27] Y.-G. K. Shin, M. D. Newton, S. S. Isied. *J. Am. Chem. Soc.* **125**, 3722 (2003).

[28] J. S. Richardson, D. C. Richardson. In *Prediction of Protein Structure and the Principles of Protein Conformation* (G. D. Fasman, ed.), pp. 1. Plenum (1989).

[29] L. Zubcevic, S.-Y. Lee. *Curr. Opin. Struct. Biol.* **58**, 314 (2019).

[30] J. Ludwiczak, A. Winski, A. M. da Silva Neto, K. Szczepaniak, V. Alva, S. Dunin-Horkawicz. *Sci. Rep.* **9**, 1 (2019).

[31] P. Kumar, M. Bansal. *FEBS J.* **282**, 4415 (2015).

[32] B. Xia, D. Bao, S. Upadhyayula, G. Jones, V. I. Vullev. *J. Org. Chem.* **78**, 1994 (2013).

[33] M. K. Ashraf, R. R. Pandey, R. K. Lake, B. Millare, A. A. Gerasimenko, D. Bao, V. I. Vullev. *Biotechnology Progress* **25**, 915 (2009).

[34] K. Rybicka-Jasinska, V. I. Vullev. *J. Photochem. Photobiol., A* **401**, 112779 (2020).

[35] K. Skonieczny, E. M. Espinoza, J. B. Derr, M. Morales, J. M. Clinton, B. Xia, V. I. Vullev. *Pure Appl. Chem.* **92**, 275 (2020).

[36] J. B. Derr, K. Rybicka-Jasińska, E. M. Espinoza, M. Morales, M. K. Billones, J. A. Clark, V. I. Vullev. *Biomolecules* **11**, 429 (2021).

[37] J. M. Larsen, E. M. Espinoza, J. D. Hartman, C.-K. Lin, M. Wurch, P. Maheshwari, R. K. Kaushal, M. J. Marsella, G. J. O. Beran, V. I. Vullev. *Pure Appl. Chem.* **87**, 779 (2015).

[38] E. M. Espinoza, J. M. Larsen, V. I. Vullev. *J. Phys. Chem. Lett.* **7**, 758 (2016).

[39] J. M. Larsen-Clinton, E. M. Espinoza, M. F. Mayther, J. Clark, C. Tao, D. Bao, C. M. Larino, M. Wurch, S. Lara, V. I. Vullev. *Phys. Chem. Chem. Phys.* **19**, 7871 (2017).

[40] J. M. Larsen, E. M. Espinoza, V. I. Vullev. *J. Photon. Energy.* **5**, 055598 (pp. 1 (2015).

[41] E. M. Espinoza, J. M. Larsen, V. I. Vullev. *ECS Trans.* **66**, 1 (2015).

[42] E. M. Espinoza, V. I. Vullev. *ECS Trans.* **77**, 1517 (2017).

[43] E. M. Espinoza, J. A. Clark, J. Soliman, J. B. Derr, M. Morales, V. I. Vullev. *J. Electrochem. Soc.* **166**, H3175 (2019).

[44] J. B. Derr, J. A. Clark, M. Morales, E. M. Espinoza, S. Vadhin, V. I. Vullev. *RSC Adv.* **10**, 24419 (2020).

Chapter 2

Biomimetic and bioinspired molecular electrets. How to make them and why does the established peptide chemistry not always work?

Abstract

"Biomimetic" and "bioinspired" define different aspects of the impacts that biology exerts on science and engineering. Biomimicking improves the understanding of how living systems work, and builds tools for bioinspired endeavors. Biological inspiration takes ideas from biology and implements them in unorthodox manners, exceeding what nature offers. Molecular electrets, i.e. systems with ordered electric dipoles, are key for advancing charge-transfer (CT) science and engineering. Protein helices and their biomimetic analogues, based on synthetic polypeptides, are the best-known molecular electrets. The inability of native polypeptide backbones to efficiently mediate long-range CT, however, limits their utility. Bioinspired molecular electrets based on anthranilamides can overcome the limitations of their biological and biomimetic counterparts. Polypeptide helices are easy to synthesize using established automated protocols. These protocols, however, fail to produce even short anthranilamide oligomers. For making anthranilamides, the residues are introduced as their nitrobenzoic-acid derivatives, and the oligomers are built from their C- to their N-termini via amide-coupling and nitro-reduction steps. The stringent requirements for these reduction and coupling steps pose non-trivial challenges, such as high selectivity, quantitative yields, and fast completion under mild conditions. Addressing these challenges will provide access to bioinspired molecular electrets essential for organic electronics and energy conversion.

Introduction

In the context of ***biomimetics*** and ***biological inspiration***, this publication describes the development of molecular electrets and focuses on the synthetic challenges for making their bioinspired analogues (Fig. 2-1). (Electrets are systems ghvb with ordered electric dipoles, i.e. they are the electrostatic analogues of magnets [1].) Description of multi-step syntheses of electret oligomers illustrates the improvements needed for making their preparation facile and accessible for the broad research and development community. Fundamental research in experimental and theoretical physical chemistry leads to the breakthroughs demonstrating the broad impact of biomimetic and bioinspired structures on a myriad of fields, such as materials engineering, energy conversion and electronics. It is, however, the ability to prepare such structures that makes this line of research and development even possible.

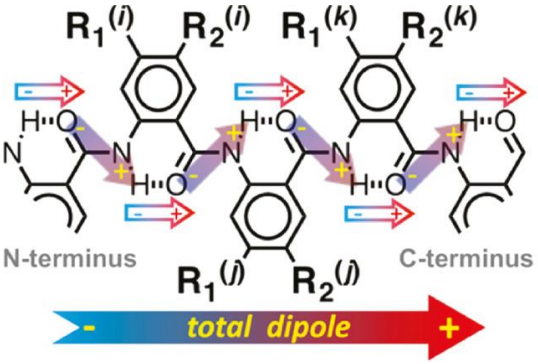

Fig. 2-1: Bioinspired molecular electrets, composed of Aa residues, showing (1) the origin of the macrodipole, i.e. the total electric dipole, from amide and hydrogen bonds, ordered in the center along the backbone, (2) the aromatic moieties providing sites for electron or hole transfer, and (3) the side chains, R_1 and R_2, modulating the electronic and optical properties of the residues.

Charge transfer (CT) is one the most important processes for sustaining life as we know it. CT not only drives vital processes in living systems such as cell respiration and photosynthesis, but also ensures the efficient performance of materials and devices essential for modern life [2-7].

Biology provides a wide range of invaluable paradigms for advances in all areas of science and engineering. Deepening and expanding the understanding of how living systems work by ***mimicking*** them, and implementing this knowledge in unorthodox manners as defined by ***biological inspiration***, illustrates the broad impacts that the transitions from ***biomimetic*** to ***bioinspired*** approaches have [1], [8]. Transformative developments in understanding and implementing CT benefit immensely from the numerous robust examples found in biological redox and energy-conversion systems.

While "biomimetic" and "bioinspired" approaches commenced as key tools for science and engineering, through the last couple decades, they evolved into independent research fields. The term "biomimetic" appeared in the early 1970s, mostly in the context of developing synthetic procedures [9-12]. It did not take long to spread to other areas of science and engineering [13-15]. Concurrently, references to "biological inspiration" in computer engineering and medicine in the 1940s and 1960s, respectively [16], [17], predate the "biomimetic" terminology. The use of the term "bioinspired," however, took off in the early 1990s [18-23], as the next step forward to broad utilization of biological concepts.

The evolution of the fields of biomimetics and biological inspiration has important impacts on the CT science and engineering. Dye-sensitized solar cells, artificial photosynthesis, enzymatic fuel cells, and solar fuels are some of the concepts that originated from understanding and implementing biological concepts in CT systems [24-32].

Electric dipoles are ubiquitous and their localized fields present largely underutilized paradigms for controlling CT, the importance of which cannot be overstated

[5]. The ideas about dipole effects on CT have evolved since the middle of the 20th century [33-35]. The initial work focused on dipoles embedded in proteins, i.e. on biological electrets.

With intrinsic dipoles of up to 5 Debye per residue, protein helices are the best-known molecular electrets [36-38]. Therefore, their biomimetic analogues, i.e. synthetic polypeptide helices of alpha amino acids, have been almost exclusively the choice for studying how electric dipoles affect CT [38-43]. However, unless cofactors or residues with redox-accessible side chains are present, proteins and their polypeptide analogues mediate CT via tunneling, limiting the practicality of its efficiency to about 2 nm [44-46]. In photosynthesis, on the other hand, arrays of cofactors effectively mediate CT over several nanometers via electron hopping [2]. Similarly, hole hopping along the electron-rich bases of DNA and PNA macromolecules allows for efficient CT at record-long distances [47-49].

Combining the structural motifs of protein helices, responsible for the intrinsic macrodipoles, with the concepts of biological arrays that mediate long-range CT, we developed bioinspired molecular electrets based on anthranilamide (Aa) structures (Fig. 2-1) [1], [50-54]. Similar to protein helices, ordered amide and hydrogen bonds generate macrodipoles along the backbones of the Aa oligomers. Unlike proteins and synthetic polypeptide helices, however, aromatic moieties, directly linked with amide bonds, provide sites for electron or hole hopping that are essential for attaining long-range CT.

Unlike the native α-amino acids, which have single side chains, the Aa residues have two side chains (R_1 and R_2, Fig. 2-1) presenting another advantage of the bioinspired

structures. Variations in these two side chains, permits a broad adjustment of the electronic and optical properties of the Aa residues. Altering between alkyl, alkyloxy and amine side chains varies the Aa reduction potentials over a span of one volt [55-57]. Furthermore, we determined that not only the mesomeric and inductive characteristics of R_1 and R_2, but also their exact position, govern the electronic properties of the Aa residues. Moving the same substituent from R_1 and R_2 changes the reduction potentials with about 100–200 mV, and results in tens of nm shifts in the optical spectra [55,56]. In addition to regulating the electronic properties of the aromatic residues, the side chains R_1 and R_2 also provide a means for improving the solubility of the Aa oligomers and controlling their self-assembly properties. This role of the side chains is closely related to the functions of the side chains of native amino acids in the formation of tertiary and quaternary protein structures.

While the first report on Aa oligomers came out more than a century ago [58], less than a couple of dozen publications on these aromatic oligoamides have appeared since then [59-69]. The studies of Aa oligomers have focused on their structural features, including their ability to serve as rigid templates for foldamers and templates with biological activity [68-72]. Recently, our analysis of the electronic properties of different Aa oligomers demonstrated for the first time, theoretically and experimentally, that they are molecular electrets [50-51]. That is, Aa oligomers possess large intrinsic electric dipoles originating from the ordered arrangements of their amide and hydrogen bonds [50]. We also determined that without side chains, i.e. R_1=R_2=H (Fig. 2-1), the Aa oligomers have a high propensity for aggregation [51], which may decrease the enthusiasm for their use as “well-behaved” structural motifs as reflected by the limited number of publications.

Because the Aa conjugates are polypeptides, we developed a set of electron-rich non-native Aa residues as building blocks for hole-transfer molecular electrets [53], [55-57], [73-75]. Using alkyl-containing substituents as side chains, especially as R_2 (Fig. 2-1), dramatically increases the solubility of the Aa residues in organic solvents and prevents their aggregation [56]. Attaching electron-deficient chromophores to them allowed us to demonstrate that even a single Aa residue can substantially rectify CT [52], [54].

The Aa conjugates are oligopeptides. Thus, it appears that with all available well-established robust protocols for polypeptide synthesis, making Aa oligomers should be trivially easy. For more than 100 years, peptide chemistry has evolved with huge amount of manpower involved in its development [76-85]. Several important breakthroughs in the second half of the 20th century led to the current state-of-the-art solid-phase peptide synthesis (SPPS) protocols that are readily automatable, allowing facile preparation of 50-residue polypeptides in a few days [86-90]. The polypeptides are built from their C- to their N-termini on a solid support. Each amino acid is introduced as free carboxylates with orthogonal protections of their amine and the side-chain groups (if needed). ***In situ*** activation of the carboxylates allows them to couple to the terminal free amines on the solid support. Amine deprotection of the amine of the coupled residue prepares it for the coupling with the next amino acid. Quantitative yields of each coupling and deprotection step ensure that the product cleaved from the solid support can be readily purified using preparative and semi-preparative HPLC [89].

Despite all the advances in peptide chemistry, however, none of these synthetic protocols are applicable for making Aa oligomers. First, the anthranilic residues are

considerably less reactive than aliphatic amino acids. The carbonyls at the ***ortho***-position decrease the nucleophilicity of the free amines. Similarly, the protected ***ortho***-amines decrease the electrophilicity of the carbonyl carbons of the activated carboxylates. Second and most important, activation of carboxyl groups at the ***ortho*** position to amides or protected amines leads to the formation of stable cyclic structures that cannot react with the aromatic free amines on the oligomer termini and suppress any further coupling all together [64].

Introducing each of the Aa residues as its 2-nitrobenzoic acid analogue addresses both issues. The strongly electron-withdrawing nitro group increases the electrophilicity of the carbonyl carbon. In addition, the nitro group does not react with the neighboring activated carboxylates to form stable structures that terminate the coupling step. Hence, Aa oligomers are synthesized from their C- to N-termini via a sequence of amide coupling and nitro-group-reduction steps [51], [64]. Despite the large number of procedures for selective reduction of nitro groups to amines [91-94], in the context of the synthesis of Aa oligomers, this step presents key challenges. It is a six-electron six-proton reduction proceeding through three intermediates. Reducing conditions that lead to complete conversion of nitro groups to amines under mild conditions, without affecting the rest of the Aa oligomer, are not quite routine.

Herein, after a brief review of biomimetics and biological inspiration, we introduce the concept of CT molecular electrets based on motifs derived from biology, i.e. dipoles originating from ordered amide and hydrogen bonds. The century of development of synthetic bioorganic chemistry produced robust and reliable tools for making biomimetic

electrets based on polypeptide α-helices, which unfortunately are not truly useful for the preparation of bioinspired Aa structures. Introducing the amines as nitro groups presents

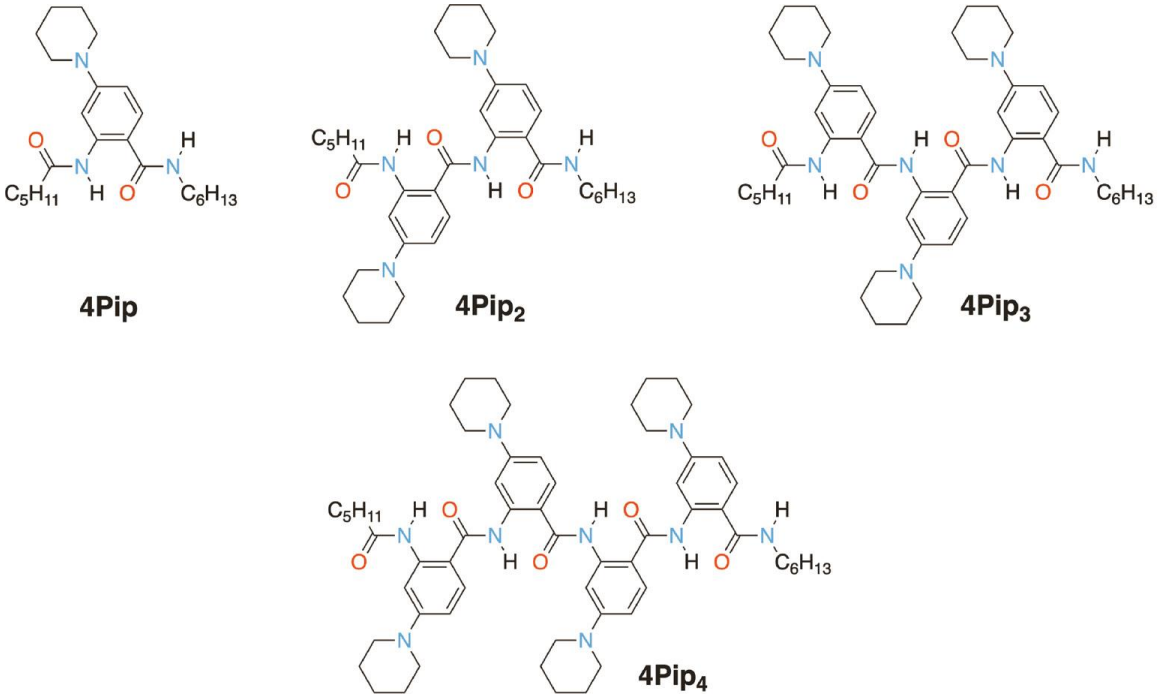

Fig. 2-2: Bioinspired molecular electret oligomers, composed of an electron-rich residue, 4Pip (R_1=piperidin-1-yl, R_2=H, Fig. 2-1) with alkyl-capped N- and C-terminal amides.

an alternative strategy for making Aa oligomers. Based on this approach, we demonstrate the synthesis of Aa dimer, trimer and tetramer composed of electron-rich residue, 4Pip (Fig. 2-2). The reduction steps essential for converting the N-terminal nitro groups into amines present some of the key challenges. We show that few of the "established" procedures for nitro reduction are feasible for Aa synthesis. Our findings demonstrate that Cr (II) in organic media provides the best means for selective reduction of a nitro-Aa derivative to the corresponding amine. Electrochemical and spectroscopic analyses of the synthesized oligomers (Fig. 2-2) reveal key insights about the electronic properties of these aromatic amides.

GENERAL CONSIDERATIONS

Biomimetic vs. bioinspired. What's the difference?

Transitions from biomimetics to biological inspiration illustrate the broadest impacts that biology can have on other areas of science and engineering. Billions of years of evolution on Earth has produced diversity of life forms with multi-scale organization of complex structural features displaying countless functionalities. Myriads of cellular functionalities emerge from specific molecular (self) assemblies. Tissue functionalities emerge from cell differentiation and organization. Organ functionalities emerge from arrangements of tissues and cells with specific properties. Organisms manifest vital functionalities that emerge from the synergy between the comprising organs. Social organizations of single-cell and multicellular organisms lead to the emergence of new properties and group behavior that the analyses of the individual participants cannot predict [95]. Such structure-function relationships at multiple spatial and temporal scales still remain not only challenging for engineers to achieve, but also far from completely understood by mathematicians, physicist, chemists, biologists and social scientists.

While ***biomimicry*** merely imitates structural features of living systems, ***biomimesis*** aims at attaining the functionality of biological entities by copying their structures [1], [8]. Hence, the biomimetic approaches are indispensable for unveiling how biology works, and for discovering important structure-function relationships in living systems by employing maquettes that are often less complex than the copied biological counterparts. Furthermore, systematic lowering of the complexity of the maquettes of the examined biological systems reveals which parameters are important for attaining certain functionalities of interest.

As engineering tools, biomimicry and biomimesis provide a direct means interfacing synthetic materials and biomedical devices with living tissue [96,97], where the interests are not only in biocompatibility, but also in biofunctionality [98]. A two-way relationship between biology and engineering has been the principal driving force behind the development of the whole field of microfluidics [99-101]. Mimicking features of the cardiovascular system leads to sophisticated microfluidic designs. Concurrently, microfluidic devices provide indispensable platforms for studying living cells and tissues under natural conditions outside the complexity of the living organisms, which frequently leads to key discoveries in biology and medicine [102-104].

While biology offers a myriad of lessons for advanced engineering, a direct implementation of biological and biomimetic structures is far from optimal for materials, devices and other manmade systems targeting similar functionalities. To achieve reasonable lifespans, for example, living systems rely on ***damage management*** via numerous self-repair mechanisms that evolved through the thousands of millennia [105-110]. That is, damages are inevitable. Hence, deviating a small portion of the life energy for driving self-repair processes ensures longevity. Conversely, engineered self-repair approaches of abiotic systems are still immensely far from what life can do. Therefore, the longevity of manmade systems relies on ***damage prevention***. It involves over-engineering in order to decrease the probability of damages to occur. While such over-engineering cannot completely prevent damages, it still increases the lifespans of devices and other manmade structures.

Biological and biomimetic structures are frequently quite less than optimal for engineering solutions. Therefore, ***biological inspiration*** provides routes for overcoming the inherent limitations of the living systems. Bioinspired approaches involve taking ideas and elements from biology and implementing them in manners different from their natural occurrence [1], [111-113]. For example, ***materials genome*** has nothing to do with DNA or other information-carrying biomolecules. Instead, materials genome encompasses biologically inspired extraction of specific structural information from huge databases for guiding the experimental development of new materials with specific targeted functionalities [114-118]. Therefore, a broad range of functionalities that surpass what nature offers can readily emerge from bioinspired approaches.

Overall, biomimetics (encompassing biomimicry and biomimesis) broadens and deepens the understanding of how living systems work, and builds toolkits for biological inspiration. Conversely, biological inspiration leads to countless unexplored possibilities for energy science, electronics, photonics, materials design and numerous other fields of science and engineering.

Molecular electrets based on amide structures

While making small magnets has inherent limitations, making large electrets can prove challenging. The drastic decrease in the Curie temperature (and the Néel temperature) with the decrease in particle size, limits how small molecular magnets can be [119-121]. Conversely, the ease of extracting charges (electrons and ions) from every medium, except vacuum, defines the practical limitations on how large molecular electrets and their dipoles can be. Therefore, bottom-up approaches are the best for pursuing designs

of electrets, and especially of molecular electrets, which provide immensely attractive paradigms for nanometer-scale control of CT.

Amide bonds are widespread rigid linkers in biomolecules and synthetic polymers. They are easy to form and possess large permanent electric dipoles [122]. Therefore, amides are an excellent choice as building blocks for molecular electrets [51], [53]. Concurrently, hydrogen-bonding networks are essential for holding together macromolecular secondary conformations and for ensuring that the electric dipoles are ordered. Formation of a hydrogen bond leads to shift of electron density from the negative pole of one dipole (e.g. from the amide oxygens) to the positive poles of another one (e.g. to the amide protons) (Fig. 2-1). This polarization extends the center the negative charges away from the first dipole and the center of the positive charges away from the second one, increasing the magnitude of both. Therefore, the collective shift of the electron density up on the formation of hydrogen-bonding network in protein helices and Aa oligomers enhances their macrodipoles [50], [123].

In addition to their roles as dipole sources, as covalent linkers, and as hydrogen-bond donors and acceptors, amides can strongly affect the electronic properties of aromatic moieties to which they are directly attached [124]. The mesomeric electron-donating properties of amides when attached via their nitrogens strongly affect the distribution of the frontier orbitals of the Aa residues. Thus, the amide linkers in Aa conjugates define not only the electronic coupling with electron donors and acceptors attached to them, but also their resistance against oxidative degradation during hole transfer processes [55].

Overall, peptide bonds, i.e. carboxyamides, have all the attractive properties for the designs of molecular electrets. The impressive advances in the peptide chemistry should ensure the synthetic procedures for an easy access to a wide variety of molecular structures with large permanent electric dipoles.

Making polypeptides

In ribosomes, the natural synthesis of proteins proceeds from their N- to their C-termini by selectively adding a single amino acid at a time [125]. Catalytic condensation between amines and non-activated carboxylates allows for chemical replication of such biosynthesis of polypeptides [126]. Nevertheless, the best established methods for chemical synthesis of polypeptides build them from their C- to their N-termini [127]. It involves a series of amide-coupling steps between the N-terminal free amines of a peptide and the activated carboxylates of the amino acids that is the next in the sequence. To ensure the selectivity of this reaction, the amine of the added amino acid is protected and the polypeptide with the free amine does not have free carboxylates that can be potentially activated. Therefore, amine deprotection follows each amide coupling step. That is, the synthesis of a polypeptide with $\boldsymbol{n}$ residues requires $2\boldsymbol{n}$ reaction steps. For reasonable amounts of the final polypeptide products, each of these steps has to undergo with a quantitative yield.

Since the first report of dipeptide synthesis in 1901 [76], peptide chemistry has evolved with exponential rates. It involved important breakthroughs, especially during the second half the 20th century, such as (1) the discovery of Boc and Fmoc protection groups, along with the protection groups with orthogonal sensitivity for the side-chain functional

groups of the native amino acids [87,88], [128-130]; (2) the development of a wide range of reagents for mild ***in situ*** activation of amino-acid carboxylates for amide coupling [131,132]; (3) the development of SPPS and the automated fast Boc and Fmoc protocols [86], [133-137], recognized by the 1984 Nobel Prize in Chemistry, awarded to R. B. Merrifield; (4) the development of resins for SPPS with different sensitivity toward acidic cleavage, i.e. allowing the use of anything from HF to weakly acidic organic solution as cleavage reagent, and producing polypeptides with different C-termini, i.e. free carboxylates and primary amides [138]; and (5) the development of preparative reverse phase HPLC for facile purification of peptides from SPPS.

The interest in the field drove the involvement of an enormous number of researchers in its development. Following the chemical synthesis of oxytocin, reported in the 1953 [77], teams led by Panayotis Katsoyannis at University of Pittsburgh and by Helmut Zahn at RWTH Aachen University independently reported the synthesis of insulin [79], [80]. Concurrently, collaborative work involving teams from Academia Sinica, Shanghai, and Peking University also led to the total chemical synthesis of insulin, the activity of which was confirmed using animal studies [81], [83]. These demonstrations of obtaining biologically active polypeptides via a chemical means provided important motivation for perfecting and further developing the procedures for peptide synthesis.

The current protocols for SPPS are readily prone to automation for expedient preparation of polypeptides that are more than 50-residue long. While protein expression, using the machinery of living cells, allows for making long sequences exceeding tens of kDa, chemical peptide synthesis provides the means for facile incorporation of synthetic

amino acids and other moieties into the polypeptide backbone [139-145], which is a key advantage in the exploration of new non-native structures essential for bioinspired science and engineering. For the Fmoc protocol, for example, each residue is introduced as a free-carboxylate derivative with Fmoc protected amine that is to be added to the polypeptide backbone, and acid-sensitive protection of the side-chain functional groups. The ***in situ*** activation of the carboxylate allows it to be coupled to the free amines (or hydroxyls) on the resin solid support. Traditionally, activating the carboxylates as halides provides the reactivity needed for the amide coupling. Acid chlorides are considerably more reactive than acid fluorides. This high reactivity, however, makes the chlorides more prone to causing side reactions, and thus, acid fluorides have made their way into the modern SPPS [131,132]. After all, the fluoride is the smallest possible leaving group for amide coupling reactions rendering acid fluorides quite desirable when steric hindrance is an issue.

Conversely, the sensitivity to moisture renders the utility of acid halides for peptide synthesis. Therefore, activating the carboxylates to form intermediates that are considerably more susceptible to nitrogen nucleophiles, rather than oxygen ones, have become the preferred route for SPPS. Carbodiimides, such as DCC, EDC and DIC, readily react with carboxylic acids under mild conditions (the presence of a base is not required) to form ***O***- or ***N***-acylisoureas. The acylisoureas are inherently unstable and susceptible to nucleophilic substitutions; the produced ureas are excellent leaving groups. Therefore, a huge excess of hydroxyl derivatives, such as ***N***-hydroxysuccinimide (NHS) or 1-hydroxybenzotriazole (HOBt) always accompanies the administration of carbodiimide reagents. Moieties, such as NHS and HOBt form esters that are quite susceptible to

nucleophilic attacks from amines (to form amides), while relatively stable in the presence of water and other oxygen nucleophiles. In fact, it is quite common to carry out NHS amide-coupling chemistry in aqueous solutions, and the commercially available HOBt reagent comes as a hydrate, e.g. HOBt·2 H_2O, and used as received.

An alternative for HOBt, 1-hydroxy-7-azabenzotriazole (HOAt), presents routes for further improvements of the yields that is invaluable for difficult amide-coupling steps. The pyridine nitrogen at position 7 in HOAt provides an extra hydrogen-bonding site for stabilizing the transition states with α-amino acids [146]. The use of HOAt instead of HOBt, however, may not necessarily prove beneficial for transition states with different geometries when coupling β- and γ-amino acids, or aminobenzoic acids.

Onium derivatives (i.e. uronium and phosphonium salts) of HOBt and HOAt (such as TBTU, BOP, HATU and PyAOP) encompass another important class of reagents for mild ***in situ*** activation of carboxylates that has revolutionized automated SPPS. In the presence of base, these electrophilic onium derivatives readily react with the deprotonated carboxylic acids to form conjugates that are susceptible to nucleophilic attacks in quantitative yields. The added large excess of HOBt or HOAt ensures the formation of the corresponding active esters that have long enough lifetimes to react with the free amines on the solid support. Because carboxylic anhydrides (that are equally good for coupling with the immobilized amines) are another outcome from such activation, the acid should be added in four-fold excess to ensure quantitative yields for the amide coupling. In addition, the molar amounts of some of these onium reagents should not exceed 95% or 99% that of the α-amino acid to prevent racemization.

Difficult coupling steps may require heating of the reaction mixtures with the solid support and protocols involving microwave heating are implemented in commercially available peptide synthesizers [147-148]. Elevated temperatures can address challenges of kinetically impeded reactions, and microwave treatment is particularly useful when the entropic components of the activation energy is the underlying reason for slow conversion rates. While such elevated temperature aid difficult coupling steps, they do not prevent low yields originating from undesired side reactions. In fact, heating may accelerate and even add new side reactions involving not only the reagent solution and the immobilized polypeptide, but also the resin may not be necessarily inert at high temperature.

Because of the dense multiple functionality in a peptide chain, the formation of five or six-member cyclic structures is frequently favored (though undesirable). If certain residues, like glycine and tryptophan, are present in the sequence, base catalyzed hydantoin formation can occur [149]. In some extreme protic conditions (e.g. in the presence of carboxylic acids in high concentrations), undesired six-member ring formation involving two neighboring residues is possible via cleavage of the ester on the C-terminal side of the dimer. The diketopiperazine formation is responsible for losses due to cleaving of the reaction intermediates from the solid support before the completion of the synthesis. Kinetic studies show that proline and valine at the C-terminal are extremely susceptible to this side reaction, especially in the presence of free carboxylic acid in the solution [150]. To avoid such a process, HOBt has to be added in large excess, so that the formation of HOBt ester will be favored over the anhydride formation.

Succinyl and glutaryl derivatives readily form by cyclization between the aspartate and glutamate side chains, respectively, and their α-carboxyl or carboxylamides. Since under the conditions of Fmoc synthesis the carboxyl side chain groups are protected as t-butyl esters, such undesirable cyclization can occur only during the deprotection. Therefore, the cleavage and deprotection times ought not to exceed 2 or 3 h [149].

Also, primary amides in the side chains (e.g. in glutamine and asparagine) are susceptible to dehydration intramolecular reactions with the α-carboxyl group under the conditions of activation with onium reagents [149]. Therefore, the use of acid-sensitive protection groups of the primary amides in the Gln and Asn ensures the decrease in the reactivity of these side chains.

Overall, the current SPPS methodologies are practically perfect for facile preparation of polypeptides of α-amino acids that fold to assume helical structures and form biomimetic molecular electrets. Furthermore, robust algorithms with excellent predicting power, along with molecular-mechanics modeling tools, offer a means for reliable selections of ***de novo*** sequences of α-amino acids that assume helix folds with high probability for various media. Also, the understanding of leucine-zipper interfacing between protein helices provides paradigms in primary sequences that ensure tertiary and quaternary folds of coil-of-coils helix bundles with co-directional orientation of the macrodipoles [151-154].

RESULTS

Making bioinspired molecular electrets

Bioinspired molecular electrets based on Aa structures are polypeptides (Fig. 2-1). With the amazing advances in peptide chemistry, it appears that the permeation of Aa oligomers should be immensely facile using automated SPPS protocols. The decades of development of the peptide-synthesis protocols, however, has targeted the preparation of polypeptides of aliphatic α-amino acids. The bioinspired molecular electrets, on the other hand, comprise aromatic β-amino acids (Fig. 2-1). The structural differences between the Aa conjugates and the derivatives of the native amino acids render the state-of-the-art peptide-synthesis protocols useless for making bioinspired molecular electrets.

The amines and the activated carboxylates of anthranilic conjugates are not as reactive as those of α-amino acids. Especially with electron-withdrawing carbonyls at ***ortho*** position, the aromatic free amines at the N-termini of Aa oligomers are not as nucleophilic as the aliphatic amines of native peptide residues. In addition, the electron-donating (protected) amines compromise the electrophilicity of the activated carboxylates next to them in the aromatic rings.

Most importantly, activation of the carboxylate in anthranilic conjugates leads to the formation of stable cyclic intermediates [64]. Similar to the intramolecular cyclization induced by activating the native glutamine and asparagine [149], this condensation upon activation of anthranilic carboxylates suppresses the progress to amide coupling [64].

We observe that treating anthranilamides with different activation reagents (i.e. halogenating, onium and carbodiimide derivatives) lead to the same products that are

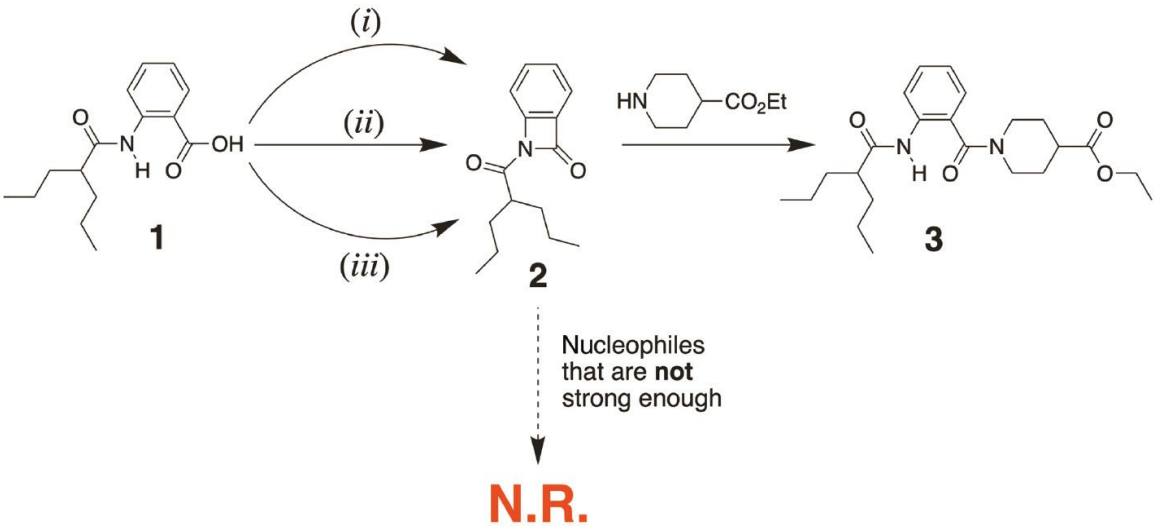

Scheme 2-1: Activation of the carboxylates of Aa residues leads to stable cyclic lactams. (***i***) $C_2O_2Cl_2$, DCM, 3 drops DMF, −78°C; (***ii***) EDC, HOBt, NMM, DMF; and (***iii***) TFFH, NMM, DMF (N.R.=no reaction).

always a water-molecule lighter than the starting materials as determined using high-resolution mass spectrometry (HRMS). The facile chromatographic isolation of these products proves their stability and allows us to determine that the preferred routes involve intramolecular reaction between the activated carboxylate and the amide or the protected amine next to them to form four-member cyclic lactams (Scheme 2-1). This finding differs from previous reports for the intermolecular condensation leading to six-member-ring azlactones upon carboxylate activation [64]. Still, the produced four-member-ring lactams are quite stable and can be opened only with strong nucleophiles, such as piperidines (Scheme 2-1). These findings render even the established peptide-synthesis protocols useless for preparing bioinspired molecular electrets based on anthranilamide structures.

Instead of using anthranilic acids with protected β-amines, introducing each residue as the corresponding derivative of the 2-nitrobenzoic acid (Scheme 2-2) addresses the grave inherent challenges for making polypeptides based on Aa structures. Thus, in lieu of

the established protocols based on amine deprotection, the building of Aa molecular electrets involves a series of amide-coupling and selective nitro-group-reduction steps [51], [64].

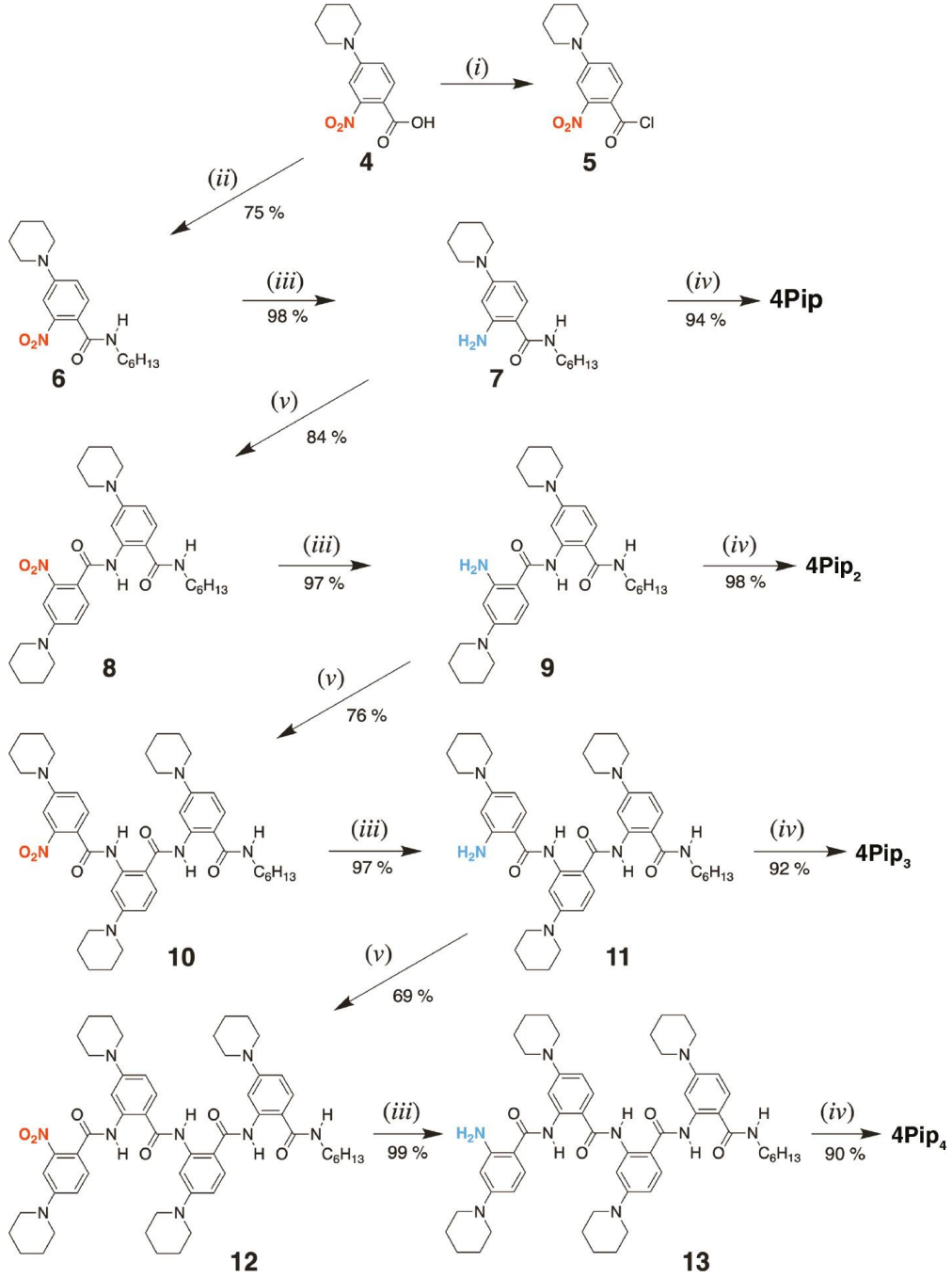

Scheme 2-2: Synthesis of bioinspired molecular electret oligomers, composed of 4Pip residues (R_1=piperidin-1-yl, R_2=H, Figs. 2-1 and 2-2) with alkyl-capped N- and C-terminal amides. (***i***) $C_2O_2Cl_2$, DCM, 3 drops DMF, −78°C; (***ii***) DIC, NHS, $H_2N–C_6H_{13}$, DMF, 0°C→r.t.; (***iii***) H_2, Pd/C, EtOAc; (***iv***) $(C_5H_{11}CO)_2O$, DCM, pyridine, 40°C; and (***v***) **5**, DCM, pyridine, r.t.

To illustrate this concept, we synthesize oligomers of an electron-rich amino-Aa residue, 4Pip (Scheme 2-2) [56] that, along with its 2-amino derivative, is quite susceptible to oxidative degradation under harsh reaction conditions. Employing chloride activation, along with heterogeneous Pd-catalyzed H2 reduction, affords the 4Pipn oligomers in high yields. Coupling alkyl acids with terminal Aa amines (using anhydride chemistry) proceeds with yields exceeding 90%. Conversely, amide coupling between Aa conjugates (using chloride chemistry) affords yields of about 70–85% (Scheme 2-2). While these latter yields are acceptable for solution-phase procedure, they are not sufficient for SPPS.

The reduction steps converting the nitro groups into amines proceed with quantitative yields (Scheme 2-2), which is quite desirable for making Aa conjugates. The heterogeneous nature of this reduction, however, precludes its utility for solid-phase procedures. Furthermore, H2 in the presence of Pd catalyst cleaves most carbon-halogen bonds and reduces certain electron-deficient aromatic compounds.

The large variety of coupling procedures developed for SPPS offers many options for improving the synthesis of Aa oligomers. Despite the importance of selective reduction of nitro groups, on the other hand, such procedures for producing amines that are potentially suitable for SPPS are scarce.

Selective reduction of nitro groups in Aa conjugates

The reduction of a nitro group to an amine is a six-electron-six-proton process. It is a sequence of three two-electron-two-proton steps, involving the reduction of nitro to nitroso group, nitroso group to hydroxylamine, and hydroxylamine to amine. Incomplete reduction leaving hydroxylamines along with the amines, followed by amide coupling,

leads to a mixture of products that are quite challenging to separate chromatographically. The acylhydroxylamine impurities, however, have distinct NMR signals and are readily detectable using HRMS, showing exact mass of the product plus an oxygen atom, which is an indication for incomplete reduction. Consumption of the reducing reagent changes the electrochemical potential of the reaction mixture. To prevent incomplete reduction, therefore, depletion of the reducing reagent should not be allowed, i.e. the reducing reagent should be added in excess in the beginning of the reaction or replenished during the progress of the reaction.

To ensure feasibility for SPPS, reactions for reducing nitro groups to amines should (1) be homogeneous, fast, and highly selective; (2) proceed with quantitative yields in organic solvents (that keep the resin swollen) at room temperature and atmospheric pressure; and (3) not leave any impurities stuck to the solid support, i.e. the resin should be easy to wash with DMF or other organic solvents after each reduction step. To survey the performance of the various reduction methods, we test the reduction of 5-bromo-2-nitro Aa analogue, 14, to the corresponding amine, 15 (Scheme 2-3). Reaction yields, prevention of debromination, mildness of the conditions (i.e. as close to room temperature as possible), and keeping the reaction solution clear (i.e. no precipitate formation for the duration of the reaction),

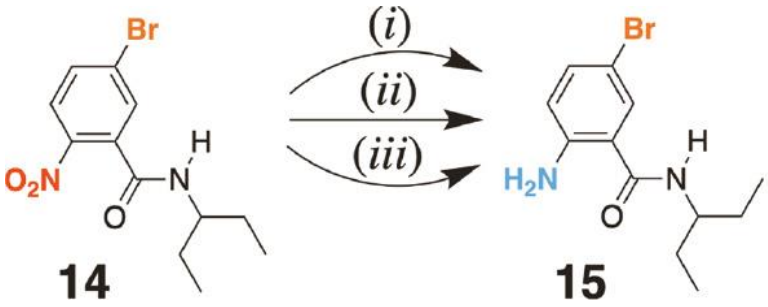

Scheme. 2-3: Reduction of a 5-bromo-2-nitro Aa analogue to the corresponding amine at room temperature: (***i***) $HSiCl_3$, DIPEA, MeCN, 0°C→r.t. (40%); (***ii***) $Na_2S_2O_4$, K_2CO_3, H_2O/heptylviologen, DCM, r.t. (64%); and (iii) $CrCl_2$, DMF, r.t. (95%).

are the criteria for the feasibility of the reduction method for implementation in SPPS protocols.

Tin (II) chloride dissolved in alcohols or other organic solvents, is one of the most popular reagents for selective reduction of nitro groups to amines [91], and we have successfully used it for the synthesis of Aa derivatives [52]. Elevated temperature is essential for driving this reduction to completion with reasonable rates.

Despite its reported use for solid-phase synthesis [155-157], the need for prolonged heating and the left over insoluble side products render $SnCl_2$ impractical for SPPS. While $SnCl_2$ has a good solubility in organic solvents and the starting reaction mixtures are clear, the requirement for large amounts of reducing agent (i.e. three Sn^{2+} ions are needed for reducing each nitro group) and the inherent humidity under basic conditions (i.e. the reduction of nitro groups consumes protons and produces water) lead to insoluble tin (IV) and tin (II) conjugates. Our tests with implementing $SnCl_2$ for SPPS show that after the first and the second reduction steps, the impurities from tin side products become impossible to remove from the resin, which severely compromises the yields of the synthesized Aa peptide. Furthermore, the conditions of tin (II) reduction cause cleavage of the C–Br bonds.

Carbon monoxide is a good reagent for selective reduction of nitro groups [93]. The need for high pressure or catalysts, however, makes CO nitro reduction somewhat undesirable for SPPS protocols. Conversely, the electrochemical potentials of many metals allow them to selectively reduce nitro groups to amines. The heterogeneous nature of such reduction methods using solid metals, however, renders such approaches unfeasible for

solid-phase protocols. Combining carbon monoxide with such metals, at zero oxidation state, presents an alternative. Dicobalt octacarbonyl is soluble in organic solvents and exhibits pronounced selectivity for reduction of nitro groups [158]. We successfully employ $Co_2(CO)_8$ for selective reducing aromatic nitrogroups to the corresponding amines in bromine-containing Aa derivatives (with yields of 75–95%) [8], [54] and in conjugates with electron-deficient chromophores susceptible to reduction (with yields of 60–70%) [7]. Such reduction with $Co_2(CO)_8$, however, requires elevated temperature and at the end of the reaction, dark-red colored precipitate of side products forms.

Focusing on room-temperature procedures, trichlorosilane appears to present an alternative as a hydrogen-donating reagent for reducing nitro groups to amines [159,160]. Using $HSiCl_3$ allows us to achieve 40% yield for reducing **14–15**. As effective as $HSiCl_3$ is as a reducing agent, it is also prone to sol gel polymerization driven by the humidity in the media.

Dithionite ion, S_2O4^{2-}, is another moiety with practically perfect electrochemical potential for selective reduction of nitro groups in molecules with complex functionality at room temperature. Sodium dithionite is a mild reducing reagent that is widely used in biochemistry and biomaterials science for mild reduction of protein cofactors and for reductive amination [161-163]. While immensely soluble in water, the readily available dithionite salts are insoluble in organic solvents. Also, making organic-soluble dithionite salts without oxidizing them is not truly straightforward [164-166]. Using solid support containing polyethylene glycol (PEG) that swells in water [167], appears as a good alternative. The hydrophobic nature of the Aa oligomers, however, can cause undesirable

folds in the hydrogels during the synthesis and prevent the exposure of the nitro groups to the aqueous media with the reducing reagent. Furthermore, the acid-halide amide coupling, which seems to the preferred route for Aa synthesis, is immensely sensitive to moisture in the reaction mixtures, making the regularly used hydrophobic polystyrene resins the preferred solid support for SPPS of bioinspired molecular electrets.

Phase-transfer catalysts (PTCs) allow for addressing the challenges with the $Na_2S_2O_4$ solubility [168-169]. It involves the implementation of two phases of immiscible liquids: (1) an aqueous solution of the dithionite reducing agent kept at basic pH; and (2) an organic solvent, such as CH_2Cl_2, in which the nitro compound is dissolved or the swollen resin is kept. Tetrabutylammonium salts with anions that are not soluble in organic solvents, such as SO_4^{2-}, present a good choice for PTC added to the aqueous phase. Ion pairing between N^+ $(C_4H_9)_4$ and $S_2O_4^{2-}$ makes the reducing agent soluble in organic media allowing it to diffuse to the nitro compounds. While it has been successfully used for solid-phase synthetic protocols [170,171], our tests reveal that this PTC approach does not produce **15** from **14** in acceptable yields.

As an alternative to PTC, the use of an organic-soluble redox couple for shuttling electrons from the dithionate in the aqueous medium to the nitro compound in the organic phase presents an excellent alternative [172]. The electrochemical potential of this redox couple should be right between the reduction potentials of the dithionite and of the targeted nitro group. Benzyl, heptyl and other hydrophobic viologens are an excellent choice for such electron shuttles and they can be successfully employed in solid-phase synthesis [172]. The use of ***n***-heptyl viologen as an electron shuttle produces **15** from **14** with 38%

yields. We observe that an increase in the equivalents of the added viologen from 0.03 to 2.7 improves the yields from 40% to 64%.

This finding brings an important point. The reduction potentials of the reaction media should be negative enough to completely reduce the nitro groups to amines, but not too negative to drive the reduction of other functional groups. Therefore, the reducing reagents with best selectivity have potentials that are quite close to those of the nitro groups. Lowering the activity (or the concentration) of the reduced form of the reagent or increasing the activity of its oxidized form can cause a positive shift in its potential just large enough to prevent the reduction of the nitro groups. If the PTC does not maintain the activity of the dithionite in the organic media large enough to ensure the required electrochemical potential for reduction of **14**, the reaction cannot proceed to completion. Similarly, the rates of viologen reduction by dithionite and of the nitro-group reduction by the reduced viologen, along with the partition coefficients of these species, control the ratio between the activities of reduced and the oxidized forms of the viologen in the organic media. Our observations show that an increase in the overall viologen concentration favors the reduction of **14**, which is consistent with increase in the amount of reduced viologen making the electrochemical potential of the organic media negative enough for the reduction of the nitro group.

Resorting to a different reducing agent, chromium (II), allows us to achieve practically quantitative yields for reducing **14**–**15** in reasonable times at room temperature. When in organic media, e.g. $CrCl_2$ in DMF, the $Cr^{3+}|Cr^{2+}$ redox couple has the reduction potential to drive the reduction of nitro groups to amines to completion. Furthermore, the

sufficient solubility of the chromium compounds in organic solvents makes this reduction procedure implementable in solid-phase synthetic protocols [173]. Unlike $SnCl_2$, $Na_2S_2O_4$, $Co_2(CO)_8$, H_2 and other reducing reagents, however, $CrCl_2$ is kinetically unstable and immensely susceptible to oxidation in air and in other oxygen-containing environment. Therefore, we carry out the reduction of **14**–**15** by chromium (II) in an argon atmosphere in a glove box where the oxygen level is under 1 ppm. The yields of this reduction exceed 95% and the washing off the chromium compounds after the completion of the reaction is quite straightforward.

Adding manganese or other solid metals maintains the level of chromium (II) in the reaction mixture [174]. That is, the $Cr^{3+}|Cr^{2+}$ redox couple aids electron shuttling from the solid metal to the nitro compound. Implementation of this procedure in solid-phase synthesis requires a closed flow system with two reaction vessels, one containing the solid metal and the other – the resin solid support [175]. The reducing metal enriches the solvent of chromium salts in Cr^{2+}, which diffuses or flows to the resin in the other compartment [175].

How does the length of the molecular electrets affect their electronic properties?

All 4Pip conjugates absorb in the UV region of the spectrum (Fig. 2-3). The increase in the number of residues does not linearly increases the absorptivity. Instead, the bathochromic shifts and the splitting of the absorption bands (as evident from the appearance of shoulders), induced by lengthening of the oligomers (Fig. 2-3), are consistent with excitonic coupling between the residues.

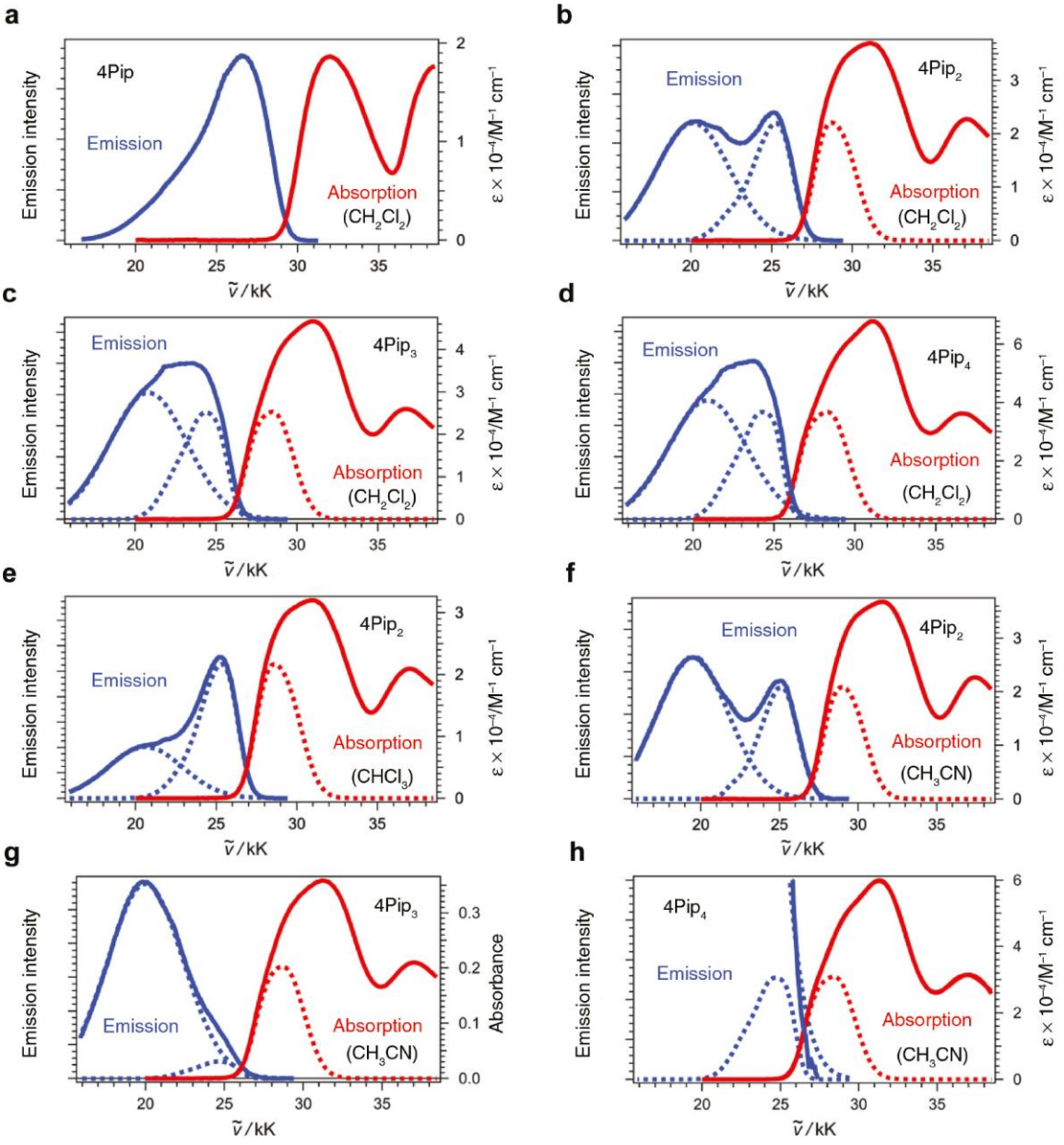

Fig. 2-3: Absorption (solid red curves) and emission (solid blue curves) spectra of the 4Pip oligomers, recorded for different solvents (λ_{ex}=330 nm for all oligomers except for the monomer, 4Pip, which is 310 nm). The dotted lines represent the products of deconvolution from fitting the spectral with sums of Gaussians. (a–d) Absorption and emission spectra of (a) 4Pip, (b) $4Pip_2$, (c) $4Pip_3$ and (d) $4Pip_4$ for CH_2Cl_2. (e, f) Absorption and emission spectra of $4Pip_2$ for (e) $CHCl_3$ and (f) CH_3CN. (g, h) Absorption and emission spectra of $4Pip_4$ for CH_3CN: (g) normalized spectral maxima; and (h) normalized deconvoluted components at the crossing spectral edges.

The emission spectra show similar splitting where the medium polarity and the number of the residues enhance the relative intensity of the low-energy band (Fig. 2-3). Two principal phenomena can account for these trends: (1) aggregation with increase propensity for long oligomers in polar media; and (2) formation of emissive CT states that cannot be directly accessed from the ground states by direct optical excitation.

Aggregation induced by increased solvent polarity is possible if these polar oligomers assemble in stacks with co-directionally oriented dipoles, e.g. forming H-like aggregates. Increasing the number of residues increases the total magnitude of the dipoles. Concurrently, polar media screen the dipole-generated localized fields responsible for repulsive interaction in the hypothesized assemblies, consistent with observation for similar Aa oligomers with no side chains and different capping moieties of their N- and C-termini (R_1=R_2=H Fig. 2-1) [51]. The identical groups capping the N- and C-termini of the 4Pip oligomers and the lack of concentration dependence in the optical spectra, however, renders the aggregation as an origin of the observed trends (Fig. 2-3) quite unlikely.

Only for the monomer, 4Pip, in relatively non-polar media, we observe aggregation as the concentration rises to hundreds of μM (Fig. 2-4a). For the dimer, trimer and tetramer, variations in sample concentration from nM to mM does not alter the optical spectra (Fig. 2-4b). While these findings may suggest for immensely small dissociation constants, we cannot exclude other reasons for the observed splits in the spectral bands.

Aromatic alkyl amines have a large propensity for forming excited twisted intramolecular charge-transfer (TICT) states. Theoretical analysis, however, reveals that

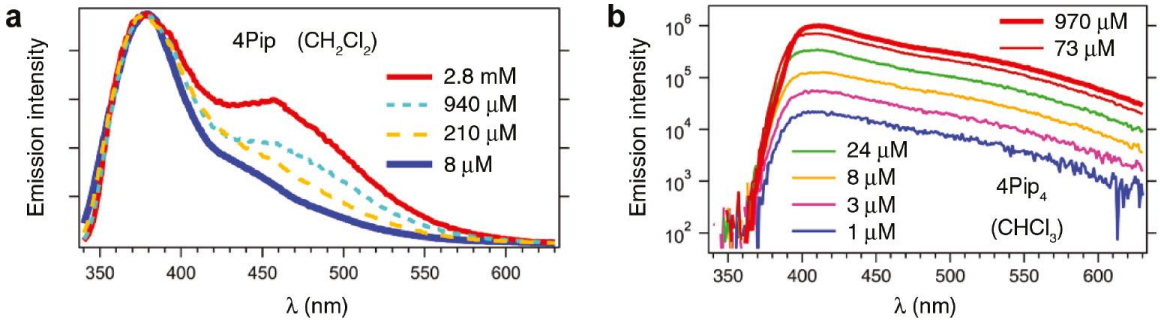

Fig. 2-4: Concentration dependence of the emission spectra of the 4Pip monomer and tetramer for chlorinated solvents. (a) Normalized spectra presented in a liner intensity scale (λ_{ex}=310 nm). (b) Spectra presented in a logarithmic intensity scale (λ_{ex}=330 nm).

Aa residues with amines at position 5, i.e. $–R_2=–NR'R''$, do not form TICT states [52]. Shifting the electron-donating amines from position 5 (R_1) to position 4 (R_2) considerably alters the electronic properties of the Aa residues. Thus, we cannot preclude a propensity of 4Pip conjugates to form TICT states, which polar media should enhance as consistent with the observed trends.

The optical excitation energy, E_{00}, as expected, decreases with an increase in the length of the oligomers (Table 2-1). This decrease is most pronounced, by about 0.3 eV, between the monomer and the dimer. A further increase in the oligomer length to a tetramer leads to only about a 0.1-eV decrease in E_{00}, which is consistent with delocalization of the frontier orbitals limited to about three residues. Specifically, the permanent dipoles elevate the energy levels of the frontier orbitals at the C-termini, and lower those at the N-termini. That is, the HOMOs of the oligomers are located at the C-terminal residues, while the LUMOs – at the N-termini [50]. Increasing the lengths of the oligomers decreases the

HOMO-LUMO overlaps and transitions from HOMO to LUMO+***n*** and from LUMO to HOMO-***n*** become characteristic of the observed features in the optical spectra.

Table 2-1: Concentration dependence of the emission spectra of the 4Pip monomer and tetramer for chlorinated solvents. (a) Normalized spectra presented in a liner intensity scale (λ_{ex}=310 nm). (b) Spectra presented in a logarithmic intensity scale (λ_{ex}=330 nm).

Solvent	**4Pip**	**4Pip$_2$**	**4Pip$_3$**	**4Pip$_4$**
$CHCl_3$	3.60	3.33	3.26	3.23
CH_2Cl_2	3.61	3.35	3.25	3.22
CH_3CN	3.65	3.36	3.28	3.25

Similar to the 4Pip monomer [57], the oligomers of this residue manifest irreversibility during electrochemical oxidation (Fig. 2-5a), suggesting for the formation of unstable radical cations. Indeed, chemical reversibility of voltammograms guarantees the stability of the oligomers to transfer charges [55]. Lack of reversibility at moderate scan rates, however, does not preclude them from successfully mediating CT in the nanosecond, picosecond and femtosecond time domains. For example, while millisecond oxidative degradation results in irreversible behavior at moderate scan rates, holes residing on a residue for less than a nanosecond during efficient CT will have negligibly short time to initiate relatively slow chemical transformations.

In the presence of supporting electrolyte (0.1 M or more), the oxidation of the oligomers occurs practically at the same potential (Fig. 2-5a,b), suggesting for a considerable localization of the radical cation under these conditions. Conversely, lowering the electrolyte concentation reveals potentially a size dependence on the propensity of these oligomers to oxidize, as reflected by the positive shift in the reduction potential with the increase in the number of residues (Fig. 2-5b,c), which could be ascribed to dipole induced

impedance of the oxidation. The experimental uncertainty of these changes as revealed by the relatively large error bars (Fig. 2-5c), however, renders the substantiality of this trend somewhat unfeasible.

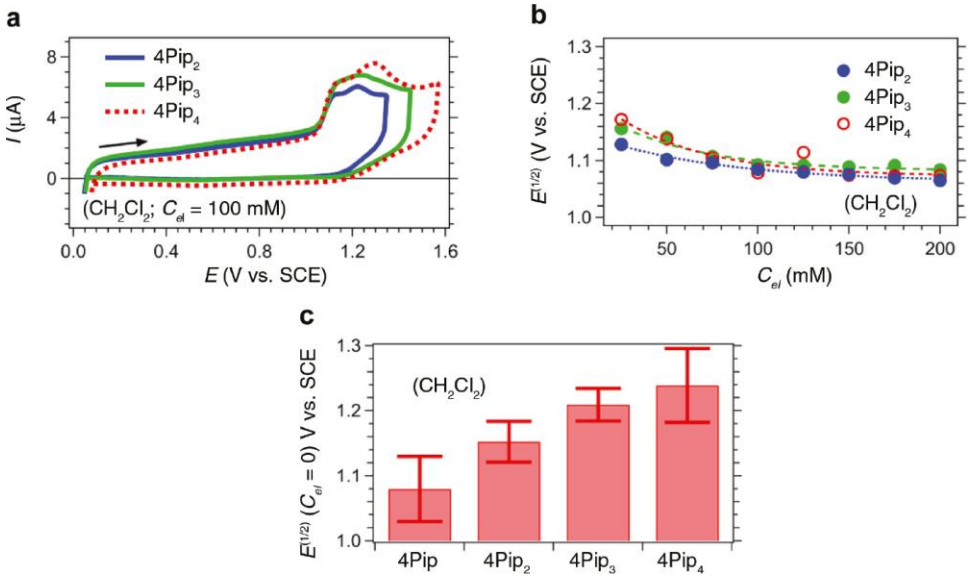

Fig. 2-5: Electrochemical characteristics of the 4Pip conjugates. (a) Cyclic voltammograms of the dimer, trimer and tetramer for dichloromethane solution in the presence of 100 mM N(***n***-$C_4H_9)_4PF_6$ (***ν***=50 mV s^{-1}). (b) Dependence of the reduction potentials of oxidation (obtained from the first inflection points of the anodic waves [176]) on the concentation of the supporting electrolyte, C_{el} [177], [178]. (c) Reduction potentials for the oxidation of the oligomers extrapolated to

Overall, the exciton of the 4Pip oligomers appears to delocalize over two-to-three residues. The radical cation, at least in electrolyte media, is localized on one or a maximum of two Aa residues. These findings suggest that while the amide bonds appear to provide rigidity and partial conjugation along the backbones of the oligomers, they do not ensure broad delocalization of the excitons and the holes on the 4Pip conjugates. The nodes on the carbonyl carbons of the frontier π-orbitals of the amide bonds [124] can be a source for this limitation of the delocalization.

Conclusions

Biomimetic molecular electrets, based on polypeptide helical structure of α-amino acids, are relatively easy to make using automated synthetic protocols. The established procedures for peptide synthesis, however, cannot produce bioinspired anthranilamide electrets. Introducing each residue as the corresponding nitrobenzoic-acid derivative places strict demands on the selective reduction of nitro groups to amines. Survey of the broad variety of available reduction methods reveals that only a few such procedures are feasible for Aa synthesis and even fewer are potentially implementable in SPPS. Our findings reveal that viologen^{2+}|viologen$^{+\bullet}$ and $Cr^{3+}|Cr^{2+}$ organic-soluble redox couples manifest some of the best electrochemical properties for selective reduction of nitro groups in Aa derivatives. Using these redox couples for shuttling electrons from reducing agents in a different solid or liquid phase offers routes for implementation in solid-phase synthesis protocols. These advances are important steps toward making the bioinspired molecular electrets readily available to wide research and development communities. Furthermore, the optical and electrochemical properties of the anthranilamide oligomers reveal relative localization of the excitons and the holes, i.e. the positive charges, placed on them.

Experimental

Cyclic lactams and opening them (Scheme 2-1)

2-(2-Propylpentanamido)benzoic acid (1)

Anthranilic acid (397 mg, 2.9 mmol) was placed in a 50 mL and suspended in DCM (3 mL), blanked with continuous flow of N_2 and placed in a dry ice/acetone bath. While the reaction was mixing 2-propylpentanoic acid (472 μL, 2.76 mmol) was slowly added

followed by the dropwise addition of NMM (1 mL, 9 mmol). The reaction mixture was allowed to warm up to room temperature and was stirred overnight. The reaction was then concentrated ***in vacuo***. Hexanes (25 mL) was added to the solution and vortex until a white precipitate formed to afford 137 mg (0.52 mmol, 18% yield) of white solid of **1**. ^{1}H NMR (600 MHz, $CDCl_3$) ***δ***/ppm: 10.95 (1 H, s), 8.78 (1H, m), 8.14 (1 H, dd, ***J***=7.9, 1.8 Hz), 7.59 (1H, m), 7.11 (1H, m), 2.34 (1H, dt, ***J***=9.6, 4.7 Hz), 1.71 (2H, m), 1.5 (2H, m), 1.37 (4H, m), 0.91 (6H, t, ***J***=7.2 Hz); ^{13}C NMR (150 MHz, $CDCl_3$) ***δ***/ppm: 175.8, 172.5, 142.00, 135.7, 131.8, 122.6, 120.6, 113.9, 49.5, 35.3, 20.7, 14.0; HRMS (ESI) calcd. for $C_{15}H_{22}NO_3$ $[M+H]^+$ 264.1600, found 264.15985.

7-(2-Propylpentanoyl)-7-azabicyclo[4.2.0]octa-1,3,5-trien-8-one (2)

1 (1 eq.) was suspended in 50 mL dry DCM in a dry argon-purged flask (1 eq), and two drops of ***N***,***N***-dimethylformamide (DMF) were added. The mixture was cooled in a dry ice/acetone bath and oxalyl chloride (1 eq.) was added dropwise. The mixture was stirred for 3 h and allowed to warm up to room temperature. After removing the solvents under reduced pressure, the crude product was purified by silica chromatography (hexane: ethyl acetate 4:1) to yield 35 mg (0.14 mmol, 83% yield) or white solid; ^{1}H NMR (400 MHz, $CDCl_3$) ***δ/***ppm: 8.19 (dd, ***J***=8.0, 1.4 Hz, 1H), 7.81–7.76 (m, 1H), 7.57 (d, ***J***=8.1 Hz, 1H), 7.51–7.46 (m, 1H), 2.70 (tt, ***J***=9.0, 5.5 Hz, 1H), 1.86–1.76 (m, 2H), 1.61 (ddt, ***J***=13.5, 10.1, 5.9 Hz, 2H), 1.41–1.28 (m, 4H), 0.91 (t, ***J***=7.3 Hz, 6H); ^{13}C NMR (100 MHz, $CDCl_3$) ***δ/***ppm: 165.8, 160.1, 146.4, 136.4, 128.4, 128.0, 126.7, 116.9, 45.4, 35.0, 20.6, 14.0; HRMS (ESI) calcd. for $C_{15}H_{20}NO_2$ $[M+H]^+$ 246.1494, found 246.1478.

Ethyl 1-(2-(2-propylpentanamido)benzoyl)piperidine-4-carboxylate (3)

Piperidine-4-carboxylic acid ethyl ester (1.2 eq.) was added to a solution of **2** (1 eq.) in DCM (50 mL). After the completion of the reaction, the reaction mixture was concentrated under reduced pressure and crystallized from methanol; Yield: 41 mg (93%). White solid; ^{1}H NMR (400 MHz, $CDCl_3$) ***δ***/ppm: 8.81 (s, 1H), 8.21 (d, ***J***=8.3 Hz, 1H), 7.43–7.37 (m, 1H), 7.18 (dd, ***J***=7.6, 1.3 Hz, 1H), 7.09 (t, ***J***=7.5 Hz, 1H), 4.74–4.25 (m, 1H), 4.14 (q, ***J***=7.1 Hz, 2H), 4.00–3.64 (m, 1H), 3.09 (t, ***J***=10.2 Hz, 2H), 2.57 (tt, ***J***=10.5, 4.0 Hz, 1H), 2.22 (tt, ***J***=9.6, 4.9 Hz, 1H), 2.11–1.84 (m, 2H), 1.82–1.68 (m, 2H), 1.70–1.60 (m, 2H), 1.49–1.39 (m, 2H), 1.39–1.28 (m, 4H), 1.25 (t, ***J***=7.1 Hz, 3H), 0.90 (t, ***J***=7.2 Hz, 6H); ^{13}C NMR (100 MHz, $CDCl_3$) ***δ***/ppm: 174.7, 173.8, 169.2, 136.5, 130.7, 126.9, 124.7, 123.5, 123.2, 60.7, 48.6, 40.8, 35.4, 28.3, 20.8, 14.2, 14.1; HRMS (ESI) calcd. for $C_{23}H_{35}N_2O_4$ $[M+H]^+$ 403.2597, found 403.2574.

Synthesis of 4Pip oligomers (Scheme 2-2)

2-Nitro-4-(piperidin-1-yl)benzoyl chloride (*5*) (i, Scheme 2-2)

The preparation of 2-nitro-4-(piperidin-1-yl)benzoic acid, **4**, was previously described [56]. To a solution of **4** (1 eq.) in DCM, placed in a dry argon-filled flask, three drops of DMF were added and the mixture was cooled in a dry ice/acetone bath. Oxalyl chloride (1 eq.) was added dropwise and the mixture was stirred for 3 h. The residual oxalyl chloride was removed by repeatedly concentrating the mixture and resuspending the residue in 3 mL dry DCM. After three resuspension and concentation steps, the crude acid chloride was used in the subsequent step without further purification.

General procedure 1: reduction of nitro compounds to amines (iii, Scheme 2-2)

The nitro compound (1 eq.) was dissolved in 75 mL of ethyl acetate and reduced at room temperature with hydrogen (1 atm.) on 10% Pd/C (0.1 eq.) as a catalyst. The conversion of the nitro group to an amine led to the appearance of blue fluorescence and the progress of the reaction was monitored with TLC. Upon completion of the reduction, the solid support with the catalyst was filtered off and the filtrate was evaporated under reduced pressure. The products were purified using recrystallization from hexane solutions.

General procedure 2: amide formation (v, Scheme 2-2)

To a solution of the amine (1 eq.) in anhydrous DCM (10 mL) was added one drop of dry pyridine and the mixture was cooled in dry ice/acetone bath while purging with argon. A solution of **5** (1 eq.) in 1 mL dry DCM was added slowly and the mixture was stirred until the reaction was completed, as monitored, using TLC. The solution was poured into 1 N HCl and the organic layer was collected, dried over $MgSO_4$ and concentrated ***in vacuo***. The product was purified by column chromatography on silica using hexane/ethyl acetate (4:1) as an eluent.

General procedure 3: capping the N-termini as hexanoic amides (iv, Scheme 2-2)

Under argon, hexanoic anhydride (1 eq.) was added dropwise to a solution of amine (1 eq.) in dry pyridine (4 mL) cooled in an ice bath. The mixture was allowed to warm up, heated to 40 °C, and stirred until the reaction was completed, as monitored using TLC. The solution was poured into 1 N HCl and the organic layer was collected, dried over $MgSO_4$ and concentrated ***in vacuo***. The product was purified by column chromatography on silica using hexane/ethyl acetate (4:1) as an eluent.

N-Hexyl-2-nitro-4-(piperidin-1-yl)benzamide (6) and 4Pip

The precursor for the C-terminal residue, **6**, and 4Pip have been previously reported [56]. Compound **6** was prepared from ***in situ*** activated **4** and 1-aminohexane, and for 4Pip, the general procedure 3 was used.

2-Amino-N-hexyl-4-(piperidin-1-yl)benzamide (7)

Yield: 450 mg (98%). White solid; ^{1}H NMR (400 MHz, $CDCl_3$) δ 7.18 (CH-CC=O, d, ***J***=8.9 Hz, 1H), 6.25 (CH–C–PIP, dd, ***J***=8.8, 2.2 Hz, 1H), 6.13 (CH–C–NH_2, s, 1H), 5.91 (NH, s, 1H), 5.76 (NH_2, s, 2H), 3.39–3.33 (m, 2H), 3.25–3.18 (m, 4H), 1.72–1.63 (m, 4H), 1.63–1.52 (m, 4H), 1.41–1.26 (m, 6H), 0.88 (t, ***J***=6.8 Hz, 3H); ^{13}C NMR (100 MHz, $CDCl_3$) δ 169.1, 154.0, 150.5, 128.2, 107.1, 105.0, 102.0, 49.4, 39.5, 31.5, 29.8, 26.7, 25.3, 24.3, 22.6, 14.0; HRMS (ESI) calcd. for $C_{18}H_{29}N_{3O}Na$ [M+Na^+] 326.2203, found 326.2203.

N-Hexyl-2-(2-nitro-4-(piperidin-1-yl)benzamido)-4-(piperidin-1-yl)benzamide (8)

Yield: 190 mg (84%). Yellow solid; ^{1}H NMR (400 MHz, $CDCl_3$) δ 12.29 (s, 1H), 8.38 (s, 1H), 7.60 (d, ***J***=8.7 Hz, 1H), 7.32 (d, ***J***=9.0 Hz, 1H), 7.23 (d, ***J***=2.5 Hz, 1H), 7.00 (dd, ***J***=8.7, 2.6 Hz, 1H), 6.55 (s, 1H), 6.12 (s, 1H), 3.41–3.28 (m, 10H), 1.73–1.53 (m, 14H), 1.41–1.27 (m, 6H), 0.88 (t, ***J***=6.9 Hz, 3H); ^{13}C NMR (100 MHz, $CDCl_3$) δ 169.0, 164.1, 154.0, 152.5, 150.1, 148.9, 141.9, 129.3, 127.6, 120.1, 117.0, 109.6, 108.7, 105.9, 48.8, 39.8, 31.4, 29.5, 26.6, 25.3, 25.1, 24.2, 24.1, 22.5, 14.1, 14.0; HRMS (ESI) calcd. for $C_{30}H_{42}N_5O_4$ [M+H^+] 536.3231, found 536.3221.

2-Amino-N-(2-(hexylcarbamoyl)-5-(piperidin-1-yl)phenyl)-4-(piperidin-1-yl)benzamide (9)

Yield: 115 mg (97%). White solid; ^{1}H NMR (400 MHz, $CDCl_3$) δ 12.13 (s, 1H), 8.36 (d, ***J***=2.5 Hz, 1H), 7.65 (d, ***J***=9.0 Hz, 1H), 7.31 (d, ***J***=8.9 Hz, 1H), 6.53 (d, ***J***=8.8 Hz, 1H), 6.37 (dd, ***J***=9.0, 2.2 Hz, 1H), 6.13 (s, 1H), 6.08 (s, 1H), 6.01 (s, 2H), 3.39 (dd, ***J***=12.9, 7.1 Hz, 2H), 3.35–3.30 (m, 4H), 3.28–3.23 (m, 4H), 1.75–1.53 (m, 14H), 1.42–1.25 (m, 6H), 0.89 (t, ***J***=6.9 Hz, 3H); ^{13}C NMR (100 MHz, $CDCl_3$) δ 169.3, 168.1, 154.1, 151.5, 142.4, 129.4, 127.5, 109.6, 108.3, 107.2, 106.3, 105.6, 101.5, 49.2, 49.0, 39.8, 31.5, 29.6, 26.7, 25.4, 25.3, 24.3, 22.6, 14.0; HRMS (ESI) calcd. for $C_{30}H_{44}N_5O_2$ [M+H$^+$] 506.3495, found 506.3573.

2-Hexanamido-N-(2-(hexylcarbamoyl)-5-(piperidin-1-yl)phenyl)-4-(piperidin-1-yl)benzamide (4Pip$_2$)

Yield: 21 mg (98%). White solid; ^{1}H NMR (400 MHz, $CDCl_3$) δ 12.43 (s, 1H), 11.84 (s, 1H), 8.41 (d, ***J***=2.1 Hz, 1H), 8.28 (d, ***J***=2.1 Hz, 1H), 7.77 (d, ***J***=9.1 Hz, 1H), 7.33 (d, ***J***=8.9 Hz, 1H), 6.63 (d, ***J***=8.0 Hz, 1H), 6.54 (d, ***J***=7.9 Hz, 1H), 6.10 (s, 1H), 3.42–3.38 (m, 2H), 3.38–3.33 (m, 8H), 2.46–2.41 (m, 2H), 1.80–1.54 (m, 16H), 1.40–1.34 (m, 6H), 1.34–1.28 (m, 4H), 0.94–0.84 (m, 6H); ^{13}C NMR (100 MHz, $CDCl_3$) δ 172.5, 169.2, 168.1, 154.2, 142.7, 141.9, 128.9, 127.6, 109.4, 108.7, 106.3, 105.3, 48.9, 48.6, 39.9, 38.7, 31.5, 31.4, 29.7, 29.6, 26.7, 25.4, 25.1, 24.4, 24.3, 22.6, 22.5, 14.0, 13.9; HRMS (ESI) calcd for $C_{36}H_{53}N_5O_3$ [(M+H)+(–H)] 603.4148, found 603.4168.

N-Hexyl-2-(2-(2-nitro-4-(piperidin-1-yl)benzamido)-4-(piperidin-1-yl)benzamido)-4-(piperidin-1-yl)benzamide (10)

Yield: 71 mg (76%). Yellow solid; ^{1}H NMR (400 MHz, $CDCl_3$) δ 12.40 (s, 2H), 8.43 (s, 1H), 8.20 (s, 1H), 7.81 (d, ***J***=9.0 Hz, 1H), 7.62 (d, ***J***=8.7 Hz, 1H), 7.34 (d, ***J***=8.4 Hz, 1H),

7.27 (d, ***J***=2.5 Hz, 1H), 7.00 (dd, ***J***=8.7, 2.5 Hz, 1H), 6.70 (s, 1H), 6.57 (s, 1H), 6.14 (s, 1H), 3.43–3.28 (m, 14H), 1.75–1.55 (m, 20H), 1.39–1.28 (m, 6H), 0.89 (t, ***J***=6.9 Hz, 3H); ^{13}C NMR (101 MHz, $CDCl_3$) δ 169.0, 168.0, 164.3, 152.6, 150.0, 142.7, 141.6, 129.8, 129.0, 127.7, 120.7, 117.1, 109.8, 109.2, 106.9, 105.7, 48.9, 39.9, 31.5, 29.5, 26.7, 25.4, 25.2, 24.3, 24.1, 22.6, 14.0; HRMS (ESI) calcd. for $C_{42}H_{56}N_7O_5$ [M+H$^+$] 738.4337, found 738.4342.

2-Amino-N-(2-((2-(hexylcarbamoyl)-5-(piperidin-1-yl)phenyl)carbamoyl)-5-(piperidin-1-yl)phenyl)-4-(piperidin-1-yl)benzamide (11)

Yield: 66 mg (97%). White solid; ^{1}H NMR (400 MHz, $CDCl_3$) δ 12.37 (s, 2H), 8.41 (d, ***J***=2.5 Hz, 1H), 8.30 (d, ***J***=2.5 Hz, 1H), 7.80 (d, ***J***=9.1 Hz, 1H), 7.71 (d, ***J***=9.0 Hz, 1H), 7.32 (d, ***J***=8.9 Hz, 1H), 6.67 (d, ***J***=9.0 Hz, 1H), 6.55 (dd, ***J***=8.7, 1.8 Hz, 1H), 6.34 (d, ***J***=8.9 Hz, 1H), 6.16 (s, 1H), 6.12–6.08 (m, 1H), 3.43–3.22 (m, 14H), 1.75–1.54 (m, 20H), 1.41–1.27 (m, 6H), 0.88 (t, ***J***=6.9 Hz, 3H); ^{13}C NMR (100 MHz, $CDCl_3$) δ 169.2, 168.2, 168.2, 154.1, 154.0, 151.5, 143.2, 141.8, 129.7, 128.9, 127.6, 109.7, 109.6, 108.8, 108.7, 106.7, 105.7, 105.4, 49.4, 49.0, 48.8, 39.9, 31.5, 29.6, 26.7, 25.5, 25.4, 25.3, 24.4, 24.3, 22.6, 14.0; HRMS (ESI) calcd. for $C_{42}H_{58}N_7O_3$ [M+H$^+$] 708.4596, found 708.4606.

2-Hexanamido-N-(2-((2-(hexylcarbamoyl)-5-(piperidin-1-yl)phenyl)carbamoyl)-5-(piperidin-1-yl)phenyl)-4-(piperidin-1-yl)benzamide (4Pip$_3$)

Yield: 22 mg (92%). White solid; ^{1}H NMR (400 MHz, $CDCl_3$) δ 12.61 (s, 1H), 12.46 (s, 1H), 11.77 (s, 1H), 8.42 (s, 1H), 8.30 (d, ***J***=9.6 Hz, 2H), 7.82 (dd, ***J***=9.0, 3.0 Hz, 2H), 7.34 (d, ***J***=8.8 Hz, 1H), 6.69 (s, 1H), 6.58 (s, 2H), 6.12 (s, 1H), 3.43–3.33 (m, 14H), 2.44 (t, J=7.5 Hz, 2H), 1.80–1.57 (m, 22H), 1.42–1.34 (m, 6H), 1.33–1.29 (m, 4H), 0.94–0.84 (m,

6H); ^{13}C NMR (100 MHz, $CDCl_3$) δ 172.5, 169.1, 168.1, 154.2, 142.6, 141.7, 129.3, 129.0, 127.6, 109.6, 109.3, 108.9, 108.6, 106.6, 105.8, 105.6, 48.7, 39.9, 38.7, 31.5, 31.4, 29.6, 26.7, 25.4, 25.3, 25.1, 24.4, 22.6, 22.5, 14.0, 13.9; HRMS (ESI) calcd. for $C_{48}H_{67}N_7O_4Na$ [M+Na^+] 828.5152, found 828.5164.

N-Hexyl-2-(2-(2-(2-nitro-4-(piperidin-1-yl)benzamido)-4-(piperidin-1-yl)benzamido)-4-(piperidin-1-yl)benzamido)-4-(piperidin-1-yl)benzamide (12)

Yield: 46 mg (69%). Yellow solid; ^{1}H NMR (400 MHz, $CDCl_3$) δ 12.61 (s, 1H), 12.46 (s, 1H), 12.35 (s, 1H), 8.44 (s, 1H), 8.31 (s, 1H), 8.22 (s, 1H), 7.86 (d, ***J***=8.9 Hz, 1H), 7.82 (d, ***J***=9.0 Hz, 1H), 7.63 (d, ***J***=8.7 Hz, 1H), 7.34 (d, ***J***=8.5 Hz, 1H), 7.27 (d, ***J***=2.5 Hz, 1H), 7.01 (dd, ***J***=8.7, 2.4 Hz, 1H), 6.79–6.47 (m, 3H), 6.13 (s, 1H), 3.43–3.31 (m, 18H), 1.78–1.58 (m, 26H), 1.40–1.27 (m, 6H), 0.89 (t, ***J***=6.9 Hz, 3H); ^{13}C NMR (100 MHz, $CDCl_3$) δ 169.1, 168.1, 164.3, 154.1, 152.6, 150.1, 142.6, 142.4, 141.7, 129.8, 129.3, 129.0, 127.7, 120.7, 117.1, 109.8, 109.1, 106.1, 48.9, 39.9, 31.5, 29.5, 26.7, 25.3, 25.2, 24.3, 24.1, 22.6, 14.0; HRMS (ESI) calcd. for $C_{54}H_{69}N_9O_6Na$ [M+Na^+] 962.5268, found 962.5436.

2-Amino-N-(2-((2-((2-(hexylcarbamoyl)-5-(piperidin-1-yl)phenyl)carbamoyl)-5-(piperidin-1-yl)phenyl)carbamoyl)-5-(piperidin-1-yl)phenyl)-4-(piperidin-1-yl)benzamide (13)

Yield: 24 mg (99%). White solid; ^{1}H NMR (400 MHz, $CDCl_3$) δ 12.59 (s, 1H), 12.44 (s, 1H), 12.33 (s, 1H), 8.42 (d, ***J***=2.4 Hz, 1H), 8.34 (d, ***J***=2.5 Hz, 1H), 8.29 (d, ***J***=2.4 Hz, 1H), 7.85 (d, ***J***=9.1 Hz, 1H), 7.81 (d, ***J***=9.1 Hz, 1H), 7.72 (d, ***J***=9.0 Hz, 1H), 7.33 (d, ***J***=8.9 Hz, 1H), 6.68 (dd, ***J***=9.0, 2.3 Hz, 1H), 6.62 (d, ***J***=7.5 Hz, 1H), 6.54 (dd, ***J***=8.8, 2.2 Hz, 1H), 6.35 (dd, ***J***=8.9, 1.9 Hz, 1H), 6.32–6.02 (m, 2H), 6.15 (s, 2H), 3.42–3.33 (m, 14H), 3.28–

3.23 (m, 4H), 1.75–1.63 (m, 26H), 1.39–1.26 (m, 6H), 0.88 (t, ***J***=6.7 Hz, 3H); ^{13}C NMR (100 MHz, $CDCl_3$) δ 169.2, 168.3, 168.2, 168.1, 154.0, 151.4, 143.2, 142.6, 141.7, 129.7, 129.2, 128.9, 127.6, 110.2, 109.7, 109.6, 109.2, 108.7, 108.6, 106.6, 106.1, 105.9, 105.8, 105.4, 49.4, 49.0, 48.8, 39.9, 31.5, 29.7, 29.6, 26.7, 25.5, 25.4, 25.3, 24.5, 24.4, 24.3, 22.6, 14.0; HRMS (ESI) calcd. for $C_{54}H_{74}N_{10}O_4$ [(M+NH_4)+(–H)] 926.5894, found 926.5865.

2-Hexanamido-N-(2-((2-((2-(hexylcarbamoyl)-5-(piperidin-1-yl)phenyl)carbamoyl)-5-(piperidin-1-yl)phenyl)carbamoyl)-5-(piperidin-1-yl)phenyl)-4-(piperidin-1-yl)benzamide (4Pip$_4$)

Yield: 27 mg (90%). White solid; ^{1}H NMR (400 MHz, $CDCl_3$) δ 12.64 (s, 1H), 12.58 (s, 1H), 12.46 (s, 1H), 11.78 (s, 1H), 8.43 (s, 1H), 8.33 (s, 2H), 8.30 (s, 1H), 7.91–7.78 (m, 3H), 7.34 (d, ***J***=8.8 Hz, 1H), 6.77–6.52 (m, 4H), 6.13 (s, 1H), 3.48–3.27 (m, 18H), 2.45 (t, ***J***=7.6 Hz, 2H), 1.79–1.62 (m, 28H), 1.40–1.34 (m, 6H), 1.33–1.29 (m, 4H), 0.94–0.85 (m, 6H); ^{13}C NMR (100 MHz, $CDCl_3$) δ 172.5, 169.1, 168.2, 168.1, 154.1, 142.6, 142.6, 142.5, 141.7, 129.3, 129.3, 129.0, 127.6, 109.3, 109.1, 108.5, 106.7, 106.1, 106.1, 106.0, 105.6, 48.8, 39.9, 38.7, 31.5, 31.4, 29.7, 29.6, 26.7, 25.4, 25.1, 24.4, 22.6, 22.5, 14.0, 13.9; HRMS (ESI) calcd. for $C_{60}H_{81}N_9O_5Na$ $[M+Na]^+$ 1030.6253, found 1030.6275.

Selective reduction of nitro groups in brominated Aa precursors (<u>Scheme 2-3</u>)

5-bromo-2-nitro-N-(pentan-3-yl)benzamide (14)

5-Bromo-2-nitrobenzoic acid (1.00 g, 4.07 mmol) was placed in a dry round bottom flask with a stir bar, and purged with Ar. Dry, Ar purged DCM (30 mL) and five drops of amine-free dry DMF were added, and the mixture was cooled in a dry ice/acetone bath. While stirring, oxalyl chloride (700 μL, 8.1 mmol) was added dropwise and allowed to react for

30 min. The progress of the reaction was monitored using TLC, i.e. a drop of the reaction was quenched with dry methanol to form methyl ester that has a distinctly different retention factor, R_f, from the starting material. After the completion of the reaction, the mixture was concentrated, resuspended in dry DCM (25 mL) and concentrated again. This resuspending and drying was repeated three times. Under argon, the dried mixture was dissolved in dry DCM (25 mL) and cooled in a dry ice/acetone bath. While stirring, 3-aminopentane (1.4 mL, 12 mmol) was added dropwise, followed by a dropwise addition of NMM (2.2 mL, 20.3 mmol). The reaction was allowed to reach room temperature and stirred for 3 h. The mixture was diluted with 5% HCl and stirred for additional 10 min. The resulting mixture was extracted with DCM (3×50 mL). The organic layers were collected, combined, dried over Na_2SO_4, and condensed. The resulting residue was dissolved in small amount of DMF, added to deionized water and filtered. The filtrate was diluted further with deionized water and extracted with DCM (3×25 mL). The organic layers were combined and dried over Na_2SO_4. The solvent was evaporated ***in vacuo*** to afforded 1.1 g (84%) of 14 as a white solid. ^{1}H NMR (600 MHz, $CDCl_3$) δ/ppm: 7.94 (d, ***J***=8.7 Hz, 1H), 7.69 (dd, ***J***=8.7, 2.2 Hz, 1H), 7.61 (d, ***J***=2.1 Hz, 1H), 5.57 (d, ***J***=9.1 Hz, 2H), 4.02–3.93 (m, 1H), 1.72–1.62 (m, 3H), 1.56–1.50 (m, 3H), 1.01 (t, ***J***=7.5 Hz, 6H). ^{13}C NMR (101 MHz, $CDCl_3$) δ/ppm: 164.69, 145.09, 135.05, 133.34, 131.80, 128.65, 126.10, 53.19, 27.15, 10.23. HRMS (ESI) ***m/z*** calcd. for $C_{12}H_{16}BrN_2O_3^+$: 315.0344 $[M+H]^+$, found 315.0216.

2-amino-5-bromo-N-(pentan-3-yl)benzamide (15)

Procedure 1: reducing with $HSiCl_3$ (i, <u>Scheme 2-3</u>)

14 (79 mg, 0.25 mmol), was transferred to a dry, argon-purged 25 mL round bottom flask with a stir bar. Dry acetonitrile (MeCN) (5 mL) was added while purging with argon, followed by followed by the addition of DIPEA (218 μL, 1.25 mmol). This solution was placed into a 0°C ice bath and stirred for 5 min. A solution of $HSiCl_3$ (91 μL, 0.9 mmol) in 2 mL MeCN was prepared separately under Ar, and added to the reaction mixture dropwise over the course of 10 min. The reaction was taken out of the ice bath and stirred overnight at room temperature. The progress of the reaction was monitored using TLC. The mixture was added to 50 mL of aqueous saturated solution of $NaHCO_3$ and extracted with DCM (3×25 mL). The organic layers were collected, combined and dried over Na_2SO_4. The solvent was evaporated ***in vauco*** and recrystallized from hexanes afforded afford 29 mg (0.10 mmol, 41% yield) of **15** as a white solid. ^{1}H NMR (600 MHz, $CDCl_3$) ***δ***/ppm: 7.38 (d, ***J***=2.3 Hz, 1H), 7.26 (dd, ***J***=8.7, 2.3 Hz, 1H), 6.57 (d, ***J***=8.7 Hz, 1H), 5.70–5.66 (m, 1H), 5.48 (s, 2H), 3.97–3.89 (m, 1H), 1.64 (dtd, ***J***=14.8, 7.4, 5.4 Hz, 2H), 1.47 (dt, ***J***=13.9, 7.5 Hz, 2H), 0.95 (t, ***J***=7.4 Hz, 6H). ^{13}C NMR (101 MHz, $CDCl_3$) ***δ/***ppm: 167.82, 147.43, 134.68, 129.32, 118.92, 118.43, 107.75, 52.29, 27.54, 10.38. HRMS (ESI) ***m/z*** calcd. for $C_{12}H_{16}BrN_2O^-$: 283.0451 $[M]^-$, found 283.0282.

Procedure 2: reducing with $Na_2S_2O_4$ (ii, <u>Scheme 2-3</u>)

14 (100 mg, 0.32 mmol), $Na_2S_2O_4$ (1.1 g, 6.37 mmol), K_2CO_3 (1.23 g, 8.9 mmol), and 1,1-diheptyl-4,4-bipyridinium dibromide (442 mg, 0.857 mmol) were placed in a dry, argon-purged 25 mL round bottom flask with a stir bar. An argon-purged mixture of 5 mL DCM and 5 mL deionized water were added, and the reaction was stirred at room temperature for 2.5 h. The instant color change of the DCM phase was an indication for the formation

of the viologen radical cation. The progress of the reaction in the organic phase was monitored using TLC. The mixture was added to 50 mL saturated aqueous solution of Na_2CO_3 and extracted with DCM (3×25 mL). The organic layers were collected, combined and dried over Na_2SO_4. The solvent was evaporated ***in vacuo*** and recrystallized from hexanes afforded afford 58 mg (0.20 mmol, 64% yield) of **15** as a white solid.

Procedure 3: reducing with $CrCl_2$ (iii, Scheme 2-3)

This reaction was performed in a glovebox filled with argon (O_2<1 ppm, H_2O<1 ppm). **14** (50 mg, 0.16 mmol) and $CrCl_2$ (310 mg, 2.5 mmol) were dissolved in 5 mL of argon purged dry DMF and transferred to a dry 100 mL round bottom flask with a stir bar. The solution was stirred for 4 h and the progress was monitored using TLC. Upon completion, the mixture was taken out of the glove box, added to 100 mL of aqueous EDTA solution (0.03 M) and extracted with ethyl acetate (3×25 mL). The organic layers were collected, combined, and dried over Na_2SO_4. The solvent was evaporated ***in vacuo*** and recrystallized from hexanes afforded afford 43 mg (0.15 mmol, 95% yield) of **15** as a white solid.

Optical absorption and emission spectroscopy

Steady-state absorption spectra were recorded in a transmission mode using a JASCO V-670 spectrophotometer (Tokyo, Japan); and steady-state emission spectra were measured, also in a transmission mode, with a FluoroLog-3 spectrofluorometer (Horiba-Jobin-Yvon, Edison, NJ, USA) as previously reported [179]. The reported fluorescence spectra, $F(\tilde{\nu}), F(\nu\tilde{})$, were obtained from the fluorescence spectra, $\boldsymbol{F}(\lambda)$, recorded vs. wavelength, i.e. $F(\tilde{\nu}) = F(\lambda)\lambda 2 . F(\nu\tilde{}) = F(\lambda)\,\lambda 2$.

Electrochemical analysis

Cyclic voltammetry is conducted using Reference 600 Potentiostat/Galvanostat/ZRA (Gamry Instruments, PA, USA), connected to a three-electrode cell, at scan rates of 50 mV s^{-1}, as previously described [177], [178]. Anhydrous solvents are employed for the sample preparation, with different concentrations of tetrabutylammonium hexafluorophosphate, $N(\boldsymbol{n}\text{-}C_4H_9)_4PF_6$, as supporting electrolyte. Prior to recording the voltammograms, the samples are extensively purged with argon while maintaining constant volume by adding more of the anhydrous solvent. For each sample and each solvent, a set of voltammograms is recorded where the electrolyte concentration is increased from 25 mM to 200 mM in increments of 25 mM. The half-wave potentials, $\boldsymbol{E}^{(1/2)}$, are determined from the first inflection point of the anodic waves, i.e. the potentials where $\boldsymbol{\partial^2 I/\partial E^2}=0$ at $\boldsymbol{\partial E/\partial t}$=constant [55], [176]. To correct for potential drifts in the reference electrode (which is SCE, connected with the cell via a salt bridge), ferrocene was used as a standard, i.e. $\boldsymbol{E}^{(1/2)}=0.45\pm0.01$ V vs. SCE for MeCN, 100 mM $N(\boldsymbol{n}\text{-}C_4H_9)_4BF_4$ [177]. Voltammograms of the standard are recorded before and after each set of measurements. From the dependence of $\boldsymbol{E}^{(1/2)}$ on the electrolyte concentration (Fig. 2-5b), the potential for neat solvents are estimated from extrapolation to zero electrolyte concentration [180].

References

[1] V. I. Vullev. ***J. Phys. Chem. Lett.*****2**, 503 (2011).

[2] J. J. Warren, J. R. Winkler, H. B. Gray. ***Coord. Chem. Rev.*****257**, 165 (2013).

[3] U. Brandt. ***BIOspektrum*****20**, 267 (2014).

[4] R. M. Metzger. ***Chem. Rev.*****115**, 5056 (2015).

[5] J. B. Derr, J. Tamayo, E. M. Espinoza, J. A. Clark, V. I. Vullev. ***Can. J. Chem.*****96**, 843 (2018).

[6] S. Ilic, A. Alherz, C. B. Musgrave, K. D. Glusac. ***Chem. Soc. Rev.*****47**, 2809 (2018).

[7] A. Purc, E. M. Espinoza, R. Nazir, J. J. Romero, K. Skonieczny, A. Jeżewski, J. M. Larsen, D. T. Gryko, V. I. Vullev. ***J. Am. Chem. Soc.*****138**, 12826 (2016).

[8] E. M. Espinoza, J. M. Larsen-Clinton, M. Krzeszewski, N. Darabedian, D. T. Gryko, V. I. Vullev. ***Pure Appl. Chem.*****89**, 1777 (2017).

[9] R. Breslow. ***Chem. Soc. Rev.*****1**, 553 (1972).

[10] C. A. Scherer, C. A. Dorschel, J. M. Cook, P. W. Le Quesne. ***J. Org. Chem.*****37**, 1083 (1972).

[11] E. Leete. ***J. Chem. Soc., Chem. Commun.*** 1091 (1972).

[12] S. M. Kupchan, R. M. Schubert. ***Science*****185**, 791 (1974).

[13] R. Y. Tam, L. J. Smith, M. S. Shoichet. ***Acc. Chem. Res.*****50**, 703 (2017).

[14] T. T. Teeri, H. Brumer, G. Daniel, P. Gatenholm. ***Trends Biotechnol.*****25**, 299 (2007).

[15] X. Chen, G. S. Lee, A. Zettl, C. R. Bertozzi. ***Angew. Chem., Int. Ed.*****43**, 6111 (2004).

[16] G. Tempesti, D. Mange, A. Stauffer. ***Riv. Biol.*****92**, 143 (1999).

[17] A. Rosas. ***J. Med.*****45**, 173 (1961).

[18] J. S. Moya Corral. ***Rev. R. Acad. Cienc. Exactas, Fis. Nat.*****90**, 97 (1996).

[19] T. Aida, D.-L. Jiang, M.-S. Choi, M. Enomoto. ***Polym. Mater. Sci. Eng.*****80**, 257 (1999).

[20] A. E. Barron, R. N. Zuckermann. ***Curr. Opin. Chem. Biol.*****3**, 681 (1999).

[21] M. Enomoto, T. Aida. ***Yuki Gosei Kagaku Kyokaishi*****57**, 924 (1999).

[22] A. Mandel, W. Schmitt, T. G. Womack, R. Bhalla, R. K. Henderson, S. L. Heath, A. K. Powell. ***Coord. Chem. Rev.*****190–192**, 1067 (1999).

[23] Z. Hu, R. D. Williams, D. Tran, T. G. Spiro, S. M. Gorun. ***J. Am. Chem. Soc.*****122**, 3556 (2000).

[24] M. K. Brennaman, R. J. Dillon, L. Alibabaei, M. K. Gish, C. J. Dares, D. L. Ashford, R. L. House, G. J. Meyer, J. M. Papanikolas, T. J. Meyer. ***J. Am. Chem. Soc.*****138**, 13085 (2016).

[25] E. L. Efurumibe, A. D. Asiegbu. ***Int. J. Phys. Sci.*****8**, 2053 (2013).

[26] D. G. Nocera. ***Acc. Chem. Res.*****45**, 767 (2012).

[27] J. Kim, I. Jeerapan, J. R. Sempionatto, A. Barfidokht, R. K. Mishra, A. S. Campbell, L. J. Hubble, J. Wang. ***Acc. Chem. Res.*****51**, 2820 (2018).

[28] N. Mano, A. de Poulpiquet. ***Chem. Rev.*****118**, 2392 (2018).

[29] R. M. Evans, B. Siritanaratkul, C. F. Megarity, K. Pandey, T. F. Esterle, S. Badiani, F. A. Armstrong. ***Chem. Soc. Rev.*****48**, 2039 (2019).

[30] M. del Barrio, M. Sensi, C. Orain, C. Baffert, S. Dementin, V. Fourmond, C. Leger. ***Acc. Chem. Res.*****51**, 769 (2018).

[31] L. Hammarstroem. ***Acc. Chem. Res.*****48**, 840 (2015).

[32] D. L. Ashford, M. K. Gish, A. K. Vannucci, M. K. Brennaman, J. L. Templeton, J. M. Papanikolas, T. J. Meyer. ***Chem. Rev.*****115**, 13006 (2015).

[33] R. A. Marcus. ***Disc. Faraday Soc.*** 21 (1960).

[34] S. Yomosa. ***Sup. Prog. Theor. Phys.*** 249 (1967).

[35] S. G. Boxer. ***Annu. Rev. Biophys. Biophys. Chem.*****19**, 267 (1990).

[36] W. G. J. Hol, P. T. Van Duijnen, H. J. C. Berendsen. ***Nature*****273**, 443 (1978).

[37] A. Wada. ***J. Chem. Phys.*****30**, 328 (1959).

[38] Y.-G. K. Shin, M. D. Newton, S. S. Isied. ***J. Am. Chem. Soc.*****125**, 3722 (2003).

[39] E. Galoppini, M. A. Fox. ***J. Am. Chem. Soc.*****118**, 2299 (1996).

[40] S. Yasutomi, T. Morita, Y. Imanishi, S. Kimura. ***Science*****304**, 1944 (2004).

[41] L. Garbuio, S. Antonello, I. Guryanov, Y. J. Li, M. Ruzzi, N. J. Turro, F. Maran. ***J. Am. Chem. Soc.*****134**, 10628 (2012).

[42] C. Shlizerman, A. Atanassov, I. Berkovich, G. Ashkenasy, N. Ashkenasy. ***J. Am. Chem. Soc.*****132**, 5070 (2010).

[43] M. Lauz, S. Eckhardt, K. M. Fromm, B. Giese. ***Phys. Chem. Chem. Phys.*****14**, 13785 (2012).

[44] H. B. Gray, J. R. Winkler. ***Proc. Natl. Acad. Sci. U.S.A.*****102**, 3534 (2005).

[45] V. I. Vullev, G. Jones II. ***Res. Chem. Intermed.*****28**, 795 (2002).

[46] G. Jones II, X. Zhou, V. I. Vullev. ***Photochem. Photobiol. Sci.*****2**, 1080 (2003).

[47] F. D. Lewis. ***Isr. J. Chem.*****53**, 350 (2013).

[48] R. Venkatramani, S. Keinan, A. Balaeff, D. N. Beratan. ***Coord. Chem. Rev.*****255**, 635 (2011).

[49] E. Wierzbinski, A. de Leon, X. Yin, A. Balaeff, K. L. Davis, S. Rapireddy, R. Venkatramani, S. Keinan, D. H. Ly, M. Madrid, D. N. Beratan, C. Achim, D. H. Waldeck. ***J. Am. Chem. Soc.*****134**, 9335 (2012).

[50] M. K. Ashraf, R. R. Pandey, R. K. Lake, B. Millare, A. A. Gerasimenko, D. Bao, V. I. Vullev. ***Biotechnol. Prog.*****25**, 915 (2009).

[51] B. Xia, D. Bao, S. Upadhyayula, G. Jones, V. I. Vullev. ***J. Org. Chem.*****78**, 1994 (2013).

[52] D. Bao, S. Upadhyayula, J. M. Larsen, B. Xia, B. Georgieva, V. Nunez, E. M. Espinoza, J. D. Hartman, M. Wurch, A. Chang, C.-K. Lin, J. Larkin, K. Vasquez, G. J. O. Beran, V. I. Vullev. ***J. Am. Chem. Soc.*****136**, 12966 (2014).

[53] J. M. Larsen, E. M. Espinoza, V. I. Vullev. ***J. Photon. Energy.*****5**, 055598 (2015).

[54] M. Krzeszewski, E. M. Espinoza, C. Cervinka, J. B. Derr, J. A. Clark, D. Borchardt, G. J. O. Beran, D. T. Gryko, V. I. Vullev. ***Angew. Chem., Int. Ed.*****57**, 12365 (2018).

[55] E. M. Espinoza, J. M. Larsen, V. I. Vullev. ***J. Phys. Chem. Lett.*****7**, 758 (2016).

[56] J. M. Larsen, E. M. Espinoza, J. D. Hartman, C.-K. Lin, M. Wurch, P. Maheshwari, R. K. Kaushal, M. J. Marsella, G. J. O. Beran, V. I. Vullev. ***Pure Appl. Chem.*****87**, 779 (2015).

[57] J. M. Larsen-Clinton, E. M. Espinoza, M. F. Mayther, J. Clark, C. Tao, D. Bao, C. M. Larino, M. Wurch, S. Lara, V. I. Vullev. ***Phys. Chem. Chem. Phys.*****19**, 7871 (2017).

[58] H. Meyer. ***Justus Liebigs Ann. Chem.*****351**, 267 (1907).

[59] K. Butler, M. W. Partridge. ***J. Chem. Soc.*** 2396 (1959).

[60] A. Hoorfar, W. D. Ollis, J. F. Stoddart, D. J. Williams. ***Tetrahedron Lett.*****21**, 4211 (1980).

[61] A. Hoofar, W. D. Ollis, J. F. Stoddart. ***J. Chem. Soc., Perkin Trans. 1***, 1721 (1982).

[62] W. D. Ollis, J. F. Stoddart. ***Inclusion Compd.*****2**, 169 (1984).

[63] K. Imagawa, H. Tsuneyuki, S. Miyata, T. Oda, K. Nishino, Y. Ikutani. ***Osaka Kyoiku Daigaku Kiyo, Dai-3-bumon*****36**, 123 (1987).

[64] Y. Hamuro, S. J. Geib, A. D. Hamilton. ***J. Am. Chem. Soc.*****118**, 7529 (1996).

[65] A. Varnavas, L. Lassiani, V. Valenta. ***Farmaco*****55**, 369 (2000).

[66] A. Varnavas, V. Valenta, F. Berti, L. Lassiani. ***Farmaco*****56**, 555 (2001).

[67] T. Minami, S. Koyamoto, M. Kobayashi, R. Tanaka, Y. Hatanaka. ***Chem. Lett.*****34**, 434 (2005).

[68] R. V. Nair, S. Kheria, S. Rayavarapu, A. S. Kotmale, B. Jagadeesh, R. G. Gonnade, V. G. Puranik, P. R. Rajamohanan, G. J. Sanjayan. ***J. Am. Chem. Soc.*****135**, 11477 (2013).

[69] K. J. Wilson, J. Xiao, C. Z. Chen, Z. Huang, I. U. Agoulnik, M. Ferrer, N. Southall, X. Hu, W. Zheng, X. Xu, A. Wang, C. Myhr, E. Barnaeva, E. R. George, A. I. Agoulnik, J. J. Marugan. ***Eur. J. Med. Chem.*****156**, 79 (2018).

[70] S. Krauthaeuser, L. A. Christianson, D. R. Powell, S. H. Gellman. ***J. Am. Chem. Soc.*****119**, 11719 (1997).

[71] Y. Hamuro, A. D. Hamilton. ***Bioorg. Med. Chem.*****9**, 2355 (2001).

[72] M. W. Giuliano, W. S. Horne, S. H. Gellman. ***J. Am. Chem. Soc.*****131**, 9860 (2009).

[73] E. M. Espinoza, V. I. Vullev. ***ECS Trans.*****77**, 1517 (2017).

[74] E. M. Espinoza, J. M. Larsen, V. I. Vullev. ***ECS Trans.*****66**, 1 (2015).

[75] E. M. Espinoza, D. Bao, M. Krzeszewski, D. T. Gryko, V. I. Vullev. ***Int. J. Chem. Kinet.*** Ahead of Print (2019).

[76] E. Fischer, E. Fourneau. ***Ber. Dtsch. chem. Ges.*****34**, 2868 (1901).

[77] V. du Vigneaud, C. Ressler, J. M. Swan, C. W. Roberts, P. G. Katsoyannis. ***J. Am. Chem. Soc.*****76**, 3115 (1954).

[78] P. G. Katsoyannis. ***J. Polym. Sci.*****49**, 51 (1961).

[79] J. Meienhofer, E. Schnabel, H. Bremer, O. Brinkhoff, R. Zabel, W. Sroka, H. Klostermeyer, D. Brandenburg, T. Okuda, H. Zahn. ***Z. Naturforsch.*****18b**, 1120 (1963).

[80] P. G. Katsoyannis, A. Tometsko, K. Fukuda. ***J. Am. Chem. Soc.*****85**, 2863 (1963).

[81] Y.-T. Kung, Y.-C. Du, W.-T. Huang, C.-C. Chen, L.-T. Ke, S.-C. Hu, R.-Q. Jiang, S.-Q. Chu, C.-I. Niu, J.-Z. Hsu, W.-C. Chang, L.-L. Chen, H.-S. Li, Y. Wang, T.-P. Loh, A.-H. Chi, C.-H. Li, P.-T. Shi, Y.-H. Yieh, K.-L. Tang, C.-Y. Hsing. ***Sci. Sin.*****14**, 1710 (1965).

[82] Y. Pan, Y. Tu, W. Hawan, C. Chen, L. Go. ***Tanpakushitsu Kakusan Koso*****11**, 603 (1966).

[83] Y.-T. Kung, Y.-C. Du, W.-T. Huang, C.-C. Chen, L.-T. Ke, S.-C. Hu, R.-Q. Jiang, S.-Q. Chu, C.-I. Niu, J.-Z. Hsu, W.-C. Chang, L.-L. Chen, H.-S. Li, Y. Wang, T.-P. Loh, A.-H. Chi, C.-H. Li, P.-T. Shi, Y.-H. Yieh, K.-L. Tang, C.-Y. Hsing. ***Sci. Sin.*****15**, 544 (1966).

[84] H. Zahn. ***Naturwissenschaften*****54**, 396 (1967).

[85] H. Zahn, G. Schmidt. ***Tetrahedron Lett.*** 5095 (1967).

[86] R. B. Merrifield. ***J. Am. Chem. Soc.*****85**, 2149 (1963).

[87] L. A. Carpino, G. Y. Han. ***J. Am. Chem. Soc.*****92**, 5748 (1970).

[88] L. A. Carpino, G. Y. Han. ***J. Org. Chem.*****37**, 3404 (1972).

[89] M. Stawikowski, G. B. Fields. ***Curr. Protoc. Protein. Sci.*****Chapter 18**, Unit 18 1 (2012).

[90] G. R. Marshall. ***Amino Acids, Pept. Proteins Org. Chem.*****3**, 253 (2011).

[91] F. D. Bellamy, K. Ou. ***Tetrahedron Lett.*****25**, 839 (1984).

[92] D. Formenti, F. Ferretti, F. K. Scharnagl, M. Beller. ***Chem. Rev.*****119**, 2611 (2019).

[93] A. M. Tafesh, J. Weiguny. ***Chem. Rev.*****96**, 2035 (1996).

[94] M. Orlandi, D. Brenna, R. Harms, S. Jost, M. Benaglia. ***Org. Process Res. Dev.*****22**, 430 (2018).

[95] Y. N. A. Harari. ***Sapiens: A Brief history of Humankind***. First U.S. edition. Harper, New York (2015).

[96] S. Gupta, M. R. Chatni, A. L. N. Rao, V. I. Vullev, L. V. Wang, B. Anvari. ***Nanoscale*****5**, 1772 (2013).

[97] B. Bahmani, Y. Guerrero, D. Bacon, V. Kundra, V. I. Vullev, B. Anvari. ***Lasers Surg Med*****46**, 582 (2014).

[98] J. Wan, M. S. Thomas, S. Guthrie, V. I. Vullev. ***Ann. Biomed. Eng.*****37**, 1190 (2009).

[99] G. M. Whitesides. ***Nature*****442**, 368 (2006).

[100] M. S. Thomas, B. Millare, J. M. Clift, D. Bao, C. Hong, V. I. Vullev. ***Ann Biomed Eng*****38**, 21 (2010).

[101] K. Chau, B. Millare, A. Lin, S. Upadhyayula, V. Nuñez, H. Xu, V. I. Vullev. ***Microfluid. Nanofluid.*****10**, 907 (2011).

[102] J. H. Sung, Y. I. Wang, N. Narasimhan Sriram, M. Jackson, C. Long, J. J. Hickman, M. L. Shuler. ***Anal. Chem.*****91**, 330 (2019).

[103] E. Cinar, S. Zhou, J. DeCourcey, Y. Wang, R. E. Waugh, J. Wan. ***Proc. Natl. Acad. Sci. U.S.A.*****112**, 11783 (2015).

[104] A. M. Forsyth, J. Wan, P. D. Owrutsky, M. Abkarian, H. A. Stone. ***Proc. Natl. Acad. Sci. U.S.A.*****108**, 10986 (2011).

[105] S. K. Y. Tang, W. F. Marshall. ***Science*****356**, 1022 (2017).

[106] T. Yamashita, K. Abe. ***Curr. Pharm. Des.*****18**, 3649 (2012).

[107] S. Kuang, M. A. Rudnicki. ***Trends Mol. Med.*****14**, 82 (2008).

[108] S. Pekovic, S. Subasic, N. Nedeljkovic, I. Bjelobaba, R. Filipovic, I. Milenkovic. "Molecular basis of brain injury and repair", in ***Neurobiological Studies–From Genes to Behaviour***, S. Ruzdijic, L. Rakic (Eds.), pp. 143–165, Research Signpost, India (2006).

[109] P. A. Beachy, S. S. Karhadkar, D. M. Berman. ***Nature*****432**, 324 (2004).

[110] R. Yatsunami, S. Nakamura. ***Kagaku to Kyoiku*****49**, 122 (2001).

[111] M. Krzeszewski, T. Kodama, E. M. Espinoza, V. I. Vullev, T. Kubo, D. T. Gryko. ***Chem. – Eur. J.*****22**, 16478 (2016).

[112] K. Skonieczny, J. Yoo, J. M. Larsen, E. M. Espinoza, M. Barbasiewicz, V. I. Vullev, C.-H. Lee, D. T. Gryko. ***Chem. – Eur. J.*****22**, 7485 (2016).

[113] A. J. Wierzba, A. Wincenciuk, M. Karczewski, V. I. Vullev, D. Gryko. ***Chem. – Eur. J.*****24**, 10344 (2018).

[114] J. A. Warren. ***MRS Bull.*****43**, 452 (2018).

[115] Z. Liu, Y. Li, D. Shi, Y. Guo, M. Li, X. Zhou, Q. Huang, S. Du. ***Scr. Mater.*****141**, 99 (2017).

[116] M. R. Norman. ***Rep. Prog. Phys.*****79**, 074502/1 (2016).

[117] A. W. Bosse, E. K. Lin. ***J. Polym. Sci., Part B Polym. Phys.*****53**, 89 (2015).

[118] L. Kaufman, J. Agren. ***Scr. Mater.*****70**, 3 (2014).

[119] W. R. Entley, G. S. Girolami. ***Science*****268**, 397 (1995).

[120] S. Bertaina, S. Gambarelli, T. Mitra, B. Tsukerblat, A. Mueller, B. Barbara. ***Nature*****453**, 203 (2008).

[121] L. Bogani, W. Wernsdorfer. ***Nat. Mater.*****7**, 179 (2008).

[122] S. Upadhyayula, D. Bao, B. Millare, S. S. Sylvia, K. M. M. Habib, K. Ashraf, A. Ferreira, S. Bishop, R. Bonderer, S. Baqai, X. Jing, M. Penchev, M. Ozkan, C. S. Ozkan, R. K. Lake, V. I. Vullev. ***J. Phys. Chem. B*****115**, 9473 (2011).

[123] J. Li, Y. Wang, J. Chen, Z. Liu, A. Bax, L. Yao. ***J. Am. Chem. Soc.*****138**, 1824 (2016).

[124] E. M. Espinoza, J. A. Clark, J. B. Derr, D. Bao, B. Georgieva, F. H. Quina, V. I. Vullev. ***ACS Omega*****3**, 12857 (2018).

[125] H.-M. Huang, H. Kries. ***Biochemistry*****58**, 73 (2019).

[126] H. Lundberg, F. Tinnis, N. Selander, H. Adolfsson. ***Chem. Soc. Rev.*****43**, 2714 (2014).

[127] I. Coin, M. Beyermann, M. Bienert. ***Nat. Protoc.*****2**, 3247 (2007).

[128] W. Klee, M. Breener. ***Helv. Chim. Acta*****44**, 2151 (1950).

[129] G. W. Anderson, R. Paul. ***J. Am. Chem. Soc.*****80**, 4423 (1958).

[130] F. Albericio. ***Biopolymers*****55**, 123 (2000).

[131] C. A. G. N. Montalbetti, V. Falque. ***Tetrahedron*****61**, 10827 (2005).

[132] E. Valeur, M. Bradley. ***Chem. Soc. Rev.*****38**, 606 (2009).

[133] R. B. Merrifield. ***Chem. Polypeptides***, 335 (1973).

[134] E. Robinson Noah, B. Robinson Arthur. ***Biopolymers*****90**, 297 (2008).

[135] R. Behrendt, P. White, J. Offer. ***J. Pept. Sci.*****22**, 4 (2016).

[136] V. Made, S. Els-Heindl, G. Beck-Sickinger Annette. ***Beilstein. J. Org. Chem.*****10**, 1197 (2014).

[137] H.-A. Klok. ***Highlights Bioorg. Chem.*** 554 (2004).

[138] C. Fromont, V. Pomel, M. Bradley. ***Integr. Drug Discovery Technol.*** 463 (2002).

[139] S. Okamoto, T. Morita, S. Kimura. ***Langmuir*****25**, 3297 (2009).

[140] K. Kitagawa, T. Morita, S. Kimura. ***Langmuir*****21**, 10624 (2005).

[141] V. I. Vullev, G. Jones. ***Tetrahedron Lett.*****43**, 8611 (2002).

[142] G. Jones II, V. I. Vullev. ***Org. Lett.*****4**, 4001 (2002).

[143] G. Jones II, V. Vullev, E. H. Braswell, D. Zhu. ***J. Am. Chem. Soc.*****122**, 388 (2000).

[144] M. A. Fox, E. Galoppini. ***J. Am. Chem. Soc.*****119**, 5277 (1997).

[145] G. Jones II, L. N. Lu, V. Vullev, D. Gosztola, S. Greenfield, M. Wasielewski. ***Bioorg. Med. Chem. Lett.*****5**, 2385 (1995).

[146] S. E. Allen, S.-Y. Hsieh, O. Gutierrez, J. W. Bode, M. C. Kozlowski. ***J. Am. Chem. Soc.*****136**, 11783 (2014).

[147] S. L. Pedersen, A. P. Tofteng, L. Malik, K. J. Jensen. ***Chem. Soc. Rev.*****41**, 1826 (2012).

[148] G. Sabatino, A. M. Papini. ***Curr. Opin. Drug Discovery Dev.*****11**, 762 (2008).

[149] M. Bodanszky, J. Martinez. ***Synthesis*** 333 (1981). DOI: 10.1055/s-1981-29442.

[150] B. F. Gisin, R. B. Merrifield. ***J. Am. Chem. Soc.*****94**, 3102 (1972).

[151] P. B. Harbury, T. Zhang, P. S. Kim, T. Alber. ***Science*****262**, 1401 (1993).

[152] K. J. Lumb, P. S. Kim. ***Science*****268**, 436 (1995).

[153] G. Jones II, V. I. Vullev. ***Org. Lett.*****3**, 2457 (2001).

[154] G. Jones II, V. I. Vullev. ***J. Phys. Chem. A*****105**, 6402 (2001).

[155] P. Verdie, G. Subra, M.-C. Averland-Petit, M. Amblard, J. Martinez. ***J. Comb. Chem.*****10**, 869 (2008).

[156] M.-K. Jeon, H. J. La, D.-C. Ha, Y.-D. Gong. ***Synlett***, 1431 (2007). DOI: 10.1055/s-2007-980368.

[157] M.-K. Jeon, M.-S. Kim, J.-J. Kwon, Y.-D. Gong, D.-H. Lee. ***Tetrahedron*****64**, 9060 (2008).

[158] H.-Y. Lee, M. An. ***Bull. Korean Chem. Soc.*****25**, 1717 (2004).

[159] M. Orlandi, F. Tosi, M. Bonsignore, M. Benaglia. ***Org. Lett.*****17**, 3941 (2015).

[160] M. Orlandi, M. Benaglia, F. Tosi, R. Annunziata, F. Cozzi. ***J. Org. Chem.*****81**, 3037 (2016).

[161] N. J. Blackburn, R. W. Strange, R. T. Carr, S. J. Benkovic. ***Biochemistry*****31**, 5298 (1992).

[162] D. R. Davydov, H. Fernando, B. J. Baas, S. G. Sligar, J. R. Halpert. ***Biochemistry*44**, 13902 (2005).

[163] B. Bahmani, S. Gupta, S. Upadhyayula, V. I. Vullev, B. Anvari. ***J. Biomed. Opt.*16**, 051303/1 (2011).

[164] A. Decken, S. Greer, F. Grein, A. Mailman, B. Mueller, T. A. P. Paulose, J. Passmore, J. M. Rautiainen, S. A. Richardson, M. J. Schriver, T. K. Whidden. ***Inorg. Chem.*55**, 5999 (2016).

[165] S. M. Lough, J. W. McDonald. ***Inorg. Chem.*26**, 2024 (1987).

[166] W. C. Hodgeman, J. B. Weinrach, D. W. Bennett. ***Inorg. Chem.*30**, 1611 (1991).

[167] E. Boll, H. Drobecq, N. Ollivier, L. Raibaut, R. Desmet, J. Vicogne, O. Melnyk. ***Chem. Sci.*5**, 2017 (2014).

[168] R. Kaplanek, V. Krchnak. ***Tetrahedron Lett.*54**, 2600 (2013).

[169] E. Schütznerová, V. Krchňák. ***ACS Comb. Sci.*17**, 137 (2015).

[170] I. Messina, I. Popa, V. Maier, M. Soural. ***ACS Comb. Sci.*16**, 33 (2014).

[171] C. McMaster, V. Fulopova, I. Popa, M. Grepl, M. Soural. ***ACS Comb. Sci.*16**, 221 (2014).

[172] R. A. Scheuerman, D. Tumelty. ***Tetrahedron Lett.*41**, 6531 (2000).

[173] A. Hari, B. L. Miller. ***Tetrahedron Lett.*40**, 245 (1999).

[174] A. Hari, B. L. Miller. ***Angew. Chem., Int. Ed.*38**, 2777 (1999).

[175] A. Hari, B. L. Miller. ***Org. Lett.*2**, 691 (2000).

[176] E. M. Espinoza, J. A. Clark, J. Soliman, J. B. Derr, M. Morales, V. I. Vullev. ***J. Electrochem. Soc.*166**, H3175 (2019).

[177] D. Bao, B. Millare, W. Xia, B. G. Steyer, A. A. Gerasimenko, A. Ferreira, A. Contreras, V. I. Vullev. ***J. Phys. Chem. A*113**, 1259 (2009).

[178] D. Bao, S. Ramu, A. Contreras, S. Upadhyayula, J. M. Vasquez, G. Beran, V. I. Vullev. ***J. Phys. Chem. B*114**, 14467 (2010).

[179] S. Upadhyayula, V. Nunez, E. M. Espinoza, J. M. Larsen, D. Bao, D. Shi, J. T. Mac, B. Anvari, V. I. Vullev. ***Chem. Sci.*****6**, 2237 (2015).

[180] E. M. Espinoza, B. Xia, N. Darabedian, J. M. Larsen, V. Nunez, D. Bao, J. T. Mac, F. Botero, M. Wurch, F. Zhou, V. I. Vullev. ***Eur. J. Org. Chem.*****2016**, 343 (2016).

Supplemental Figures

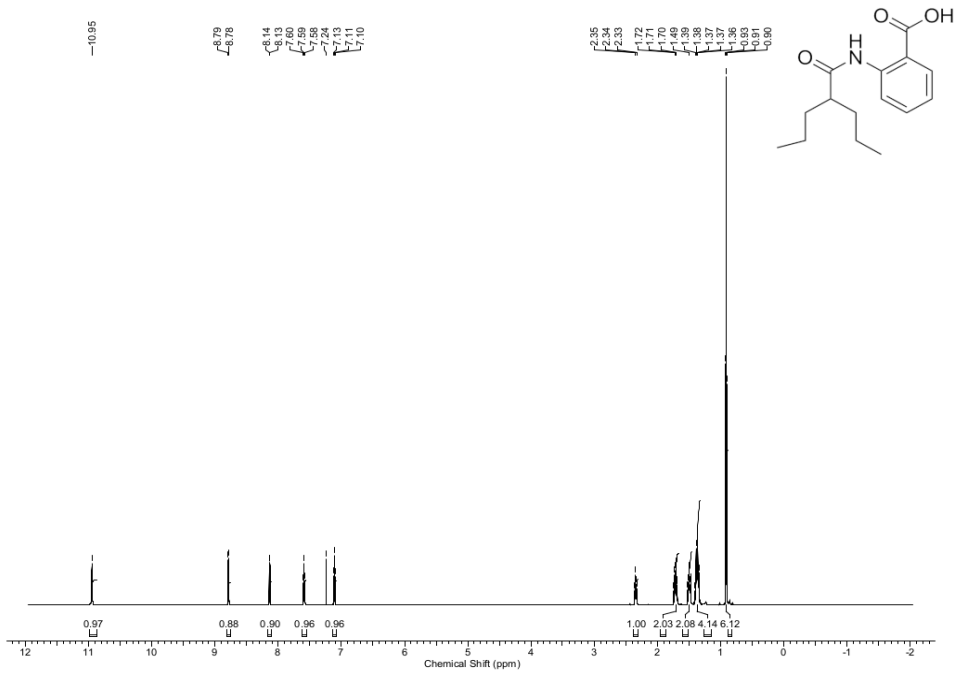

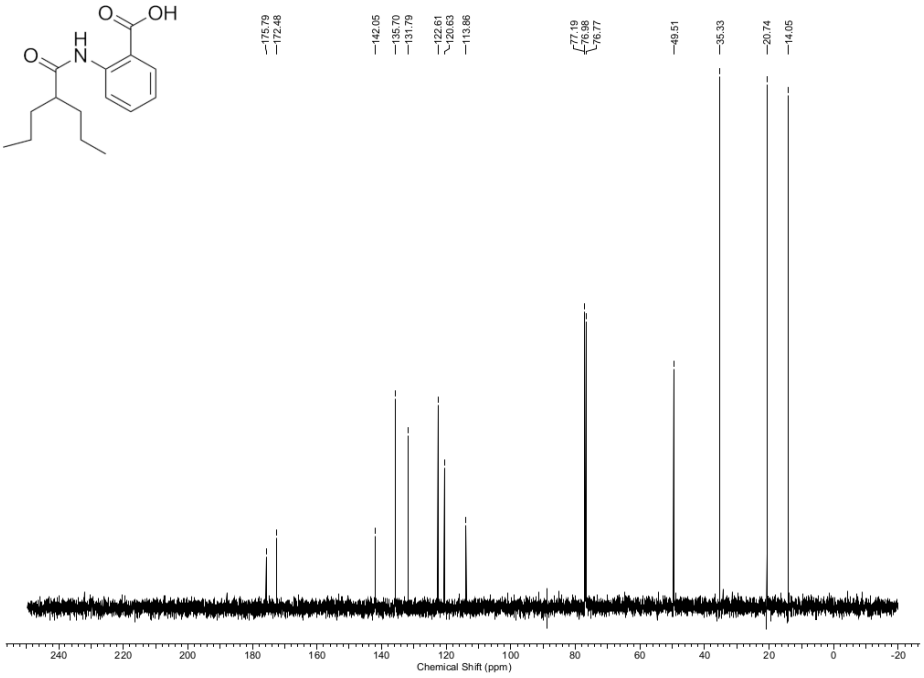

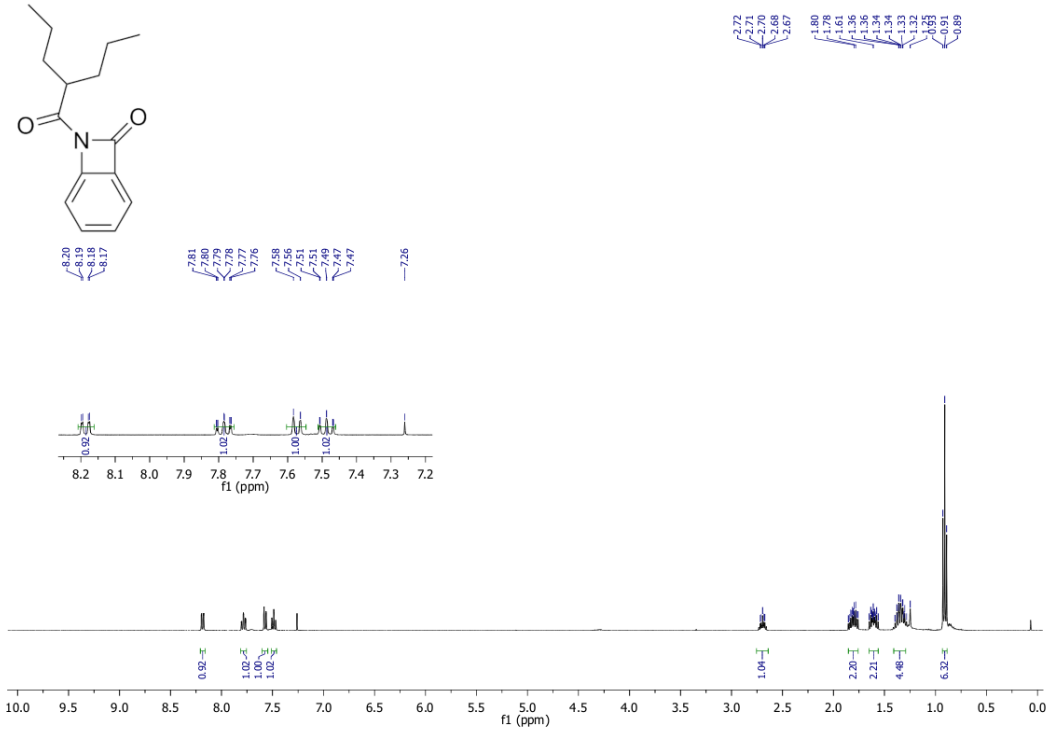
2.72
2.71
2.70
2.68
2.67
1.80
1.78
1.61
1.36
1.36
1.34
1.34
1.33
1.32
0.93
0.91
0.89
8.20
8.19
8.18
8.17
7.81
7.80
7.79
7.78
7.77
7.76
7.58
7.56
7.51
7.51
7.49
7.47
7.47
7.26
0.92
1.02
1.00
1.02
f1 (ppm)
0.92
1.02
1.00
1.02
1.04
2.20
2.21
4.48
6.32
f1 (ppm)

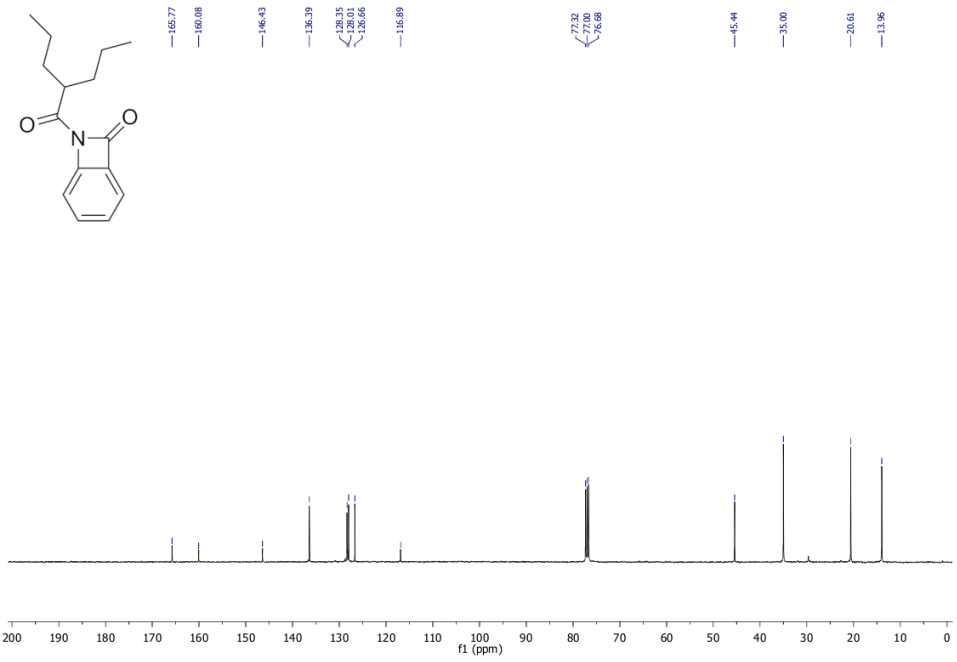
165.77
160.08
146.43
136.39
128.35
128.01
126.66
116.89
77.32
77.00
76.68
45.44
35.00
20.61
13.96
f1 (ppm)

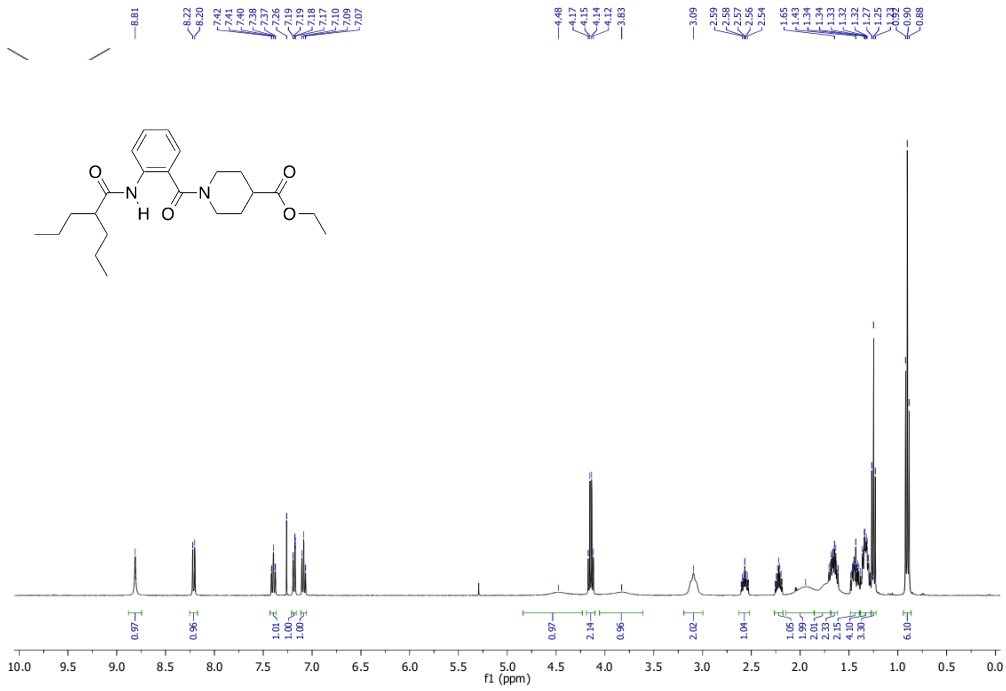
8.81
8.22
8.20
7.42
7.41
7.40
7.38
7.37
7.26
7.19
7.19
7.18
7.17
7.10
7.09
7.07
4.48
4.17
4.15
4.14
4.13
3.83
3.09
2.59
2.58
2.57
2.56
2.54
1.65
1.43
1.34
1.34
1.33
1.32
1.32
1.27
1.25
0.92
0.90
0.88
0.97
0.96
1.01
1.00
1.00
0.97
2.14
0.96
2.02
1.04
1.05
1.99
2.01
2.33
2.15
4.10
3.39
6.10
f1 (ppm)

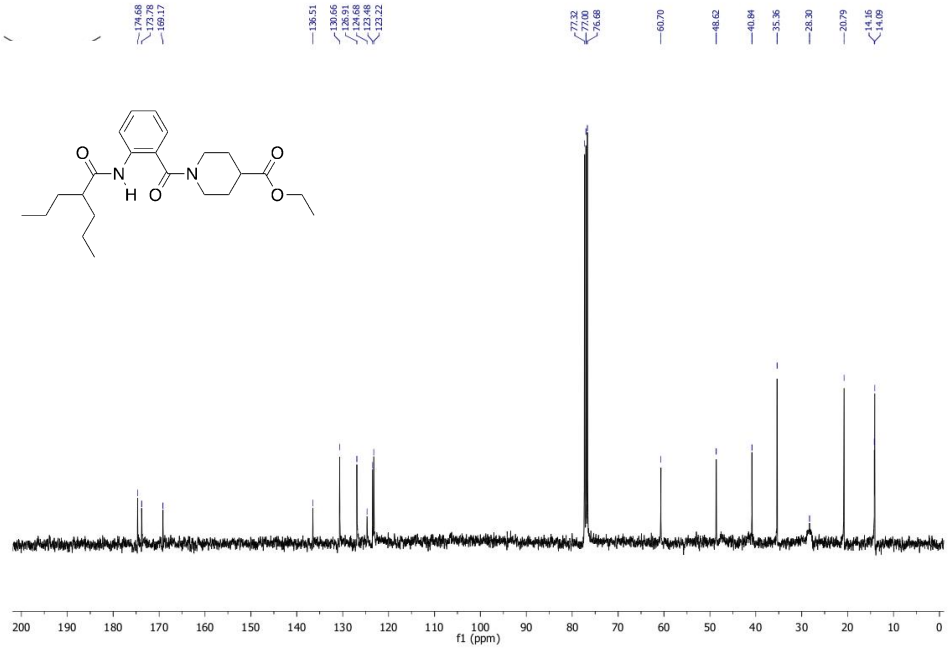
174.68
173.78
169.17
136.51
130.66
126.91
124.68
123.48
123.22
77.32
77.00
76.68
60.70
48.62
40.84
35.36
28.30
20.79
14.16
14.09
f1 (ppm)

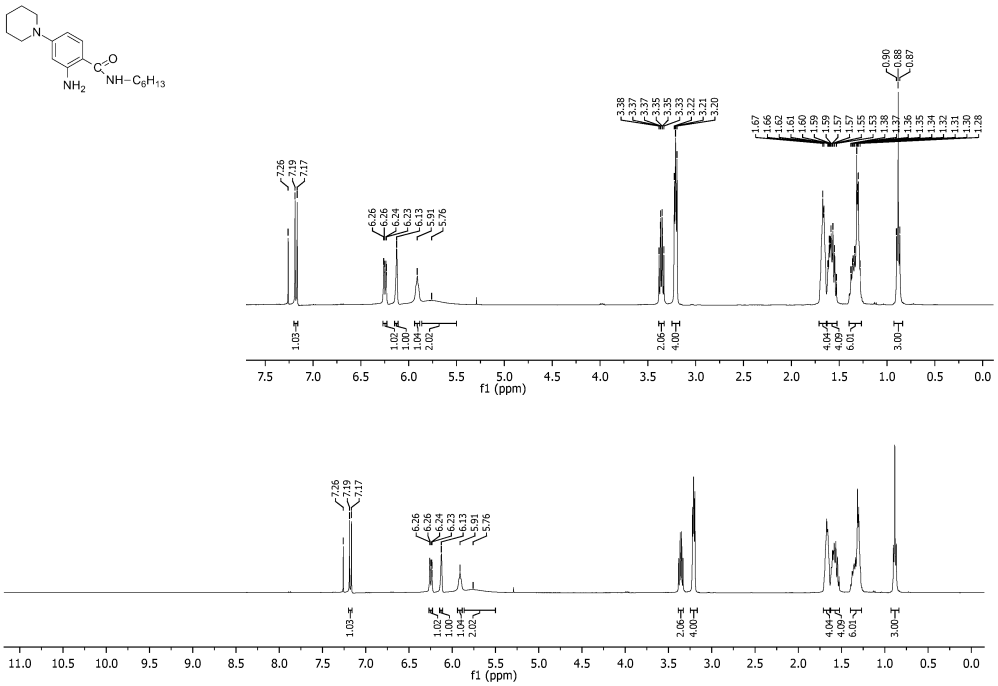
NH2
NH–C6H13
7.26
7.19
7.17
6.26
6.26
6.24
6.23
6.13
5.91
5.76
3.38
3.37
3.37
3.35
3.35
3.33
3.22
3.21
3.20
1.67
1.66
1.62
1.61
1.60
1.59
1.59
1.57
1.57
1.55
1.53
1.38
1.37
1.36
1.35
1.34
1.32
1.31
1.30
1.28
0.90
0.88
0.87
1.03
1.02
1.00
1.04
2.02
2.06
4.00
4.04
4.09
6.01
3.00
f1 (ppm)

7.26
7.19
7.17
6.26
6.26
6.24
6.23
6.13
5.91
5.76
1.03
1.02
1.00
1.04
2.02
2.06
4.00
4.04
4.09
6.01
3.00
f1 (ppm)

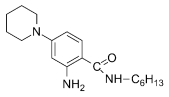
NH2
NH–C6H13

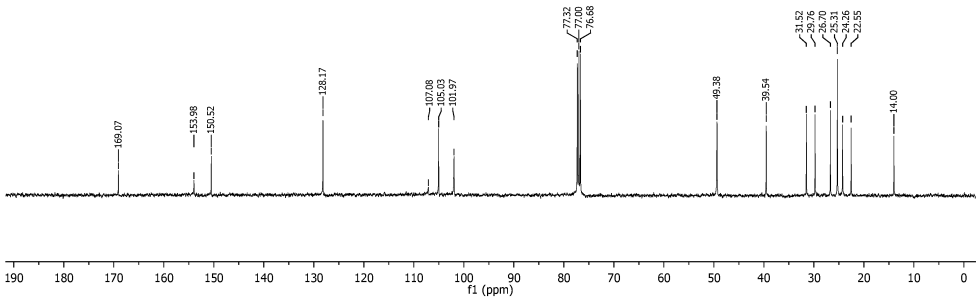
169.07
153.98
150.52
128.17
107.08
105.03
101.97
77.32
77.00
76.68
49.38
39.54
31.52
29.26
26.70
25.31
24.26
22.55
14.00
f1 (ppm)

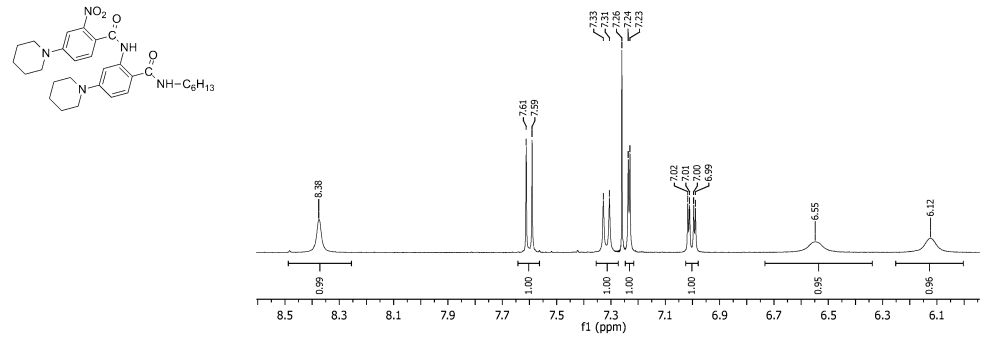
NO2
O
NH
O
NH–C6H13
N
N
8.38
7.61
7.59
7.33
7.31
7.26
7.24
7.23
7.02
7.01
7.00
6.99
6.55
6.12
0.99
1.00
1.00
1.00
1.00
0.95
0.96
f1 (ppm)

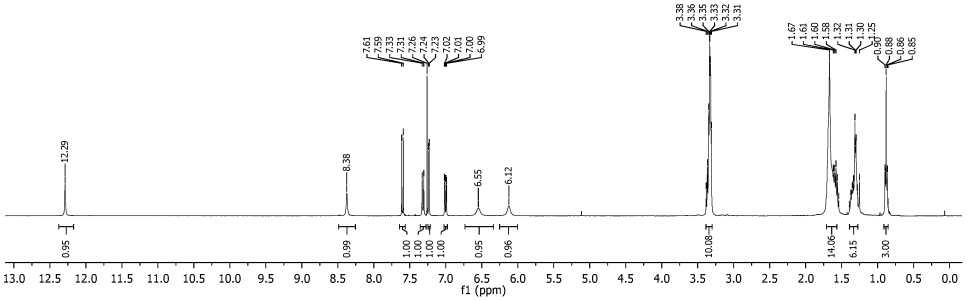
12.29
8.38
7.61
7.59
7.33
7.31
7.26
7.24
7.23
7.02
7.01
7.00
6.99
6.55
6.12
3.38
3.36
3.35
3.33
3.32
3.31
1.67
1.61
1.60
1.58
1.32
1.31
1.30
1.25
0.88
0.86
0.85
0.95
0.99
1.00
1.00
1.00
1.00
0.95
0.96
10.08
14.06
6.15
3.00
f1 (ppm)

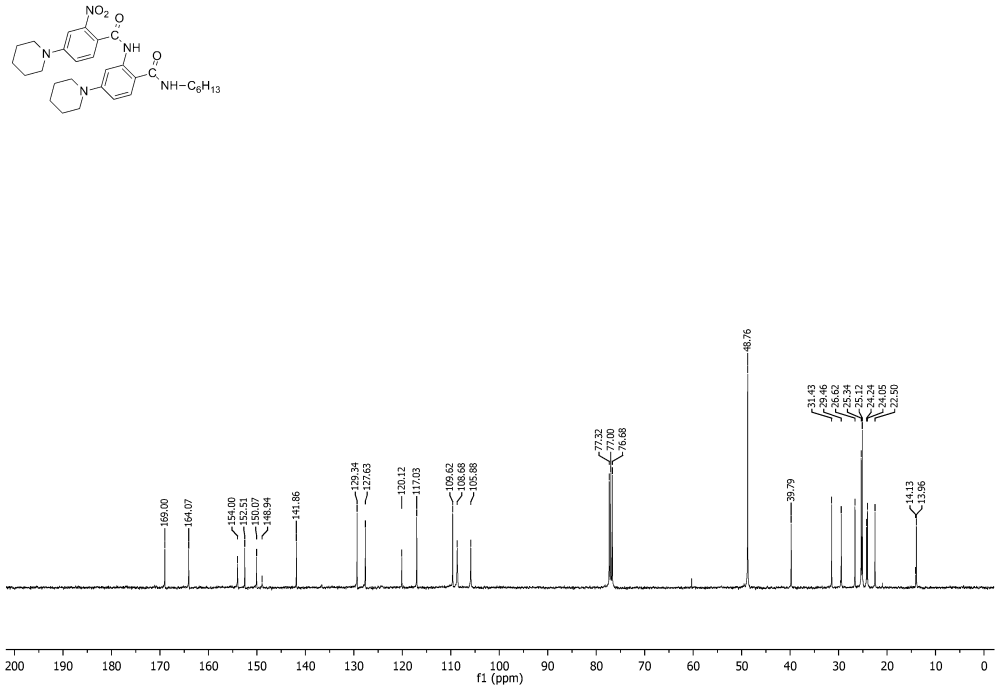
NO2
O
NH
O
NH–C6H13
N
N
169.00
164.07
154.00
152.51
150.07
148.94
141.86
129.34
127.63
120.12
117.03
109.62
108.68
105.88
77.32
77.00
76.68
48.76
39.79
31.43
29.46
26.62
25.34
25.12
24.24
24.05
21.90
14.13
13.96
f1 (ppm)

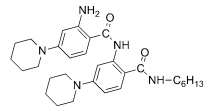
NH2
O
NH
O
NH–C6H13
N
N

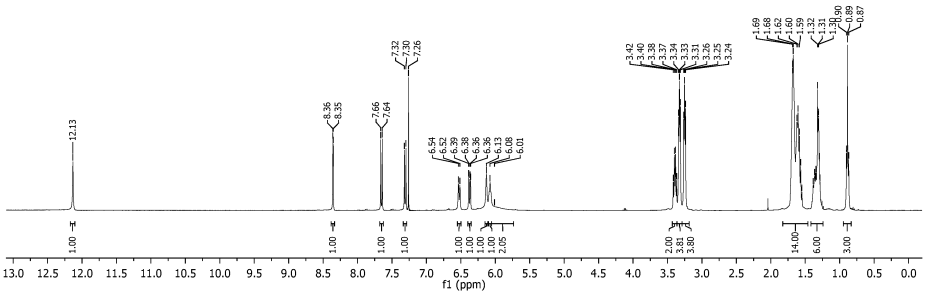
12.13
8.36
8.35
7.66
7.64
7.32
7.30
7.26
6.54
6.52
6.39
6.38
6.36
6.36
6.13
6.08
6.01
3.42
3.40
3.38
3.37
3.34
3.33
3.31
3.26
3.25
3.24
1.69
1.68
1.62
1.60
1.59
1.32
1.31
0.90
0.89
0.87
1.00
1.00
1.00
1.00
1.00
1.00
1.05
2.05
2.00
3.81
3.80
14.00
6.00
3.00
f1 (ppm)

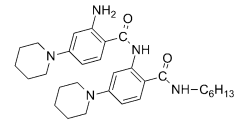
NH2
O
NH
O
NH–C6H13
N
N

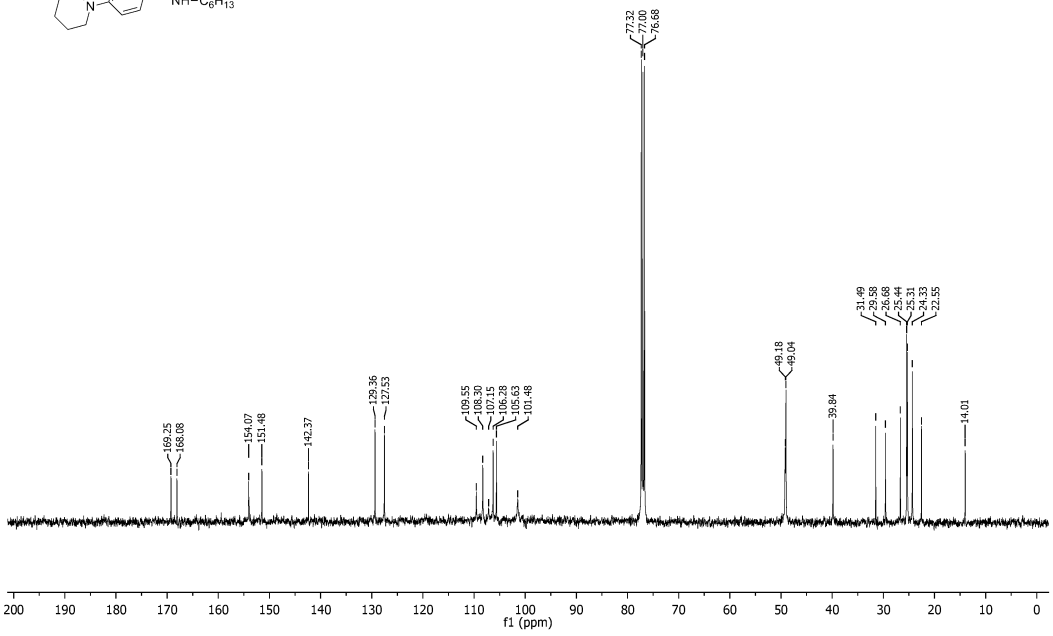
77.32
77.00
76.68
169.25
168.08
154.07
151.48
142.37
129.36
127.53
109.55
108.30
107.15
106.28
105.63
101.48
49.18
49.04
39.84
31.49
29.58
26.68
25.44
25.31
24.33
22.55
14.01
f1 (ppm)

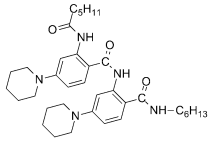

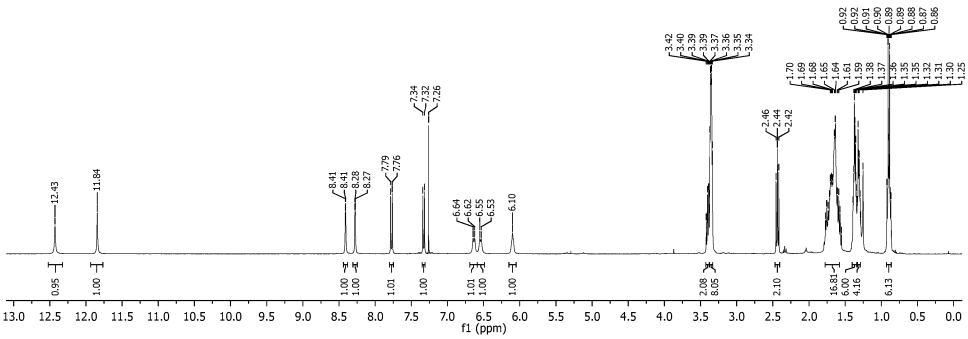

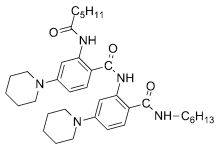

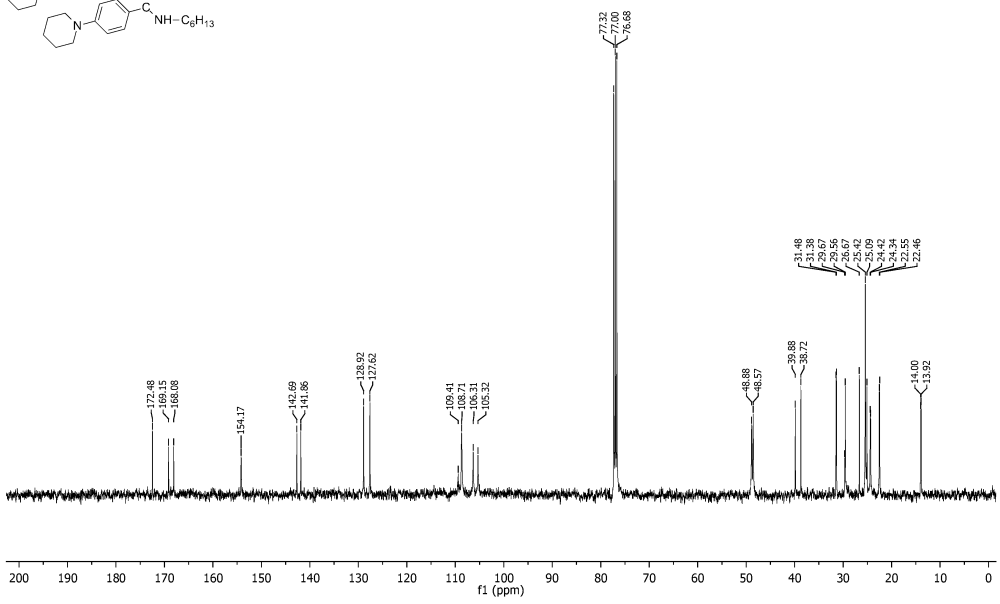

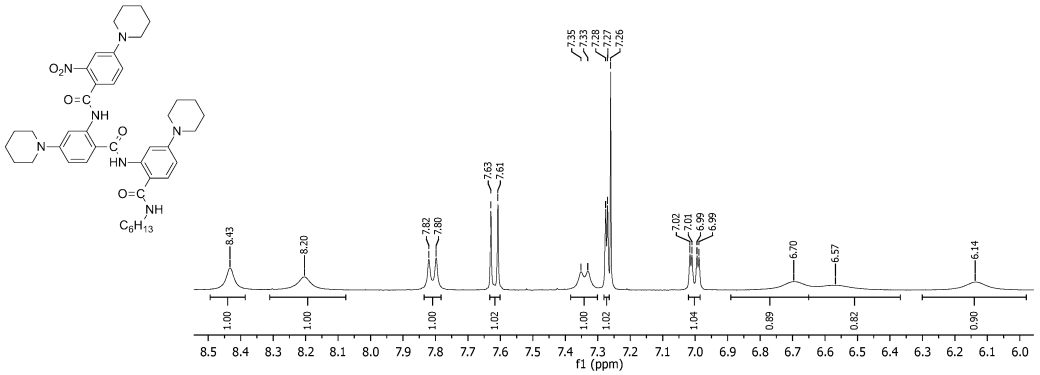
8.43
8.20
7.82
7.80
7.63
7.61
7.35
7.33
7.28
7.27
7.26
7.02
7.01
6.99
6.99
6.70
6.57
6.14
f1 (ppm)

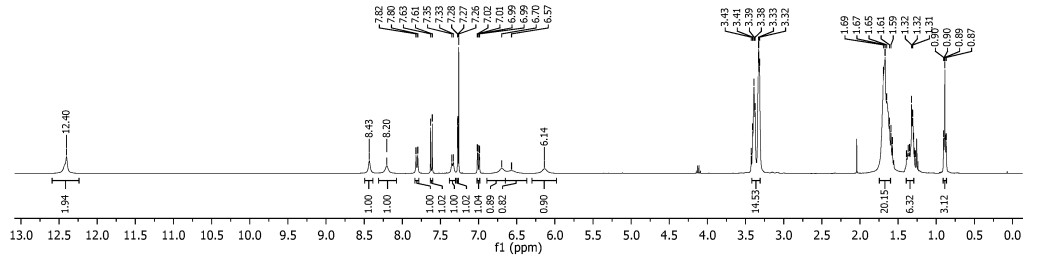
12.40
8.43
8.20
6.14
3.43
3.41
3.39
3.38
3.33
3.32
1.69
1.67
1.65
1.61
1.59
1.32
1.32
1.31
0.90
0.89
0.87
f1 (ppm)

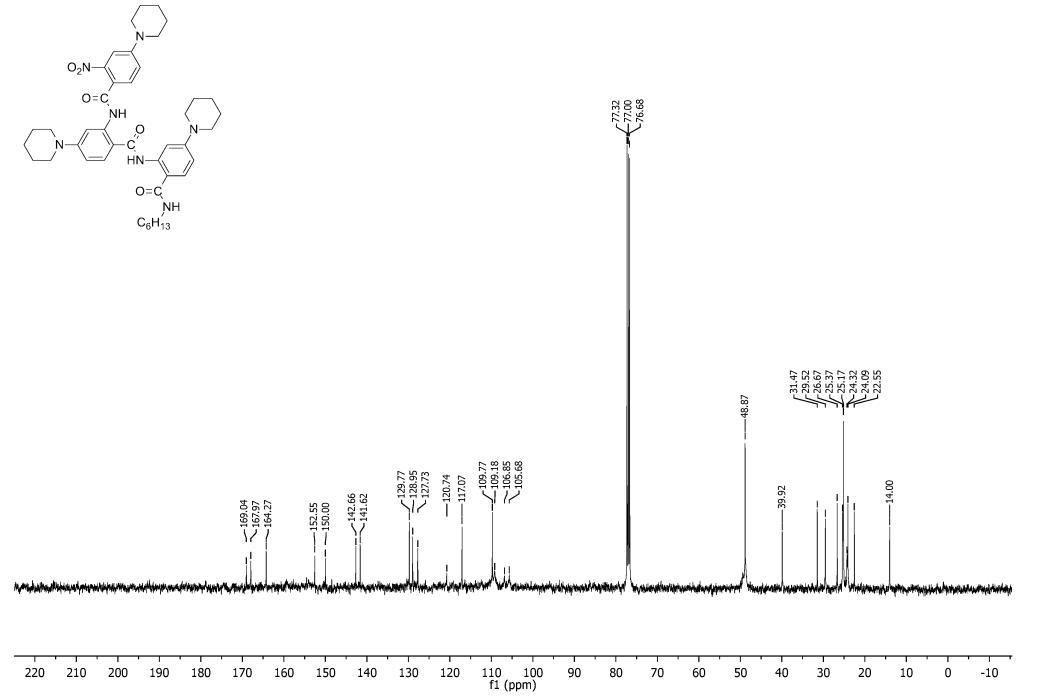
77.32
77.00
76.68
48.87
39.92
31.47
29.52
26.67
25.37
25.17
24.32
24.09
22.55
14.00
169.04
167.97
164.27
152.55
150.00
142.66
141.62
129.77
128.95
127.73
120.74
117.07
109.77
109.18
106.85
105.68
f1 (ppm)

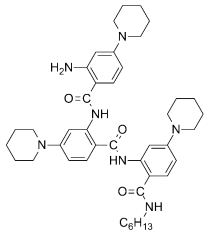

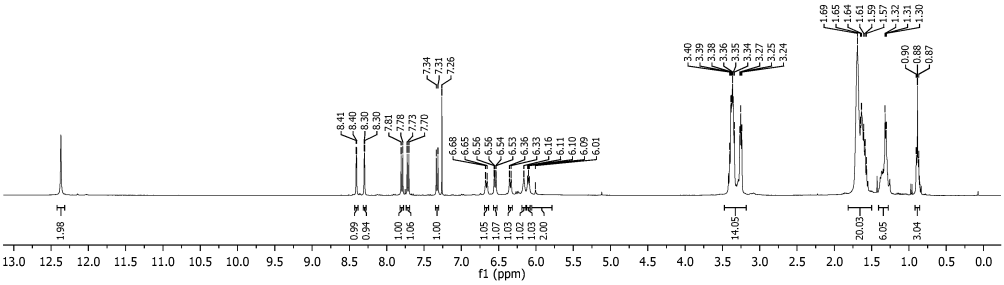
8.41
8.40
8.30
8.29
7.81
7.78
7.73
7.70
7.34
7.31
7.26
6.68
6.65
6.56
6.55
6.54
6.53
6.36
6.33
6.16
6.11
6.10
6.09
6.01
3.40
3.39
3.38
3.36
3.35
3.34
3.27
3.25
3.24
1.69
1.65
1.64
1.61
1.59
1.57
1.32
1.31
1.30
0.90
0.88
0.87
1.98
0.99
0.94
1.00
1.06
1.00
1.05
1.07
1.03
1.02
1.03
2.00
14.05
20.03
6.05
3.04
f1 (ppm)

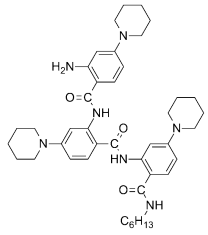

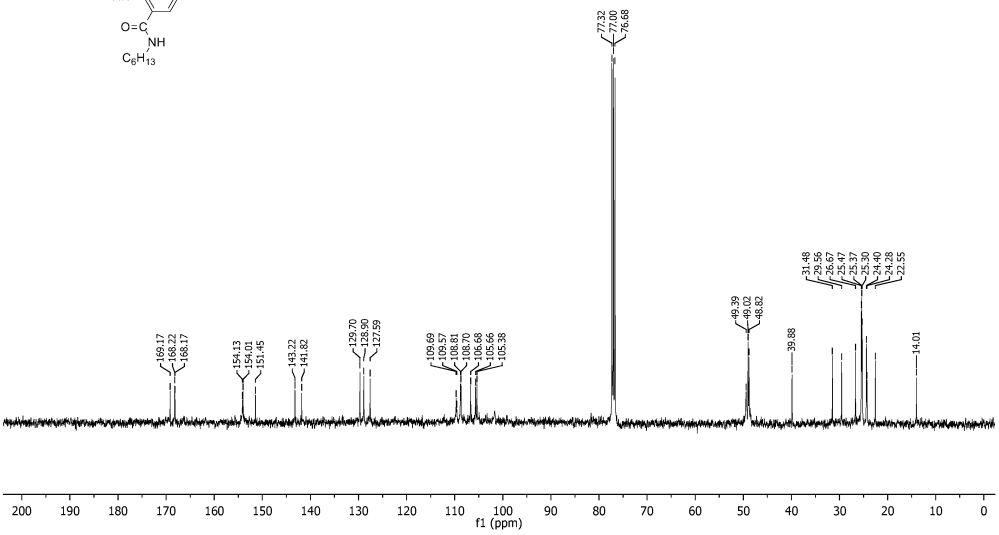
77.32
77.00
76.68
169.17
168.22
168.17
154.13
147.01
151.45
143.22
141.82
129.70
128.90
127.59
109.69
109.57
108.81
108.70
106.68
105.66
105.38
49.39
49.02
48.82
39.88
31.48
29.56
26.67
25.47
25.37
25.30
24.40
24.28
22.55
14.01
f1 (ppm)

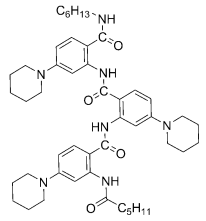

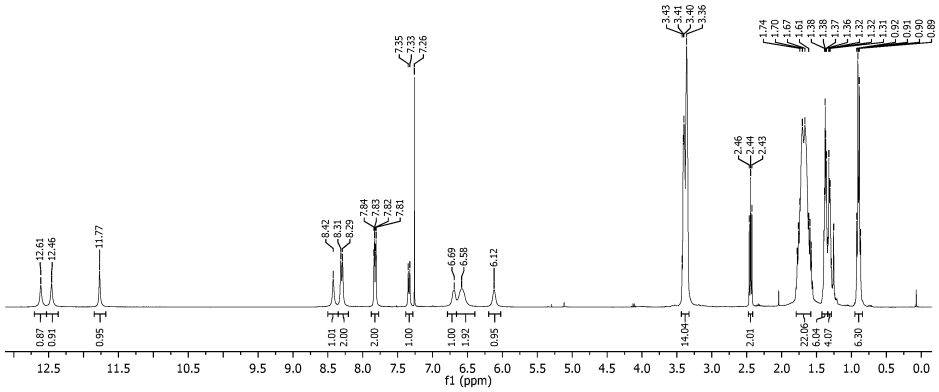
12.61
12.46
11.77
8.42
8.31
8.29
7.84
7.83
7.82
7.81
7.35
7.33
7.26
6.69
6.58
6.12
3.43
3.41
3.40
3.36
2.46
2.44
2.43
1.74
1.70
1.67
1.61
1.38
1.37
1.36
1.32
1.31
0.92
0.91
0.90
0.89
0.87
0.91
0.95
1.01
2.00
2.00
1.00
1.00
1.92
0.95
14.04
2.01
22.06
6.04
4.07
6.30
f1 (ppm)

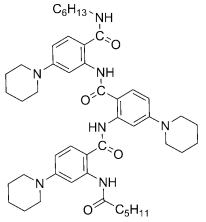

172.53
169.13
168.12
154.19
142.59
141.72
129.25
129.03
127.63
109.59
109.28
108.85
108.55
106.61
105.77
105.56
77.32
77.00
76.68
48.71
39.89
38.70
31.48
31.37
29.55
26.67
26.43
25.34
25.08
24.39
22.55
22.46
14.00
13.92
f1 (ppm)

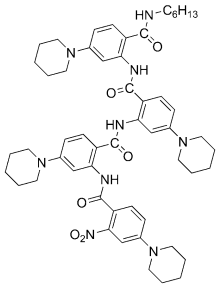

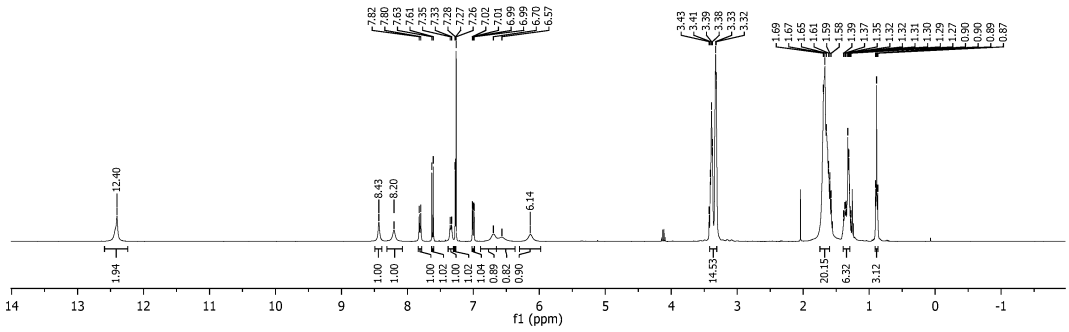
12.40
8.43
8.20
6.14
7.82
7.80
7.63
7.61
7.35
7.33
7.28
7.27
7.26
7.02
7.01
6.99
6.99
6.70
6.57
3.43
3.41
3.39
3.38
3.33
3.32
1.69
1.67
1.65
1.61
1.59
1.58
1.39
1.37
1.35
1.32
1.32
1.31
1.30
1.29
1.27
0.90
0.90
0.90
0.89
0.87
1.94
1.00
1.00
1.00
1.02
1.00
1.02
1.04
0.89
0.83
0.90
14.53
20.15
6.32
3.12
f1 (ppm)

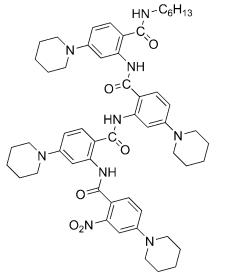

77.32
77.00
76.68
169.10
168.05
164.27
154.14
152.59
150.10
142.58
142.41
141.68
130.76
129.29
129.02
127.68
120.65
117.06
109.80
109.05
106.14
48.89
39.91
31.48
29.54
26.68
25.34
25.18
24.31
24.11
22.56
14.01
f1 (ppm)

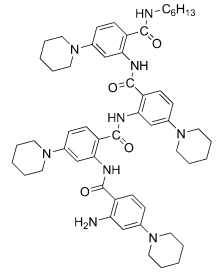

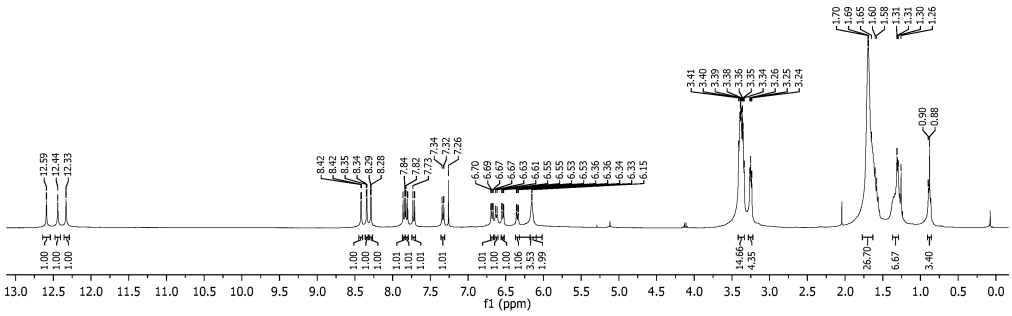
12.59
12.44
12.33
8.42
8.42
8.35
8.34
8.29
8.28
7.84
7.82
7.73
7.34
7.32
7.26
6.70
6.69
6.67
6.63
6.61
6.55
6.55
6.53
6.53
6.36
6.36
6.34
6.33
6.15
3.41
3.40
3.39
3.38
3.36
3.35
3.34
3.26
3.25
3.24
1.70
1.69
1.65
1.60
1.58
1.31
1.31
1.30
1.26
0.90
0.88
1.00
1.00
1.00
1.00
1.00
1.00
1.01
1.01
1.01
1.01
1.01
1.00
1.00
1.06
3.53
1.99
14.66
4.35
26.70
6.67
3.40
f1 (ppm)

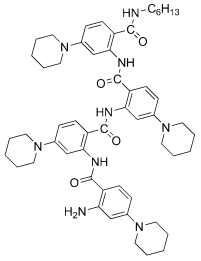

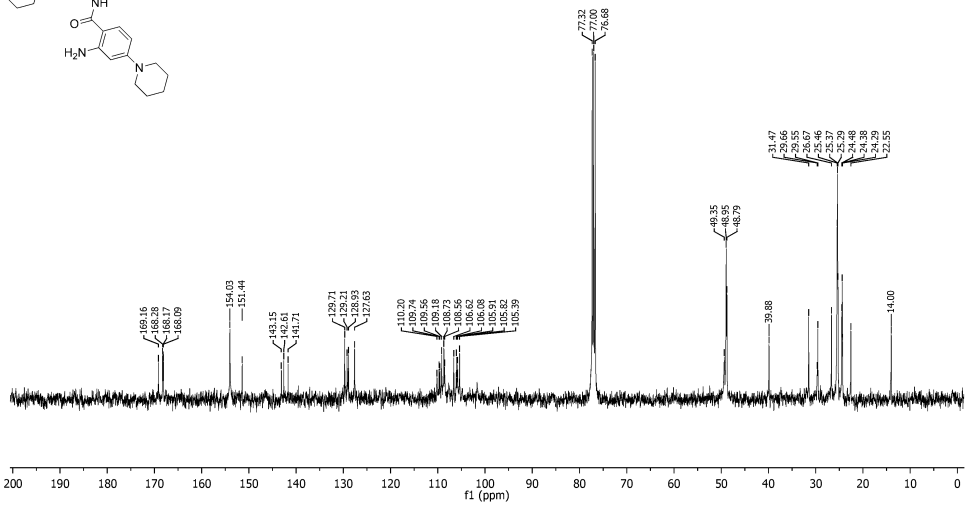
77.32
77.00
76.68
49.35
48.95
48.79
31.47
29.66
29.55
25.67
25.46
25.37
25.29
24.48
24.38
24.29
23.55
39.88
14.00
169.16
168.28
168.17
168.09
154.03
151.44
143.15
141.61
141.71
129.71
129.21
128.88
127.63
110.20
109.74
109.56
109.18
108.73
108.56
106.62
106.08
105.91
105.82
105.39
f1 (ppm)

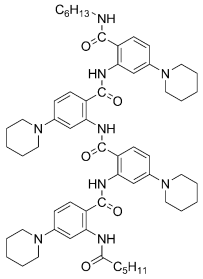
C6H13
NH
O
HN
N
C5H11

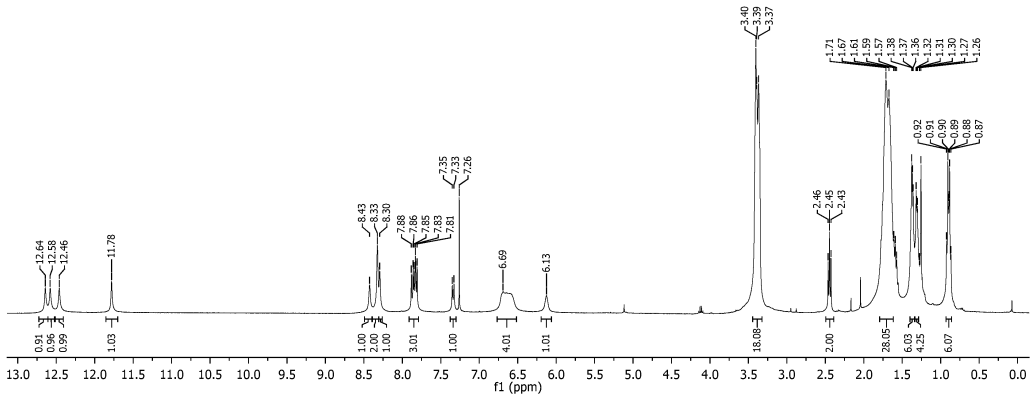
12.64
12.58
12.46
11.78
8.43
8.33
8.30
7.88
7.86
7.85
7.83
7.81
7.35
7.33
7.26
6.69
6.13
3.40
3.39
3.37
2.46
2.45
2.43
1.71
1.67
1.61
1.59
1.57
1.38
1.37
1.36
1.32
1.31
1.30
1.27
1.26
0.92
0.91
0.90
0.89
0.88
0.87
0.91
0.96
0.99
1.03
1.00
2.00
1.00
3.01
1.00
4.01
1.01
18.08
2.00
28.05
6.03
4.25
6.07
f1 (ppm)

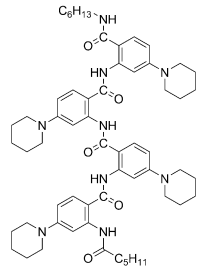
C6H13
NH
O
HN
N
C5H11

77.32
77.00
76.68
172.49
168.72
168.17
168.11
154.12
142.59
142.56
142.49
141.71
129.33
129.29
128.99
127.64
109.30
108.95
108.54
106.68
106.14
106.08
105.98
105.55
48.80
39.90
38.71
31.48
31.37
29.68
29.55
26.67
25.36
25.08
24.38
22.55
22.46
14.00
13.93
f1 (ppm)

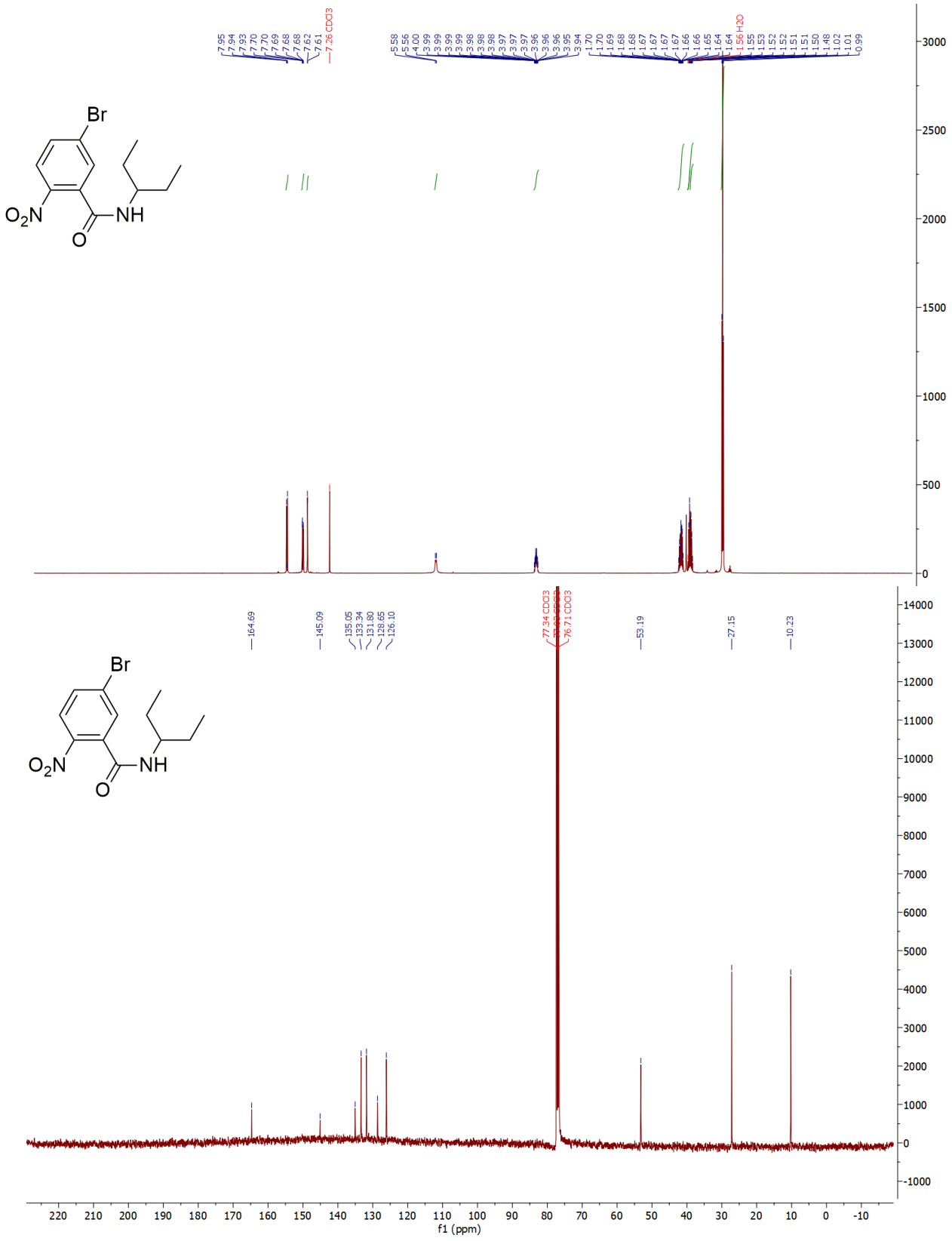
Br
O2N
NH
O
7.95
7.94
7.93
7.70
7.70
7.69
7.68
7.68
7.62
7.61
7.26 CDCl3
5.58
5.56
4.00
3.99
3.99
3.99
3.99
3.98
3.98
3.98
3.97
3.97
3.97
3.96
3.96
3.96
3.95
3.94
1.70
1.70
1.69
1.68
1.68
1.67
1.67
1.67
1.67
1.66
1.66
1.65
1.64
1.64
1.56 H2O
1.55
1.53
1.52
1.52
1.51
1.51
1.50
1.48
1.02
1.01
0.99
3000
2500
2000
1500
1000
500
0
164.69
145.09
135.05
133.34
131.80
128.65
126.10
77.34 CDCl3
76.71 CDCl3
53.19
27.15
10.23
14000
13000
12000
11000
10000
9000
8000
7000
6000
5000
4000
3000
2000
1000
0
-1000
220
210
200
190
180
170
160
150
140
130
120
110
100
90
80
70
60
50
40
30
20
10
0
-10
f1 (ppm)

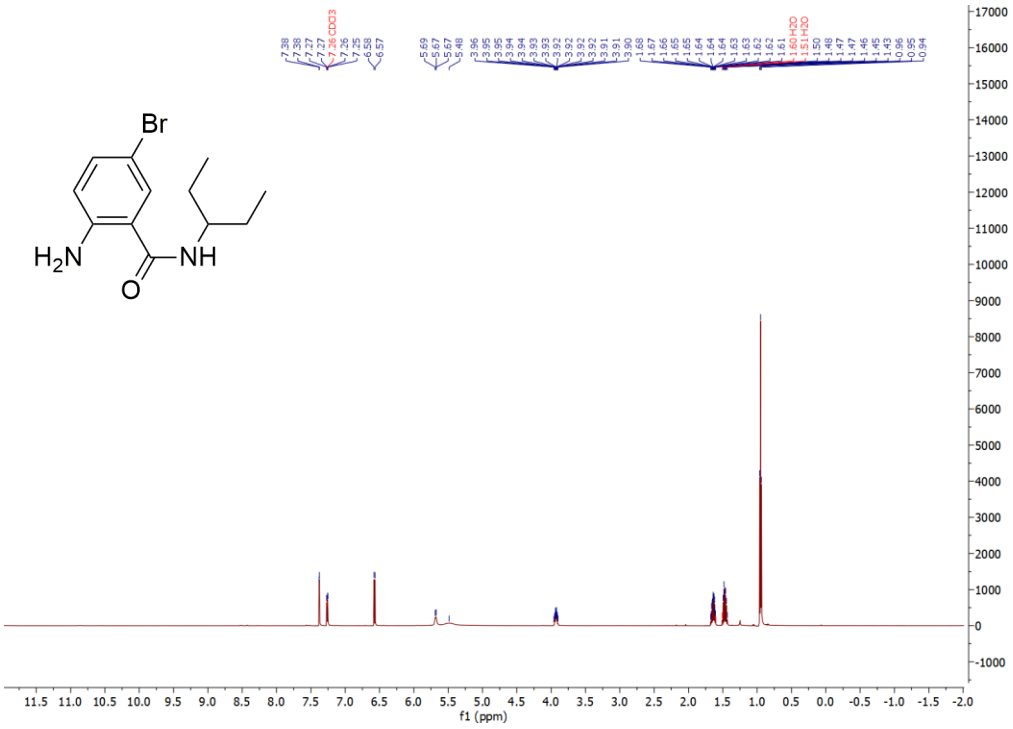

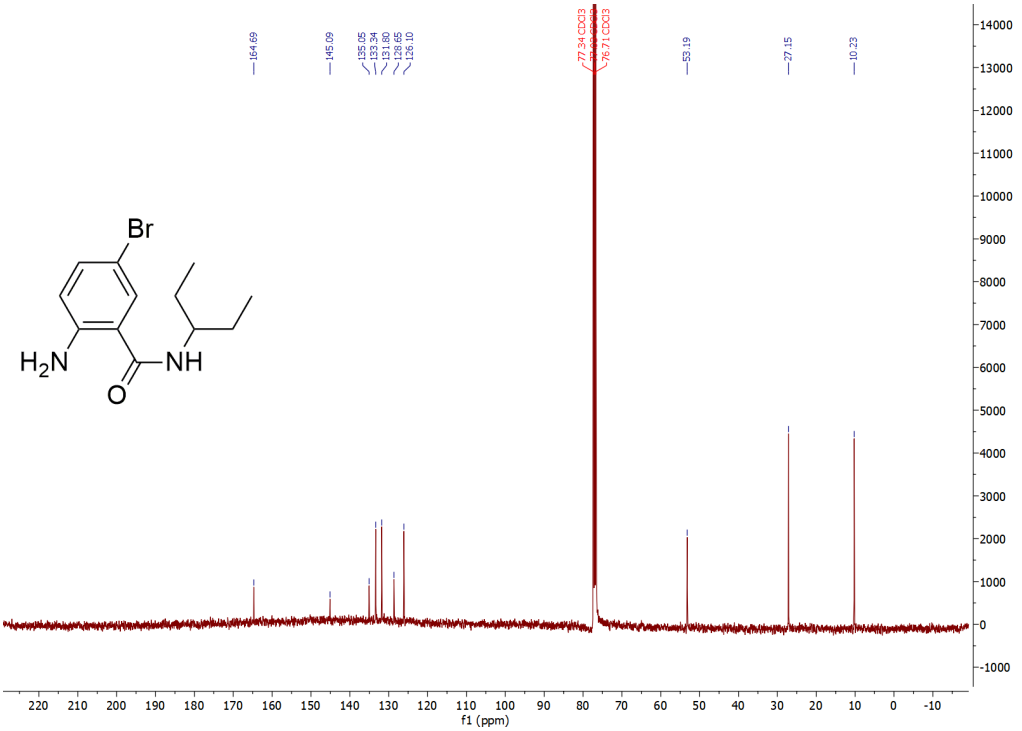

(a) ^{1}H

Chapter 3

Solvent-induced selectivity of Williamson etherification in the pursuit of amides resistant against oxidative degradation

ABSTRACT

This article reports two discoveries. (1) 2-Methoxyethanol induces unprecedented selectivity for etherification of 5-hydroxy-2-nitrobenzic acids without forming undesired esters. (2) Such compounds are precursors for amides showing unusual robustness against oxidative degradation, essential for molecular electrets that transfer strongly oxidizing holes at about −6.4 eV vs. vacuum.

Introduction

Williamson etherification (WE), involving alcohols and alkanes with good leaving groups as starting materials, remains the most broadly used method for the preparation of ethers.[1] WE offers an important means for adding electron-donating groups to aromatic conjugates, essential for preparing electron-rich *p*-conducting organic materials. Despite its immense importance, the lack of selectivity presents challenges for the utility of WE.[1c]

To harness dipole effects on charge transfer (CT),[2] we develop bioinspired molecular electrets that are based on polypeptide structures composed of anthranilamide (**Aa**) residues.[3] (Electrets are systems with ordered electric dipole moments.) The amide and hydrogen bonds of the electrets are a source for their intrinsic dipole moments.[4] The side chains of **Aa**, R_1 and R_2 (Chart 3-1a), on the other hand, provide a means for controlling their electronic properties.[4a,5] Indeed, electric dipoles present key paradigms for controlling CT, which is of tremendous importance for energy conversion and organic electronics, among many other fields.[2a] Molecular dipoles rectify CT,[2b,2c,3c,3d] affecting charge separation and charge recombination.[3c]

Chart 3-1: (a) Molecular anthranilamide (**Aa**) electret with its permanent electric dipole. (b–e) Electret **Aa** residues with either side chains that are highlighted.

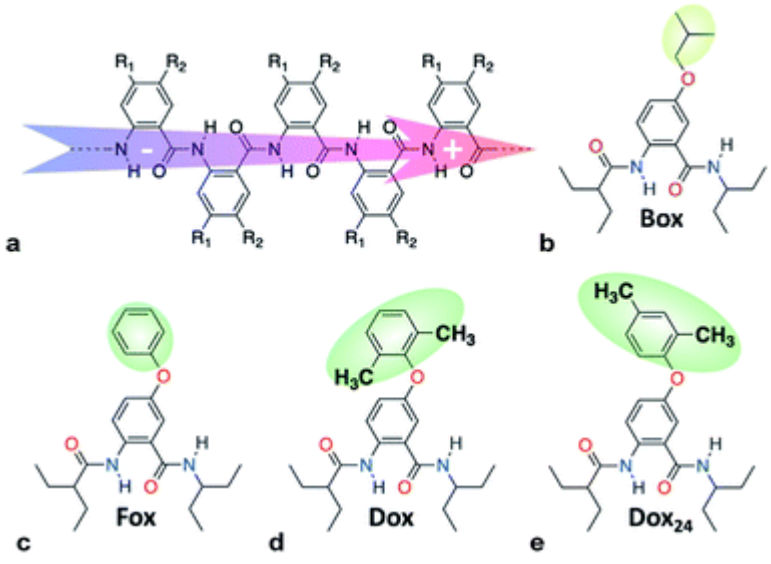

Electron-donating side chains afford hole-transfer electrets.[5d] For long-range CT in organic materials, it is important to attain a hopping (or incoherent) mechanism, for which the kinetics exhibits negligible distance dependence beyond about 1 nm.[6] In order to prevent oxidative degradation of electrets mediating such hole hopping, it is crucial for the comprising **Aa** residues to form stable radical cations, $\mathbf{Aa}^{\bullet+}$.[5a–c] For attaining such stability, we have determined that: (1) the spin density distribution (SDD) of $\mathbf{Aa}^{\bullet+}$ should not extend over its C-terminal amide;[5b] and (2) the reduction potentials for oxidizing **Aa**, should not be too large, *i.e.*, $E_{\mathrm{Aa}^{\bullet+}|\mathrm{Aa}} < 1.5$ V *vs.* SCE, to prevent the inherent oxidative degradation of the amides.[5b] The latter places a limit on how oxidizing the transferred holes can be. Hole hopping along moieties with as positive $E_{\mathrm{Aa}^{\bullet+}|\mathrm{Aa}}$ as possible ensures the potency of the holes for attaining large open-circuit voltages and for driving chemical transformations. Because placing alkoxy side chains on **Aa** residues brings the reduction potentials of their radical cations, $\mathbf{Aa}^{\bullet+}$, to the limit of 1.5 V *vs.* SCE,[5a–c] such ether conjugates present a key paradigm in the pursuit of organic derivatives that can transduce strongly oxidizing charge carriers.

Established peptide-synthesis procedures, used on aromatic β-amino acids with protected amines, lead to non-reactive cyclic intermediates, preventing the formation of **Aa** derivatives.[5f,7] Therefore, in the synthesis of **Aa** conjugates, we introduce each residue as its 2-nitrobenzoic acid (**NBA**) analogue.

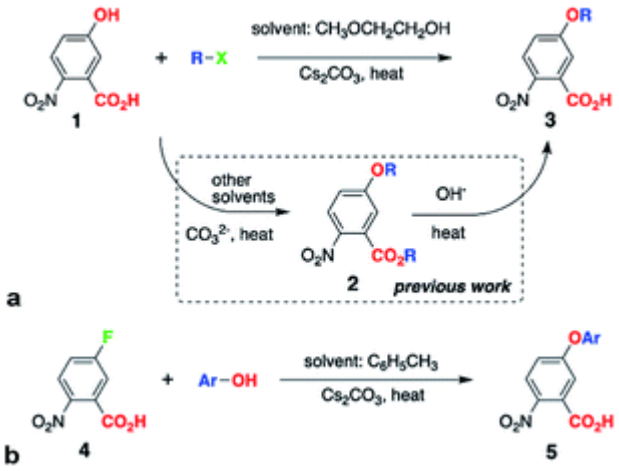

Scheme 3-1: Etherification of 2-nitrobenzoic acid (**NBA**) derivatives. (a) –X = –Cl, –Br, –I; –R = –$(CH_2)_3CH_3$, $–CH_2CH(CH_3)_2$, $–CH(CH_3)C_2H_5$, $–C(CH_3)_3$; for direct conversion of **1** to **3**, 1 equiv. **1**, 4 equiv. RX and 3 equiv. Cs_2CO_3; microwave heating: 2× 30 s, 60 W, temperature set to 130 °C, and ambient-pressure control; or conventional heating: 12 h, pressure tube at 130 °C; (b) –Ar = $–C_6H_5$, $–2,6\text{-}C_6H_3(CH_3)_2$ and $−2,6\text{-}C_6H_3(CH_3)_2$; 1 equiv. **4**, 2–4 equiv. ArOH and 3–6 equiv. Cs_2CO_3; conventional heating: 12 h, pressure tube at 110 °C.

WE offers a means for synthesizing alkyloxy derivatives of **NBA** from alkyl halides and the corresponding **NBA** hydroxy analogues, **1** (Scheme 3-1a).[5a] Because the carboxyl of **1** has a smaller pK_a value than the hydroxyl, both are deprotonated under the basic conditions of WE and can act as nucleophiles, leading to the formation of the esters of the alkoxy **NBA** derivatives, **2** (Scheme 3-1a).[5a] This lack of selectivity of WE sets the requirement for an additional step, *i.e.*, hydrolysis, for obtaining the free-acid precursor, **3**, for **Aa** synthesis (Scheme 3-1a).[5a]

Herein, we present the discovery of conditions for WE that allow for selective

Table 3-1: Reaction yields of direct formation of **3** from **1** and X–R[a]

	X =		
–R =	I	Br	Cl
$–(CH_2)_3CH_3$	97%	34%	15%
$–CH_2CH(CH_3)_2$	40%	19%	Trace[b]
$–CH(CH_3)CH_2CH_3$	41%	Trace[b]	Trace[b]
$–C(CH_3)_3$	Trace[b]	Trace[b]	N.D.[c]

Yields are based on isolated and purified products, 3 (Scheme 1a). b Products are not apparent on TLC but are detected using HRMS. c Not detected with HRMS.

etherification of **1** without forming the undesired esters. Employing 2-methoxyethanol (**2ME**) as a solvent for WE of **1** with 1-iodobutane under microwave irradiation, affords 5-butoxy-2-nitrobenzoic acids, **3**, in quantitative yields (R = *n*-C_4H_9, Scheme 3-1a, Table 3-1).

Reacting **1** with other butyl halides under the same conditions, also results in direct production of **3** without formation of the ester, **2**, or other side products. Reversing the WE paradigm, by taking advantage of the propensity of electron-deficient **NBA** fluorides to undergo nucleophilic aromatic substitution, provides routes to phenoxy **NBA** derivatives (Scheme 3-1b). As examined with cyclic voltammetry (CV), the electrochemical oxidation of the butoxy **Aa** derivatives barely shows any reversibility at scan rates of about 0.1 V s^{-1} or less. Conversely, some of the phenoxy **Aa** conjugates show not only improved chemical reversibility, but also $E_{Aa^{\bullet+}|Aa}$ exceeding 1.5 V *vs.* SCE by about 200 mV. This result appears surprising because aliphatic and aromatic carboxamides readily undergo irreversible oxidative degradation at about 1.5 V *vs.* SCE.[8] Therefore, these ether **Aa** conjugates have the potential to transduce strongly oxidizing holes making them comparable to a wide range of inorganic CT materials.

Results

Others and we have shown the two-step synthesis of 3, starting with the preparation of 2 using polar solvent media at about 150 °C (Scheme 3-1a).[5a,9] To lower the temperature and considerably shorten the reaction times, we resort to microwave radiation instead of conventional heating. Microwaving mixtures of 1 and various butyl halides dissolved in different solvents that are traditionally used for this reaction, such as *N,N*-

dimethylacetamide and *N,N*-dimethylformamide (in the presence of Cs_2CO_3), does not produce even detectable amounts of either 2 or 3, as confirmed with high-resolution mass spectrometry (HRMS) of the reaction mixtures.

Polar solvents, however, are not usually beneficial for microwave-driven reactions. Medium polarity and hydrogen bonding can, indeed, stabilize transition states and lower activation energies. In such reaction mixtures, however, the polar solvents, rather than the reactants, tend to be the principal absorbers of the microwave energy. Conversely, non-polar solvents with high boiling points ensure that reactants absorb substantial amount of the microwave radiation. This direct transfer of energy to the reactants is a principal advantage that microwave-driven chemical conversions have over reactions under conventional heating.

Using low-polarity solvents, such as toluene and ethyl acetate, allows the formation of only traces of 3, as detected with HRMS. This minute conversion of 1 to 3 renders it impractical. Medium-polarity aprotic solvents, such as tetrahydrofuran (THF) and halogenated alkanes, do not produce even traces of 2 or 3. This lack of conversion extends even to the neat-reaction conditions, *i.e.*, when the butyl halide reactant is the solvent.

Conversely, when 2ME is the solvent for the same WE reaction of 1 with butyl halides, we observe the formation solely of the free acid, 3, as NMR analysis, *i.e.*, NOESY, confirms (see ESI†). Using other alcohols as solvents, such as isopropanol, also affords traces of 3 without 2, as HRMS reveals. While employing ethylene glycol for WE results in chromatographically detectable amounts of 3, the minute yields of a few percent renders it impractical. Ether solvents, such as THF and 1,2-dimethoxyethane, conversely, do not

mediate the conversion of 1 to 3. While similar to ethylene glycol and 1,2-dimethoxyethane (R′O–CH_2CH_2–OR″, R′ and R″ = H or CH_3), 2ME provides a unique reaction environment that under microwave radiation allows for etherification of the phenol OH of 1, without the side reaction of esterification of the carboxyl. This finding of the 2ME-mediated selectivity of WE is a key breakthrough of this study, eliminating the need for the second step, *i.e.*, hydrolysis of 2 (Scheme 3-1a).

As a variation of WE, Purdie–Irvine alkylation, involving Ag_2O as a reagent with high affinity for the formed halide ions, allows for monomethylation of diols.[10] Cs^+ are the only available metal ions in the WE for converting 1 into 3 (Scheme 3-1a), and they do not have the chelation properties of Ag^+. Conversely, strongly basic conditions involving treating alcohols with NaH or Na, and excess of these alkoxides when reacting them with chloro- or bromo-acetic acid, produce ethers capped with free carboxylates.[10c,11] Such conditions keep the media dry and the dryness of the base is important for enhancing the WE yields.[12] In the contrary to the previously reported synthesis of ethers with free carboxylates, we use: (1) a relatively mild base, Cs_2CO_3, (2) a hydroxyl-carboxyl starting material, 1, and (3) halides in four-fold excess (Scheme 3-1a). In addition to its selectivity, all these features represent key advantages of the 2ME-mediated WE.

The reaction yields of the direct synthesis of 3 from 1 manifest dependence not only on the halide, but also on the alkyl chain. Improving the leaving group, by varying the starting materials from chloride to bromide and iodide, increases the reaction yields (Table 3-1). Concurrently, branched primary butyls, X–$CH_2CH(CH_3)_2$, show lower yields than the linear ones, X–$(CH_2)_3CH_3$. The yields decrease further for secondary butyls, X–

$CH(CH_3)C_2H_5$; and for tertiary, $X–C(CH_3)_3$, we observe only traces of 3 or no product at all (Table 3-1). These effects of the halides and the alkyl chains on the yields are consistent with the S_N^2 mechanism expected for such WE reactions. In addition, the inherent instability of *t*-butyl ethers of electron-deficient phenols reflects the negligible and no yields of 3 when $R = C(CH_3)_3$.

The cleanliness of this WE reaction represents a principal advantage. Reacting 1 with 1-iodobutane produces the *n*-butyl analogue of 3 in quantitative yields (Table 3-1). For the other butyl halides the isolated-product yields are under 50%. Nevertheless, the reason for these yields was a lack of conversion despite the left over starting material 1, rather than a production of side products. Increasing the reaction times does not increase the ratio between 3 and 1, and does not improve the yields.

Transferring this microwave synthetic procedure to pressure-tube settings provides the means for scaling up and for using less expensive conventional heating sources. Heating for 12 hours at 130 °C, *i.e.*, about 5° above the boiling point of 2ME under normal pressure, results in similar selectivity of the production of 3. Monitoring the progress of the reaction, using TLC and HRMS, reveals formation of the ester 2, but with isolated yields that do not exceed 1%. Often, 2 disappears with extended reaction times. This finding suggests that 2ME has the perfect proticity resulting in pH of the reaction mixture that ensures the ether formation, but makes the ester unstable. Even if the ester 2 forms, the traces of water that build up with the progress of the reaction can drive its hydrolysis.

Switching the WE pattern allows for pursuing the synthesis of phenoxy Aa precursors. Instead of starting with halide derivatives of the side chains

(Scheme 3-1a), we introduce the side chains as the WE nucleophiles (Scheme 3-1b). Fluorines on electron-deficient aromatic rings are immensely susceptible to nucleophilic aromatic substitution. Hence, introducing the side chain as the corresponding phenolate to fluorinated NBA, 4, allows for making the precursors, 5, for phenoxy Aa residues (Scheme 3-1b). The reaction yields for the phenoxy and 2,4-dimethylphenoxy analogues of 5, *i.e.*, the precursors for Fox and Dox_{24} (Chart 3-1c and e), are about 90%. The synthesis of the precursor of Dox, however, proceeds with yields smaller than 45%, most likely because of the steric hindrance induced by the two methyl groups at the ortho positions of the phenoxy side chain (Chart 3-1d).

Attempts to employ this nucleophilic aromatic substitution (Scheme 3-1b) for the synthesis of alkoxy Aa derivatives prove unfeasible. While the formation of the alkoxide ions, using metal sodium or strong imide bases, is quite trivial, 4 appears unstable under such extremely basic conditions.

Oxidation reversibility at relatively high potentials

Converting the ether **NBA**s (**3** and **5**, Scheme 3-1) to their amide analogues capped with alkyls (Chart 3-1b and e), allows for examining the electrochemical properties of these **Aa** residues.[5a–c,5e] We select one aliphatic and three aromatic ether derivatives: **Box** (with isobutyl), **Fox** (with phenyl), **Dox** (with 2,6-dimethylphenyl) and **Dox_{24}** (with 2,4-dimethylphenyl) (Chart 3-1b and e). In **Dox** and **Dox_{24}**, the *ortho* and *para* positions of the electron-donating methyls ensure strong electronic coupling with the **Aa** ring. When both methyls are *ortho* to the oxygen, they can enforce orthogonality between the two aromatic rings and impede rotations around the ether linker,

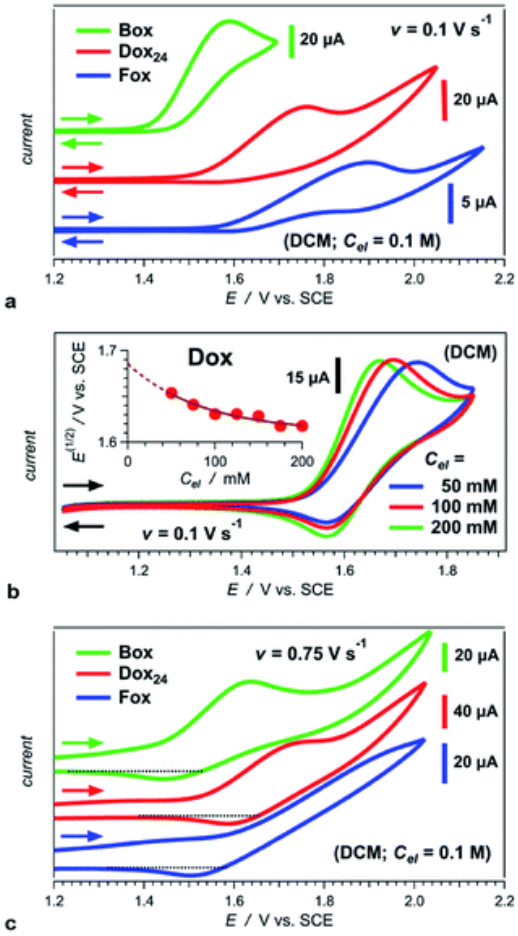

Fig. 3-1: Cyclic voltammograms of **Aa** ether residues (Chart 3-1b and e) for DCM in the presence of an electrolyte, $N(n\text{-}C_4H_9)_4PF_6$, with varied concentration, C_{el}. (a) Irreversible oxidation of **Box**, **Fox** and **Dox$_{24}$** at scan rate, v = 0.1 V s^{-1}, and C_{el} = 100 mM. (b) Oxidation of **Dox** showing reversibility at 0.1 V s^{-1}. Inset: dependence of the half-wave potential on C_{el} and extrapolation of its value for neat DCM, *i.e.*, for C_{el} = 0 M. (c) Partial reversibility of the oxidation of **Box**, **Fox** and **Dox$_{24}$** at 0.75 V s^{-1}.

which represent the principal difference between **Dox** and **Dox$_{24}$** (Chart 3-1d and e).

At moderate scan rates, **Box** exhibits irreversible oxidation at about 1.5 V *vs.* SCE for dichloromethane (**DCM**) media (Fig. 3-1a), which is consistent with the behaviour of other **Aa** residues with alkyloxy side chains.[5a] Replacing the aliphatic with aromatic ether, methylated at the two *ortho* positions, leads to reversible oxidation at potential of about 1.7 V *vs.* SCE (*i.e.*, **Box***vs.***Dox**, Fig. 3-1b and Table 3-2), which is unprecedented for amides.

At the same scan rates of 0.1 V s^{-1} and smaller, the other two aromatic-ether residues, **Fox** and **Dox$_{24}$**, exhibit irreversible oxidation similar to **Box**. Like **Dox**, however, **Fox** and **Dox$_{24}$** oxidize at more positive potentials than **Box** (Fig. 3-1a).

Increasing the scan rates beyond 0.5 V s^{-1} leads to partial oxidation reversibility of **Box**, **Fox** and **Dox$_{24}$**, as evident from the small cathodic peaks that appear in their voltammograms (Fig. 3-1c). These findings indicate that the lifetimes of their radical

cations are in the order of 1 s, which is sufficiently long for most CT applications. This oxidation reversibility (even if only partial), at potentials as high as 1.7 and 1.8 V *vs.* SCE, reveals an important effect that ethers have on aromatic amides.

Employing acetonitrile (MeCN) as a solvent yields the same trends as DCM. As expected, the reduction potentials for MeCN are not as positive as those for DCM (Table 3-2).

The **Aa** residues with aromatic ethers are harder to oxidize than the one with an alkyloxy group. Adding two methyls to the phenyloxy substituents causes a slight negative shift in the reduction potentials, *i.e.*, **Fox***vs.***Dox** and **Dox**$_{24}$ (Table 3-2). While the latter agrees with the methyl electron-donating properties, the former appears counter-intuitive assuming that the phenyloxy groups extend the π-conjugation of the residues. Nevertheless, the zero-to-zero energies, $\mathcal{E}_{00}$, of all ether residues are similar, around 3.5 eV (Table 3-2), regardless the aromatic *vs.* aliphatic nature of the substituent. It suggests that the resonance effect of the aromatic ethers on the π-conjugation does not necessarily dominate the electronic properties of the residues.

The Hammett constants and the field Swain–Lupton parameters of phenyloxy groups are more positive than those of alkyloxy substituents.[15] When the conformations supress the resonance effects, allowing the inductive ones to dominate, the phenyloxy groups are stronger electron-withdrawers than the alkyloxy ones, which is consistent with our

findings.

Table 3-2: Reduction potentials and optical excitation energies of **Aa** ether residues

	$E^{(1/2)}_{Aa^{\bullet+}\|Aa}$/V *vs.* SCE [a]	
	DCM	**MeCN**
Box	1.56 ± 0.05	1.42 ± 0.07
Fox	1.82 ± 0.03	1.57 ± 0.02
Dox	1.69 ± 0.02	1.55 ± 0.03
Dox_{24}	1.70 ± 0.04	1.56 ± 0.04

Values for neat solvents, *i.e.*, extrapolated to C_{el} = 0 M (Fig. 3-1b) from cyclic voltammograms recorded at 0.05 and 0.1 V s^{-1}. For irreversible oxidation, the values of the half-wave potentials at various C_{el} are obtained from the inflection points at the rise of the anodic peaks.[13] b **Estimated from the wavelengths, λ_{00}, where the normalized absorption and fluorescence spectra cross, $\mathscr{E}_{00} = h\upsilon/\lambda_{00}$, [5c,14] which is a rough approximation for the transition-dipole-moment representation.[14a]**

Why do the methyls at the *ortho* positions of the phenyloxy substituent provide extra stability of the radical cations of **Dox**? The sterics of the *ortho*-methyls forces orthogonality between the two aromatic rings of **Dox**, and SDD does not extend over the phenyl side chain. That is, **Dox** and **Box** manifest similar SDD that extends over the N-terminal amide and the ether oxygen (Fig. 3-2). Conversely, the aromatic rings of **Fox** and **Dox_{24}** are not orthogonal to each other, and the SDD expands over the phenyls of the side chains (Fig. 3-2).

These contrasts between SDD of **$Dox^{\bullet+}$** and of the radical cations of the other two aromatic ethers could account for the difference between the reversibility of their oxidation. Conversely, **Dox** shows reversibility at low scan rates, while **Box** does not. Yet, they have

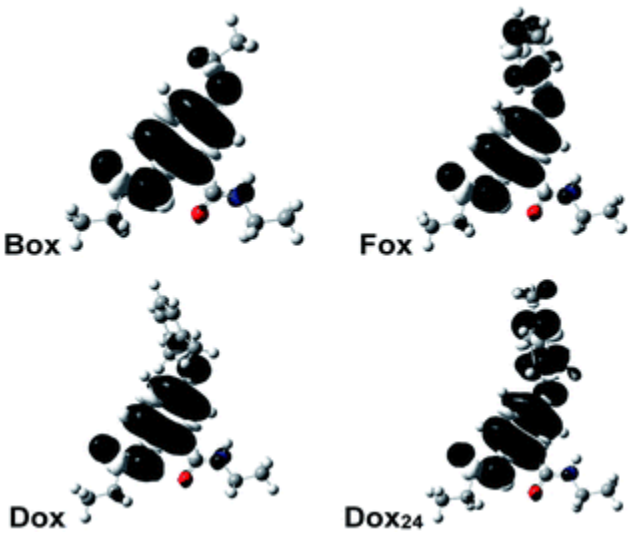

Fig. 3-2: Spin-density distributions (SDDs) of the radical cations of the **Aa** ether residues (*anti* conformers) showing the delocalization of the positive charge. For the DFT computations, the alkyls chains are truncated to ethyls.

quite similar SDDs (Fig. 3-2).

Two conformers of **Dox** provide orthogonality between its aromatic rings: *i.e.*, with the phenyloxy at *syn vs. anti* orientation in relevance to the C-terminal amide. While the computed energy differences between the *syn*- and *anti*-**Dox** are comparable to the thermal energy, k_BT at $T \approx$ 20 °C, the NMR spectra show a single set of peaks for the 2,6-dimethylphenyloxy protons. We ascribe it to an interexchange between the two conformers that is faster than the NMR acquisition timescales. The structural features of **Dox** make the electronic properties of its radical cation similar to those of **Box**$^{\bullet+}$, rather than **Fox**$^{\bullet+}$ and **Dox$_{24}$**$^{\bullet+}$. Unlike **Box**$^{\bullet+}$, however, **Dox**$^{\bullet+}$ has a polarizable aromatic side chain.

This strategy for decreasing the susceptibility of aromatic amides to oxidative degradation by adding ether substituents is considerably more attractive than an alternative means involving modification of their –CONH– groups. Introducing capping groups with quaternary carbons that connect to the amides of **Aa** residues does not detectably improve the stability of their radical cations. Oligomers of **Aa** residues that oxidize irreversibly, still show irreversible voltammograms.[5f] Conversely, converting the C-terminal amide, **Aa**–

CONH–R, to a tertiary amide, *i.e.*, to **Aa**–$CONR_2$, induces partial reversibility in the voltammograms of residues that oxidize irreversibly.[5b] It is consistent with the importance of the proton of the C-terminal amide for the pathways of oxidative degradation. In an **Aa** oligomer (Chart 3-1a), however, the introduction of such tertiary amides along its back bone would disrupt the hydrogen-bonding pattern that is important for its extended conformation and macrodipole. The C-terminal protons of such oligomers are not involved in the hydrogen bonding network, as NMR studies show.[3b] Therefore, capping the C-terminus of an **Aa** oligomer with tertiary amide will not disrupt its conformational integrity. Still, computational analysis show that the positive charge of a singly oxidized oligomer, composed of identical **Aa** units, localizes on the N-terminal residue. Therefore, tertiary amide on C-terminus would prove beneficial only if the hole transfer away from the C-terminal residue is slower than its oxidative degradation. In light of this discussion, gaining oxidation reversibility *via* adding ether side chains is a superb strategy because it does not involve disruption of the amides along the backbone that maintain the extended secondary conformation of the **Aa** oligomers.

Conclusions

Ether substituents show important propensity for stabilizing oxidized amides. Ethers are strong enough electron-donating groups to remove the positive charge in the radical cations from the amide groups susceptible to oxidative degradation, but not strong enough to cause drastic negative shifts in reduction potentials. Orthogonality of the aromatic rings of such ether substituents is especially promising for the design of hole-transfer amides. Selectivity for etherification of aromatic hydroxyls in the presence of other

nucleophilic groups is important for the synthesis of such charge-transfer conjugates that, along with their newly discovered electronic properties, opens new doors for organic electronics and energy science.

REFERENCES

[1] (a) A. Williamson Philos. Mag. Ser. 3, 1850, **37** , 350 —356. (b) R. Gigg and P. M. Carroll , *Nature*, 1961, **191** , 495 —496. (c) M. Sauthier , A. Mortreux and I. Suisse , Carbohydrate Chemistry , A. P. Rauter, T. K. Lindhorst and Y. Queneau, *Royal Society of Chemistry*, 2014, vol. 40, pp. 73–98. (d) S. Mandal , S. Mandal , S. K. Ghosh , P. Sar , A. Ghosh , R. Saha and B. Saha , *RSC Adv*., 2016, **6** , 69605 —69614.

[2] (a) J. B. Derr , J. Tamayo , E. M. Espinoza , J. A. Clark and V. I. Vullev , *Can. J. Chem*., 2018, **96** , 843 —858. (b) E. Galoppini and M. A. Fox , *J. Am. Chem. Soc*., 1996, **118** , 2299 —2300. (c) S. Yasutomi , T. Morita , Y. Imanishi and S. Kimura , *Science*, 2004, **304** , 1944 —1947. (d) C. Shlizerman , A. Atanassov , I. Berkovich , G. Ashkenasy and N. Ashkenasy , *J. Am. Chem. Soc*., 2010, **132** , 5070 —5076. (e) Y. Chen , J. Viereck , R. Harmer , S. Rangan , R. A. Bartynski and E. Galoppini , *J. Am. Chem. Soc.*, 2020, **142** , 3489 —3498.

[3] (a) V. I. Vullev. *J. Phys. Chem. Lett.*, 2011, **2** , 503 —508. (b) B. Xia , D. Bao , S. Upadhyayula , G. Jones and V. I. Vullev , *J. Org. Chem*., 2013, **78** , 1994 —2004. (c) D. Bao , S. Upadhyayula , J. M. Larsen , B. Xia , B. Georgieva , V. Nunez , E. M. Espinoza , J. D. Hartman , M. Wurch , A. Chang , C.-K. Lin , J. Larkin , K. Vasquez , G. J. O. Beran and V. I. Vullev , *J. Am. Chem. Soc*., 2014, **136** , 12966 —12973. (d) M. Krzeszewski , E. M. Espinoza , C. Cervinka , J. B. Derr , J. A. Clark , D. Borchardt , G. J. O. Beran , D. T. Gryko and V. I. Vullev , *Angew. Chem., Int. Ed*., 2018, **57** , 12365 —12369.

[4] (a) M. K. Ashraf , R. R. Pandey , R. K. Lake , B. Millare , A. A. Gerasimenko , D. Bao and V. I. Vullev , *Biotechnol. Prog*., 2009, **25** , 915 —922. (b) S. Upadhyayula , D. Bao , B. Millare , S. S. Sylvia , K. M. M. Habib , K. Ashraf , A. Ferreira , S. Bishop , R. Bonderer , S. Baqai , X. Jing , M. Penchev , M. Ozkan , C. S. Ozkan , R. K. Lake and V. I. Vullev , *J. Phys. Chem*. B, 2011, **115** , 9473 —9490.

[5] (a) J. M. Larsen , E. M. Espinoza , J. D. Hartman , C.-K. Lin , M. Wurch , P. Maheshwari , R. K. Kaushal , M. J. Marsella , G. J. O. Beran and V. I. Vullev , *Pure Appl. Chem*., 2015, **87** , 779 —792. (b) E. M. Espinoza , J. M. Larsen and V. I. Vullev , *J. Phys. Chem. Lett.,* 2016, **7** , 758 —764. (c) J. M. Larsen-Clinton , E. M. Espinoza , M. F. Mayther , J. Clark , C. Tao , D. Bao , C. M. Larino , M. Wurch , S. Lara and V. I. Vullev , *Phys. Chem. Chem. Phys*., 2017, **19** , 7871 —7876. (d) J. M. Larsen , E. M. Espinoza and V. I. Vullev , *J. Photonics Energy*, 2015, **5** , 055598. (e) E. M. Espinoza , J. M. Larsen-Clinton , M. Krzeszewski , N. Darabedian , D. T. Gryko and V. I. Vullev , Pure Appl. Chem., 2017, **89** , 1777 —1797. (f) K. Skonieczny , E. M. Espinoza , J.

B. Derr , M. Morales , J. M. Clinton , B. Xia and V. I. Vullev , *Pure Appl. Chem*., 2020, **92** , 275 —299.

[6] J. Jortner , M. Bixon , T. Langenbacher and M. E. Michel-Beyerle , *Proc. Natl. Acad. Sci. U. S. A*., 1998, **95** , 12759 —12765.

[7] Y. Hamuro , S. J. Geib and A. D. Hamilton , *J. Am. Chem. Soc*., 1996, **118** , 7529 —7541

[8] (*a*) J. F. O'Donnell and C. K. Mann , *J. Electroanal. Chem. Interfacial Electrochem.*, 1967, **13** , 157 —162. (*b*) T. Golub and J. Y. Becker , *Org. Biomol. Chem.*, 2012, **10** , 3906 —3912.

[9] (*a*) A. Andersson , J. B. Baell , P. J. Duggan , J. E. Graham , R. J. Lewis , N. G. Lumsden , C. E. Tranberg , K. L. Tuck and A. Yang , *Bioorg. Med. Chem.*, 2009, **17** , 6659 —6670. (*b*) H. Bertrand , R. Guillot , M.-P. Teulade-Fichou and D. Fichou , *Chem.–Eur. J.*, 2013, **19** , 14654 —14664. (*c*) A. F. Donnell , Y. Zhang , E. M. Stang , D. D. Wei , A. J. Tebben , H. L. Perez , G. M. Schroeder , C. Pan , C. Rao , R. M. Borzilleri , G. D. Vite and S. Gangwar , *Bioorg. Med. Chem. Lett.*, 2017, **27** , 5267 —5271.

[10] (*a*) T. Purdie and J. C. Irvine , *J. Chem. Soc., Trans.*, 1903, **83** , 1021 —1037. (*b*) A. Bouzide and G. Sauve , *Tetrahedron Lett.*, 1997, **38** , 5945 —5948. (*c*) A. Tuchscherer , D. Schaarschmidt , S. Schulze , M. Hietschold and H. Lang , *Dalton Trans.*, 2012, **41** , 2738 —2746.

[11] O. Zech , M. Kellermeier , S. Thomaier , E. Maurer , R. Klein , C. Schreiner and W. Kunz , *Chem.–Eur. J.*, 2009, **15** , 1341 —1345.

[12] B. Abribat , Y. Le Bigot and A. Gaset , *Tetrahedron*, 1996, **52** , 8245 —8256.

[13] (*a*) E. M. Espinoza , J. A. Clark , J. Soliman , J. B. Derr , M. Morales and V. I. Vullev , *J. Electrochem. Soc.*, 2019, **166** , H3175 —H3187. (*b*) A. Purc , E. M. Espinoza , R. Nazir , J. J. Romero , K. Skonieczny , A. Jeżewski , J. M. Larsen , D. T. Gryko and V. I. Vullev , *J. Am. Chem. Soc.*, 2016, **138** , 12826 —12832. (*c*) E. M. Espinoza , B. Xia , N. Darabedian , J. M. Larsen , V. Nunez , D. Bao , J. T. Mac , F. Botero , M. Wurch , F. Zhou and V. I. Vullev , *Eur. J. Org. Chem.*, 2016, **2016** , 343 —356. (*d*) D. Bao , S. Ramu , A. Contreras , S. Upadhyayula , J. M. Vasquez , G. Beran and V. I. Vullev , *J. Phys. Chem. B*, 2010, **114** , 14467 —14479. (*e*) D. Bao , B. Millare , W. Xia , B. G. Steyer , A. A. Gerasimenko , A. Ferreira , A. Contreras and V. I. Vullev , *J. Phys. Chem. A*, 2009, **113** , 1259 —1267.

[14] (*a*) G. Angulo , G. Grampp and A. Rosspeintner , *Spectrochim. Acta, Part A*, 2006, **65A** , 727 —731. (*b*) S. Guo , D. Bao , S. Upadhyayula , W. Wang , A. B. Guvenc , J. R. Kyle , H. Hosseinibay , K. N. Bozhilov , V. I. Vullev , C. S. Ozkan and M. Ozkan , *Adv. Funct. Mater.*, 2013, **23** , 5199 —5211.

[15] (*a*) C. Hansch , A. Leo and R. W. Taft , *Chem. Rev.*, 1991, **91** , 165 —195. (*b*) C. G. Swain and E. C. Lupton Jr , *J. Am. Chem. Soc.*, 1968, **90** , 4328 —4337.

Experimental

MATERIALS

General methods. All chemicals were used as received unless otherwise specified. The reported ^{1}H NMR, ^{13}C NMR, and NOESY spectra were recorded on 400 MHz, 500 MHz and 600 MHz spectrometers. ^{1}H chemical shifts (δ) are reported in ppm relative to $CHCl_3$ in $CDCl_3$ (δ = 7.26 ppm); ^{13}C δ are reported in ppm relative to $CDCl_3$ (δ = 77.23 ppm). Data for ^{1}H NMR are reported as follows: chemical shift, integration, multiplicity (s = singlet, d = doublet, t = triplet, q = quartet, p = pentet/quintet, h = hextet/sextet, e = eptet(from επτά)/heptet, m = multiplet), and coupling constants. All ^{13}C NMR spectra were recorded with complete proton decoupling. High-resolution mass spectrometry (HRMS) was performed using Agilent LCTOF (6200) mass spectrometer (Agilent Technologies, Santa Clara, CA). Analytical thin layer chromatography was performed using 0.25 mm silica gel 60-F plates. Flash chromatography was performed using 60 Å, 32−63 μm silica gel.

Synthetic procedures

Scheme 3S-1. Synthesis of ether derivatives, **3** (Scheme 3-1a).

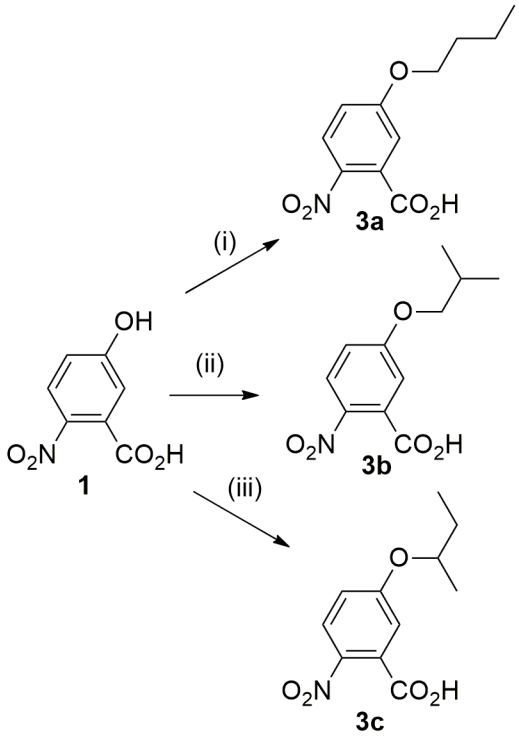

(i) C_4H_9X, Cs_2CO_3, 2ME, 130°C, 30 sec, 97%; (ii) C_4H_9X, Cs_2CO_3, 2ME, 130°C, 30 sec, 40%; (iii) C_4H_9X, Cs_2CO_3, 2ME, 130°C, 30 sec, 41%.

Scheme 3S-2. Synthesis of Box.

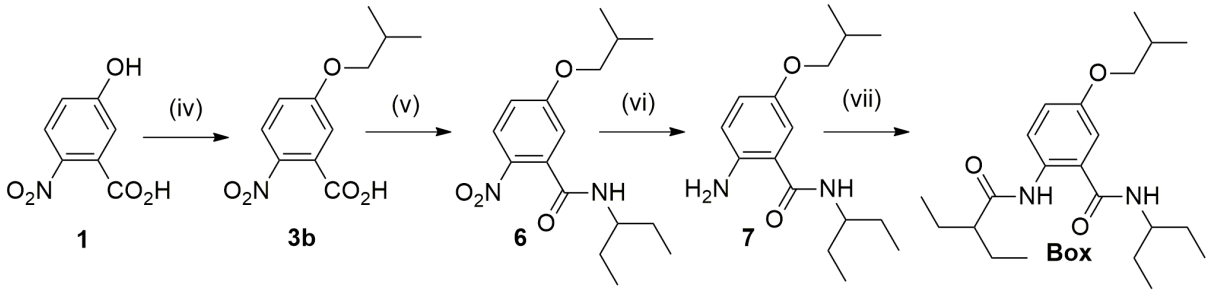

(iv) 1-iodo-2-methylpropane, Cs_2CO_3, 2ME, 130°C, overnight, 40%; (v) 3-aminopentane, HATU, HOAt, DIPEA, DMF, r.t., Overnight, 81%; (vi) Pd/C, H_2, Ethyl Acetate, r.t., Overnight; (vii) 2-ethylbutyric acid, HATU, HOAt, DIPEA, DMF, r.t., Overnight, 71%.

Scheme 3S-3. Synthesis of Fox.

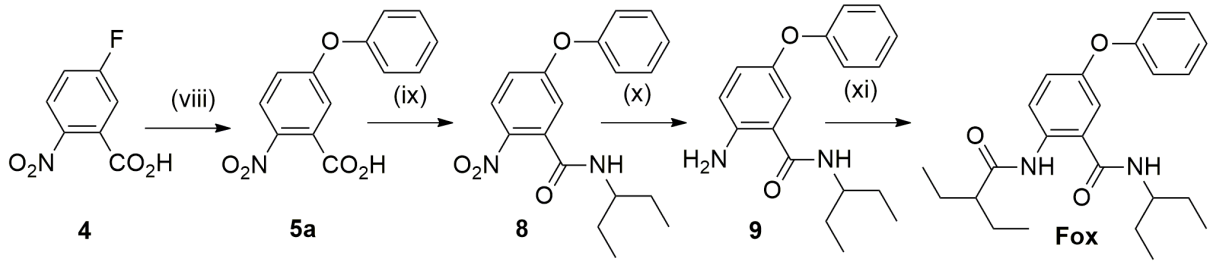

(viii) Phenol, Cs_2CO_3, Toluene, 110°C, Overnight, 92%; (ix) (1) $(COCl)_2$, DCM, DMF, -78 °C to r.t., 1 hr, 72%; (2) 3-aminopentane, DCM, NMM, -78 °C to r.t., 6h, 72%; (x) Pd/C, H_2, Ethyl Acetate, r.t., Overnight; (xi) 2-ethylbutanoyl chloride, DCM, NMM, -78 °C to r.t., 4h, 25%.

Scheme 3S-4. Synthesis of Dox.

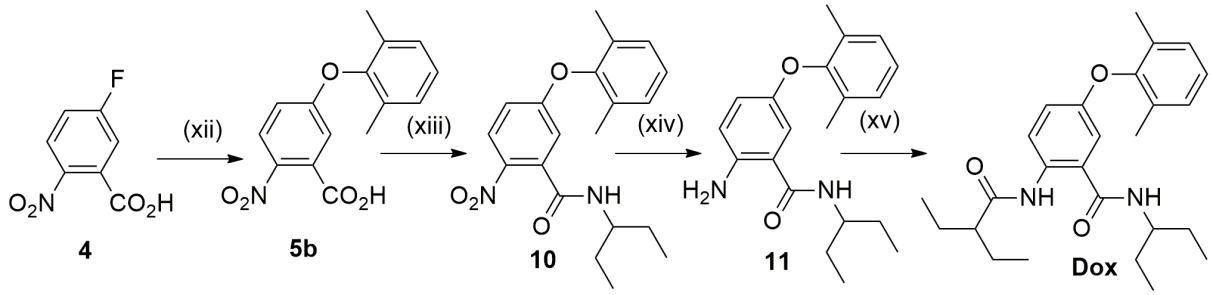

(xii) 2,6-Dimethylphenol, Cs_2CO_3, Toluene, 110°C, Overnight, 42%; (xiii) (1) $(COCl)_2$, DCM, DMF, -78 °C to r.t., 1 hr; (2) 3-aminopentane, DCM, NMM, -78 °C to r.t., 6h, 26%; (xiv) Pd/C, H_2, Ethyl Acetate, r.t., Overnight; (xv) 2-ethylbutanoyl chloride, DCM, NMM, -78 °C to r.t., 4h, 29%.

Scheme 3S-5. Synthesis of Dox_{24}.

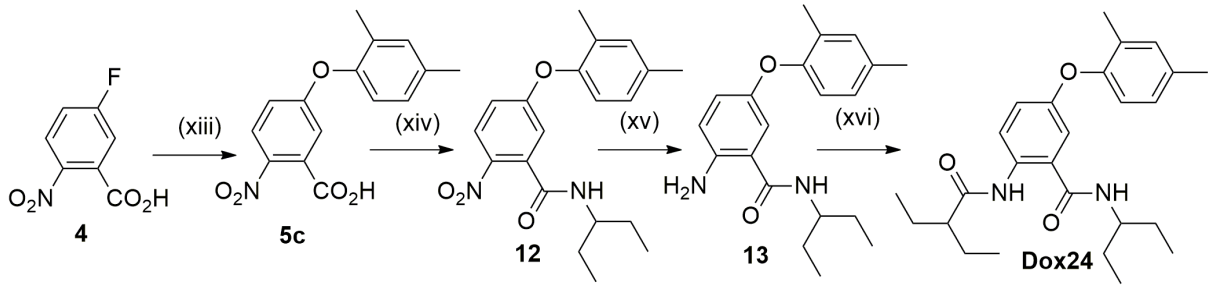

(xiii) 2,4-Dimethylphenol, Cs_2CO_3, Toluene, 110°C, Overnight, 88%; (xiv) (1) $(COCl)_2$, DCM, DMF, -78 °C to r.t., 1 hr; (2) 3-aminopentane, DCM, NMM, -78 °C to r.t., 6h, 64%; (xv) Pd/C, H_2, Ethyl Acetate, r.t., Overnight; (xvi) 2-ethylbutyric acid, HATU, HOAt, DIPEA, DMF, r.t., Overnight, 58%.

Optimization of solvent and reaction times. Our previous work on synthesis of alkyloxy NBA derivatives provides the initial choices of a base (i.e., Cs_2CO_3) and reactant equivalents (i.e., 4:1 equivalents of halide to **1**, except for neat reaction where we use the

halide as a solvent). The microwave synthesis is conducted using a Discover LabMate reactor equipped with IntelliVent Pressure control (CEM Corporation, Matthews, NC, USA). The temperature limit is set for 130 ºC, and the power – to 60 W. The pressure control (set for ambient pressure) prevents the reaction mixture from overheating and the solvent from boiling out of the reaction vessel. We employ consecutive treatment of 30 seconds each. After each treatment, we examine the reaction mixture using TLC. After completing the reaction, use HRMS to examine the crude reaction mixture and each spot on the TLC (which we scrape off the TLC and extract with methanol for analysis with ESI HRMS).

As an example, for the synthesis of **3b**, from **1** and 1-iodo-2-methylpropane (Scheme 3S-1), we examine a wide variety of solvents (Table 3S-1). For a substantial number of the examined solvents, the TLC results are identical for before and after the reaction (2×30 s microwave treatment), and the HRMS does not detect product, **3b**, in the crude reaction mixture. Reactions employing other set of solvents, mostly alcohols, yield traces of **3b**, detectable with HRMS from the crude mixture, and may or may not show additional spot on the TLC, identified with the product (Table 3S-1). While reactions in ethylene glycol produce both, a small product spot on the TLC confirmed with HRMS, the overall isolated yields were less than 5%, which renders this solvent as unfeasible for further pursuits.

By far, 2-methoxyethanol (2ME) produces the highest yields (Table 3S-1). As evident from the intensities of the product and starting-material spots on the TLC, even 30-s microwave treatments result in higher conversions for 2ME than for the other solvents for 2×30 s reaction times. An increase in the reaction times for 2ME to 60 s improves the conversion

(Table 3S-2). Additional increases in the reaction times, however, does not result in further improvements of the conversion, as the TLC analysis and the ratio between the intensities for the peaks for 3b and 1 show on the mass spectra show. The reactions of **1** with the other butyl halides reveal similar trends.

Table 3S-1. Solvent optimization for direct conversion of 1 to 3b (Scheme 3-1a and 3S-1).[a]

Solvent	Conversion
2-Methoxyethanol	Notable [b]
Methanol	Minimal [c]
Ethanol	Minimal
Isopropyl Alcohol	Minimal
Ethylene Glycol	Minimal
Dichloromethane	None [d]
1,2-Dichloroethane	None
1-Iodo-2-Methylpropane	None
1,2-Dimethoxyethane	None
N,*N*-Dimethylformamide	None
N,*N*-Dimethylacetamide	None
Tetrahydrofuran	None
Toluene	Minimal
Ethyl Acetate	Minimal

[a] Reaction conditions: substrate **1** (0.5 mmol), halide **2** (4 equiv.), Cs_2CO_3 (3 equiv.), dry solvent (1mL); two 30-second intervals of microwave treatment: temperature set to 130 °C at 60 W power, pressure sensor set for ambient pressure, under argon atmosphere. [b] Notable conversion: isolated product yields exceed 5%. [c] Minimal conversion: detectable with HRMS, but yields smaller than 5%; also may or may not be detectable on TLC. [d] No conversion: product not detected with HRMS.

Table 3S-2. Optimization of reaction times for conversion of 1 to 3b (Scheme 3-1a and 3S-1).[a]

time / s [b]	Conversion
30	Partial [c]
60	Complete [d]
90	No Further Conversion [e]
120	No Further Conversion
170	No Further Conversion

[a] Reaction conditions: substrate **1** (0.5 mmol), halide **2** (4 equiv.), Cs_2CO_3 (3 equiv.), dry 2ME (1 mL); Microwave treatment: temperature set to 130 °C at 60 W power, pressure sensor set for ambient pressure, under argon atmosphere. [b] The reaction time varies in increment of 30 s for the first 2 min, and additional 50 s after that. [c] Partial conversion: further microwave treatments lead to a visible increase in the ratio between **3b** and **1** (as determined by TLC and HRMS). [d] Complete conversion: further microwave treatments do not improve the ratio between **3b** and **1**. [e] No further conversion: no visible improvement in the ration between **3b** and **1**.

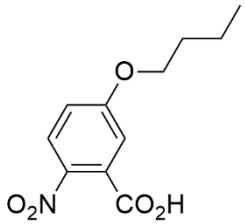

5-butoxy-2-nitrobenzoic acid (3a) (Scheme 3S-1). Cs_2CO_3 (488 mg, 1.5 mmol) was placed in a microwave vial, and purged with argon. **(1)** 5-hydroxy-2-nitrobenzoic acid (91.6 mg, 0.5 mmol). was added, followed by the 1-iodobutane (230 μL, 2.0 mmol) and 1mL of 2-methoxyethanol (2ME). The microwave vial was capped and put into the microwave. The parameters were set to 130°C, 60 W, 2×30 seconds. After the first interval the reaction mixture was allowed to cool for 5 minutes and then microwaved again at the same exact parameters giving a dark orange solution. The progress of the reaction was monitored via TLC. The mixture was diluted with 5% HCL and extracted with DCM (3×25mL). The organic layer was dried Na_2SO_4 and condensed. The product was purified using flash chromatography (stationary phase: silica gel; eluent gradient: 0:1 (v:v) to 1:1 (v:v) of ethyl acetate and hexanes. The 1:1 elution was mixed with 1% acetic acid. The product was condensed to afford 116 mg (97%) of **(3a)**. white crystals. ^{1}H NMR (600 MHz, Chloroform-*d*) δ 8.00 (d, *J* = 9.1 Hz, 1H), 7.17 (d, *J* = 2.7 Hz, 1H), 7.04 (dd, *J* = 9.1, 2.7

Hz, 1H), 4.08 (t, *J* = 6.5 Hz, 2H), 1.81 (dq, *J* = 8.7, 6.6 Hz, 2H), 1.55 – 1.45 (m, 2H), 0.98 (t, *J* = 7.4 Hz, 3H). ^{13}C NMR (151 MHz, $CDCl_3$) δ 171.56, 163.15, 140.13, 130.09, 126.88, 116.91, 114.96, 77.44, 77.23, 77.02, 69.22, 31.04, 19.25, 13.90. HRMS (ESI) m/z calculated for $C_{11}H_{12}NO_5$: $[M-H]^-$ 238.0721, found 238.0741.

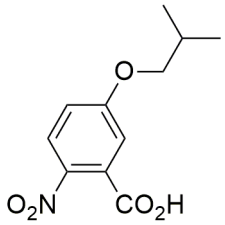

5-isobutoxy-2-nitrobenzoic acid (3b) (Scheme 3S-1). Cs_2CO_3 (488 mg, 1.5 mmol) was placed in a microwave vial, and purged with argon. **(1)** 5-hydroxy-2-nitrobenzoic acid (91.6 mg, 0.5 mmol). was added, followed by the 1-iodo-2-methylpropane (230 μL, 2.0 mmol) and 1mL of 2ME. The microwave vial was capped and put into the microwave. The parameters were set to 130°C, 60 W, 2×30 seconds. After the first interval the reaction mixture was allowed to cool for 5 minutes and then microwaved again at the same exact parameters giving a dark orange solution. The progress of the reaction was monitored via TLC. The mixture was diluted with 5% HCL and extracted with DCM (3×25mL). The organic layer was dried Na_2SO_4 and condensed. The product was purified using flash chromatography (stationary phase: silica gel; eluent gradient: 0:1 (v:v) to 1:1 (v:v) of ethyl acetate and hexanes. The 1:1 elution was mixed with 1% acetic acid. The product was condensed to afford 116 mg (40%) of (2). White Crystals. Tan powder of **(3b)**. ^{1}H NMR (600 MHz, Chloroform-*d*) δ 8.02 (d, *J* = 9.1 Hz, 1H), 7.17 (d, *J* = 2.7 Hz, 1H), 7.05 (dd, *J* = 9.1, 2.7 Hz, 1H), 3.84 (d, *J* = 6.5 Hz, 2H), 2.13 (dq, *J* = 13.3, 6.7 Hz, 1H), 1.05 (d, *J* =

6.7 Hz, 6H). ^{13}C NMR (151 MHz, $CDCl_3$) δ 163.27, 140.13, 130.28, 126.92, 116.87, 114.97, 77.44, 77.23, 77.02, 75.71, 29.92, 28.34, 19.27, 19.14. HRMS (ESI) m/z calculated for $C_{11}H_{12}NO_5$: $[M-H]^-$ 238.0721, found 238.0827.

Conventional Heating

(1) (3.7 g, 20 mmol), was placed in in a pressure tube bottom flask with a stir bar, and purged with argon. Fifteen mL of 2ME was added, followed by the cesium carbonate (9.77 g, 30 mmol), and 1-bromo-2-methylpropane (4.3 mL, 40 mmol). The mixture was stirred at 130°C overnight. The progress of the reaction was monitored via TLC. The reaction was taken out of the oil bath for 10 minutes to cool and then diluted with 200 mL of 5% HCl and extracted with DCM (3×25mL). Dried over Na_2SO_4 and vacuum filtered. The filtrate was condensed. The product was purified using flash chromatography (stationary phase: silica gel; eluent gradient: 0:1 (v:v) to 1:1 (v:v) of ethyl acetate and hexanes. The 1:1 elution was mixed with 1% acetic acid. The product was condensed to afford 901 mg (18%) of **(3b)**. Tan powder.

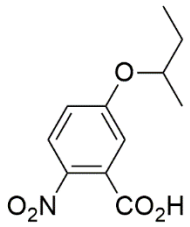

5-(2-*n*-butoxy)-2-nitrobenzoic acid (3c) (Scheme 3S-1). Cs_2CO_3 (488 mg, 1.5 mmol) was placed in a microwave vial, and purged with argon. **(1)** 5-hydroxy-2-nitrobenzoic acid (91.6 mg, 0.5 mmol). was added, followed by the 2-iodobutane (230 μL, 2.0 mmol) and 1mL of 2ME. The microwave vial was capped and put into the microwave. The parameters

were set to 130°C, 60 W, 2×30 seconds. After the first interval the reaction mixture was allowed to cool for 5 minutes and then microwaved again at the same exact parameters giving a dark orange solution. The progress of the reaction was monitored via TLC. The mixture was diluted with 5% HCL and extracted with DCM (3×25mL). The organic layer was dried Na_2SO_4 and condensed. The product was purified using flash chromatography (stationary phase: silica gel; eluent gradient: 0:10 (v:v) to 1:1 (v:v) of ethyl acetate and hexanes. The 1:1 elution was mixed with 1% acetic acid. The product was condensed to afford 116 mg (41%) of **(3c)**. White Crystals. ^{1}H NMR (600 MHz, $CDCl_3$) δ 10.33 (s, 1H), 8.01 (d, *J* = 9.1 Hz, 1H), 7.15 (d, *J* = 2.7 Hz, 1H), 7.02 (dd, *J* = 9.1, 2.7 Hz, 1H), 4.46 (h, *J* = 6.1 Hz, 1H), 1.79 (ddd, *J* = 13.8, 7.5, 6.3 Hz, 1H), 1.74 – 1.64 (m, 1H), 1.35 (d, *J* = 6.1 Hz, 3H), 0.99 (t, *J* = 7.5 Hz, 3H. ^{13}C NMR (151 MHz, $CDCl_3$) δ 171.72, 162.50, 139.80, 130.18, 127.01, 117.63, 115.77, 77.44, 77.23, 77.02, 76.83, 29.90, 29.13, 19.11, 9.78. HRMS (ESI) m/z calculated for $C_{11}H_{12}NO_5$: $[M-H]^-$ 238.0721, found 238.1227

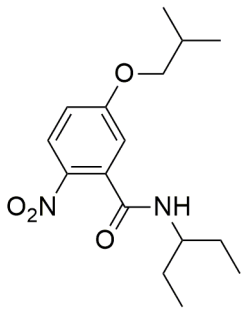

5-isobutoxy-2-nitro-N-(pentan-3-yl)benzamide (6) (Scheme 3S-2). (3a) (1.26 g, 5.29 mmol), 1-[Bis(dimethylamino)methylene]-1H-1,2,3-triazolo[4,5-b]pyridinium 3-oxide hexafluorophosphate (HATU) (2.8 g, 7.41 mmol), 1-hydroxy-7-azabenzotriazole (HOAt)

(1.0 g, 7.41 mmol), and N-diisopropylethylamine (DIPA) (1.3 mL, 7.41 mmol) was dissolved in 15 mL of DMF in a dry, argon purged 100 mL round bottom flask with a stir bar. This was stirred for 15 minutes and then 3-aminopentane (860 μL, 7.41 mmol) was transferred and stirred overnight. The progress of the reaction was monitored via TLC. The mixture quenched with 100 mL of saturated Na_2CO_3 was extracted with DCM (3×50mL). The organic layer was dried Na_2SO_4 and condensed. The product was purified using flash chromatography (stationary phase: silica gel; eluent gradient: 0:10 (v:v) to 3:2 (v:v) of ethyl acetate and hexanes in 200 mL increments.to afford 1.39 g (81%) of **(6)**. White powder. ^{1}H NMR (500 MHz, Chloroform-*d*) δ 8.07 (d, *J* = 9.1 Hz, 1H), 6.92 (dd, *J* = 9.1, 2.7 Hz, 1H), 6.87 (d, *J* = 2.7 Hz, 1H), 5.56 (d, *J* = 9.1 Hz, 1H), 3.96 (dtt, *J* = 8.9, 7.5, 5.5 Hz, 1H), 3.80 (d, *J* = 6.5 Hz, 2H), 2.11 (hept, *J* = 6.7 Hz, 1H), 1.64 (dddd, *J* = 14.9, 13.0, 7.5, 5.5 Hz, 2H), 1.51 (dt, *J* = 13.9, 7.4 Hz, 2H), 1.06 – 0.96 (m, 12H). ^{13}C NMR (126 MHz, cdcl$_3$) δ 166.64, 163.65, 138.68, 136.33, 127.38, 114.88, 114.79, 77.48, 77.23, 76.98, 75.53, 53.05, 28.32, 27.24, 19.25, 10.40. HRMS (ESI) m/z calculated for $C_{16}H_{24}N_2O_4$: $[M+H]^+$ 309.1814, found 309.2099

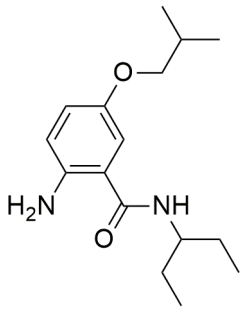

2-amino-5-isobutoxy-N-(pentan-3-yl)benzamide (7) (Scheme 3S-2). (6) (1.28 g, 3.94 mmol), Pd/C (192 mg, 15% by weight), and 15 mL of ethyl acetate was transferred in a dry, Ar purged 100 mL round bottom flask with a stir bar. The round bottom was then vacuumed for 5 min. H_2 gas was attached to the round bottom and the reaction was stirred overnight. The reaction was then vacuumed filtered and condensed giving crude **(7)**. Black oil. HRMS (ESI) m/z calculated for $C_{16}H_{25}N_2NaO_2$: $[M+Na]^+$ 300.1819, found 299.8578.

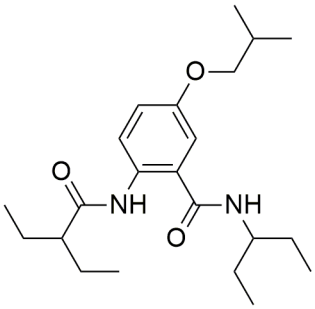

2-(2-ethylbutanamido)-5-isobutoxy-N-(pentan-3-yl)benzamide (b, Box) (Scheme 3S-2). HATU (2.1 g, 5.52 mmol), and HOAt (751 mg, 5.52 mmol), 2-ethylbutaric acid (696 μL, 5.52 mmol), DIPEA (960 μL, 5.52 mmol) was dissolved in 15 mL of DMF in a dry, argon purged 100 mL round bottom flask with a stir bar. This was stirred for 15 minutes and then **(7)** (3.94 mmol) was transferred and stirred overnight. The progress of the reaction was monitored via TLC. The mixture quenched with 100 mL saturated Na_2CO_3 was extracted with DCM (3×50mL). The organic layer was dried Na_2SO_4 and condensed. The product was purified using flash chromatography (stationary phase: silica gel; eluent gradient: 0:10 (v:v) to 2:3 (v:v) of ethyl acetate and hexanes in 200 mL increments.to afford 1.06 g (71%) of **(Box)**. White powder. ^{1}H NMR (500 MHz, Chloroform-*d*) δ 10.49 (s, 1H),

8.46 (d, *J* = 9.1 Hz, 1H), 6.99 (dd, *J* = 9.1, 2.9 Hz, 1H), 6.94 (d, *J* = 2.9 Hz, 1H), 5.80 (d, *J* = 9.2 Hz, 1H), 3.96 (dtd, *J* = 13.6, 8.4, 5.2 Hz, 1H), 3.72 (d, *J* = 6.6 Hz, 2H), 2.13 – 2.01 (m, 2H), 1.68 (qdd, *J* = 12.7, 8.3, 6.2 Hz, 5H), 1.61 – 1.40 (m, 4H), 1.03 (d, *J* = 6.7 Hz, 6H), 0.94 (dt, *J* = 12.1, 7.4 Hz, 12H). ^{13}C NMR (126 MHz, cdcl$_3$) δ 174.74, 168.81, 154.70, 132.28, 123.59, 116.91, 113.38, 77.49, 77.23, 76.98, 75.21, 52.88, 52.85, 28.55, 27.79, 26.01, 19.45, 12.23, 10.54. HRMS (ESI) m/z calculated for $C_{22}H_{36}N_2O_3$: $[M+H]^+$ 377.5387, found 377.2986.

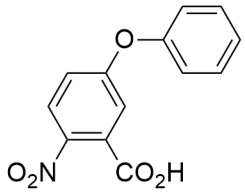

2-nitro-5-phenoxybenzoic acid (5a) (Scheme 3S-3). (4) (3.50 g, 18.9 mmol) was placed in in a pressure tube bottom flask with a stir bar, and purged with argon. Twenty mL of dry toluene was added, followed by the cesium carbonate (18.5 g, 56.7 mmol), and phenol (7.11 g, 75.6 mmol). The mixture was stirred at 110°C overnight. The progress of the reaction was monitored via TLC. The reaction was taken out of the oil bath for 10 minutes to cool and then diluted with 200 mL of 5% HCl and extracted with DCM (3×25mL). Dried over Na_2SO_4 and vacuum filtered. The filtrate was condensed. The product was crashed out in DCM and Hexanes. The product was condensed to afford 4.52 g of (92%) of **(5a)**. White crystals. ^{1}H NMR (500 MHz, Chloroform-*d*) δ 8.03 – 7.97 (m, 2H), 7.52 (dd, *J* = 7.8, 2.8 Hz, 2H), 7.49 – 7.42 (m, 1H), 7.36 (ddd, *J* = 9.0, 7.2, 2.8 Hz, 2H), 7.15 – 7.08 (m,

1H). ^{13}C NMR (151 MHz, $CDCl_3$) δ 168.97, 162.26, 130.76, 129.87, 126.92, 126.09, 120.79, 119.39, 117.64, 115.21, 77.44, 77.23, 77.02.

HRMS (ESI) m/z calculated for $C_{13}H_8NO_5$: $[M-H]^-$ 258.0408, found 258.0438

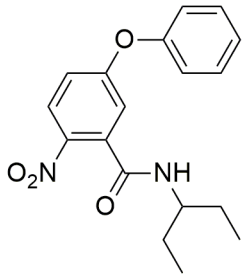

2-nitro-N-(pentan-3-yl)-5-phenoxybenzamide (8) (Scheme 3S-3). (5a) (1.06 g, 4.09 mmol) was transferred to a dry, Ar purged 100 mL round bottom flask, with a stir bar. This was dissolved in 20 mL of DCM, with 3 drops of DMF. The reaction mixture was cooled to -78°C and was stirred for 5 minutes. Then, (1.37 mL, 16 mmol) of oxalyl chloride was added dropwise, the stirred for 1 hr. The reaction was monitored via TLC by taking a few drops of reaction mixture and adding it to methanol. This would generate the ester from and move up the TLC plate. The reaction mixture was condensed 3 times, each time adding 20 mL of DCM. The condensed product was dissolved in 20 mL of DCM and cooled to -78°C for 5 min. 3-aminopentane (0.93 mL, 8 mmol) was added dropwise followed by *N*-methylmorpholine (NMM) (2.2 mL, 20 mmol). This was raised to room temperature and reacted overnight. Upon completion of the reaction, the mixture was quenched with 100 mL of 5% HCl. The mixture was extracted with DCM (3×25mL). The organic layer was dried Na_2SO_4 and condensed. The product was purified using flash chromatography (stationary phase: silica gel; eluent gradient: 0:10 (v:v) to 3:2 (v:v) of ethyl acetate and

hexanes in 200 mL increments. The product was condensed to afford 0.96 g (72%) of **(8)**. White crystals. ^{1}H NMR (500 MHz, Chloroform-*d*) δ 8.06 (d, *J* = 9.1 Hz, 1H), 7.43 (t, *J* = 8.0 Hz, 2H), 7.30 – 7.23 (m, 1H), 7.10 – 7.04 (m, 2H), 6.99 (d, *J* = 2.6 Hz, 1H), 6.96 (dd, *J* = 9.1, 2.7 Hz, 1H), 5.55 (d, *J* = 9.1 Hz, 1H), 3.94 (dtd, *J* = 8.9, 7.6, 3.8 Hz, 1H), 1.64 (dqd, *J* = 14.7, 7.4, 5.4 Hz, 2H), 1.54 – 1.43 (m, 2H), 0.96 (t, *J* = 7.4 Hz, 6H). ^{13}C NMR (151 MHz, $CDCl_3$) δ 169.00, 162.29, 130.79, 129.90, 126.95, 126.12, 120.82, 119.42, 117.67, 115.24, 77.47, 77.26, 77.05. HRMS (ESI) m/z calculated for $C_{18}H_{20}N_2NaO_4$: $[M+Na]^+$ 351.1321, found 351.1067.

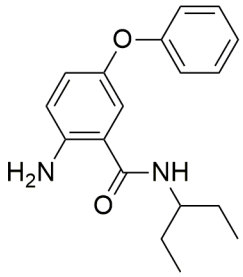

2-amino-N-(pentan-3-yl)-5-phenoxybenzamide (9) (Scheme 3S-3). (6) (400 mg, 2.94 mmol), Pd/C (60 mg, 15% by weight), and 5mL of ethyl acetate was transferred in a dry, Ar purged 100 mL round bottom flask with a stir bar. The round bottom was then vacuumed for 5 min. H_2 gas was attached to the round bottom and the reaction was stirred overnight. The reaction was then vacuumed filtered and condensed giving crude **(9)**. Black oil. HRMS (ESI) m/z calculated for $C_{18}H_{23}N_2O_2$: $[M+H]^+$ 299.1760, found 299.1658.

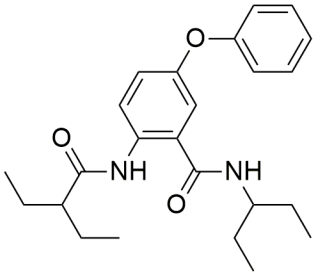

2-(2-ethylbutanamido)-N-(pentan-3-yl)-5-phenoxybenzamide (c, Fox) (Scheme 3S-3). 2-ethylbutyric acid (460 μL, 3.63 mmol) was placed in a 100 mL round bottom flask with a stir bar, and purged with argon. The reagent was dissolved in DCM, with 3 drops of DMF. The reaction mixture was cooled to -78°C and was stirred for 5 minutes. Then, (921 μL, 11.9 mmol) of oxalyl chloride was added dropwise, the stirred for 1 hr. The reaction was monitored via TLC by taking a few drops of reaction mixture and adding it to methanol. This would generate the ester from and move up the TLC plate. The reaction mixture was condensed 3 times, each time adding 20 mL of DCM. The condensed product was dissolved in 20 mL of DCM and cooled to -78°C for 5 min. **(9)** (1.21 mmol) was dissolved in DCM and added dropwise followed by NMM (2.00 mL, 18.5 mmol). This was raised to room temperature and reacted overnight. Upon completion of the reaction, the mixture was quenched with 100 mL of 5% HCl. The mixture was extracted with DCM (3×25mL). The organic layer was dried Na_2SO_4 and condensed. The product was purified using flash chromatography (stationary phase: silica gel; eluent gradient: 0:10 (v:v) to 2:3 (v:v) of ethyl acetate and hexanes in 200 mL increments. The product was condensed to afford 117 mg (25%) of **(Fox)**. White crystals. ^{1}H NMR (500 MHz, Chloroform-*d*) δ 8.06 (d, *J* = 9.0 Hz, 1H), 7.47 – 7.40 (m, 2H), 7.27 (td, *J* = 7.4, 1.2 Hz, 1H), 7.10 – 7.04 (m, 2H), 6.99 (d, *J* = 2.6 Hz, 1H), 6.96 (dd, *J* = 9.1, 2.7 Hz, 1H), 5.55 (d, *J* = 9.1 Hz, 1H), 3.94 (dtd, *J* = 8.9,

7.6, 3.8 Hz, 1H), 1.63 (dtd, *J* = 14.8, 7.4, 5.5 Hz, 2H), 1.54 – 1.43 (m, 2H), 0.96 (t, *J* = 7.4 Hz, 6H). ^{13}C NMR (151 MHz, $CDCl_3$) δ 180.66, 175.05, 168.39, 160.00, 157.58, 151.74, 135.06, 130.04, 123.76, 123.47, 123.40, 123.04, 118.19, 117.43, 77.44, 77.23, 77.02, 53.22, 52.95, 52.91, 48.71, 27.68, 27.38, 25.96, 24.99, 12.18, 11.94, 10.48, 10.41. HRMS (ESI) m/z calculated for $C_{24}H_{32}N_2NaO_3$: $[M+Na]^+$ 419.2311, found 419.2108

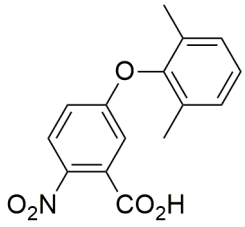

5-(2,6-dimethylphenoxy)-2-nitrobenzoic acid (5b) (Scheme 3S-4). (4) (1.85 g, 10 mmol), was placed in in a pressure tube bottom flask with a stir bar, and purged with argon. Twenty mL of dry toluene was added, followed by the cesium carbonate (4.9 g, 56.7 mmol), and 2,6-Dimethylphenol (2.44 g, 20 mmol). The mixture was stirred at 110°C overnight. The progress of the reaction was monitored via TLC. The reaction was taken out of the oil bath for 10 minutes to cool and then diluted with 200 mL of 5% HCl and extracted with DCM (3×25mL). Dried over Na_2SO_4 and vacuum filtered. The filtrate was condensed. The product was crashed out in DCM and hexanes at room temperature. The product was condensed to afford 1.21 g of (42%) of **(5b)**. Light yellow crystals. ^{1}H NMR (500 MHz, Chloroform-*d*) δ 7.98 (d, *J* = 9.0 Hz, 1H), 7.13 (d, *J* = 16.6 Hz, 4H), 6.92 (dd, *J* = 9.0, 2.6 Hz, 1H), 2.12 (s, 6H). ^{13}C NMR (126 MHz, $cdcl_3$) δ 171.02, 161.70, 150.04, 141.25, 130.91, 130.31, 129.76, 127.20, 126.58, 116.96, 115.68, 77.51, 77.26, 77.00, 16.39. HRMS (ESI) m/z calculated for $C_{15}H_{12}NO_5$: $[M-H]^-$ 286.0721, found 286.0756.

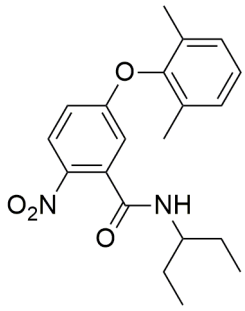

5-(2,6-dimethylphenoxy)-2-nitro-N-(pentan-3-yl)benzamide (10) (Scheme 3S-4). (5b) (9.87 g, 34 mmol) was transferred to a dry, Ar purged 150 mL round bottom flask, with a stir bar. This was dissolved in 40 mL of DCM, with 3 drops of DMF. The reaction mixture was cooled to -78°C and was stirred for 5 minutes. Then, (6.9 mL, 80 mmol) of oxalyl chloride was added dropwise, the stirred for 1 hr. The reaction was monitored via TLC by taking a few drops of reaction mixture and adding it to methanol. This would generate the ester from and move up the TLC plate. The reaction mixture was condensed 3 times, each time adding 20 mL of DCM. The condensed product was dissolved in 20 mL of DCM and cooled to -78°C for 5 min. 3-aminopentane (4.7 mL, 40 mmol) was added dropwise followed by NMM (11 mL, 100 mmol). This was raised to room temperature and reacted overnight. Upon completion of the reaction, the mixture was quenched with 200 mL of 5% HCl. The mixture was extracted with DCM (3×50mL). The organic layer was dried Na_2SO_4 and condensed. The product was purified using flash chromatography (stationary phase: silica gel; eluent gradient: 0:10 (v:v) to 3:2 (v:v) of ethyl acetate and hexanes in 400 mL increments. The product was condensed to afford 3.19 g (26%) of **(10)**. Light yellow

powder. ^{1}H NMR (600 MHz, Chloroform-*d*) δ 13.21 – 13.15 (m, 1H), 12.28 (d, *J* = 4.6 Hz, 3H), 12.10 (dd, *J* = 4.7, 2.6 Hz, 1H), 11.84 (ddt, *J* = 6.7, 4.6, 2.7 Hz, 1H), 10.81 (dd, *J* = 9.4, 4.9 Hz, 1H), 9.11 (h, *J* = 7.2, 5.1 Hz, 1H), 7.28 – 7.23 (m, 6H), 6.85 – 6.76 (m, 2H), 6.65 (dtt, *J* = 14.4, 7.5, 3.8 Hz, 2H), 6.13 (tt, *J* = 7.5, 3.7 Hz, 6H). ^{13}C NMR (126 MHz, cdcl$_3$) δ 166.30, 163.03, 149.94, 136.48, 136.13, 132.85, 130.25, 128.52, 127.52, 121.07, 116.28, 115.95, 77.49, 77.23, 76.98, 53.11, 27.28, 21.03, 16.14, 10.35. HRMS (ESI) m/z calculated for $C_{20}H_{24}N_2NaO_4$: $[M+Na]^+$ 379.1628, found 379.1608.

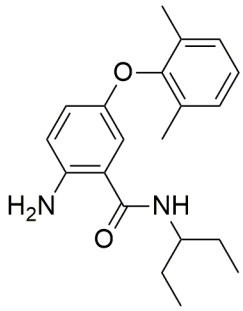

2-amino-5-(2,6-dimethylphenoxy)-N-(pentan-3-yl)benzamide (11) (Scheme 3S-4). (10) (3.19 g, 8.97 mmol), Pd/C (1.6 g, 15% by weight), and 15 mL of ethyl acetate was transferred in a dry, Ar purged 100 mL round bottom flask with a stir bar. The round bottom was then vacuumed for 5 min. H_2 gas was attached to the round bottom and the reaction was stirred overnight. The reaction was then vacuumed filtered and condensed giving crude **(11)**. Black oil. HRMS (ESI) m/z calculated for $C_{20}H_{24}N_2NaO_2$: $[M+Na–2H]^+$ 347.1735, found 347.0353.

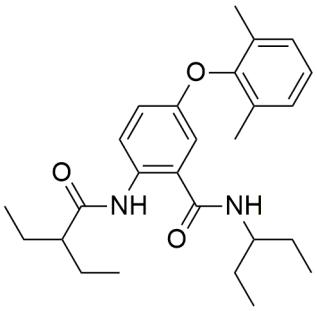

5-(2,6-dimethylphenoxy)-2-(2-ethylbutanamido)-N-(pentan-3-yl)benzamide (d, Dox) (Scheme 3S-4, Chart 3-1d). 2-ethylbutyric acid (2.3 mL, 18 mmol) was placed in a 100 mL round bottom flask with a stir bar, and purged with argon. The reagent was dissolved in DCM, with 3 drops of DMF. The reaction mixture was cooled to -78°C and was stirred for 5 minutes. Then, (3.0 mL, 36 mmol) of oxalyl chloride was added dropwise, the stirred for 1 hr. The reaction was monitored via TLC by taking a few drops of reaction mixture and adding it to methanol. This would generate the ester from and move up the TLC plate. The reaction mixture was condensed 3 times, each time adding 20 mL of DCM. The condensed product was dissolved in 20 mL of DCM and cooled to -78°C for 5 min. **(1)** (8.97 mmol) was dissolved in DCM and added dropwise followed by NMM (5.0 mL, 45 mmol). This was raised to room temperature and reacted overnight. Upon completion of the reaction, the mixture was quenched with 100 mL of 5% HCl. The mixture was extracted with DCM (3×25mL). The organic layer was dried Na_2SO_4 and condensed. The product was purified using flash chromatography (stationary phase: silica gel; eluent gradient: 0:10 (v:v) to 3:2 (v:v) of ethyl acetate and hexanes in 200 mL increments. The product was condensed to afford 1.10 g (29%) of **Dox**. White crystals ^{1}H NMR (600 MHz, Chloroform-*d*) δ 10.49 (s, 1H), 8.36 (d, *J* = 9.1 Hz, 1H), 7.10 (d, *J* = 6.3 Hz, 1H), 7.09 – 7.05 (m, 1H),

7.04 (d, *J* = 2.8 Hz, 1H), 6.59 (dd, *J* = 9.1, 2.8 Hz, 1H), 5.81 (d, *J* = 9.1 Hz, 1H), 3.95 (dt, *J* = 9.0, 5.2 Hz, 1H), 2.11 (s, 6H), 2.07 (dt, *J* = 9.3, 5.1 Hz, 1H), 1.72 – 1.61 (m, 5H), 1.57 – 1.51 (m, 2H), 1.51 – 1.43 (m, 2H), 0.93 (dt, *J* = 14.8, 7.4 Hz, 12H). ^{13}C NMR (151 MHz, $CDCl_3$) δ 174.80, 168.65, 153.24, 150.86, 132.93, 131.52, 129.38, 125.67, 123.98, 123.84, 116.91, 113.07, 77.44, 77.23, 77.02, 52.91, 27.73, 26.03, 16.56, 12.24, 10.50. HRMS (ESI) m/z calculated for $C_{26}H_{35}N_2O_3$: $[M-H]^-$ 423.5667, found 423.2622.

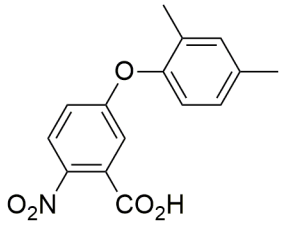

5-(2,4-dimethylphenoxy)-2-nitrobenzoic acid (5c) (Scheme 3S-5). (4) (1.89 g, 10 mmol), was placed in in a pressure tube bottom flask with a stir bar, and purged with argon. Twenty mL of dry toluene was added, followed by the cesium carbonate (4.9 g, 56.7 mmol), and 2,4-Dimethylphenol (2.4 mL, 20 mmol). The mixture was stirred at 110°C overnight. The progress of the reaction was monitored via TLC. The reaction was taken out of the oil bath for 10 minutes to cool and then diluted with 200 mL of 5% HCl and extracted with DCM (3×25mL). Dried over Na_2SO_4 and vacuum filtered. The filtrate was condensed. The product was crashed out in DCM and hexanes at room temperature. The product was purified using flash chromatography (stationary phase: silica gel; eluent gradient: 0:10 (v:v) to 6:4 (v:v) of ethyl acetate and hexanes in 200 mL increments. At the 1:1 (v:v) gradient, 1% of acetic acid was added to the elution. The product was condensed to afford 2.36 g of (88%) of **(5c)**. Tan powder. ^{1}H NMR (500 MHz, Chloroform-*d*) δ 7.98

(d, *J* = 9.0 Hz, 1H), 7.12 (t, *J* = 2.9 Hz, 2H), 7.07 (dd, *J* = 8.2, 2.2 Hz, 1H), 7.01 (dd, *J* = 9.0, 2.7 Hz, 1H), 6.90 (d, *J* = 8.1 Hz, 1H), 2.36 (s, 3H), 2.13 (s, 3H). ^{13}C NMR (126 MHz, cdcl$_3$) δ 170.39, 162.59, 149.89, 141.27, 136.26, 132.96, 130.24, 130.02, 128.67, 127.01, 121.12, 118.14, 116.38, 77.49, 77.23, 76.98, 21.06, 16.14. HRMS (ESI) m/z calculated for $C_{15}H_{12}NO_5$: $[M–H]^-$ 286.0721, found 286.0722.

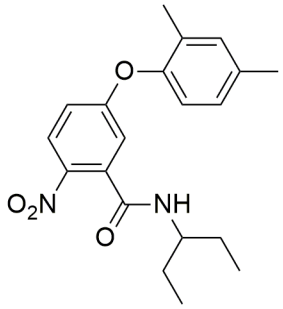

5-(2,4-dimethylphenoxy)-2-nitro-N-(pentan-3-yl)benzamide (12) (Scheme 3S-5). (5c) (1.99 g, 7.52 mmol) was transferred to a dry, Ar purged 100 mL round bottom flask, with a stir bar. This was dissolved in 20 mL of DCM, with 3 drops of DMF. The reaction mixture was cooled to -78°C and was stirred for 5 minutes. Then, (2.5 mL, 30.1 mmol) of oxalyl chloride was added dropwise, the stirred for 1 hr The reaction was monitored via TLC by taking a few drops of reaction mixture and adding it to methanol. This would generate the ester from and move up the TLC plate. The reaction mixture was condensed 3 times, each time adding 20 mL of DCM. The condensed product was dissolved in 20 mL of DCM and cooled to -78°C for 5 min. 3-aminopentane (1.8 mL, 15 mmol) was added dropwise followed by NMM (4.1 mL, 37.6 mmol). This was raised to room temperature and reacted overnight. Upon completion of the reaction, the mixture was quenched with 200 mL of 5%

HCl. The mixture was extracted with DCM (3×50mL). The organic layer was dried Na_2SO_4 and condensed. The product was purified using flash chromatography (stationary phase: silica gel; eluent gradient: 0:10 (v:v) to 3:2 (v:v) of ethyl acetate and hexanes in 400 mL increments. The product was condensed to afford 1.83 g (64%) of **(12)**. Light yellow crystals. ^{1}H NMR (500 MHz, Chloroform-*d*) δ 8.04 (d, *J* = 9.1 Hz, 1H), 7.11 (d, *J* = 2.2 Hz, 1H), 7.04 (dd, *J* = 8.2, 2.2 Hz, 1H), 6.96 (d, *J* = 2.7 Hz, 1H), 6.86 (d, *J* = 8.1 Hz, 1H), 6.80 (dd, *J* = 9.1, 2.7 Hz, 1H), 5.46 (d, *J* = 9.1 Hz, 1H), 3.97 (dtt, *J* = 9.0, 7.6, 5.5 Hz, 1H), 2.35 (s, 3H), 2.12 (s, 3H), 1.65 (dddd, *J* = 14.9, 13.0, 7.5, 5.5 Hz, 2H), 1.56 – 1.44 (m, 2H), 0.98 (t, *J* = 7.4 Hz, 6H). ^{13}C NMR (151 MHz, $CDCl_3$) δ 166.31, 163.02, 149.93, 139.74, 136.47, 136.12, 132.84, 130.24, 128.52, 127.50, 121.06, 116.28, 115.94, 77.44, 77.23, 77.02, 53.10, 27.26, 21.02, 16.13, 10.34. HRMS (ESI) m/z calculated for $C_{20}H_{24}N_2NaO_4$: $[M+Na]^+$ 379.1634, found 379.0181.

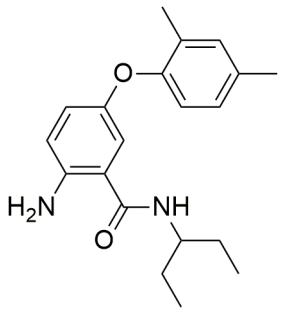

2-amino-5-(2,4-dimethylphenoxy)-N-(pentan-3-yl)benzamide (13) (Scheme 3S-5). (12) (2.41 g, 6.76 mmol), Pd/C (362 mg, 15% by weight), and 15 mL of ethyl acetate was transferred in a dry, Ar purged 100 mL round bottom flask with a stir bar. The round bottom was then vacuumed for 5 min. H_2 gas was attached to the round bottom and the reaction

was stirred overnight. The reaction was then vacuumed filtered and condensed giving crude **(13)**. Black oil. HRMS (ESI) m/z calculated for $C_{20}H_{26}N_2NaO_2$: $[M+Na]^+$ 349.1892, found 348.9783.

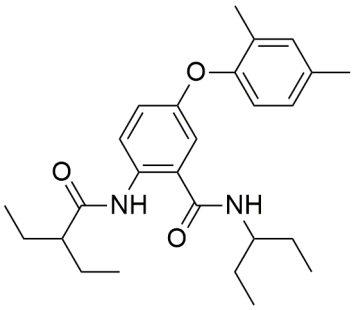

5-(2,4-dimethylphenoxy)-2-(2-ethylbutanamido)-N-(pentan-3-yl)benzamide (e, Dox$_{24}$) (Scheme 3S-5). HATU (3.6 g, 9.47 mmol), and HOAt (1.4 g, 9.47 mmol), 2-ethylbutaric acid (1.2 mL, 9.47 mmol), DIPEA (1.2 mL, 9.47 mmol) was dissolved in 20 mL of DMF in a dry, argon purged 100 mL round bottom flask with a stir bar. This was stirred for 15 minutes and then **(13)** (6.76 mmol) was transferred and stirred overnight. The progress of the reaction was monitored via TLC. The mixture quenched with 100 mL saturated Na_2CO_3 was extracted with ethyl acetate (3×50mL). The organic layer was dried Na_2SO_4 and condensed. The product was purified using flash chromatography (stationary phase: silica gel; eluent gradient: 0:10 (v:v) to 1: (v:v) of ethyl acetate and hexanes in 400 mL increments.to afford 1.66 g (58%) of **(Dox$_{24}$)**. White crystals. ^{1}H NMR (500 MHz, Chloroform-*d*) δ 10.61 (s, 1H), 8.46 (d, *J* = 9.1 Hz, 1H), 7.08 (dd, *J* = 9.7, 2.5 Hz, 2H), 6.96 (dd, *J* = 8.1, 2.2 Hz, 1H), 6.87 (dd, *J* = 9.1, 2.8 Hz, 1H), 6.74 (d, *J* = 8.2 Hz, 1H), 5.77 (d, *J* = 9.2 Hz, 1H), 3.95 (ddt, *J* = 13.5, 8.3, 4.3 Hz, 1H), 2.31 (s, 3H), 2.19 (s, 3H), 2.11

(tt, *J* = 9.0, 5.3 Hz, 1H), 1.75 – 1.61 (m, 4H), 1.60 – 1.51 (m, 2H), 1.46 (dt, *J* = 13.8, 7.5 Hz, 2H), 0.94 (td, *J* = 7.4, 4.2 Hz, 12H). ^{13}C NMR (126 MHz, cdcl$_3$) δ 174.89, 168.54, 153.16, 152.28, 133.98, 132.43, 129.50, 127.93, 123.72, 123.49, 120.50, 119.20, 115.53, 77.49, 77.23, 76.98, 52.92, 27.73, 26.01, 20.91, 16.30, 12.23, 10.49. HRMS (ESI) m/z calculated for $C_{26}H_{35}N_2O_3$: $[M-H]^-$ 423.2653, found 423.2646.

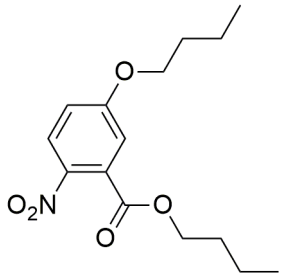

butyl 5-butoxy-2-nitrobenzoate (2a). (1) (1.8 g, 10 mmol), was placed in in a pressure tube bottom flask with a stir bar, and purged with argon. Fifteen mL of 2ME was added, followed by the cesium carbonate (4.89 g, 15 mmol), and 1-iodobutane (2.3 mL, 20 mmol). The mixture was stirred at 130°C overnight. The progress of the reaction was monitored via TLC. The reaction was taken out of the oil bath for 10 minutes to cool and then diluted with 200 mL of 5% HCl and extracted with DCM (3×25mL). Dried over Na_2SO_4 and vacuum filtered. The filtrate was condensed. The product was purified using flash chromatography (stationary phase: silica gel; eluent gradient: 0:10 (v:v) to 1:1 (v:v) of ethyl acetate and hexanes in 200 mL increments. The product was condensed to afford 10 mg (0.3%) of **(2a)**. Brown oil. ^{1}H NMR (500 MHz, Chloroform-*d*) δ 7.98 (d, *J* = 9.0 Hz, 1H), 7.01 (d, *J* = 2.7 Hz, 1H), 6.97 (dd, *J* = 9.0, 2.7 Hz, 1H), 4.31 (t, *J* = 6.7 Hz, 2H), 4.04

(t, J = 6.4 Hz, 2H), 1.82 – 1.64 (m, 4H), 1.53 – 1.34 (m, 4H), 0.94 (dt, J = 15.0, 7.4 Hz, 6H). HRMS (ESI) m/z calculated for $C_{15}H_{20}NO_5$: $[M-H]^-$ 294.1347, found 294.3283.

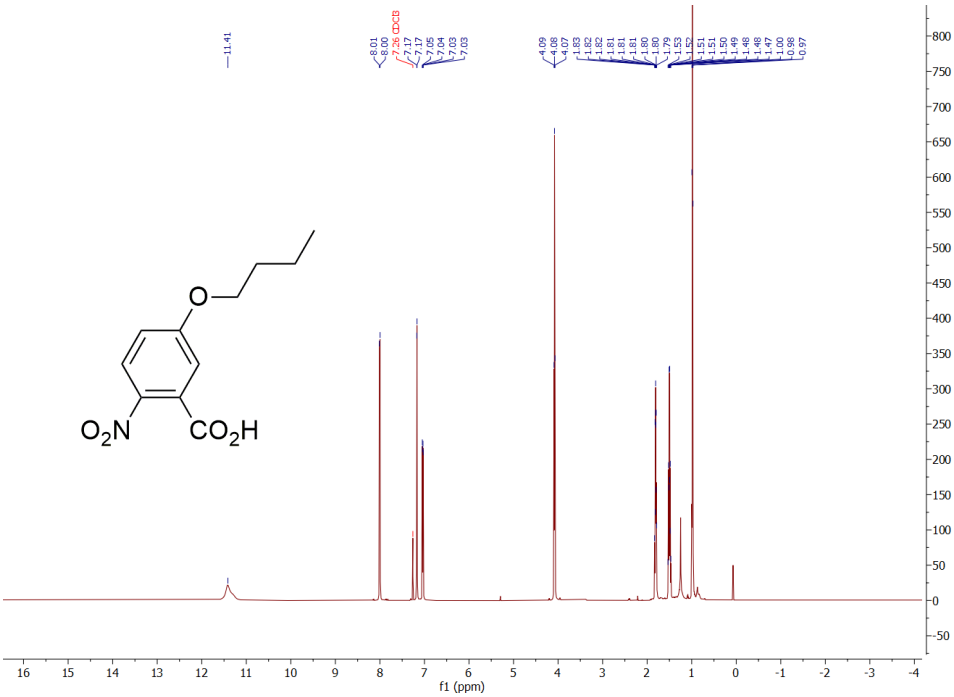

a

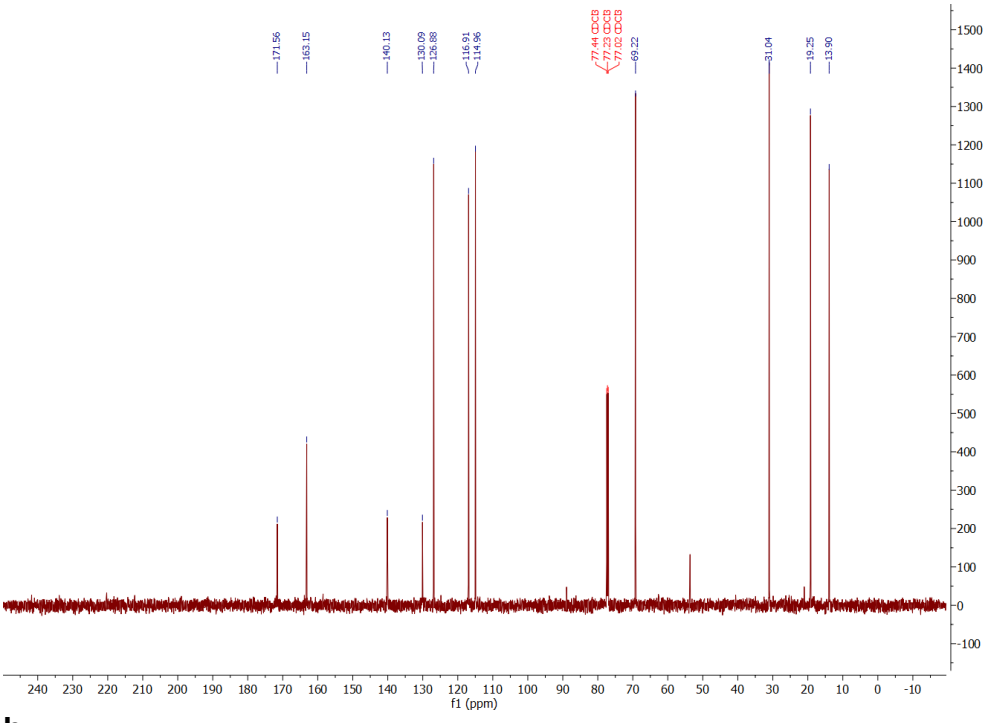

b

Figure 3S-1. (a) ^{1}H NMR of **(3a)** (600 MHz, $CDCl_3$); (b) ^{13}C NMR of **(3a)** (151 MHz, $CDCl_3$).

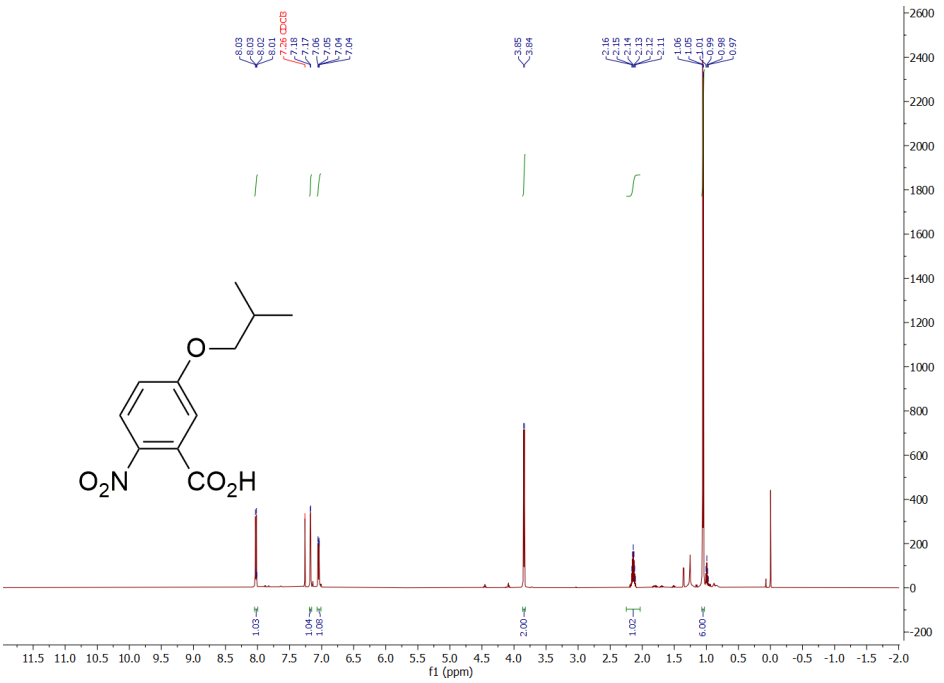

a

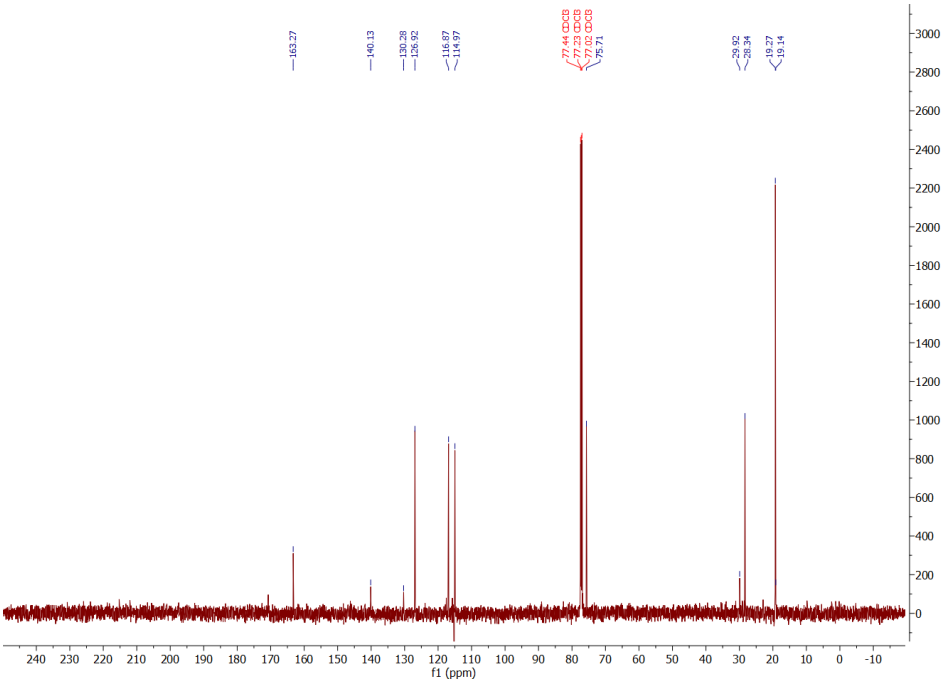

b

Figure 3S-2. (a) ^{1}H NMR of **(3b)** (600 MHz, $CDCl_3$); (b) ^{13}C NMR of **(3b)** (151 MHz, $CDCl_3$).

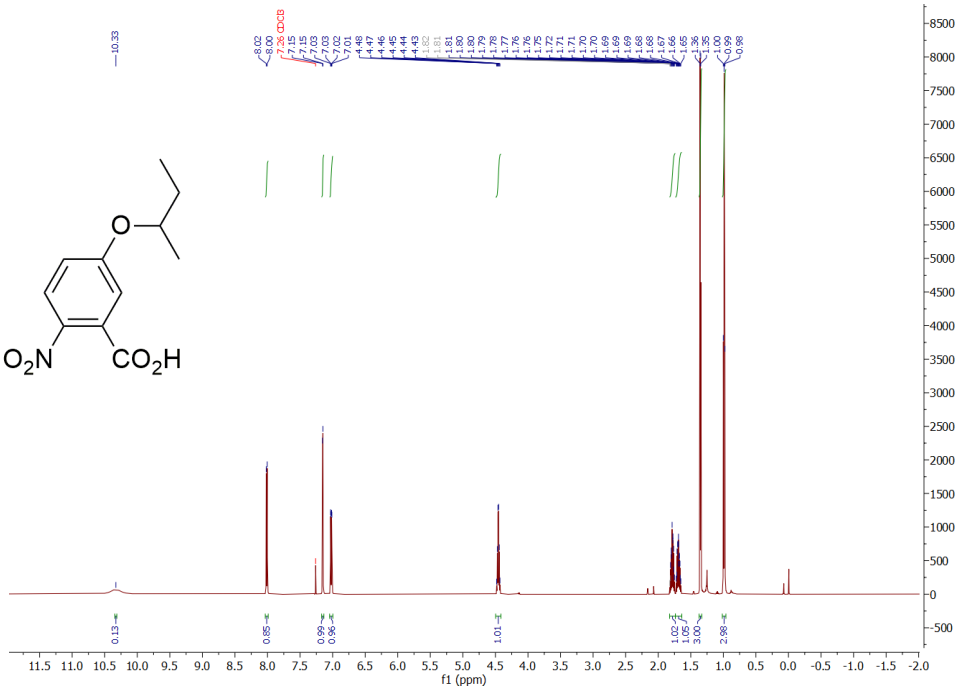

a

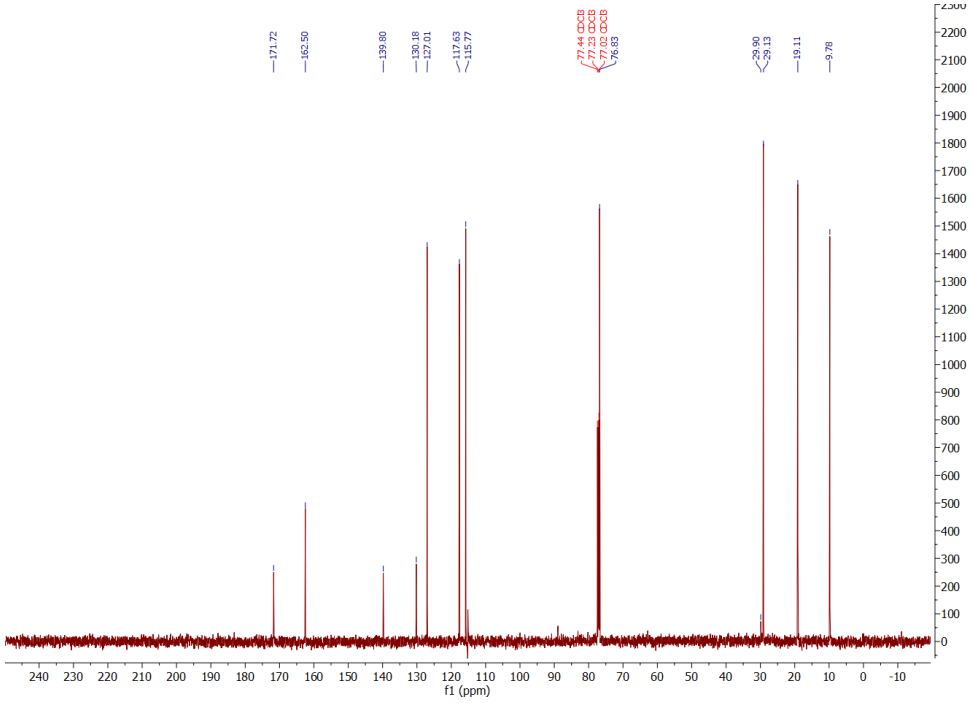

b

Figure 3S-3. (a) ^{1}H NMR of **(3c)** (600 MHz, $CDCl_3$); (b) ^{13}C NMR of **(3c)** (151 MHz, $CDCl_3$).

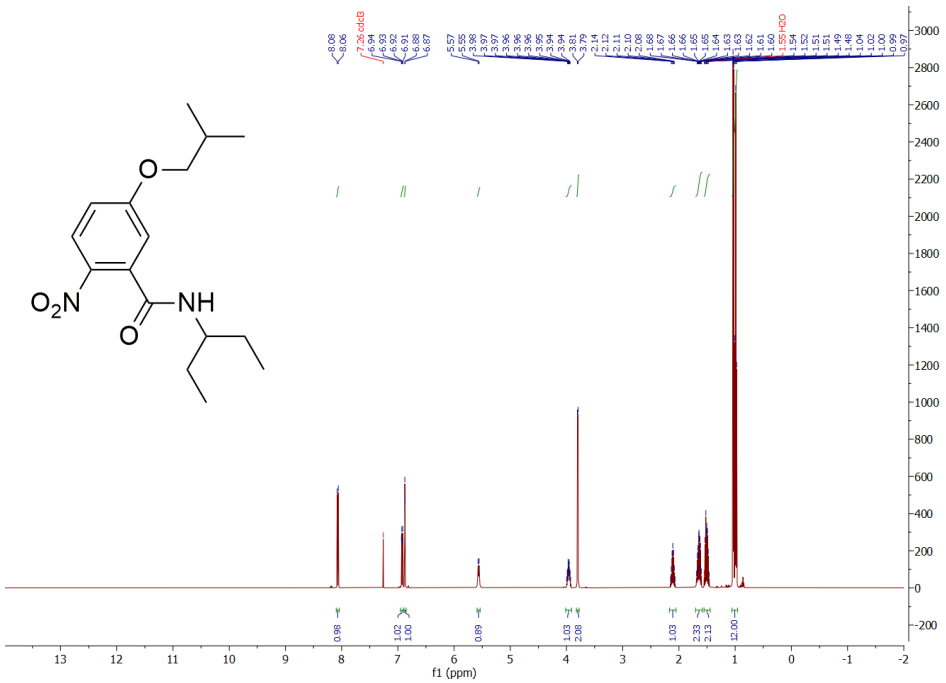

a

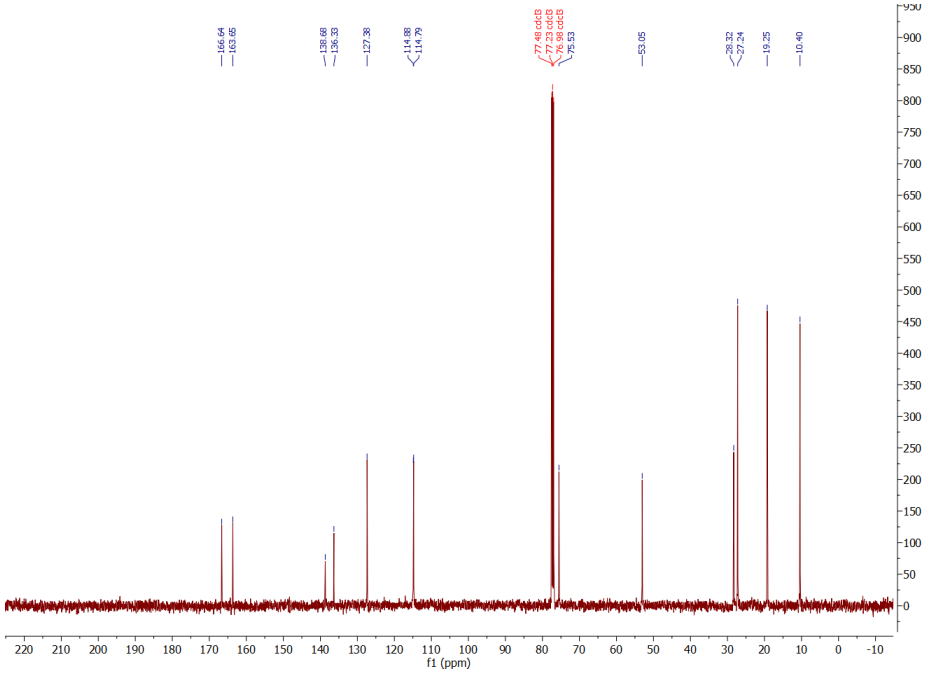

b

Figure 3S-4. (a) ^{1}H NMR of **(6)** (500 MHz, $CDCl_3$); (b) ^{13}C NMR of **(6)** (126 MHz, $CDCl_3$).

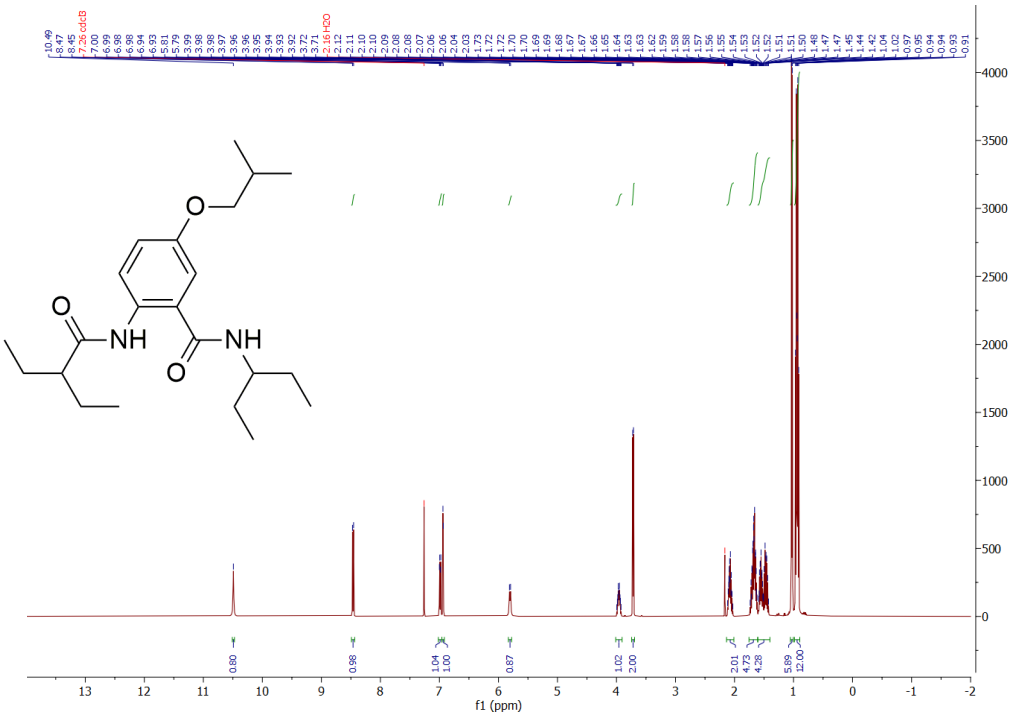

a

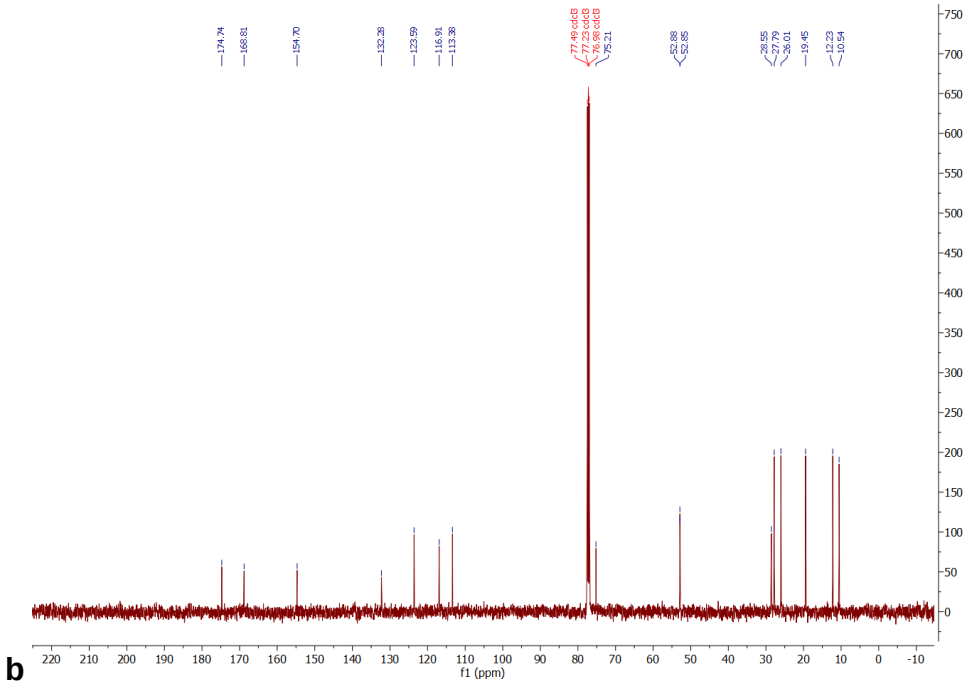

b

Figure 3S-5. (a) ^{1}H NMR of **(b, Box)** (500 MHz, $CDCl_3$); (b) ^{13}C NMR of **(b)** (126 MHz, $CDCl_3$).

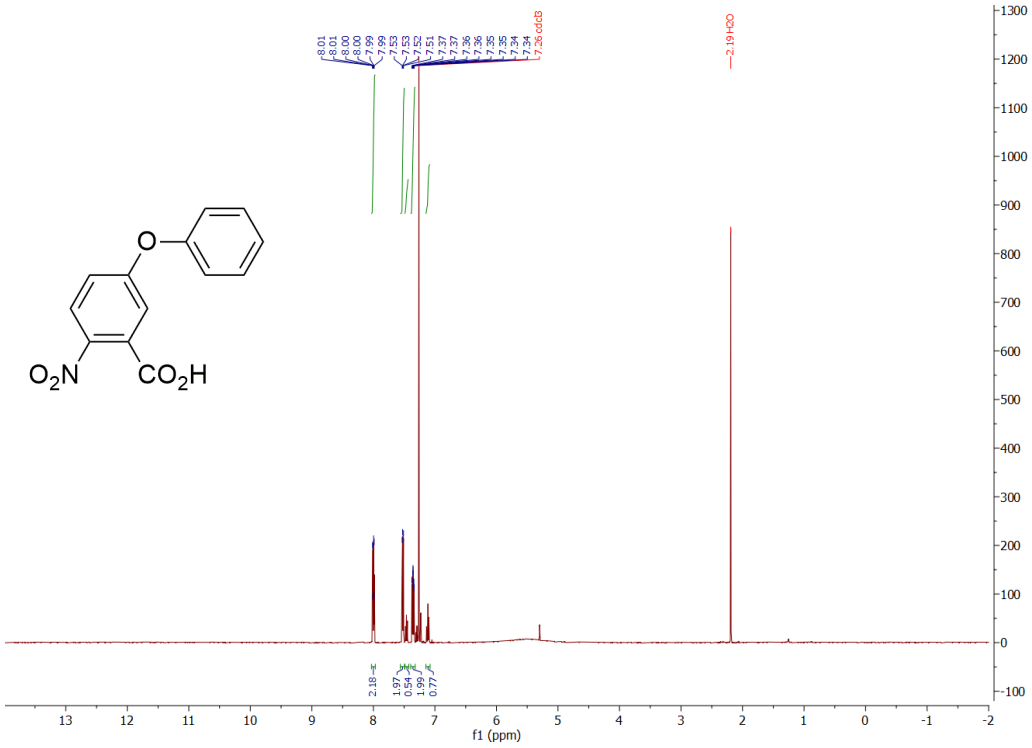

a

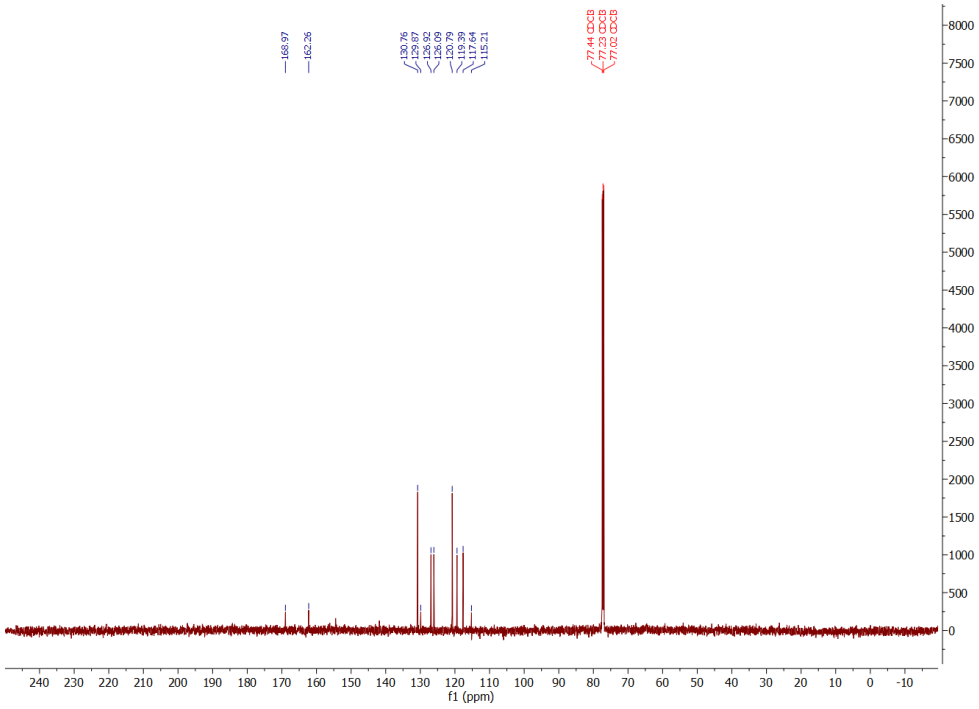

b

Figure 3S-6. (a) ^{1}H NMR of **(5a)** (500 MHz, $CDCl_3$); (b) ^{13}C NMR of **(5a)** (151 MHz, $CDCl_3$).

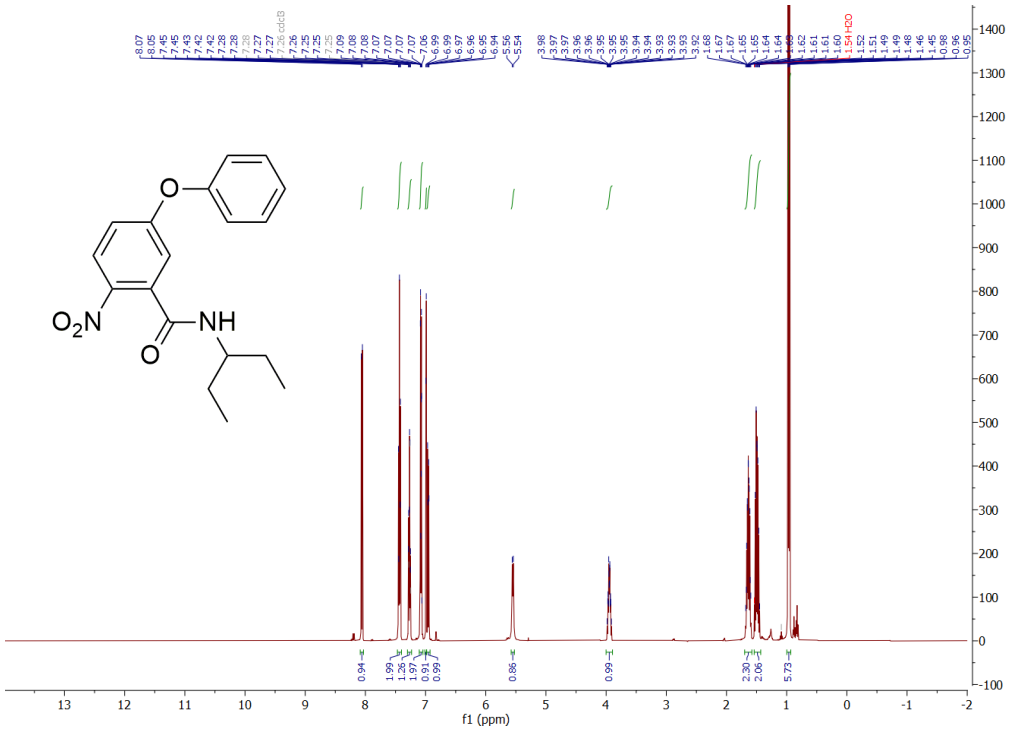

a

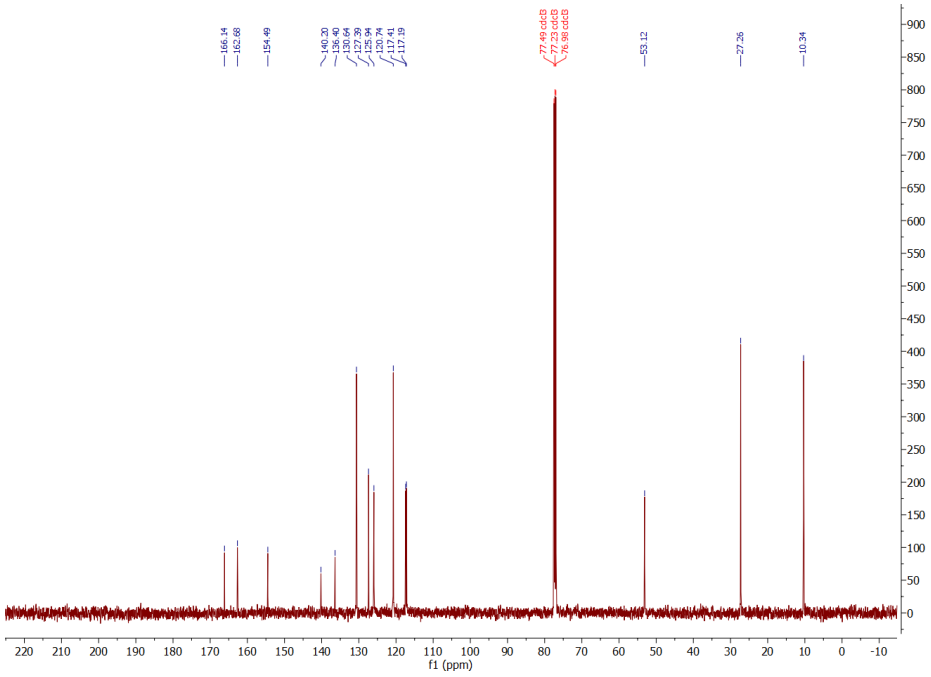

b

Figure 3S-7. (a) ^{1}H NMR of **(8)** (500 MHz, $CDCl_3$); (b) ^{13}C NMR of **(8)** (151 MHz, $CDCl_3$).

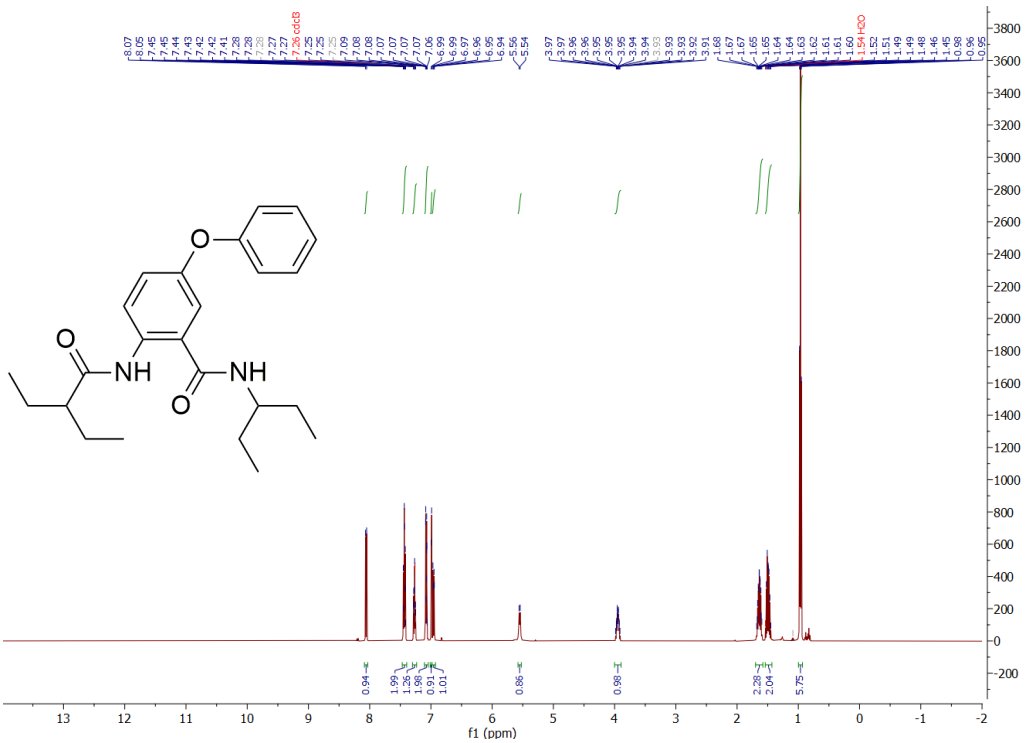

a

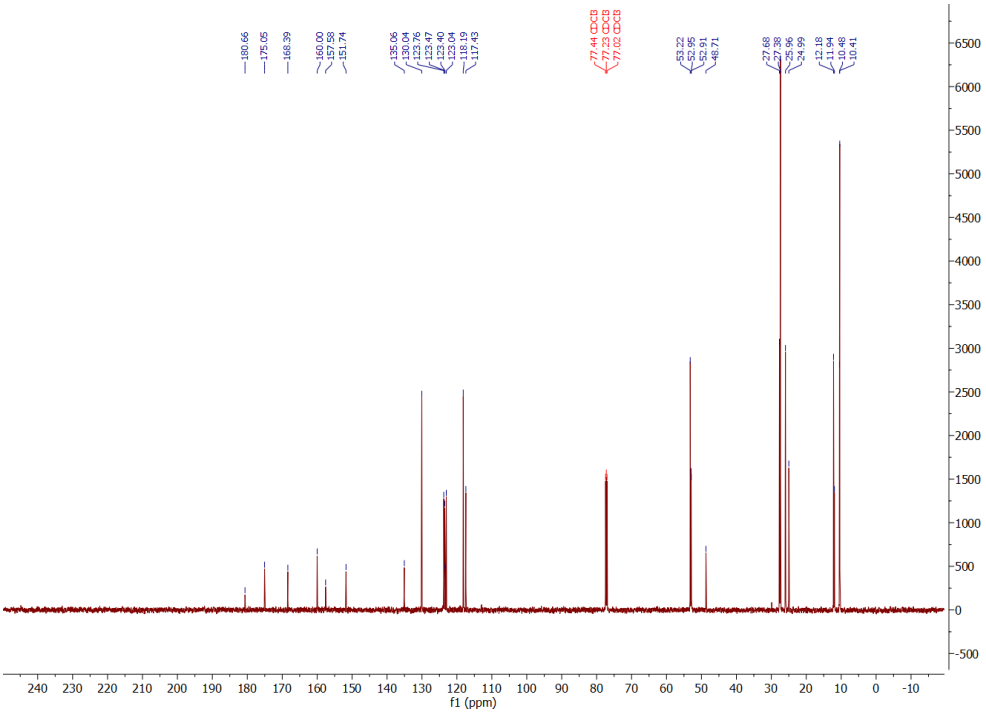

b

Figure 3S-8. (a) ^{1}H NMR of **(c, Fox)** (600 MHz, $CDCl_3$); (b) ^{13}C NMR of **Fox** (126 MHz, $CDCl_3$).

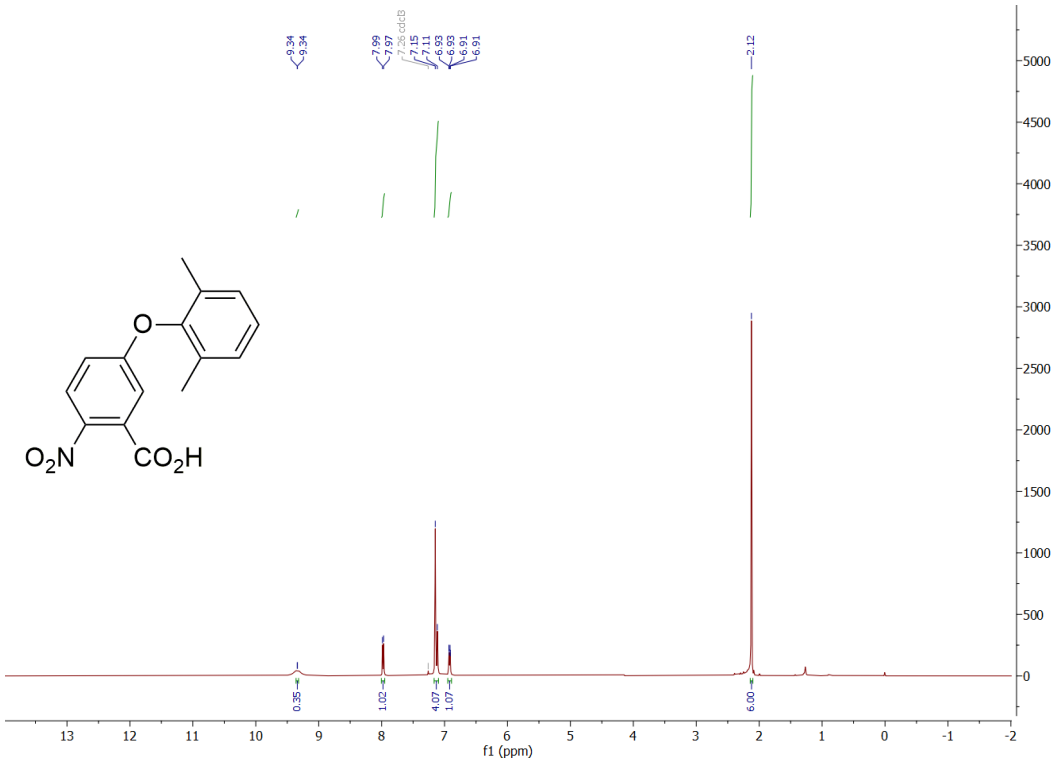

a

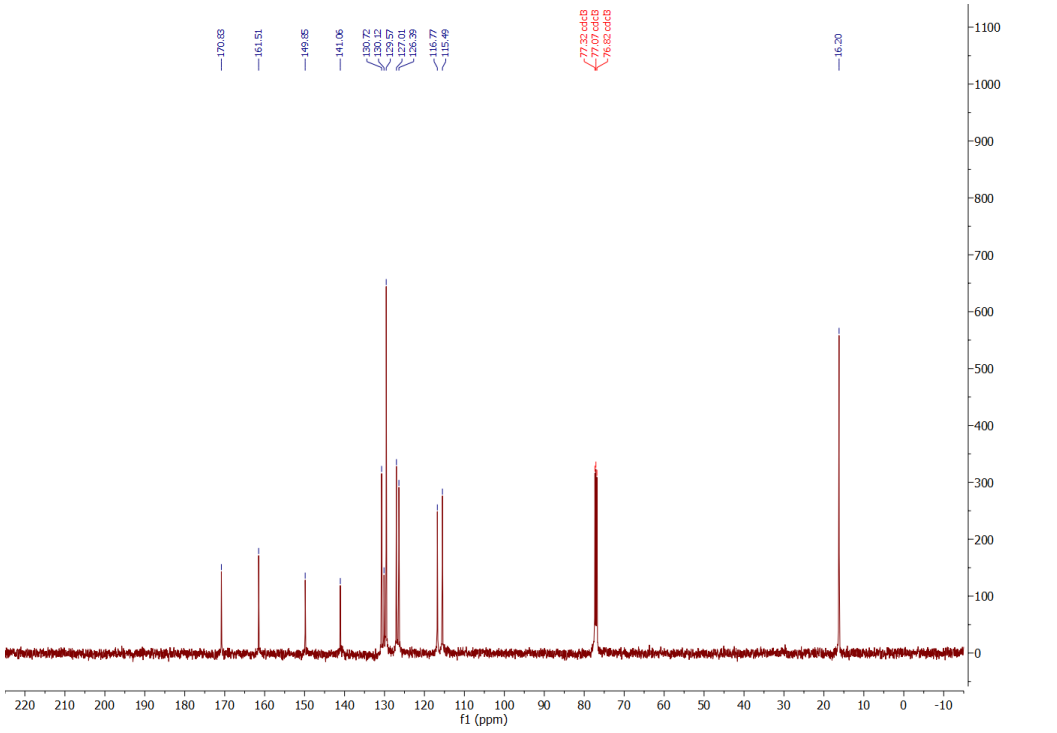

b

Figure 3S-9. (a) ^{1}H NMR of **(5b)** (500 MHz, $CDCl_3$); (b) ^{13}C NMR of **(5b)** (126 MHz, $CDCl_3$).

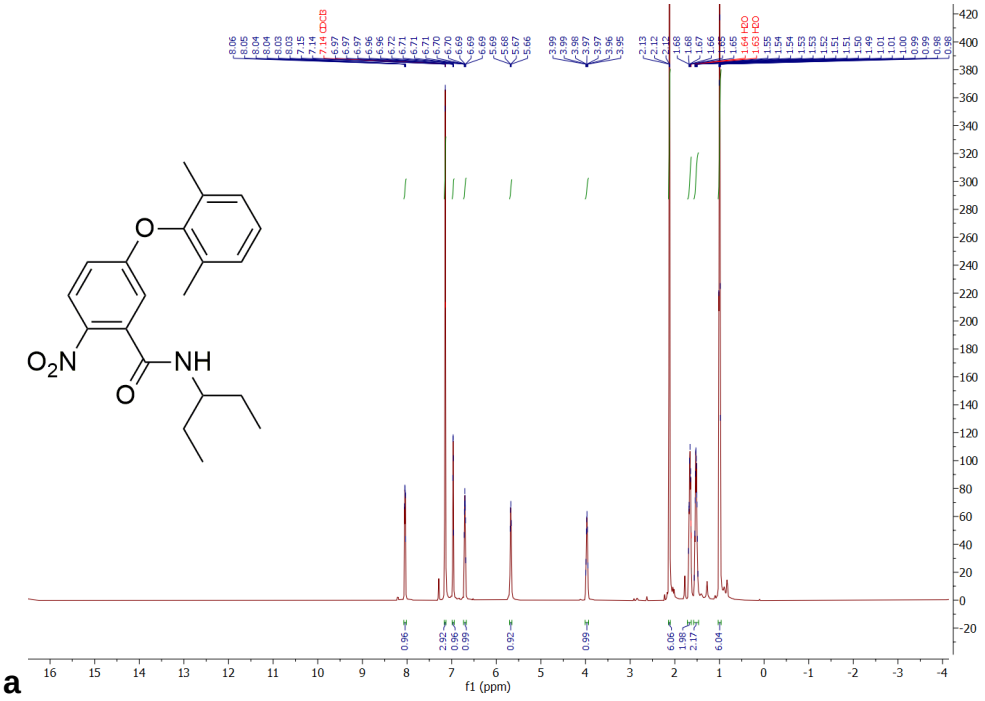

a

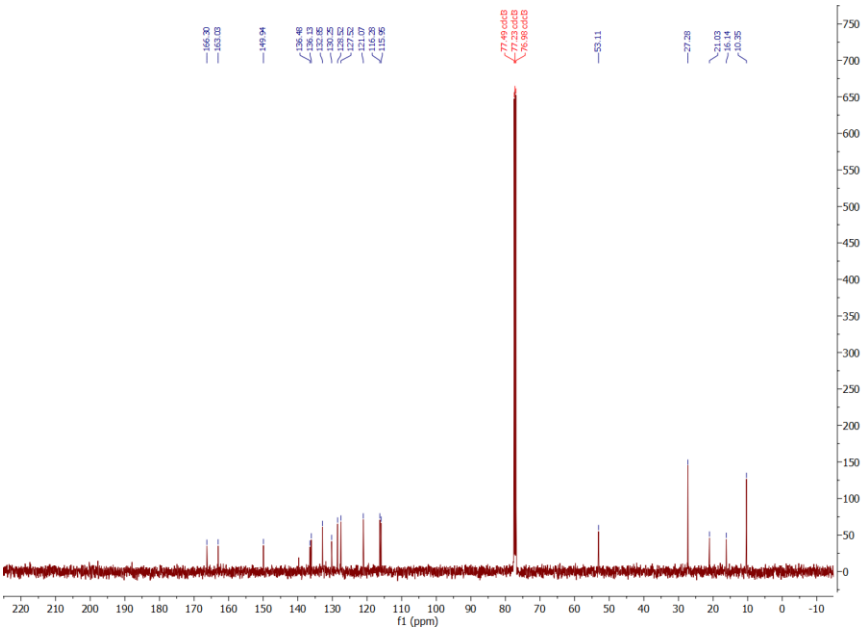

b

Figure 3S-10. (a) ^{1}H NMR of **(10)** (600 MHz, $CDCl_3$); (b) ^{13}C NMR of **(10)** (126 MHz, $CDCl_3$).

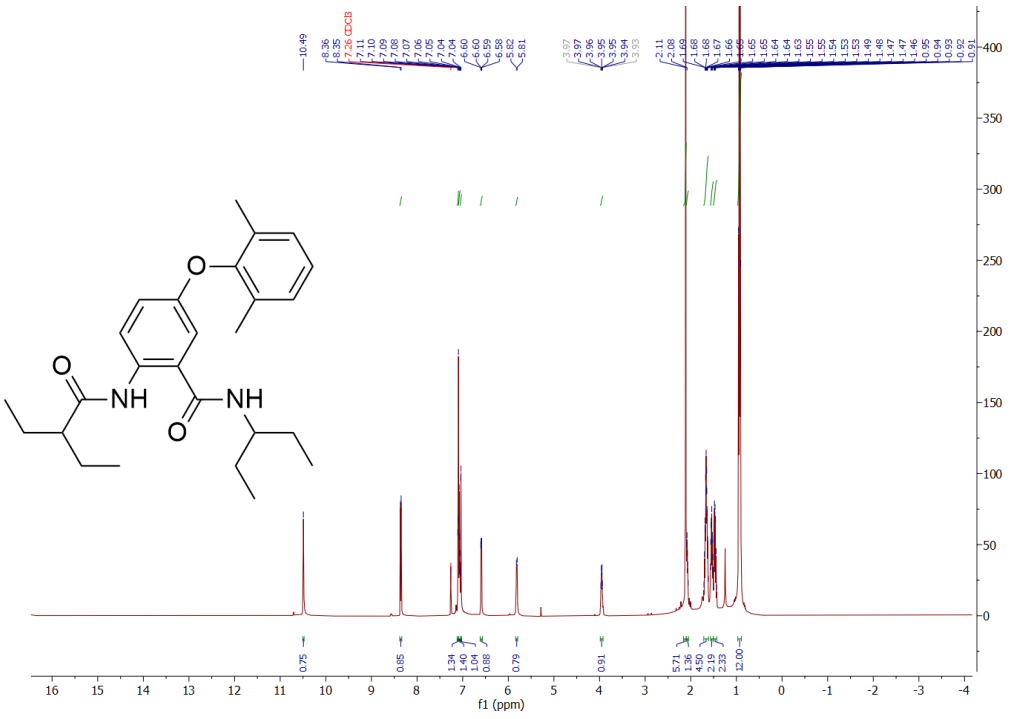

a

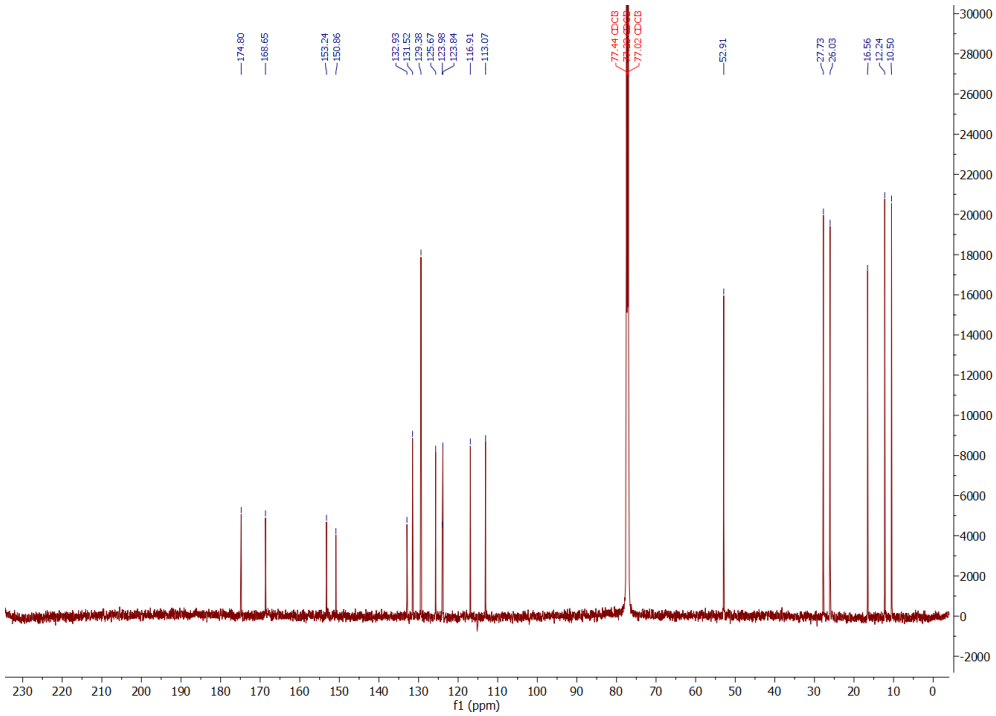

b

Figure 3S-11. (a) ^{1}H NMR of **(d, Dox)** (500 MHz, $CDCl_3$); (b) ^{13}C NMR of **Dox** (151 MHz, $CDCl_3$).

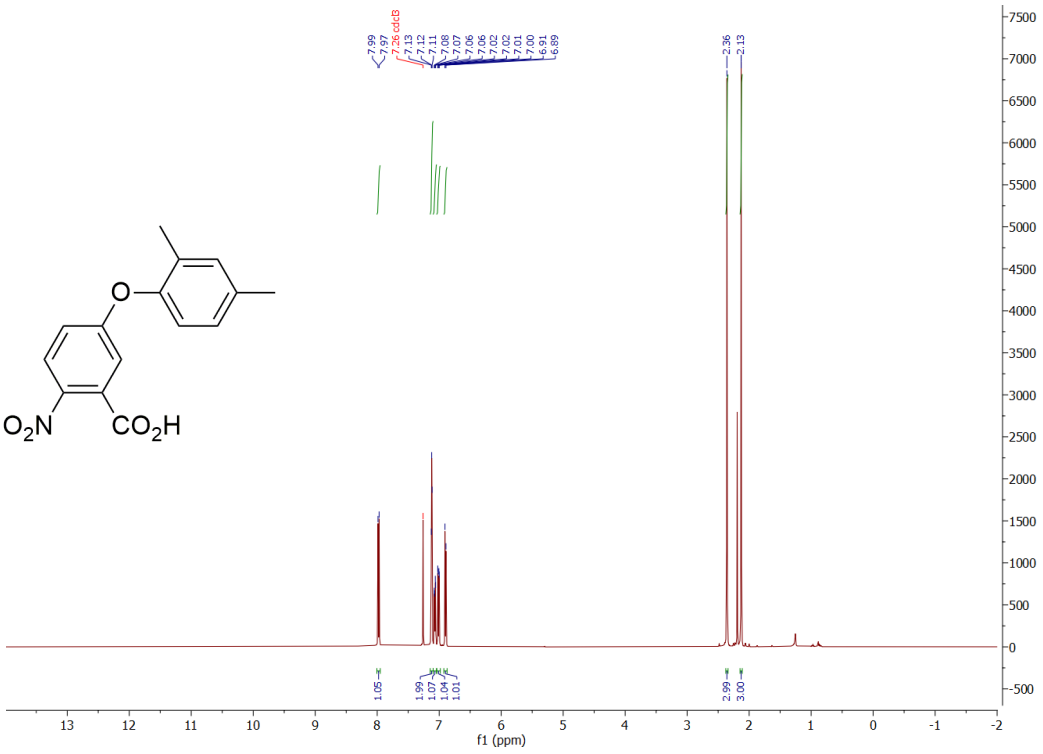

a

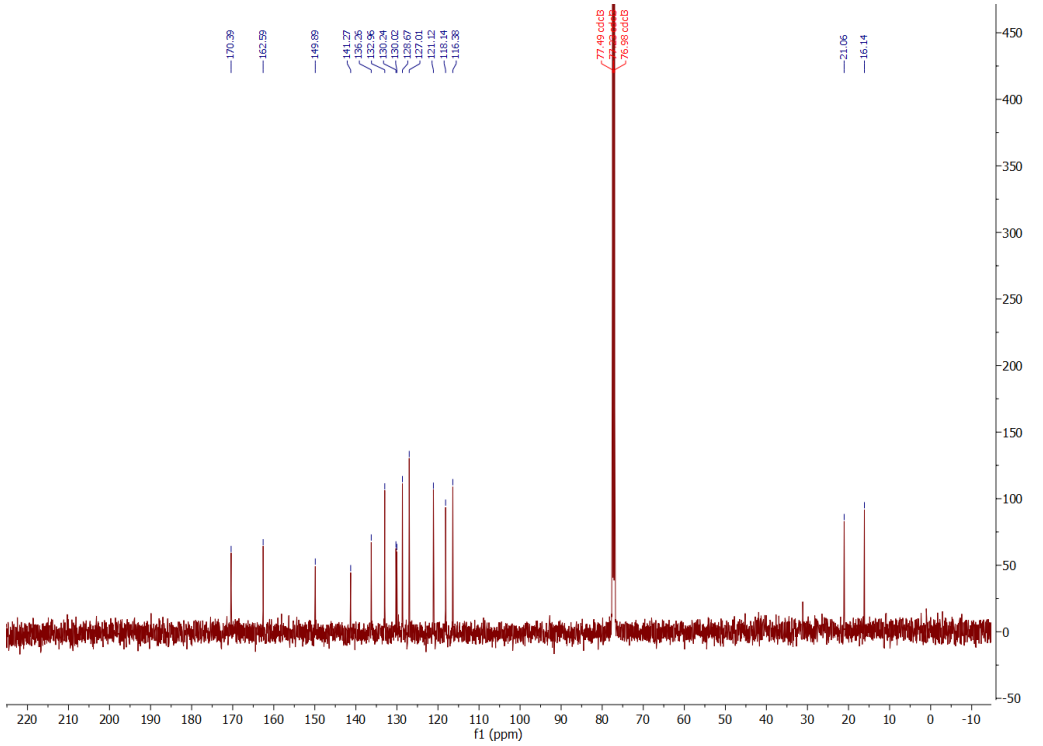

b

Figure 3S-12. (a) ^{1}H NMR of **(5c)** (500 MHz, $CDCl_3$); (b) ^{13}C NMR of **(5c)** (126 MHz, $CDCl_3$).

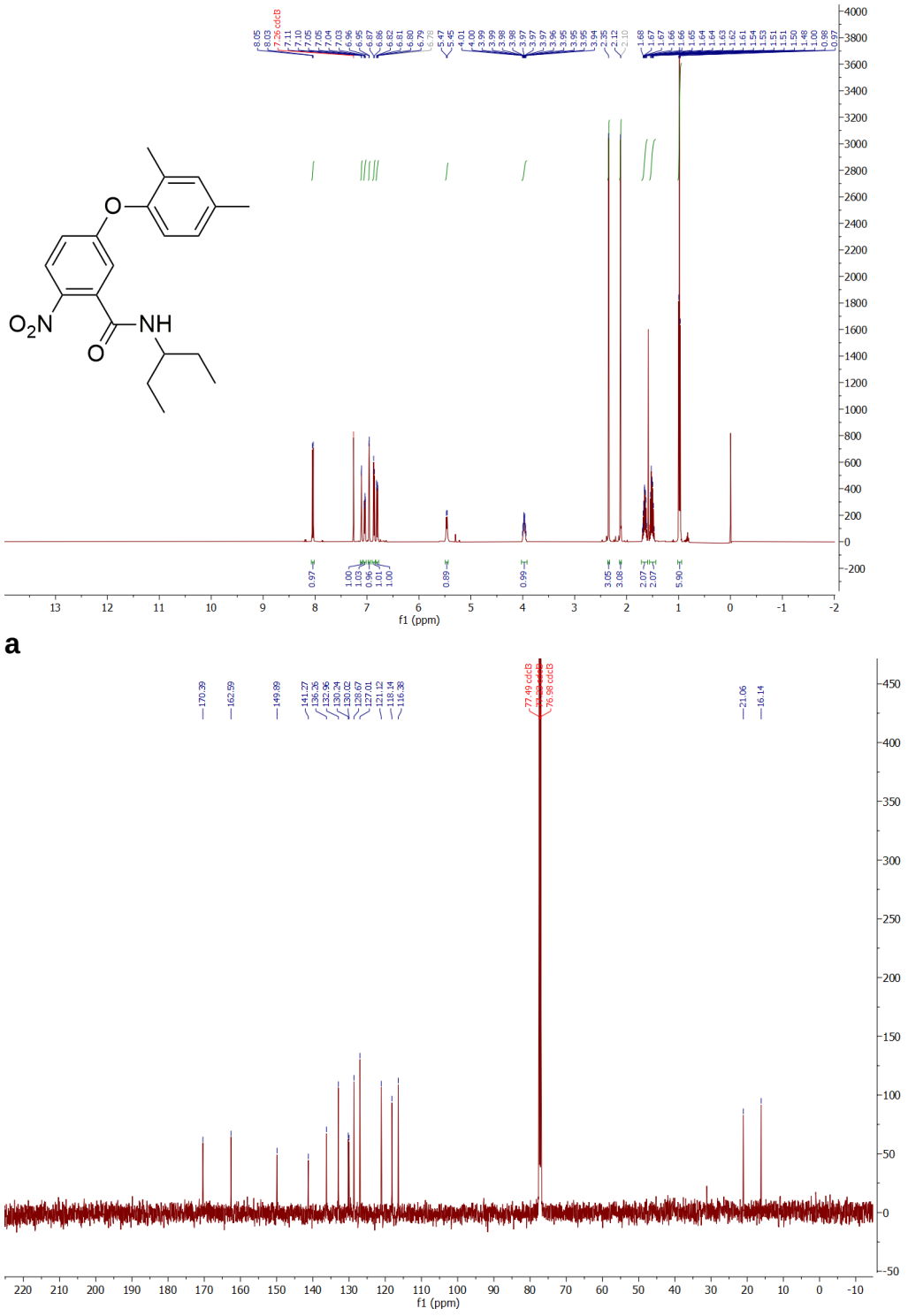

Figure 3S-13. (a) ^{1}H NMR of **(12)** (500 MHz, $CDCl_3$); (b) ^{13}C NMR of **(12)** (151 MHz, $CDCl_3$).

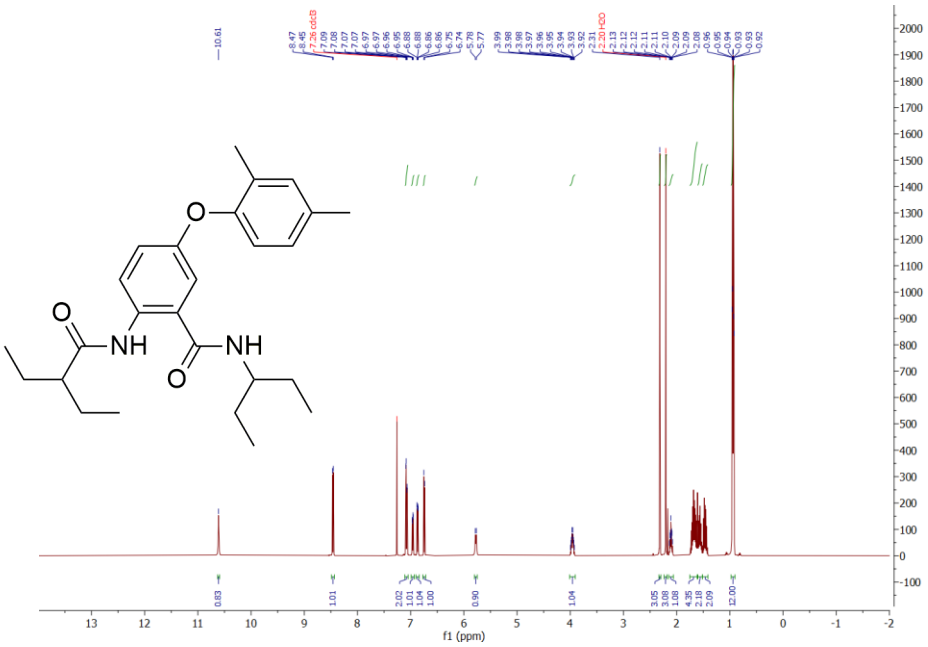

a

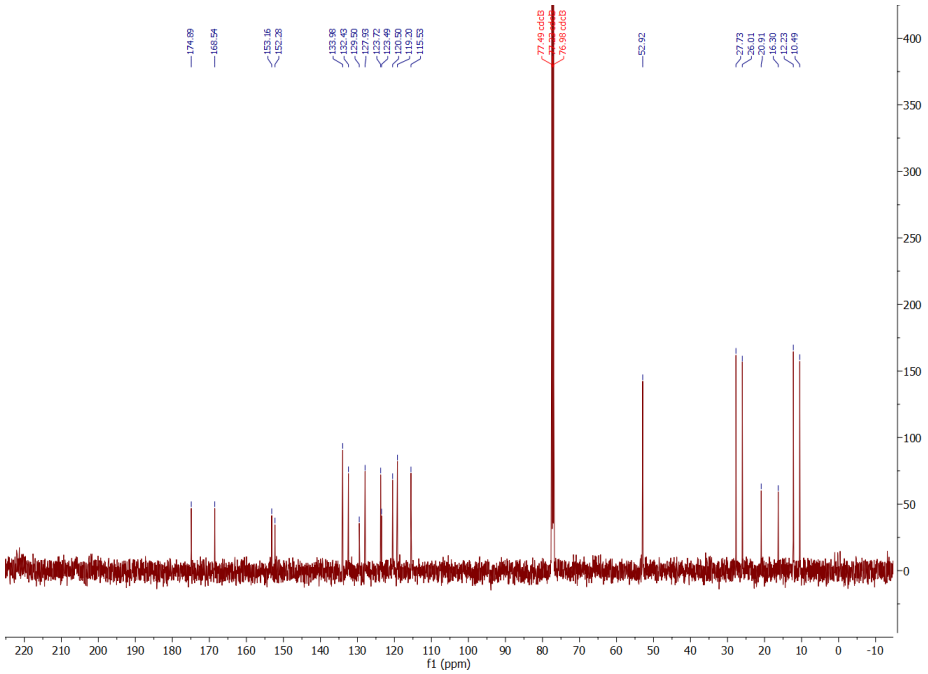

b

Figure 3S-14. (a) ^{1}H NMR of **(e, Dox$_{24}$)** (500 MHz, $CDCl_3$); (b) ^{13}C NMR of **Dox$_{24}$** (126 MHz, $CDCl_3$).

Proofs for the selective formation of ethers, rather than esters. Etherification in 2ME selectively produces the ether derivatives of 2-nitrobenziuc acid, **3** (Scheme 3-1a), as one-dimensional NMR spectra and HRMS confirm. The products of etherification of the hydroxyl and esterification of the carboxyl of 5-hydroxy-2-nitrobenzoic acid, however, have similar ^{1}H and ^{13}C NMR spectra and identical exact masses obtainable by HRMS analysis. Therefore, we resort to through-space correlation structural analysis, as implemented by NOESY, to examine if products **3** are ethers or esters. For comparison, we prepare the disubstituted (ether, ester) derivatives, **2** (Scheme 3-1), using conventional heating.

The NOESY spectrum of the product, **3a**, from reacting **1** with *n*-butyl halides in 2ME under microwave radiation (Scheme 3-1a, 3S-1) shows correlations between the α-proton of the butyl chain, b_1, and the anthranilic protons at positions 4 and 6, a_4 and a_6 (Chart 3S-1a, Figure 3S-15). A through-space NOE correlation between a_6 and b_1 (Chart 3S-1a) is, indeed, plausible regardless if the butyl is coupled as ether at position 5 or as ester with the carboxyl at position 1. Observing an NOE correlation between a_4 and b_1 (Chart 3S-1a, Figure 3S-15), however, is highly unlikely if the butyl is bonded to the carboxyl as an ester. Therefore, the through-space correlation between a_4 and b_1 suggests that treating 2-nitrobenzoic acid, **1**, with alkyl halide in 2ME leads to selective formation of ether derivatives, **3** (Scheme 3-1a, 3S-1)

To further assure that the products from reacting **1** with alkyl halides in 2ME leads to ethers, rather than esters, we undertake NOE analysis of ether ester derivative, **2**, with R = *n*-C_4H_9. The NOESY spectra of **2a** reveal that both α-butyl protons, b_1 and c_1, show strong

correlations with the other alkyl protons, but only one of them correlates with aryl protons a_4 and/or a_6 (Chart 3-S1, Figure 3S-16). These findings are consistent with assigning the proton that correlates with a_4 and a_6 to the α-butyl protons to the ether alkyl chain. The other α-butyl protons belong to the ester alkyl chain (Chart 3S-1b). It suggests that most prevailing conformer of **2a** is the one in which the butyl of the ester is pointing away from the aromatic ring, and the relaxation of c_1 through c_2 and c_3 dominates, making the NOE correlation between c_1 and a_6 (Figure 3S-16b).

Reacting **3** with amines, under carboxyl-activating conditions, produces amide with good yields, e.g., **10** (Scheme 3S-2). Esters with free hydroxyl groups cannot produce amides under such conditions. Therefore, **3** must have free carboxylate and the butyl chain has to be attached to the hydroxyl at position 5 in order obtaining amides, such as 10, to be possible. That is, the products **3** are ether derivatives.

Chart 3S-1. Structures of **(3a)** and **(2a)** with key through-space correlations obtained from the NOESY analysis (Figure 3S-15b, 3S-16b).

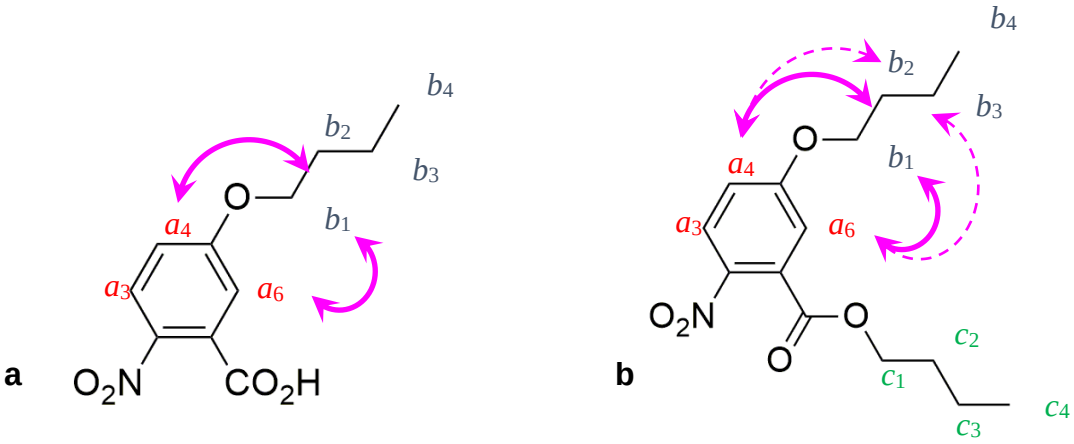

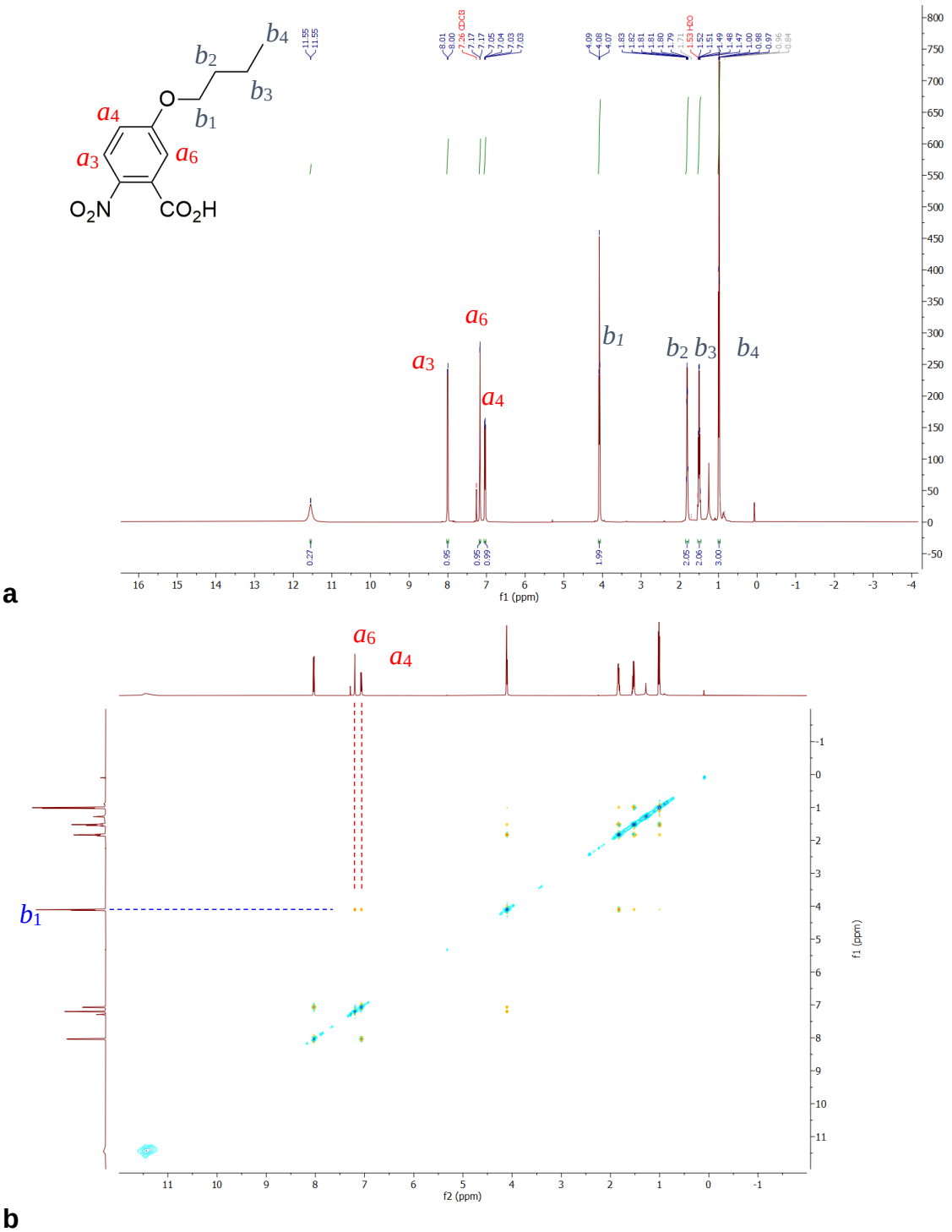

Figure 3S-15. (a) ^{1}H NMR and (b) NOESY spectra of **(3a)** (600 MHz, $CDCl_3$).

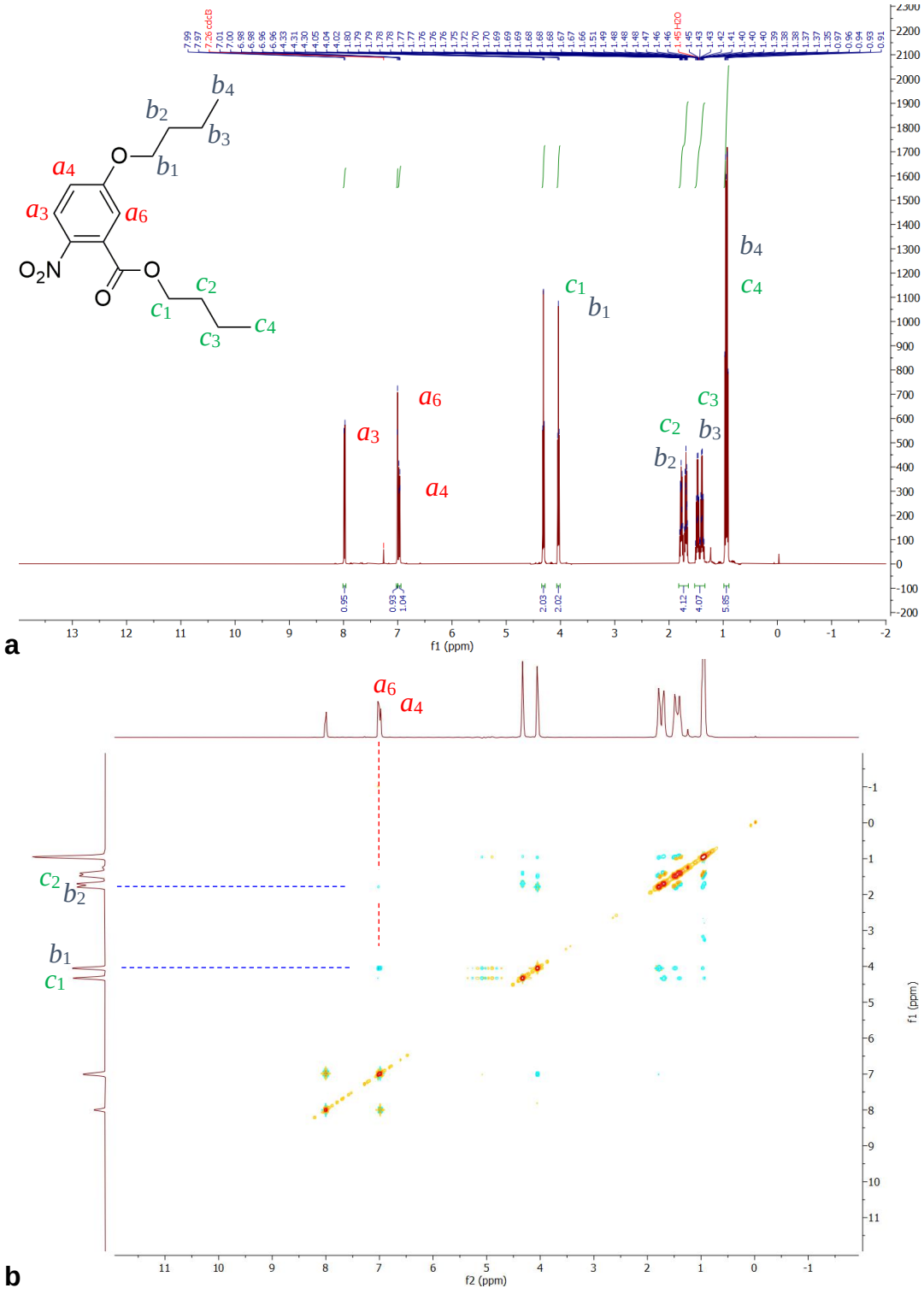

Figure 3S-16. (a) ^{1}H NMR and (b) NOESY spectra of **(2a)** (500 MHz, $CDCl_3$).

***Syn* and *anti* conformers of Dox.** DFT computational analysis reveals that *anti* conformers of the phenoxy Aa residues are energetically slightly more stable than the *syn* conformers (Table 3S-3). This finding is consistent with the steric hindrance between the phenoxy side chains at position 5 and the amide at position 1 (Figure 3S-16). Nevertheless, the energy difference between the *syn* and *anti* conformers of Dox, $\Delta\mathscr{E}$(Dox), is smaller that k_BT for room temperature. Furthermore, polarizable and polar solvating media depletes these energy differences, i.e., $\Delta\mathscr{E}(\text{Dox}) \rightarrow 0$ (Table 3S-3). These findings indicate that at room temperature both conformers of Dox should be present in significant amounts under thermodynamic equilibrium. For the gas phase, for example, $\Delta\mathscr{E}$(Dox) = 17 meV that indicates for 66% *anti* and 34% *sin* conformers of Dox. The solvent-induced decrease in $\Delta\mathscr{E}$(Dox) decreases the difference between the equilibrium concentrations of the two conformers to less than 20% difference, i.e., $|[anti] / [syn]| < 1.5$. Oxidizing the phenoxy Aa residues slightly increases the difference between the energy of *syn* and *anti* conformers, as apparent from the differences between the ionization energies, ΔIE, that are larger than $\Delta\mathscr{E}$(Table 3S-3).

Despite the computationally predicted abundance of both *anti* and *syn* conformers (Table 3S-3), the ^{1}H and ^{13}C NMR spectra of Dox reveal a single set of chemical shifts for the methyls at positions 2 and 6, for the protons and the carbons at positions 3 and 5, and for the carbons at position 2 and 6 of the 2,6-dimethylphenyloxy group (Figure 3S-11). These results suggest that (1) either the synthesis produced only one of the *syn* or *anti* isomer of Dox that remains conformationally locked; or (2) the exchange between the *syn* and *anti* conformers is faster than the NMR acquisition timescales. NOESY spectra of Dox

do not reveal any though-space correlations between the phenyloxy protons at positions 3, 4 and 5 and the other protons of the Dox molecule. This NOESY result, therefore, does not provide information about the conformer(s) present in the Dox solutions. Mechanistic consideration of the nucleophilic aromatic substation used for preparing the precursor for Dox suggest that the only plausible way for obtaining only a single isomers, *anti*, is if (1) phenolate attack the aromatic carbon (to replace the fluorine) equatorially, with the two six-member rings orthogonal to each other; and (2) the carboxylate completely prevents the attack from the direction of position 6 that produces the *syn* conformer. Both *syn* and *anti* conformers, however, are present in considerable amounts (Table 3S-3), suggesting that the amide or carboxyl group at position 1 cannot completely prevent the Dox precursors from assuming *syn* geometry. That is, the carboxyl group, however, is not large enough to completely prevent such attack and the *syn* conformer should still form in detectable amounts. Because the NMR spectra do not reveal two separate isomers, we conclude that the *syn* and *anti* Dox interexchange and these conformational transformation occur in the millisecond range or faster.

Table 3S-3. Differences between the energies of the *syn* and *anti* conformers of the Aa ether derivatives.

	$\Delta\mathscr{E}$(Aa) / eV [a]			ΔIE / eV [b]		
	gas phase	CH_2Cl_2 [c]	CH_3CN [c]	gas phase	CH_2Cl_2 [c]	CH_3CN [c]
Fox	< 0.010	< 0.010	< 0.010	0.050	0.015	0.010
Dox	0.017	< 0.010	< 0.010	0.042	0.013	< 0.010
Dox$_{24}$	0.014	< 0.010	< 0.010	0.064	0.027	0.020

[a] ΔE = E (*syn*) – E (*anti*): The E (*syn*) and E (*anti*) are of the DFT-optimized structures of the ground-states of the conformers. Hartree-Fock calculations also yield E (*syn*) > E (*anti*), but with ΔE ≲ 5 meV for all cases; [c] From the computed ionization energies (IE) of the conformers, i.e., ΔIE = IE(*syn*) – IE(*anti*). Using Koopmans' theorem allows for estimating IE from the difference between the computed energies of the doublet (singly oxidized) and the ground-state singlet states. [d.] Implemented using polarizable continuum model (PCM).

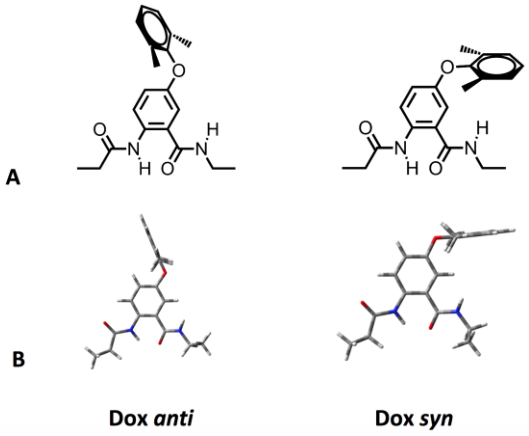

Figure 3S-17. Representation of the *anti* and *syn* conformers of Dox using (A) ChemDraw and (B) Gaussview of the DFT optimized structures using the tube view.

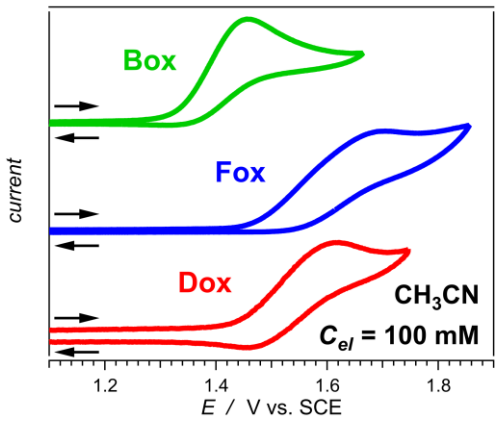

Figure 3S-18. Cyclic voltammograms of Aa ether residues (Chart 3-1b-e) for acetonitrile in the presence of 100 mM electrolyte, N(*n*-$C_4H_9)_4PF_6$, at scan rate, v = 0.1 V s^{-1}, showing irreversible oxidation of Box and Fox and partial reversibility of the oxidation of Dox.

METHODS

Cyclic voltammetry. Electrochemical studies are conducted using Reference 600^{TM} Potentiostat/ Galvanostat/ZRA (Gamry Instruments, PA, U.S.A.), connected to a three-electrode cell. Glassy carbon electrode and platinum wire serve as working and counter electrode, respectively. The reference saturated calomel electrode (SCE) is connected with the cell via a salt bridge filled with 100 mM N(*n*-$C_4H_9)_4PF_6$ solution in acetonitrile. Using such electrolyte solution in the bridge that is missile with aqueous and non-polar organic solvents aids with challenging potential drops at the junctions. To correct for potential drifts in the reference electrode (which is SCE, connected with the cell via a salt bridge), ferrocene is used as a standard ($E^{(1/2)}$ = 0.45 ± 0.01 V vs. SCE for CH_3CN, 100 mM N(*n*-$C_4H_9)_4BF_4$). Voltammograms of the standard are recorded before and after each set of measurements. Anhydrous aprotic solvents with different polarity are employed with different concentrations of supporting electrolyte, N(*n*-$C_4H_9)_4PF_6$. Specifically, we employ

dichloromethane (Figure 3-1) and acetonitrile (Figure 3S-18) for this study. Prior to recording each voltammogram, each sample is extensively purged with high-purity argon while maintaining its volume constant by adding more of the anhydrous solvent. For each solvent, a set of voltammograms is recorded where the electrolyte concentration is increased from 25 mM to 200 mM in increments of 25 mM. The half-wave potentials, $E^{(1/2)}$, are determined (1) from the midpoints between the cathodic and anodic peak potentials, E_c and E_a, respectively, for reversible or quasireversible voltammograms; and (2) from the inflection points of the waves for irreversible oxidation and reduction. The values of E_a and E_c are determined from the zero points of the first derivatives of the voltammograms, i.e., the potentials where $\partial I/\partial E = 0$ at $\partial E/\partial t =$ constant. The inflection points are determined from the zero point of the second derivatives of the voltammograms, $\partial^2 I/\partial E^2 = 0$ at $\partial E/\partial t =$ constant. The second derivatives of reversible and quasi-reversible voltammograms show that the inflection-point potentials are quite close to the mid-points between E_a and E_c, ensuring the reliability for the estimates of $E^{(1/2)}$ from the inflection points of irreversible voltammograms. The voltammograms are recorded at a scan rate from 50 to 750 mV s^{-1}. For each solvent, the dependence of $E^{(1/2)}$ on the electrolyte concentration, C_{el}, allows for extrapolating the values of the potentials for $C_{el} = 0$, i.e., the values of the potentials for the neat solvent.

Steady-state optical spectroscopy. UV/visible absorption spectra were recorded in a transmission mode using a JASCO V-670 spectrophotometer (Tokyo, Japan); and steady-

state emission spectra were measured, also in a transmission mode, with a FluoroLog-3 spectrofluorometer (Horiba-Jobin-Yvon, Edison, NJ, USA). Despite the noticeably large Stokes' shifts (Table 3S-4), the wavelength of the crossing point of the normalized absorption and emission spectra, λ_{00}, provide estimates for the optical excitation energy, $\mathscr{E}_{00} = h\,c\,/\,\lambda_{00}$. (Figure 3S-19, Table 3-2).

Table 3S-4. Absorption and emission maxima of the ether Aa derivatives (Chart 3-1b-e).

	CH_2Cl_2		CH_3CN	
	$\lambda_{abs}^{(max)}$ / nm	$\lambda_{fl}^{(max)}$ / nm	$\lambda_{abs}^{(max)}$ / nm	$\lambda_{fl}^{(max)}$ / nm
Box	320	399	318	397
Fox	314	396	311	394
Dox	315	396	315	395
Dox$_{24}$	317	397	314	395

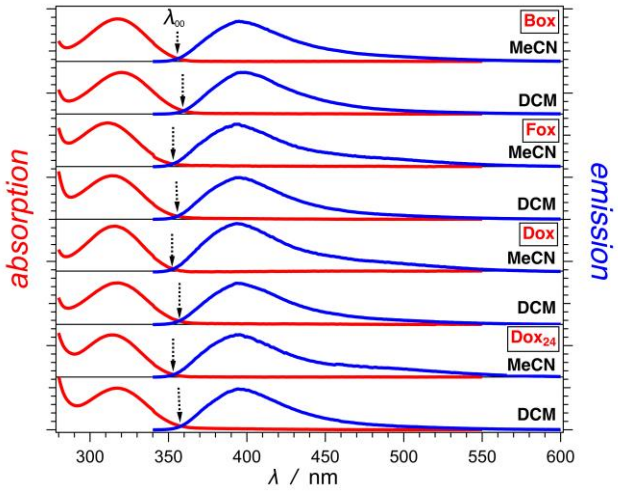

Figure 3S-19. Optical spectra of the ether Aa derivatives (Chart 3-1b-e) for acetonitrile (MeCN) and dichloromethane (DCM). The dotted arrows represent the wavelengths, λ_{00}, corresponding the zero-to-zero transition energies, $\mathscr{E}_{00}$ (Table 3-1).

Computational methods. The *N*-acylated Aa ether residues are modeled using density functional theory (DFT). The alkyl chains at the C- and N- termini are truncated to ethyls. The DFT calculations are performed at the B3LYP/6-311+G(d,p) level of theory, for the gas phase, using Gaussian 09, leading to convergence to the *syn* and *anti* conformers (Figure 3S-17). Spin-unrestricted calculations are used for radical-cation (doublet state) modeling (Figure 3-2, 3S-20). We report frontier-orbital distributions for the Aa ether residues in the gas phase (Figure 3S-21). Solvent effects were estimated by comparing the results from gas-phase calculations to those in an integral equation formalism polarizable continuum model (PCM). Basis on the Koopmans' theorem, we use the difference between the energies of the radical cation doublet states and the ground states of each of the conformers for estimating the ionization energy (IE) of the *syn* and *anti* conformers of the Aa residues.

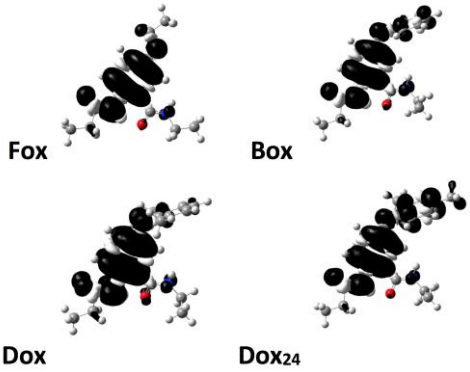

Figure 3S-20. Spin density distributions (SDDs) of the radical cation showing the delocalization of the positive charge of the Aa ether residues (*syn* conformers) using DFT calculations. The alkyl chains from the C- and N- termini are truncated to ethyls for the computational studies.

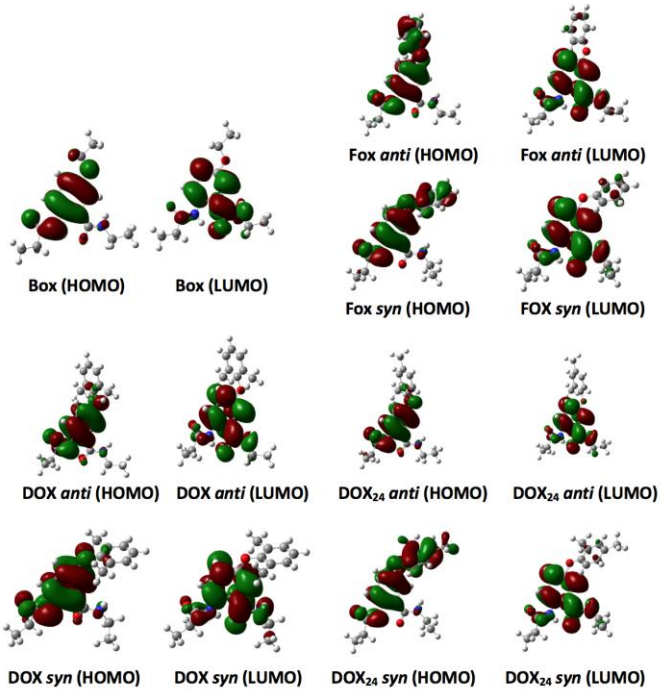

Figure 3S-21. Frontier orbitals of the Aa ether residues (*syn* and *anti* conformers) for the gas phase, obtained using DFT calculations. The alkyl chains at the C- and N-termini are truncated to ethyls for the computational studies.

Chapter 4

On the Search of a Silver Bullet for the Preparation of Bioinspired Molecular Electrets with Propensity to Transfer Holes at High Potentials

Abstract

Biological structure-function relationships offer incomparable paradigms for charge-transfer (CT) science and its implementation in solar-energy engineering, organic electronics, and photonics. Electrets are systems with co-directionally oriented electric dopes with immense importance for CT science, and bioinspired molecular electrets are polyamides of anthranilic-acid derivatives with designs originating from natural biomolecular motifs. This publication focuses on the synthesis of molecular electrets with ether substituents. As important as ether electret residues are for transferring holes under relatively high potentials, the synthesis of their precursors presents formidable challenges. Each residue in the molecular electrets is introduced as its 2-nitrobenzoic acid (NBA) derivative. Hence, robust and scalable synthesis of ether derivatives of NBA is essential for making such hole-transfer molecular electrets. Purdie-Irvine alkylation, using silver oxide, produces with 90% yield the esters of the NBA building block for iso-butyl ether electrets. It warrants additional ester hydrolysis for obtaining the desired NBA precursor. Conversely, Williamson etherification selectively produces the same free-acid ether derivative in one-pot reaction, but a 40% yield. The high yields of Purdie-Irvine alkylation and the selectivity of the Williamson etherification provide important guidelines for synthesizing building blocks for bioinspired molecular electrets and a wide range of other complex ether conjugates.

Introduction

In its many forms, charge transfer (CT) is the fundamental process that sustains life on Earth and makes our modern ways of living possible [**1**]. Biological, biomimetic, and bioinspired systems encompass some of the most important templates for advancing CT science and engineering [**2**]. The Marcus semiclassical transition-state theory has revolutionized the understanding of biological CT and bioenergetics at a molecular level [**3**]. The diabatic nature of CT mediated by biomolecules has made Marcus-Hush and Marcus-Levich-Jortner formalisms perfect for the analysis of such systems [**1**]. At the same time, biological CT has driven the evolution of CT science, resulting in new theories and unprecedented ways of thinking [**4**-**9**].

The ubiquity of electric dipoles makes the understanding how they affect CT crucially important not only for biology, but also for materials science and device engineering [**10**]. The first ideas about dipole effects on CT originated in the mid-20th century from considerations of CT through protein structures with numerous polar moieties [**11**,**12**]. In the 1990s, CT through biological and bioinspired molecules provided the experimental evidence for such effects [**13**-**16**]. As the field took off, the focus was on dipolar biomolecules on one hand, and on small polar organic conjugates on the other, limiting the range of CT to 2 nm, and the mechanism predominantly to tunneling or superexchange [**1**,**6**,**10**]. To take the field out of this confinement, we developed the concept for CT bioinspired molecular electrets (**Figure 4-1**) [**17**-**29**].

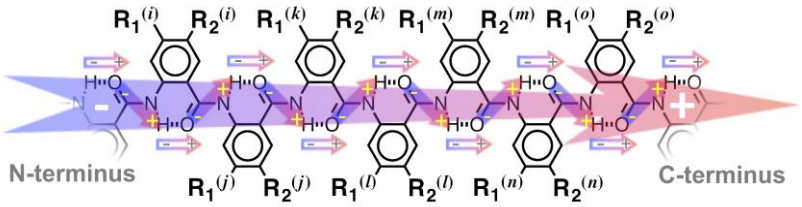

Fig. 4-1: Bioinspired molecular electrets composed of anthranilamide (Aa) residues and the origin of their macrodipoles from ordered arrangement of amides and polarization upon the formation of hydrogen bonds.

Comprising ordered electric dipole moments, electrets are the electrostatic analogues of magnets. Some of the best molecular electrets are biomolecules such as protein α-, 3_{10}-, and polyproline I helices [**30**]. Peptide bonds (i.e., aliphatic N-acyl amides) are a small group with substantial permanent dipole moments [**31**]. Therefore, the arrangement of peptide bonds in protein helical folds results in macrodipoles of about 4 D per residue [**30**]. Hydrogen bonding in α-, and 3_{10}-helices shifts the electron density from the carbonyl oxygens on one loop to the amide protons on the next one. This polarization further enhances the macrodipoles, which for protein α-helices can exceed 5 D per residue with an increment of 0.15 nm. That is, 3-nm stretches of α-helices, comprising 20 amino acids arranged in about 5.6 loops, have dipoles of 100 D, which generate electric fields of tenths of GV m^{-1} in the vicinity of these biomolecules. It does not come as a surprise, therefore, that polypeptide helices have been the principal templates for investigating dipole effects on CT [**32**-**36**].

The propensity for oxidative degradation of amides, however, limits CT to about a 2-nm range attainable by electron tunneling through such biomolecules [**37**-**39**]. Potentials of about 1.4–1.5 V vs. saturated calomel electrode (SCE), indeed, allow for hole injection in peptide bonds. A couple of σ-bonds separate each two peptide bonds in proteins, decreasing the electronic coupling between them by a factor of eight. It results in hole

residence times on the amides that are long enough to permit their oxidative degradation, as evident from the irreversibility of their electrochemical oxidation [**40**,**41**].

When it comes to efficient long-range hole transfer through insulating materials, another class of biomolecules present some of the best paradigms. Deoxyribonucleic-acid (DNA) and peptide-nucleic-acid (PNA) efficiently transfer holes over tens of nanometers along their π-stacked electron-rich bases [**42**].

Considering the desirable features of these two completely different classes of biomolecules (i.e., protein helices and DNA/PNA strands), we designed bioinspired molecular electrets based on anthranilamide (Aa) structural motifs (**Figure 4-1**) [**28**].

Like for protein helices, the ordered amide and hydrogen bonds of the bioinspired electrets generate a macrodipole of about 3 D per residue [**17**,**19**]. The Aa aromatic moieties not only provide hopping sites for electrons or holes to ensure long range CT, but also take away a part of the electron density from the amide bonds to prevent oxidative degradation [**22**]. The side chains, R_1 and R_2 (**Figure 4-1**), of the non-native Aa amino acids play a crucial role in controlling their electronic properties. Electron-donating R_2 substituents stabilize the radical cations of such Aa residues by pulling the spin density away from their C-terminal amides, making them excellent candidates for mediating hole transfer via long-range hopping. Electron-donating substituents, however, also lower the reduction potentials of these radical cations, precluding the transduction of holes with high enough energy to drive certain chemical transformations or to ensure large voltages at the termini of energy-conversion devices [**1**,**43**,**44**]. Therefore, we focused on ether-functionalized Aa conjugates. Ethers as R_2 substituents are electron-withdrawing enough to ensure stability

of the Aa radical cations, but not too polarizing to lower their reduction potential to ≤1 V vs. SCE, as we observe for amines [**20**,**24**]. As we show, aromatic ether substituents such as R_2, sterically locked in orthogonality with the Aa ring, lead to reversible electrochemical oxidation at about 1.7 V vs. SCE at scan rates of 100 mV s^{-1} or less [**27**]. Upon increasing the scan rates beyond 0.5 V s^{-1}, aliphatic and other aromatic ethers of Aa residues commence to show reversibility at a potential between 1.5 and 1.9 V vs. SCE [**27**]. Considering the timescales of electrochemical measurements ensures that the oxidative degradation of the ether Aa residues showing even partial reversibility is orders of magnitude slower than the residence time of holes on them during CT through Aa electrets. Furthermore, the potentials exceeding 1.5 V vs. SCE are the highest known under which amides can undergo reversible, or even partially reversible, oxidation [**27**].

A principal task in this line of research was making the Aa bioinspired molecules [**28**,**29**], which is the focus of this publication. While they are polypeptides of aromatic β-amino acids, none of the strategies for chemical or biochemical synthesis of biological and biomimetic peptides works for making Aa conjugates (**Figure 4-2**a) [**29**]. Using Fmoc- or *t*Boc-protected derivatives, or any form of amine or amide at the ortho positions next to the activated carboxylate has two detrimental effects: (1) lowers the electrophilicity of the carbonyl carbon of the activated acid, which lessens the efficiency of the amide coupling to the N-terminal amine; and (2) efficiently drives the formation of cyclic β-lactams that are pronouncedly stabile (**Figure 4-2**a). As we show, only strong nucleophiles such as piperidine can open these cyclic lactams [**29**], rendering them impractical for the synthesis of Aa conjugates.

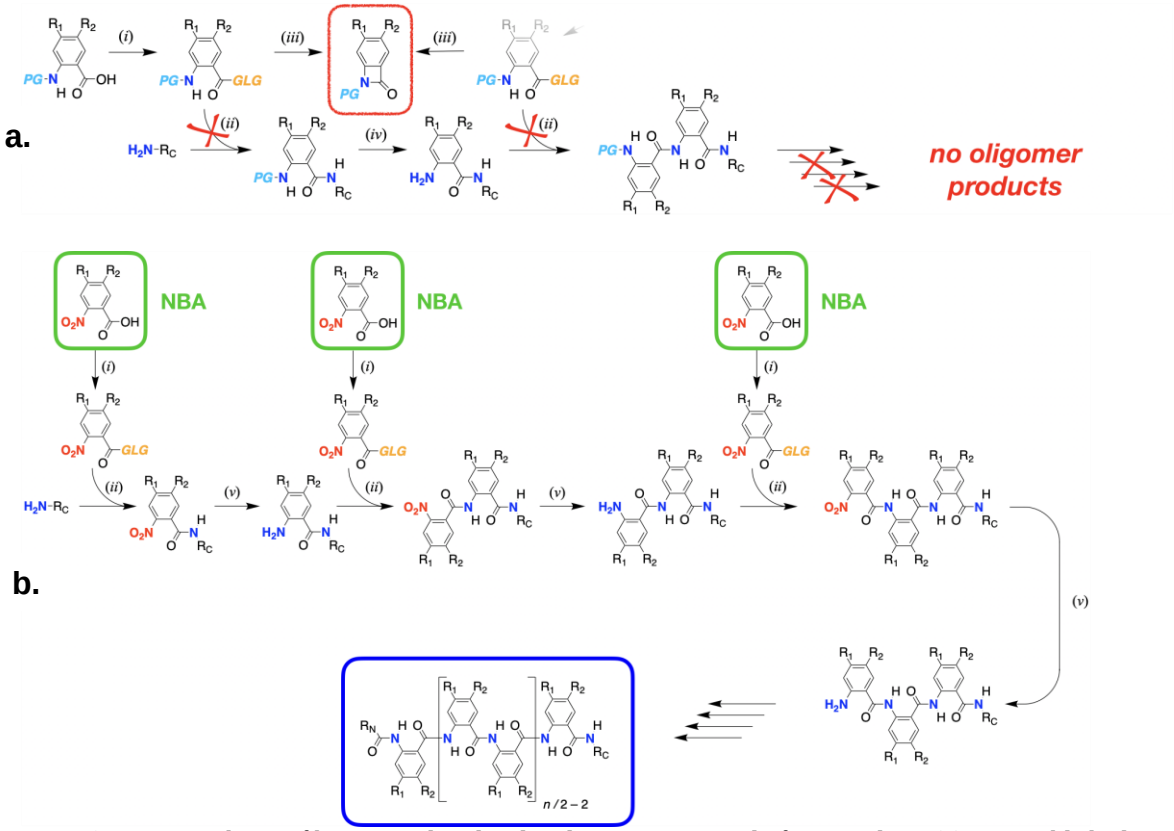

Fig. 4-2: Synthesis of bioinspired molecular electrets composed of Aa residues. (**a**) An established protocol for peptide synthesis where each residue is introduced as its protected-amine derivative, with a protection group (*PG*) such as Fmoc or *t*Boc. Ideally, the synthesis of the polyamide molecular electrets should involve a sequence of repetitions of carboxylate-activation (*i*) and amide-coupling (*ii*) steps, followed by amine deprotection (*iv*). The enormous efficiency of the intramolecular formation of stable cyclic *β*-lactams (in the red frame) (*iii*), however, precludes the intermolecular amide coupling (*ii*), rendering this synthetic strategy unacceptable. (**b**) An alternative protocol for the synthesis of Aa molecular electrets with *n* Aa units (in the blue frame), capped with R_N and R_C at the N- and C-termini, respectively, where each residue is introduced as its 2-nitrobenzoic acid (NBA) derivative (in the green frames). The multistep synthesis involves repetitions of carboxylate activation (*i*), amide coupling (*ii*), and nitro reduction (*v*). Steps (*i*) and (*ii*) can be carried out separately or in the same pot involving in situ carboxylate activation in the presence of the free amine. Specifically, the involved reaction steps are: (*i*) activation of the carboxylic acid by attaching a good living group (*GLG*) to the electrophilic carbonyl carbon via: (*i*.1) halogenation (i.e., *GLG* = -Cl or -F); (*i*.2) a reaction with a carbodiimide reagent in the presence of hydroxyl derivatives such as *N*-hydroxysuccinimide (HOSu) (i.e., *GLG* = -OSu, 1-hydroxybenzotriazole (HOBt), i.e., *GLG* = -OBt, or 1-hydroxy-7-azabenzotriazole (HOAt), i.e., *GLG* = -OAt); (*i*.3) a reaction with an onium reagent such as HOBT or HATU in the presence of HOBt or HOAt; (*ii*) coupling between the activated acid and a primary (or secondary) amine (i.e., amide coupling); (*iii*) formation of a stable cyclic β-lactam (in the red frame): the close proximity of a weakly nucleophilic nitrogen (in a protected amine or in an amide) at the ortho position to the activated carboxylate makes it immensely prone to intramolecular amide coupling leading to a cyclic lactam; (*iv*) deprotection of the amine (e.g., using base for Fmoc *PG*, and acid for *t*Boc *PG*), and (*v*) selective reduction of the N-terminal nitro group to an amine.

To build the Aa strands from the C- to the N-terminus, we introduced each of the amino acids as its 2-nitrobenzoic acid (NBA) analogues (**Figure 4-2**b). Instead of introducing an *N*-protected amino acid at each step, which is selectively deprotected for attaching the next one, we coupled a NBA analogue to the N-terminal amine and selectively reduced $-NO_2$ to $-NH_2$ to prepare it for the attachment of the next residue (**Figure 4-2**b) [**29**]. Addition of the residue building blocks such as NBA derivatives via a sequence of amide-coupling and nitro-reduction steps yields Aa oligomers of different lengths and complexity [**29**]. Alkyloxy derivatives of NBA are essential for building ether-functionalized Aa conjugates to serve as molecular electrets that can mediate the transfer of high-energy holes via hopping (i.e., incoherent CT that has the key advantage of covering long distances) [**1**]. The capability to make highly pure NBA derivatives in large quantities, with as few synthetic and purification steps as possible, is essential for advancing the pursuit for new Aa bioinspired molecular electrets.

Nucleophilic aromatic substitution of fluorinated NBAs in a solvent-free environment allows for amine derivatives of NBA to be obtained in excellent yields [**18**,**20**,**24**]. Employing aliphatic amines with long alkyl chains, however, places a certain demand on this synthetic procedure such as the use of microwave heating to drive the reaction. Unlike conventional heating, microwave radiation aids in overcoming the entropic contributions to the transition-state energy where only a few of the enormous possible conformers of the collision complexes between the starting materials lead to the desired product.

Employing nucleophilic aromatic substitution for the synthesis of alkyloxy NBAs, however, has proven utterly unfeasible. Fluorinated NBA derivatives can react with phenoxy nucleophiles in the presence of a carbonate base in organic solvent to produce aromatic ethers of NBA [**27**]. Unfortunately, the same NBAs decompose in the presence of alkyloxy nucleophiles, requiring strong bases or alkaline metals to generate them. Therefore, we resorted to etherification of hydroxyl derivatives of NBA with alkyl halides. This leads to the ether-ester derivatives of NBA, which sets the requirement for an additional step in the synthesis: hydrolysis to convert the ether-ester derivative to the corresponding free acid ether-NBAs needed for the synthesis of the electrets (**Figure 4-2**b) [**20**].

Recently, we discovered a variation of Williamson etherification (WE) that selectively yields ether derivatives of NBA without ester products [**27**]. The most crucial requirement of our WE is the solvent, 2-methoxyethanol (2ME), which selectively produces ether NBAs in good to excellent yields [**27**]. Other alcoholic solvents produce only traces of the desired products, at best. Employing neat conditions (where the alkyl halide acts as a reagent and solvent) does not lead to even traces of the products [**27**]. These outcomes warrant the search for alternative etherification procedures under mild conditions that do not necessarily involve strong bases.

As a variation of WE, Purdie-Irvine alkylation (PIA), also referred to as Purdie methylation and Irvine-Purdie methylation, accommodates the reaction of alcohols with alkyl halides in the presence of solid silver oxide, Ag_2O [**45**]. In spite of the disputes over the exact name of this reaction, A. Wurtz was the first to report such Ag_2O-driven ether

formation from different iodides and alcohols about half a century before Purdie and Irvine published their findings [**46**]. Decades of work on the esterification of silver and mercury salts of carboxylic acids with alkyl iodides provided an important platform for Purdie's research, establishing Ag^+ and aliphatic halides as a promising combination of reagents for alkylation [**47**].

Despite some misconceptions [**48**], Ag_2O is not a catalyst, but a consumable reactant where the strong affinity of Ag^+ for halide ions drives the reaction forward (i.e., $2R'X + 2ROH + Ag_2O \rightarrow 2R'OR + 2AgX + H_2O$). Nevertheless, PIA can still benefit from adding catalysts [**49**]. Silver oxide is a weak Lewis base that, while aiding the process by neutralizing the released protons, makes PIA an excellent choice for etherification involving base-sensitive reactants and products. Furthermore, prolonged reaction times allow PIA to achieve quantitative yields under relatively mild conditions. These desirable features have established PIA as the preferred method for the methylation of sugars [**50-53**], which is essential for carbohydrate analysis and have proven important for the development of glycomics [**54-57**]. With few exceptions [**58-60**], however, PIA remains largely unexplored beyond the methylation of carbohydrates, which Purdie and Irvine described more than a century ago [**45**,**53**].

Herein, we present an investigation of the utility of PIA for the synthesis of ether NBA derivatives under neat conditions where iso-butyliodide acts as a reagent and a solvent (**Figure 4-3**). Microwave heating leads to the formation of the ether derivative of NBA, **3**, and its ester, **4**, with overall yield of 40%. PIA employing conventional heating, on the other hand, produces ester **4** in 90% yield. With ether **3** in hand, we demonstrate the

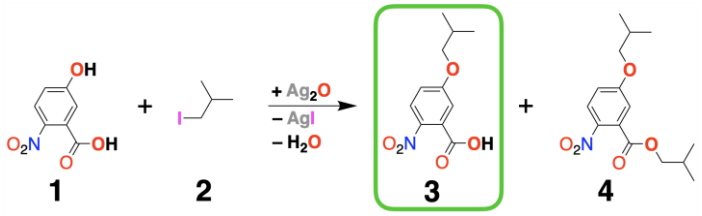

Fig. 4-3: Purdie-Irvine alkylation (PIA) leading to an ether 2-nitrobenzoic acid (NBA) precursor (in the green frame) for the synthesis of Aa bioinspired molecular electrets (**Figure 4-1**; **Figure 4-2**b). The exact masses of the products, obtained using as high-resolution mass spectrometry (HRMS), along with their ^{1}H and ^{13}C nuclear magnetic resonance (NMR) spectra (**Figure 4S-1 and 4S-2**), confirm the identities of **3** and **4**.

synthesis of electret oligomers that revealed substantial differences in the reactivities for coupling different residues together. These findings about PIA and on building the oligomers provide key guidelines for the design of the synthesis not only of bioinspired molecular electrets, but also for a wide range of ether derivatives.

Results and Discussion

2.1. Choice of Substrates

The synthesis of Aa molecular electrets involves adding each residue as its NBA analogue from the C- to the N-terminus [**29**]. The ortho nitro group in the NBA derivatives enhances the electrophilicity of the carbonyl carbon of the activated carboxylate. It is essential for coupling the NBA with the N-terminal amine (i.e., the amine of the previous residue), which is not strongly nucleophilic and experiences some steric hindrance. Activating the NBAs as acyl chlorides provides the necessary reactivity. Furthermore, the small size of -COCl is beneficial for attacking the N-terminal aromatic amine next to an *ortho* positioned amide. Therefore, synthesis of NBA analogues of the Aa residues is the first and most important step in the preparation of the bioinspired molecular electrets.

Placing ethers at the fifth position of Aa residues (R_2, **Figure 4-1**) allows for attaining reversible oxidation at unusually high potentials for amides [**27**]. Our recent

electrochemical studies showed that placing a 2,6-dimethylphenyloxy substituent at position 5 provided the most pronounced stability of the Aa radical cation at potentials that no amide has been previously known to sustain [**27**]. Alkyloxy-functionalized Aa residues manifest only partial reversibility during electrochemical oxidation. Nevertheless, the aliphatic sidechains of such Aa ethers substantially improve their solubility in organic media, which is a key consideration for the design of Aa oligomers to facilitate the work with them. Etherification of 5-hydroxy-2-nitrobenzoic acid (**1**, **Figure 4-3**) with alkyl halides provides the best route for synthesizing the NBA precursors for such Aa derivatives.

Attaching an ether with a long aliphatic flexible chain substantially improves the solubility of such derivatives. Leftover alkyl halide starting martials with a large molecular weight are not volatile enough to be readily removed from the reaction mixture, warranting the employment of chromatography [**20**]. While light-weight alkyl halides can be readily removed in vacuo at low temperature, their short aliphatic chains would not prove too beneficial for solubilizing the Aa oligomers. Butyl halides present the best compromise because they are small enough to readily remove them from the reaction mixtures. At the same time, butyls are large enough chains, especially when branched, to ensure sufficient solubilization of the ether Aa conjugates in organic solvents. The iso-butyl side chain of leucine **(Leu)** ensures substantial lipophilicity Leu-rich protein segments [**61**-**76**]. These side chains also drive the formation of leucine zippers as a part of amphipathic motifs that hold tertiary and quaternary protein structures together. Therefore, etherification

of **1** with *iso*-butyliodide (**2**, **Figure 4-3**) presents an excellent choice for examining the utility of PIA for making ether Aa derivatives.

2.2. Synthesis Design

PIA is immensely important for methylation of sugars in aqueous and other polar media. Using methyl iodide leads to the formation of methyl ethers where hydroxyls previously were. Employing it in polysaccharides, followed by their hydrolysis, to the comprising monomers provides access to useful structural information [**77**]. The polarity and the hydrogen-bonding propensity of the aqueous media is essential for dissolving the carbohydrates and for lowering the transition-state energy essential for attaining acceptable reaction rates. Such conditions, however, are not feasible for the etherification of alcohols and phenols that are not soluble in water. It warrants the use of an organic solvent, providing a good compromise between dissolving the hydroxyl reactants and suspending the solid Ag_2O.

Conducting the PIA reaction under neat conditions provides an attractive choice for pursuing green-chemistry strategies where scaling up does not require an increase in solvent consumption. The capability to suspend the NBA reactant, **1**, and the solid Ag_2O in the alkyl halide, **2**, while keeping the reaction mixture fluent enough to stir, sets the limits on the minimum amounts of halide needed. Our aim at butylation, rather than methylation, of **1** requires the suspension of the reaction mixture in **2**, which is a less polar solvent than methyl iodide. Nevertheless, using ×8 to ×9 molar excess of **2**, allows the other two reactants to be suspended in it for heating in a microwave reactor. Eight-to-nine fold excess of the liquid halide may seem excessive when claiming the benefits of solvent-free

conditions. Nevertheless, it exceeded by only about a factor of two excess of **2** for etherification of **1** in an optimized solvent environment. When employing 2ME as a solvent, we used four times excess of the halide, **2**, for etherification of **1** in the presence of Cs_2CO_3 [**27**].

The optimal temperature for the microwave-driven PIA between **1** and **2** was 130 °C at 60 W exerted for two intervals of 30 s. This high temperature, exceeding the boiling point of **2** by about 10 °C, is necessary for the reaction to proceed, but must be halted after 30 s to prevent the risk of evaporating the halide too fast, which can cause splashing of the reaction mixture out of the vessel. Further microwave irradiation does not improve the reaction yields. The capabilities of microwave radiation to induce localized heating, especially for heterogeneous reactions with solids that have strong absorptivity for GHz electromagnetic waves, indicates that what we recorded using infrared sensors is an average temperature. That is, while the bulk of the halide **2** could be relatively cool because it is not a strong microwave absorber, at the Ag_2O surface, the local temperatures can be exuberantly high.

These microwave synthetic conditions lead to the formation of the desired NBA ether, **3**, and its ester derivative, **4** (**Figure 4-3**, **Scheme 4S-1**). Doubling the loading of Ag_2O from 1 to 2 equivalents, relevant to **1**, increased the overall yield by about 50% (i.e., from 27% to 40%) while doubling the yield of **3** (i.e., from 9% to 20%) (**Table 4-1**). An increase in the oxide loading beyond two equivalents requires extra amounts of **2** to keep the suspension fluent, which decreases the concentration of **1** and does not truly improve the yields of the isolated product. Needless to say, increasing the Ag_2O loading also

challenges the cost-efficiency of the procedure. The two equivalents of oxide show the need of four Ag^+ cations for each I^- anion produced. While it may appear excessive, it should be considered that most of the silver ions are inside the Ag_2O solid and not exposed to the

liquid phase of the reaction.

These findings, along with the results about WE from our previous work [**27**], reveal an important mechanistic insight. Reacting **1** and **2** under microwave radiation in

Table 4-1: Optimization of silver-oxide loading for microwave reaction conditions.

$n(Ag_2O)/n(1)$ [a,b,c]	Yield of 3 [d]	Yield of 4 [d]
1	9%	18%
1.5	10%	23%
2	20%	20%
Previous studies: [e] $n(Cs_2CO_3)/n(1)$		
3	40%	0%

the presence of Cs_2CO_3 suspended in 2ME also gave a 40% yield, but only of **3**, with no traces of **4** [**27**]. That is, Ag_2O under neat conditions and the carbonate in 2ME drove the conversion of **1** to products with quite similar propensities. The alkaline carbonate was more basic than Ag_2O, and 2ME was protic and more hygroscopic than 2. Hence, Cs_2CO_3 suspension in 2ME provided more favorable conditions for base-catalyzed irreversible ester hydrolysis than Ag_2O suspension in **2**. This shows that the selectivity of the formation of **3** over **4**, which 2ME, and no other solvent, induces, is not due to the suppression of the carboxylate nucleophilicity or the halide reactivity. The pK_a of 4-nitrophenol is about 7 and of 2-nitrobenzoic acid is about 2. Additionally, the nitro group dominates the electronic properties of **1**, considering the Hammett constants for the three substituents: $\sigma_p(NO_2) = 0.78$; $\sigma_m(CO_2H) = 0.37$; and $\sigma_m(OH) = 0.12$ [**78**]. This indicates that under any conditions where the hydroxyl of **1** is deprotonated and can act as a good

nucleophile, its carboxyl is also deprotonated, warranting the formation of ester under any conditions that favor etherification. What the 2ME/Cs_2CO_3 medium offers are conditions for fast irreversible hydrolysis of **4** to **3**, rather than the selectivity of forming **3** over **4** (i.e., the conditions for etherification of **1** always favor the production of ester derivatives). Once again, why is 2ME such a unique solvent for making ether derivatives of NBA from **1** [**27**]? Using media with stronger basicity than the carbonate suspension in 2ME will favor the hydrolysis, but (1) will interfere with the etherification by reacting with the halide, for example, and (2) lead to degradation of the formed products. Conversely, too low a basicity would fail to deprotonate the phenol, which is needed for making it a good nucleophile for etherification. In addition, considering the kinetic aspects of the processes suggests that at the reflux temperature of the 2ME/Cs_2CO_3 mixture, the etherification, esterification, and hydrolysis are faster than the undesired side reactions. Indeed, using other alcohols as solvents leads to traces of products, but nothing like the conversion yields observed for 2ME [**27**]. In its uniqueness, the **2**/Ag_2O medium is almost as good as the 2ME/Cs_2CO_3 mixture. While the weak basicity of Ag_2O does not drive the hydrolysis of **4** to **3** to completion, the strong affinity of Ag^+ ions for halides ensures efficient alkylation of the hydroxyl and the carboxyl.

2.3. Testing Beyond Ag_2O

Among all readily available compounds, Ag_2O is the richest in silver cations (i.e., 93% of the weight of Ag_2O is from Ag^+). Nevertheless, the use of two equivalents of silver oxide added for each mole of **1**, and considering the product yields (20% of **3** and 20% of **4**) giving 0.8 equivalents of I^- based on the assumption that all of **3** originates from the

hydrolysis of initially formed **4**, suggests that only 20% of the Ag^+ ions are consumed in the formation of AgI (**Figure 4-3**). While this appears to be a small number, a lot less than 20% of the silver ions are on the surfaces of the micrometer size Ag_2O particles used for this reaction. Therefore, the process involves silver ions not only on the surface, but also in the bulk of Ag_2O. The need for accessing the bulk ions can be a considerable hurdle for the reaction.

The lack of solubility of Ag_2O in organic media and the needed five-fold excess of silver ions suggests that most of the Ag^+ cations, in the bulk of the crystal lattice, are not easily accessible to the other reagents and to the hydrogen iodide that forms. To examine the potential effects of solubilizing the inorganic reactant, we carried out the same procedure but instead of Ag_2O, we used silver salts with different solubilities in organic media. Microwaving a mixture of **1** and **2** in the presence of some of the most readily available silver compounds, Ag_2SO_4, $AgNO_3$, $Ag(CH_3CO_2)$, and $Ag(CF_3SO_3)$ produced neither **3** nor **4**. After the heating treatment, the reaction mixtures predominantly contained the starting materials **1** and **2**, along with small amounts of side products that were not **3**, **4**, or an ester of **1** with a free hydroxyl. While $Ag(CH_3CO_2)$ and $Ag(CF_3SO_3)$ are soluble in organic solvents, Ag_2SO_4 and $AgNO_3$, are not. Hence, the solubility of the silver compound is not a deterministic factor for the PIA of **1**.

Reacting silver carboxylates with aliphatic halides is an established method for esterification. The weakly basic nature of Ag_2O makes it prone to dissolution by acidic compounds such as **1** to form the corresponding silver salts (e.g., $Ag^+\mathbf{1}^-$ and $Ag^+_2\mathbf{1}^{2-}$). Reactions of silver phenoxides and carboxylates with aliphatic halides should generate

ethers and esters, respectively. If the formation of silver salts of **1** is necessary for PIA, Ag_2SO_4, $AgNO_3$, and $Ag(CF_3SO_3)$ should not drive the conversion to **3** and **4** because of the negative pK_a values of sulfuric, nitric, and triflic acids. That is, nitrobenzoic acids and nitrophenols cannot protonate sulfate, nitrate, and triflate anions, rendering the formation of silver salts of **1** from Ag_2SO_4, $AgNO_3$, and $Ag(CF_3SO_3)$ impossible.

Following this line of thinking suggests that $Ag(CH_3CO_2)$ should lead to at least some alkylation of **1** because the pK_a of acetic acid is larger than the pK_a of 2-nitrobenzoic acid. Nevertheless, $Ag(CH_3CO_2)$ is as inefficient for driving the conversion as the other silver salts. This finding points to the fact that the desirable solubility of $Ag(CH_3CO_2)$ in organic media actually originates from the stable non-charged cyclic complex, disilver diacetate, in which $Ag(CH_3CO_2)$ preferentially exists. Hence, breaking the coordination of the silver ions with the bidentate acetate ligands in $[Ag_2(CH_3CO_2)_2]$ in order to form silver salts of **1**, requires from **1** to form complexes with Ag^+, which have stability and solubility in non-polar media that are comparable to those of disilver diacetate. The requirement for solubility in **2** is especially challenging for species with doubly charged ions such as $Ag^{+2}\mathbf{1}^{2-}$. In addition, the reactivity of the acetate ion under these alkylation conditions can make $[Ag_2(CH_3CO_2)_2] + 2\ IC_4H_9 \rightarrow 2\ CH_3CO_2C_4H_9 + 2\ AgI$ the dominating reaction.

While esterification reactions involving silver carboxylate salts may provide an appealing premise for the need to dissolve Ag_2O by **1**, the efficiency of PIA involving aliphatic alcohols renders this requirement as unnecessary. The weak acidity of alkyl alcohols precludes the possibility of dissolving the solid Ag_2O in the form of salts (i.e., silver alkoxides). Therefore, structural considerations of the solid materials can prove

important for understanding why Ag_2O is uniquely efficient for driving this heterogeneous PIA. Later in this section, the discussion will focus on comparing the crystal-lattice characteristics of the starting material, Ag_2O, and the produced AgI (**Table 4-2**).

Table 4-2: Characteristics of the oxides and iodides of silver(I), thallium(I), and lead(II) [**79**].

Oxide or Iodide	Crystal Lattice [a]	$\Delta G_f^{(0)}$/eV per Atom [b]	ρ/g cm^{-3} [c]	Yield/% [d]
Ag_2O	cubic ($m\bar{3}m$, $Pn\bar{3}m$ [224]), stable	−0.328	6.78	40 (90) [e]
	triclinic (1, P1 [1])	−0.219	6.87	
	trigonal ($m\bar{3}m$, $P\bar{3}m1$ [164])	−0.208	8.61	
AgI	cubic ($\bar{4}3m$, $F\bar{4}3m$ [216]), stable	−0.281	5.32	—
	cubic ($m\bar{3}m$, $Fm\bar{3}m$ [225])	−0.188	6.64	
	cubic ($m\bar{3}m$, $Pm\bar{3}m$ [221])	−0.109	6.80	
	hexagonal (6mm, P63mc [186])	−0.280	5.33	
	hexagonal (6mm, P63mc [186])	−0.234	5.29	
	tetragonal ($\bar{4}2m$, $I\bar{4}m2$ [119])	−0.279	5.32	
	tetragonal (4/mmm, P4/nmm [129])	−0.256	5.55	
	monoclinic (2/m, P21/m [11])	−0.177	6.69	
Tl_2O	trigonal ($\bar{3}m$, $R\bar{3}m$ [166]) stable	−0.826	9.41	0
TlI	cubic ($m\bar{3}m$, $Fm\bar{3}m$ [225]) stable	−0.682	6.05	—
	cubic ($m\bar{3}m$, $Pm\bar{3}m$ [221])	−0.629	6.98	
	orthorhombic (mmm, Cmcm [63])	−0.658	6.55	
PbO	orthorhombic (mmm, Pbcm [57]) stable	−1.477	8.31	0
	orthorhombic (mmm, Pbcm [57])	−1.458	8.74	
	orthorhombic (mm2, Pca21 [29])	−1.456	7.89	
	tetragonal (4/mmm, P4/nmm [129])	−1.476	8.47	
	tetragonal (4/mmm, P42/mmc [131])	−1.064	8.37	
PbI_2	hexagonal (6mm, P63mc [186]) stable	−0.668	5.12	—
	hexagonal (6mm, P63mc [186])	−0.668	5.13	
	trigonal (3m, P3m1 [156])	−0.668	5.34	
	trigonal ($\bar{3}m$, $P\bar{3}m1$ [164])	−0.667	5.36	
	trigonal ($\bar{3}m$, $R\bar{3}m1$ [166])	−0.668	5.11	
	trigonal ($\bar{3}m$, $R\bar{3}m1$ [166])	−0.666	5.34	

[a] Crystal system (point group, Hermann-Mauguin notation with the corresponding [space-group number]). For each compound, "stable" designates the most stable structures to which other ones may rearrange. [b] Formation energy. [c] Mass density. [d]Yields of conversion of **1** to **3** and **4** under microwave heating. [e] The value in the parentheses represents the yield under conventional heating.

Why are the silver ions so unique for this type of etherification? Along with Hg_2^{2+}, Pb^{2+}, and Tl^+, Ag^+ is in the first analytical group of cations, characterized by the propensity for forming halides with pronouncedly small solubility products for aqueous media (e.g., $K_{sp}(Hg_2I_2) = 3.4 \times 10^{-28}\ M^3$, $K_{sp}(PbI_2) = 4.5 \times 10^{-9}\ M^3$, $K_{sp}(AgI) = 2.0 \times 10^{-16}\ M^2$, and $K_{sp}(TlI) = 4.4 \times 10^{-8}\ M^2$ [**80-85**]). That is, Ag^+ has the second highest affinity for I^-, surpassed only by Hg_2^{2+}. In the presence of 10 μM of Ag^+, for example, the activity of I^- in a solution cannot exceed 20 pM. Conversely, in the presence of 10 μM of Hg_2^{2+}, $a_{I^-} \leq 6$ pM, and for 10 μM of Pb^{2+} and Tl^+, $a_{I^-} \leq 21$ and 4.4 mM, respectively. In addition, the pK_{sp} of CuI is about 12, which makes Cu^+ also a good iodine-ion "sponge." The redox properties of copper (I) and the catalytic activity of some of its chelates make its oxide and salts prone to causing undesirable side reactions. While these K_{sp} values are for the ion activities in aqueous media, they provide key guidelines showing that Ag^+ is a halide "sponge," almost as potent as Hg_2^{2+}, and considerably outperforms Tl^+ and Pb^{2+}. Similar to $Ag(CH_3CO_2)$, the acetates of these two ions, $Tl(CH_3CO_2)$ and $Pb(CH_3CO_2)_2$, do not drive product formation. In contrast to Ag_2O, their oxides, Tl_2O and PbO also proved as inefficient as their salts, which can be ascribed to the affinity of Tl^+ and Pb^{2+} for I^-, which is an order to two-orders of magnitude smaller than that of Ag^+.

While the K_{sp} values offer good guidelines for the propensity of iodide formation, they do not truly represent the PIA reaction conditions. Most of the available information on the K_{sp} of these halides is for an aqueous solution and not for the aprotic organic media that we employed for PIA. During the reaction, the dispersed solid phase in the mixture must convert from oxide to iodide. Examining the crystal-lattice properties of the different

solid oxides and iodides revealed important trends that are strikingly consistent with the observed results for PIA. Ag_2O and AgI are both polymorphic with their most stable structures assuming cubic lattice arrangements (**Table 4-2**). The oxide is slightly more stable than the iodide, but only by less than *2kBT* at room temperature, considering the most stable polymorphs of the two compounds (**Table 4-2**). This indicates the thermal plausibility of transforming Ag_2O to AgI in the presence of iodide and proton sources to bind O^{2-} ions of the oxide and replace them with I^-.

The porous structure of the cubic Ag_2O (i.e., with the ions assuming face-centered antifluorite arrangement in the lattice) is quite beneficial for heterogeneous reactions. With a pore size of about 8 nm and specific surface area exceeding 9 $m^2\ g^{-1}$, cubic Ag_2O is an attractive material for heterogeneous catalysis [**86**]. While Ag_2O is a reagent in PIA, rather than a catalyst, the accessibility of the starting materials from the liquid phase into its porous bulk is an important feature for this alkylation. In addition, the face-centered cubic AgI is a highly promising ion conductor [**87**]. This ion mobility in such materials is important for the replacement of O^{2-} with 2 I^- as the crystal lattice rearranges during the PIA reaction. Furthermore, AgI exhibits higher solubility in certain aprotic organic solvents than in aqueous media (i.e., K_{sp}(AgI) is about two to four orders of magnitude smaller for acetonitrile and DMSO, respectively, than for water) [**88**]. While an increase in K_{sp}(AgI) increases the thermodynamic driving force toward the products, in the case of heterogeneous reactions involving a solid starting material and a solid product, partial solubility of at least one of these solids can lower the energy of the transition states and the intermediates, which increases the reaction rates proving beneficial for the kinetics of the

reaction. That is, partial desolation of the formed AgI in the organic liquid environment (especially, at elevated temperatures), prior to deposition on a solid phase, can aid the transformation from Ag_2O to AgI.

Extending this thermodynamic line of thinking to Tl^+ revealed that its oxide was more than 140 meV more stable than its iodide (**Table 4-2**), precluding a direct transformation of Tl_2O into TlI. Initial dissolution of Tl_2O in acidic solution, followed by treatment with a soluble metal halide, MX_n, is required to form the corresponding TlX. Following this train of thought revealed that transforming the Pb^{2+} oxide into iodide is even more preposterously impossible than for Tl^+, considering the energy of formation of PbO is 800 meV lower than that of PbI_2 (**Table 4-2**).

These thermodynamic considerations feasibly outline the reasons why Ag_2O led to 40% conversion of **1** into **3** and **4** (**Figure 4-3**), while Tl_2O and PbO did not generate even traces of the products detectable via MS. In addition, it is important to consider possible intermediate structures that can affect the kinetics of transforming the oxides into iodides in aprotic organic media where dissolution of the inorganic phase is negligible to impossible. The stable polymorphs of Ag_2O and AgI assume the form of the cubic lattices: not the same space groups, but still strikingly similar structures. Therefore, gradual transformation of silver oxide into its iodide does not require significant lattice rearrangements that may impose bindery energies that can be attributed to a decrease in the reaction rates. On the other hand, the significant lattice differences between Tl_2O and TlI, and between PbO and PbI_2 (**Table 4-2**), can induce further impedance on the oxide-to-iodide transformations, in addition to the thermodynamic infeasibility.

The solubility of the products and the lattice characteristics of the involved solids unequivocally show why Ag_2O is such a good PIA reactant, while Tl_2O and PbO are completely incapable of driving the reaction. However, what about mercury(I)? Among the iodides, Hg_2I_2 exhibits an impressively large pK_{sp} of about 21 [**80**]. Tests with Hg_2SO_4 as a iodide-"sponge" reactant for PIA did not yield even traces of products. This is consistent with the enormous stability of the solid Hg_2SO_4 (monoclinic lattice), exhibiting $\Delta Gf^{(0)}$ of about −1.45 eV per atom [**79**]. At the same time, Hg_2O is unstable and disproportionate to HgO and Hg, making it an unfeasible candidate for a PIA reactant. The pK_{sp} of HgI_2, amounting to about 12, suggests the possible utility of the oxidatively stable Hg^{2+} as an iodide "sponge." Nevertheless, the use of HgO for PIA is thermodynamically unfeasible: $\Delta G_f^{(0)}$ of HgO (orthorhombic) and HgI_2 (tetragonal) is −0.65 and 0.31 eV per atom, respectively [**79**].

All these considerations illustrate the uniqueness of Ag_2O as an efficient scavenger of the hydrogen halides produced during etherification of alcohols with organic halides. Indeed, replacement of silver reagents with compounds comprising non-precious metal seems to be an important motivation in the search of alternative halide "sponges." As the 67th and 68th for their abundance, Hg and Ag have practically the same rarity amounting to about 50 to 80 ppb of the Earth's crust. Thallium is about 10 times more abundant than silver, but Tl^+ has lesser affinity for halides than Ag^+. As the 36th most abundant element, lead composes more than 10 ppm of the Earth's crust, and from that point of view, it may present a feasible avenue to pursue in the search for alternative PIA reactants. Nevertheless,

despite the 200 times planetary excess of lead over silver, toxicity and environmental considerations make silver by far the preferred choice.

Overall, the pronounced toxicity of mercury makes the pursuit of using its compounds for a reactant hugely unfeasible and impractical. Thallium and lead compounds are also immensely toxic. In contrast, silver compounds are some of the safest to use. After all, following the discovery of the photovoltaic effect with AgCl junction in the 19th century [**89**], AgBr was crucial for the development of photography [**90**,**91**]. Despite the toxicity of mercury, silver amalgams are a popular material for dental fillings. In fact, the United States Environmental Protection Agency's recommended safety level of silver ions in drinking water (about 0.1 mg L^{-1}) are almost the same as the admissible one of iron (about 0.3 mg L^{-1}). Conversely, the amounts of mercury must not exceed 2 ppb, thallium must be less than 0.5 μg L^{-1}, and lead must be below 15 μg L^{-1}. These safety and environmental consideration provide a strong argument for the utility of silver compounds for etherification reactants. Fortunately, our findings unequivocally show that among the readily commercially available compounds of ions with potentially high affinity for halides, Ag_2O is not only the best performing, but it is the only one that drives the etherification transformation (**Table 4-2**, **Figure 4-3**).

2.4. Microwave vs. Conventional Heating

For methylating carbohydrates in aqueous suspensions, PIA leads to high yields when carried out for extended periods of time. Lowering medium polarity increases the energy of the transition states, leading to a decrease in reaction rates. For PIA in non-polar media, heating is essential for ensuring the completion of the conversion in reasonable

time. Employing microwave heating led to the maximum conversion of 40% in 1 min, producing an equimolar mixture of **3** and **4**. Transferring the microwave conditions to conventional heating in a pressure tube (i.e., 1 mmol of **1** and 2 mmol of Ag_2O suspended in **2** and heated at 130 °C overnight) led to a 90% conversion to **4** with no traces of **3**. In comparison with the optimized base-driven etherification, PIA led to superbly higher yields (i.e., WE in 2ME in the presence of Cs_2CO_3 resulted in 40% transformation of **1** to **3** [**27**]), while PIA under conventional heating led to 90% conversion of **1** to **4**.

This drastic difference between the yields and the products from microwave and convectional heating reveals important features of the reaction (**Figure 4-3**). Under the former conditions, Ag_2O is the principal absorber of the microwave radiation and it is heated considerably faster than the surrounding organic media. The short microwave bursts, along with the finite rates of heat transfer from the solid oxide to the liquid, make the solution at the surface of the Ag_2O crystals hotter than that in the bulk of the organic phase. On the other hand, under conventional heating, the liquid phase is heated at the walls of the reaction vessel and transfers the heat to the solid oxide. Conversion of **1** to **4** is the first reaction step. Consequent hydrolysis of **4** leads to the formation of **3**. The considerably higher overall PIA yield for conventional rather than microwave heating suggests that the elevated temperature of the organic liquid is of primary importance for successful PIA, leading to etherification and esterification. Conversely, heat concentration on the basic solid oxide and at its interface with the organic reactants is essential for ester hydrolysis. These findings potentially have broad applicability in the design of heterogeneous synthetic procedures and the use of microwave heating only where it is most beneficial.

2.5. Box-Containing Oligomers

With NBA derivatives in hand, the coupling/reduction protocol offers synthetic routes for bioinspired molecular electrets with diverse lengths (i.e., *n*) and sequence composition (i.e., R_1 and R_2 side chains on each of the Aa residues) (**Figure 4-2**). To demonstrate the utility of the ether NBA for composing oligomers with Box residues for which **3** is a precursor, we synthesized trimers and tetramers that also contained brominated Aa residues, Baa (**Figure 4-4**). 5-bromo-2-nitrobenzoic acid, **5**, is the NBA precursor for Baa. Baa residues are of outmost importance for post-synthetic modification of Aa molecular electrets. Homogeneous catalysis allows for replacement of the Br substituent with other functional groups. For example, catalytic replacement of Br with azide and its consequential reduction to amine provide sites for amide coupling of other moieties to the specific Baa sites of the electret sequence [**25**]. This strategy is essential for attaching potent electron acceptors to the Aa conjugates. Most electron acceptors and electron-deficient photosensitizers cannot sustain the reducing conditions required for converting the N-terminal nitro groups to amines before each coupling step. Building the Aa sequences with Baa residues allows for mild conversation of -Br to $-NH_2$ in the synthesized oligomers, to which a carboxylate derivative of the electron-deficient moieties is readily attached [**25**].

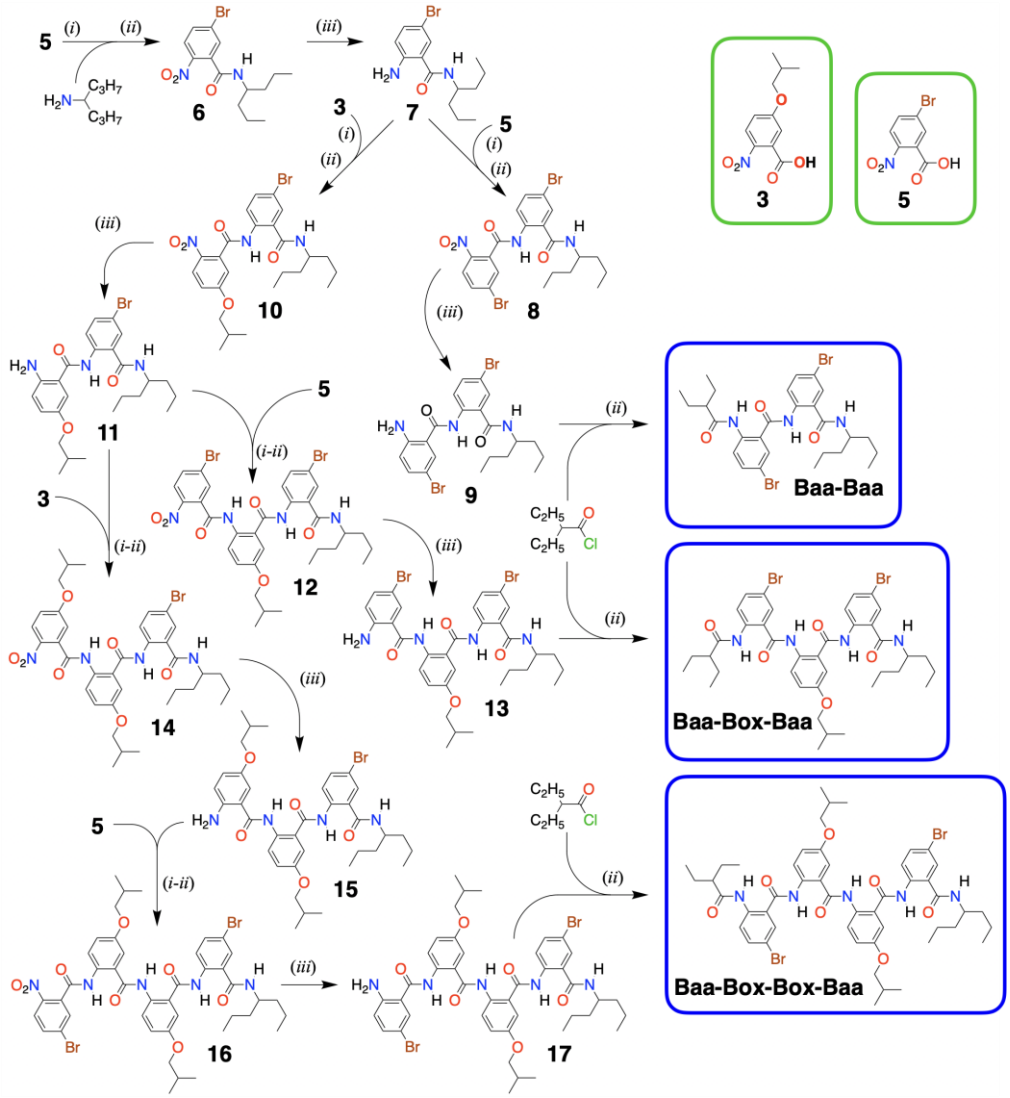

Fig. 4-4: Synthesis of different bioinspired molecular electrets (in the blue frames) from two NBA precursors for Aa residues (i.e., **3** for Box and **5** for Baa (in the green frames)) employing (*i*) carboxylate activation, (*ii*) amid coupling, and (*iii*) nitro reduction; (*i*,*ii*) designates in situ activation (i.e., the carboxylate activation is carried out in the presence of the N-terminal amine). To attach NBA derivatives to a Baa N-terminal amine, chlorination activation (*i*) of the NBA carboxylates was carried out separately, prior to amid coupling (*ii*) (i.e., (1) NBA, $(COCl)_2$, DCM, DMF, −78 °C to r.t., 1 h; (2) N-terminal amine, DCM, pyridine, −78 °C to r.t., overnight, 59% yield for **7** → **8** and 33% for **7** → **10**). To attach NBA derivatives to a Box N-terminal amine, carbodiimide carboxylate activation was carried out in situ with amid coupling (*i*,*ii*) (i.e., NBA, N-terminal amine, DIC, HOAt, DMAP, pyridine, DMF, r.t., overnight, 80% for **11** → **14** and 56% for **15** → **16**). Dicobalt octacarbonyl allows for selective reduction of the nitro groups (*iii*) (i.e., $Co_2(CO)_8$, 1,2-dimethoxyethane, 90 °C, 4 h; for N-terminal NO_2 on Baa: 72% for **6** → **7**, 75% for **8** → **9** and 34% for **16** → **17**; and for N-terminal NO_2 on Box: 33% for **10** → **11** and 47% for **14** → **15**). The results from HRMS, and ^1H and ^{13}C NMR analyses (**Figures 4S-3–4S-14**), confirm the identities of the products.

Building the Aa oligomers comprising Baa and Box revealed important features about the coupling and the reduction steps in the protocol. For the selective reduction of the N-terminal nitro groups, we used dicobaltum octacarbonyl, $Co_2(CO)_8$ [**92**,**93**]. Using organic solutions of $CrCl_2$ at room temperature offers the best yields for selective reduction of nitro groups to amines attached to Aa residues [**29**]. Nevertheless, the high sensitivity of $CrCl_2$ to oxygen warrants carrying out such reduction reactions in an oxygen-free glove box, which renders their applicability for routine synthesis somewhat unfeasible. The relative kinetic stability of $Co_2(CO)_8$ provides an attractive alternative for employing it as a reducing agent. While the yields of converting $-NO_2$ to $-NH_2$ with $Co_2(CO)_8$ are relatively high (i.e., usually exceed 70%), introducing a Box residue in the sequence tends to lower them to about 30% to 50% (**Figure 4-4**, **Scheme 4S-2**). Box is more electron-rich than Baa. Additionally, while Box manifests reversibility of its electrochemical oxidation at increased scan rates, the reduction potential of $Box^{\bullet+}$ exceeded 1.5 V vs. SCE [**27**], making it and its derivatives relatively susceptible to oxidative degradation. These electronic characteristics of ether Aa derivatives can render the formation of stable oligomers with amines on or near Box residues quite unfavorable.

The susceptibility of amines on N-terminal Box residues also governs the choice of amide coupling conditions. Activating the NBA precursors by converting them to acyl chlorides provides some of the most favorable conditions for building Aa oligomers [**17**,**29**]. For building Baa-Baa and Box-Baa sequence motifs, we chlorinated the acyl chlorides of **3** and **5** and added them to a cold solution of Baa with a free terminal amine, **7** (**Figure 4-4**). Similarly, we used aliphatic acyl chloride to cap the Baa N-terminal

amines of **9**, **13**, and **17** (**Figure 4-4**). The same synthetic strategy, however, proved unfeasible for attaching the NBA derivatives **3** and **5** to the Box N-terminal amines of **11** and **15** (**Figure 4-4**).

Carboxyl chlorides are immensely strong acetylating agents. In addition, the small size of chloride and fluoride leaving groups makes these acyl halides immensely favorable for avoiding steric hindrance during amide coupling with the not-too electrophilic aromatic amines at the N-termini. The favored strong reactivity of acyl chlorides is also their demise. Even traces of moisture readily hydrolyze the chlorides to the corresponding carboxylic acid. Impurities of even weak and sterically hindered nucleophiles, formed from solvent degradation, for example, can lead to side products. Carboxylates activated as HOSu, HOBt, and HOAt esters, on the other hand, preferentially react with amine nucleophiles. Furthermore, the hydrogen-bonding propensity of the nitrogen in the benzene ring of HOAt can stabilize the transition states during amide coupling, making it a considerably more potent reagent than its HOBt analogue. Therefore, for amide coupling to Box N-terminal amines of **11** and **15**, we employed in situ carbodiimide activation in the presence of HOAt (**Figure 4-4**, **Scheme 4S-2**).

These findings point out the underlying complexity in the design of synthetic strategies for making Aa molecular electrets (**Figure 4-2**). Electron-donating R_2 substituents increase the electrophilicity of the N-terminal amine. The free amine on such electron-rich residues may readily increase their susceptibility to oxidative degradation. Conversely, hydrogen bonding with the carbonyl oxygen at the ortho position forces the N-terminal amine to be coplanar with the aromatic ring, which decreases its

nucleophilicity. Hence, it is essential to select strong enough activation of the NBA carboxylate that undergoes amide coupling under mild enough conditions to prevent deuteriation of the amine starting material. Such optimal selection of activation and coupling strategies varies among the different sequence motifs of the Aa oligomers and warrants good understanding of the electronic properties of the comprising residues.

Conclusion

As promising as ether Aa residues are for hole-transfer bioinspired molecular electrets, their preparation is essential for exploring their utility and potential benefits. Robust and scalable methodologies for the synthesis of the ether derivatives of the 2-nitrobenzoic acid, NBA, precursors determine how accessible such electret conjugates can be. Is Ag_2O -driven Purdie-Irvine alkylation the silver bullet for such synthetic goals? Considering the 90% overall conversion yield under solvent-free conditions and conventional heating in the presence of Ag_2O, warrants a definite "yes" for an answer. The highest yields from reacting **1** and **2** under the conditions of optimized Williamson etherification were about 40% (**Table 4-1**). The Purdie-Irvine alkylation led to the formation of the ester of the desired ether derivative of the nitrobenzoic acid, warranting an additional hydrolysis step. The basic conditions of Williamson etherification ensure completion of the ester hydrolysis to produce the desired ether derivative of nitrobenzoic acid, but it does not lead to nearly as high yields as the Ag_2O driven transformations. The close-to-quantitative yields that Purdie-Irvine reaction reveal important potential pathways for addressing the shortcomings of the Williamson etherification.

References

1. Derr, J.B.; Tamayo, J.; Clark, J.A.; Morales, M.; Mayther, M.F.; Espinoza, E.M.; Rybicka-Jasinska, K.; Vullev, V.I. Multifaceted aspects of charge transfer. *Phys. Chem. Chem. Phys.* **2020**, *22*, 21583–21629.

2. Vullev, V.I. From Biomimesis to Bioinspiration: What's the Benefit for Solar Energy Conversion Applications? *J. Phys. Chem. Lett.* **2011**, *2*, 503–508.

3. Marcus, R.A.; Sutin, N. Electron Transfers in Chemistry and Biology. *Biochim. Biophys. Acta* **1985**, *811*, 265–322.

4. Beratan, D.N.; Betts, J.N.; Onuchic, J.N. Protein Electron-Transfer Rates Set by the Bridging Secondary and Tertiary Structure. *Science* **1991**, *252*, 1285–1288.

5. Beratan, D.N.; Onuchic, J.N.; Winkler, J.R.; Gray, H.B. Electron-Tunneling Pathways in Proteins. *Science* **1992**, *258*, 1740–1741.

6. Gray, H.B.; Winkler, J.R. Electron tunneling through proteins. *Q. Rev. Biophys.* **2003**, *36*, 341–372.

7. Skourtis, S.S.; Balabin, I.A.; Kawatsu, T.; Beratan, D.N. Protein dynamics and electron transfer: Electronic decoherence and non-Condon effects. *Proc. Natl. Acad. Sci. USA* **2005**, *102*, 3552–3557.

8. Beratan, D.N.; Liu, C.R.; Migliore, A.; Polizzi, N.F.; Skourtis, S.S.; Zhang, P.; Zhang, Y.Q. Charge Transfer in Dynamical Biosystems, or The Treachery of (Static) Images. *Acc. Chem. Res.* **2015**, *48*, 474–481.

9. Ing, N.L.; El-Naggar, M.Y.; Hochbaum, A.I. Going the Distance: Long-Range Conductivity in Protein and Peptide Bioelectronic Materials. *J. Phys. Chem. B* **2018**, *122*, 10403–10423.

10. Derr, J.B.; Tamayo, J.; Espinoza, E.M.; Clark, J.A.; Vullev, V.I. Dipole-induced effects on charge transfer and charge transport. Why do molecular electrets matter? *Can. J. Chem.* **2018**, *96*, 843–858.

11. Marcus, R.A. Exchange reactions and electron transfer reactions including isotopic exchange. Theory of oxidation-reduction reactions involving electron transfer. Part 4—A statistical-mechanical basis for treating contributions from solvent, ligands, and inert salt. *Discuss. Faraday Soc.* **1960**, 21–31.

12. Yomosa, S. Charge-Transfer Molecular Compounds in Biological Systems. *Sup. Prog. Theor. Phys.* **1967**, *40*, 249–263.

13. Steffen, M.A.; Lao, K.Q.; Boxer, S.G. Dielectric Asymmetry in the Photosynthetic Reaction-Center. *Science* **1994**, *264*, 810–816.

14. Galoppini, E.; Fox, M.A. Effect of the electric field generated by the helix dipole on photoinduced intramolecular electron transfer in dichromophoric alpha-helical peptides. *J. Am. Chem. Soc.* **1996**, *118*, 2299–2300.

15. Fox, M.A.; Galoppini, E. Electric field effects on electron transfer rates in dichromophoric peptides: The effect of helix unfolding. *J. Am. Chem. Soc.* **1997**, *119*, 5277–5285.

16. Knorr, A.; Galoppini, E.; Fox, M.A. Photoinduced intramolecular electron transfer in dichromophore-appended alpha-helical peptides: Spectroscopic properties and preferred conformations. *J. Phys. Org. Chem.* **1997**, *10*, 484–498.

17. Xia, B.; Bao, D.; Upadhyayula, S.; Jones, G.; Vullev, V.I. Anthranilamides as Bioinspired Molecular Electrets: Experimental Evidence for a Permanent Ground-State Electric Dipole Moment. *J. Org. Chem.* **2013**, *78*, 1994–2004.

18. Bao, D.; Upadhyayula, S.; Larsen, J.M.; Xia, B.; Georgieva, B.; Nunez, V.; Espinoza, E.M.; Hartman, J.D.; Wurch, M.; Chang, A.; et al. Dipole-Mediated Rectification of Intramolecular Photoinduced Charge Separation and Charge Recombination. *J. Am. Chem. Soc.* **2014**, *136*, 12966–12973.

19. Ashraf, M.K.; Pandey, R.R.; Lake, R.K.; Millare, B.; Gerasimenko, A.A.; Bao, D.; Vullev, V.I. Theoretical design of bioinspired macromolecular electrets based on anthranilamide derivatives. *Biotechnol. Prog.* **2009**, *25*, 915–922.

20. Larsen, J.M.; Espinoza, E.M.; Hartman, J.D.; Lin, C.-K.; Wurch, M.; Maheshwari, P.; Kaushal, R.K.; Marsella, M.J.; Beran, G.J.O.; Vullev, V.I. Building blocks for bioinspired electrets: Molecular-level approach to materials for energy and electronics. *Pure Appl. Chem.* **2015**, *87*, 779–792.

21. Larsen, J.M.; Espinoza, E.M.; Vullev, V.I. Bioinspired molecular electrets: Bottom-up approach to energy materials and applications. *J. Photon. Energy* **2015**, *5*, 055598.

22. Espinoza, E.M.; Larsen, J.M.; Vullev, V.I. What Makes Oxidized *N*-Acylanthranilamides Stable? *J. Phys. Chem. Lett.* **2016**, *7*, 758–764.

23. Espinoza, E.M.; Larsen-Clinton, J.M.; Krzeszewski, M.; Darabedian, N.; Gryko, D.T.; Vullev, V.I. Bioinspired Approach Toward Molecular Electrets: Synthetic Proteome for Materials. *Pure Appl. Chem.* **2017**, *89*, 1777–1797.

24. Larsen-Clinton, J.M.; Espinoza, E.M.; Mayther, M.F.; Clark, J.; Tao, C.; Bao, D.; Larino, C.M.; Wurch, M.; Lara, S.; Vullev, V.I. Fluorinated aminoanthranilamides: Non-native amino acids for bringing proteomic approaches to charge-transfer systems. *Phys. Chem. Chem. Phys.* **2017**, *19*, 7871–7876.

25. Krzeszewski, M.; Espinoza, E.M.; Cervinka, C.; Derr, J.B.; Clark, J.A.; Borchardt, D.; Beran, G.J.O.; Gryko, D.T.; Vullev, V.I. Dipole Effects on Electron Transfer are Enormous. *Angew. Chem. Int. Ed.* **2018**, *57*, 12365–12369.

26. Espinoza, E.M.; Bao, D.; Krzeszewski, M.; Gryko, D.T.; Vullev, V.I. Is it common for charge recombination to be faster than charge separation? *Int. J. Chem. Kinet.* **2019**, *51*, 657–668.

27. Derr, J.B.; Clark, J.A.; Morales, M.; Espinoza, E.M.; Vadhin, S.; Vullev, V.I. Solvent-induced selectivity of Williamson etherification in the pursuit of amides resistant against oxidative degradation. *RSC Adv.* **2020**, *10*, 24419–24424.

28. Rybicka-Jasinska, K.; Vullev, V.I. Molecular electrets—Why do dipoles matter for charge transfer and excited-state dynamics? *J. Photochem. Photobiol. A* **2020**, *401*, 112779.

29. Skonieczny, K.; Espinoza, E.M.; Derr, J.B.; Morales, M.; Clinton, J.M.; Xia, B.; Vullev, V.I. Biomimetic and bioinspired molecular electrets. How to make them and why does the established peptide chemistry not always work? *Pure Appl. Chem.* **2020**, *92*, 275–299.

30. Shin, Y.-G.K.; Newton, M.D.; Isied, S.S. Distance Dependence of Electron Transfer Across Peptides with Different Secondary Structures: The Role of Peptide Energetics and Electronic Coupling. *J. Am. Chem. Soc.* **2003**, *125*, 3722–3732.

31. Upadhyayula, S.; Bao, D.; Millare, B.; Sylvia, S.S.; Habib, K.M.M.; Ashraf, K.; Ferreira, A.; Bishop, S.; Bonderer, R.; Baqai, S.; et al. Permanent Electric Dipole Moments of Carboxyamides in Condensed Media: What Are the Limitations of Theory and Experiment? *J. Phys. Chem. B* **2011**, *115*, 9473–9490.

32. Yasutomi, S.; Morita, T.; Imanishi, Y.; Kimura, S. A Molecular Photodiode System That Can Switch Photocurrent Direction. *Science* **2004**, *304*, 1944–1947.

33. Cordes, M.; Kottgen, A.; Jasper, C.; Jacques, O.; Boudebous, H.; Giese, B. Influence of amino acid side chains on long-distance electron transfer in peptides: Electron hopping via "Stepping Stones". *Angew. Chem. Int. Edit.* **2008**, *47*, 3461–3463.

34. Shlizerman, C.; Atanassov, A.; Berkovich, I.; Ashkenasy, G.; Ashkenasy, N. De Novo Designed Coiled-Coil Proteins with Variable Conformations as Components of Molecular Electronic Devices. *J. Am. Chem. Soc.* **2010**, *132*, 5070–5076.

35. Becucci, L.; Guryanov, I.; Maran, F.; Guidelli, R. Effect of a Strong Interfacial Electric Field on the Orientation of the Dipole Moment of Thiolated Aib-Oligopeptides Tethered to Mercury on Either the N- or C-Terminus. *J. Am. Chem. Soc.* **2010**, *132*, 6194–6204.

36. Chen, Y.; Viereck, J.; Harmer, R.; Rangan, S.; Bartynski, R.A.; Galoppini, E. Helical peptides design for molecular dipoles functionalization of wide band gap oxides. *J. Am. Chem. Soc.* **2020**, *142*, 3489–3498.

37. Gray, H.B.; Winkler, J.R. Long-range electron transfer. *Proc. Natl. Acad. Sci. USA* **2005**, *102*, 3534–3539.

38. Vullev, V.I.; Jones, G., II. Photoinduced charge transfer in helical polypeptides. *Res. Chem. Intermed.* **2002**, *28*, 795–815.

39. Jones, G., II; Lu, L.N.; Vullev, V.; Gosztola, D.; Greenfield, S.; Wasielewski, M. Photoactive peptides. 6. Photoinduced electron transfer for pyrenesulfonamide conjugates of tryptophan-containing peptides. Mitigation of fluoroprobe behavior in N-terminal labeling experiments. *Bioorg. Med. Chem. Lett.* **1995**, *5*, 2385–2390.

40. O'Donnell, J.F.; Mann, C.K. Controlled-Potential Oxidation of Aliphatic Amides. *J. Electroanal. Chem. Interf. Electrochem.* **1967**, *13*, 157–162.

41. Espinoza, E.M.; Clark, J.A.; Soliman, J.; Derr, J.B.; Morales, M.; Vullev, V.I. Practical Aspects of Cyclic Voltammetry: How to Estimate Reduction Potentials When Irreversibility Prevails. *J. Electrochem. Soc.* **2019**, *166*, H3175–H3187.

42. Venkatramani, R.; Keinan, S.; Balaeff, A.; Beratan, D.N. Nucleic acid charge transfer: Black, white and gray. *Coord. Chem. Rev.* **2011**, *255*, 635–648.

43. Guo, S.; Bao, D.; Upadhyayula, S.; Wang, W.; Guvenc, A.B.; Kyle, J.R.; Hosseinibay, H.; Bozhilov, K.N.; Vullev, V.I.; Ozkan, C.S.; et al. Photoinduced Electron Transfer Between Pyridine Coated Cadmium Selenide Quantum Dots and Single Sheet Graphene. *Adv. Funct. Mater.* **2013**, *23*, 5199–5211.

44. Lu, H.; Bao, D.; Penchev, M.; Ghazinejad, M.; Vullev, V.I.; Ozkan, C.S.; Ozkan, M. Pyridine-coated lead sulfide quantum dots for polymer hybrid photovoltaic devices. *Adv. Sci. Lett.* **2010**, *3*, 101–109.

45. Purdie, T.; Irvine, J.C. The alkylation of sugars. *J. Chem. Soc.* **1903**, *83*, 1021–1037.

46. Wurtz, A. Note sur un nouveau mode de formation de l'éther ordinaire et de ses homologues. *Ann. Chim. Phys.* **1856**, *46*, 222–226.

47. Lander, G.D. LXIV—Alkylation by means of dry silver oxide and alkyl halides. *J. Chem. Soc. Trans.* **1900**, *77*, 729–753.

48. Thiem, J.; Wessel, H.-P. Reaktionen von Benzyliden-D-tetrosen. *Liebigs Ann. Chem.* **1982**, 595–606.

49. Sauthier, M.; Mortreux, A.; Suisse, I. From conventional to greener catalytic approaches for carbohydrates etherification. *Carbohydr. Chem. R. Soc. Chem.* **2014**, *40*, 73–98.

50. Hudson, C.S. Relations between rotatory power and structure in the sugar groups. XIV. The determination of ring structures in the glucose, mannose and rhamnose series. *J. Am. Chem. Soc.* **1926**, *48*, 1434–1443.

51. Sugihara, J.M.; Wolfrom, M.L. Maltotriose and its crystalline β-D-hendecaacetate. *J. Am. Chem. Soc.* **1949**, *71*, 3357–3359.

52. Whistler, R.L.; Kazeniac, S.J. Preparation of crystalline methyl 4-O-methyl-α-D-glucopyranoside and its triacetate. *J. Am. Chem. Soc.* **1954**, *76*, 3044–3045.

53. Purdie, T.; Irvine, J.C. The stereoisomeric tetramethyl methylglucosides and tetramethyl glucose. *J. Chem. Soc.* **1904**, *85*, 1049–1070.

54. Mahmud, I.; Garrett, T.J. Mass Spectrometry Techniques in Emerging Pathogens Studies: COVID-19 Perspectives. *J. Am. Soc. Mass Spectrom.* **2020**, *31*, 2013–2024.

55. Cipollo, J.F.; Parsons, L.M. Glycomics and glycoproteomics of viruses: Mass spectrometry applications and insights toward structure-function relationships. *Mass Spectrom. Rev.* **2020**, *39*, 371–409.

56. Smith, D.F.; Cummings, R.D.; Song, X. History and future of shotgun glycomics. *Biochem. Soc. Trans.* **2019**, *47*, 1–11.

57. Nurcombe, V.; Ling, L.; Hondermarck, H.; Cool, S.M.; Smith, R.A.A. Bringing Heparan Sulfate Glycomics Together with Proteomics for the Design of Novel Therapeutics: A Historical Perspective. *Proteomics* **2019**, *19*, 1800466.

58. Sureshan, K.M.; Das, T.; Shashidhar, M.S.; Gonnade, R.G.; Bhadbhade, M.M. Sulfonate protecting groups: Synthesis of D- and L-myo-inositol-1,3,4,5-tetrakisphosphate precursors by a novel silver(I) oxide-mediated O-alkylation of 2,4(6)-di-O-acyl-6(4)-O-sulfonyl-myo-inositol 1,3,5-orthoformate derivatives through intramolecular assistance of the sulfonyl group. *Eur. J. Org. Chem.* **2003**, 1035–1041.

59. Ren, B.; Lv, J.; Zhang, Y.; Tian, J.; Dong, H. Highly Efficient Selective Benzylation of Carbohydrates Catalyzed by Iron(III) with Silver Oxide and Bromide Anion as Co-catalysts. *ChemCatChem* **2017**, *9*, 950–953.

60. Das, T.; Shashidhar, M.S. Silver(I) oxide assisted O-alkylation of 2,3-di-O-benzyl-myo-inositol-1,3,5-orthoformate and its 6-O-substituted derivatives: Transannular participation of oxygen. *Carbohydr. Res.* **1997**, *297*, 243–249.

61. Harbury, P.B.; Zhang, T.; Kim, P.S.; Alber, T. A Switch between 2-Stranded, 3-Stranded and 4-Stranded Coiled Coils in Gcn4 Leucine-Zipper Mutants. *Science* **1993**, *262*, 1401–1407.

62. Robertson, D.E.; Farid, R.S.; Moser, C.C.; Urbauer, J.L.; Mulholland, S.E.; Pidikiti, R.; Lear, J.D.; Wand, A.J.; DeGrado, W.F.; Dutton, P.L. Design and synthesis of multi-heme proteins. *Nature* **1994**, *368*, 425–432.

63. Shoemaker, K.R.; Kim, P.S.; York, E.J.; Stewart, J.M.; Baldwin, R.L. Tests of the helix dipole model for stabilization of α-helices. *Nature* **1987**, *326*, 563–567.

64. Kerppola, T.; Curran, T. Zen and the art of Fos and Jun. *Nature* **1995**, *373*, 199–200.

65. Rabanal, F.; DeGrado, W.F.; Dutton, P.L. Toward the synthesis of a photosynthetic reaction center maquette: A cofacial porphyrin pair assembled between two subunits of a synthetic four-helix bundle multiheme protein. *J. Am. Chem. Soc.* **1996**, *118*, 473–474.

66. Jones, G., II; Vullev, V.; Braswell, E.H.; Zhu, D. Multistep Photoinduced Electron Transfer in a de Novo Helix Bundle: Multimer Self-Assembly of Peptide Chains Including a Chromophore Special Pair. *J. Am. Chem. Soc.* **2000**, *122*, 388–389.

67. Kornilova, A.Y.; Wishart, J.F.; Xiao, W.; Lasey, R.C.; Fedorova, A.; Shin, Y.-K.; Ogawa, M.Y. Design and Characterization of A Synthetic Electron-Transfer Protein. *J. Am. Chem. Soc.* **2000**, *122*, 7999–8006.

68. Jones, G., II; Vullev, V.I. Contribution of a Pyrene Fluorescence Probe to the Aggregation Propensity of Polypeptides. *Org. Lett.* **2001**, *3*, 2457–2460.

69. Jones, G., II; Vullev, V.I. Photoinduced Electron Transfer between Non-Native Donor-Acceptor Moieties Incorporated in Synthetic Polypeptide Aggregates. *Org. Lett.* **2002**, *4*, 4001–4004.

70. Vullev, V.I.; Jones, G. Photoinduced electron transfer in alkanoylpyrene aggregates in conjugated polypeptides. *Tetrahedron Lett.* **2002**, *43*, 8611–8615.

71. Fedorova, A.; Chaudhari, A.; Ogawa, M.Y. Photoinduced electron-transfer along α-helical and coiled-coil metallopeptides. *J. Am. Chem. Soc.* **2003**, *125*, 357–362.

72. Jones, G., II; Zhou, X.; Vullev, V.I. Photoinduced electron transfer in alpha -helical polypeptides: Dependence on conformation and electron donor-acceptor distance. *Photochem. Photobiol. Sci.* **2003**, *2*, 1080–1087.

73. Ghirlanda, G.; Osyczka, A.; Liu, W.; Antolovich, M.; Smith, K.M.; Dutton, P.L.; Wand, A.J.; DeGrado, W.F. *De Novo* Design of a D2-Symmetrical Protein that Reproduces the Diheme Four-Helix Bundle in Cytochrome bc1. *J. Am. Chem. Soc.* **2004**, *126*, 8141–8147.

74. Di Santo, J.P. A defining factor for natural killer cell development. *Nat. Immunol.* **2009**, *10*, 1051–1052.

75. Murphy, T.L.; Tussiwand, R.; Murphy, K.M. Specificity through cooperation: BATF-IRF interactions control immune-regulatory networks. *Nat. Rev. Immunol.* **2013**, *13*, 499–509.

76. Jang, Y.; Champion, J.A. Self-Assembled Materials Made from Functional Recombinant Proteins. *Acc. Chem. Res.* **2016**, *49*, 2188–2198.

77. Jay, A. The methylation reaction in carbohydrate analysis. *J. Carbohydr. Chem.* **1996**, *15*, 897–923.

78. Hansch, C.; Leo, A.; Taft, R.W. A Survey of Hammett Substituent Constants and Resonance and Field Parameters. *Chem. Rev.* **1991**, *91*, 165–195.

79. Jain, A.; Ong, S.P.; Hautier, G.; Chen, W.; Richards, W.D.; Dacek, S.; Cholia, S.; Gunter, D.; Skinner, D.; Ceder, G.; et al. Commentary: The Materials Project: A materials genome approach to accelerating materials innovation. *APL Mater.* **2013**, *1*, 011002.

80. Hansen, L.D.; Izatt, R.M.; Christensen, J.J. Thermodynamics of metal-halide coordination in aqueous solution. I. 'Equilibrium constants for several mercury(I)-

and mercury(II)-halide systems as a function of temperature. *Inorg. Chem.* **1963**, *2*, 1243–1245.

81. Clever, H.L.; Johnston, F.J. The solubility of some sparingly soluble lead salts: An evaluation of the solubility in water and aqueous electrolyte solution. *J. Phys. Chem. Ref. Data* **1980**, *9*, 751–784.

82. Chao, E.E.; Cheng, K.L. Stepwise titration of some anion mixtures and determination of Ksp of silver precipitates with silver ion selective electrode. *Anal. Chem.* **1976**, *48*, 267–271.

83. Alexander, R.; Ko, E.C.F.; Mac, Y.C.; Parker, A.J. Solvation of ions. XI. Solubility products and instability constants in water methanol, formamide, dimethylformamide, dimethylacetamide, dimethyl sulfoxide, acetonitrile, and hexamethylphosphorotriamide. *J. Am. Chem. Soc.* **1967**, *89*, 3703–3712.

84. Mussini, P.R.; Cipolli, A.; Mussini, T.; Rondinini, S. Standard aqueous potentials for the {thallium amalgam|thallium(I) iodide} electrode, and thermodynamic solubility product of thallium(I) iodide at temperatures from 298.15 K to 328.15 K. *J. Chem. Thermodyn.* **1993**, *25*, 1055–1059.

85. Davies, C.W.; Robinson, R.A. The solubility product of thallous iodide at 25°. *Trans. Faraday Soc.* **1937**, *33*, 633–635.

86. Subalakshmi, A.; Kavitha, B.; Karthika, A.; Nikhil, S.; Srinivasan, N.; Rajarajan, M.; Suganthi, A. Design of Mn and Zr incorporated Ag2O nanoparticles and their enhanced photocatalytic activity driven by visible light irradiation for degradation of rose bengal dye. *New J. Chem.* **2021**, *45*, 1876–1886.

87. Ono, S.; Tomizawa, R.; Nagai, T. Ion conduction mechanisms of silver halides under high pressures. *Phase Transit.* **2020**, *93*, 856–864.

88. Waghorne, W.E. Solubilities of the silver halides in aqueous mixtures of methanol, acetonitrile, and dimethylsulfoxide. *Monatsh. Chem.* **2003**, *134*, 655–667.

89. Becquerel, A.-E. Mémoire sur les effets électriques produits sous l'influence des rayons solaires. *Comptes Rendus* **1839**, *9*, 561–567.

90. Abeyweera, S.C.; Rasamani, K.D.; Sun, Y. Ternary Silver Halide Nanocrystals. *Acc. Chem. Res.* **2017**, *50*, 1754–1761.

91. Van Renterghem, W.; Goessens, C.; Schryver, D.; Van Landuyt, J.; Bollen, D.; De Keyzer, R.; Van Roost, C. Influence of twinning on the morphology of AgBr and AgCl microcrystals. *J. Imaging Sci. Technol.* **2001**, *45*, 349–356.

92. Lee, H.-Y.; An, M. Selective reduction of the nitro-group using Co2(CO)8-H2O. *Bull. Korean Chem. Soc.* **2004**, *25*, 1717–1719.

93. Purc, A.; Espinoza, E.M.; Nazir, R.; Romero, J.J.; Skonieczny, K.; Jeżewski, A.; Larsen, J.M.; Gryko, D.T.; Vullev, V.I. Gating That Suppresses Charge Recombination–The Role of Mono-*N*-Arylated Diketopyrrolopyrrole. *J. Am. Chem. Soc.* **2016**, *138*, 12826–12832

Experimental

MATERIALS

General methods. All chemicals were used as received unless otherwise specified. The reported ^{1}H NMR, ^{13}C NMR, and NOESY spectra were recorded on 400 MHz, 500 MHz and 600 MHz spectrometers. ^{1}H chemical shifts (δ) are reported in ppm relative to $CHCl_3$ in $CDCl_3$ (δ = 7.26 ppm); ^{13}C δ are reported in ppm relative to $CDCl_3$ (δ = 77.23 ppm). Data for ^{1}H NMR are reported as follows: chemical shift, integration, multiplicity (s = singlet, d = doublet, t = triplet, q = quartet, p = pentet/quintet, h = hextet/sextet, e = eptet(from επτά)/heptet, m = multiplet), and coupling constants. All ^{13}C NMR spectra were recorded with complete proton decoupling. High-resolution mass spectrometry (HRMS) was performed using Agilent LCTOF (6200) mass spectrometer (Agilent Technologies, Santa Clara, CA). Analytical thin layer chromatography was performed using 0.25 mm silica gel 60-F plates. Flash chromatography was performed using 60 Å, 32−63 μm silica gel.

Synthetic procedures

Scheme 4S-1. Synthesis of acid and ether derivatives.

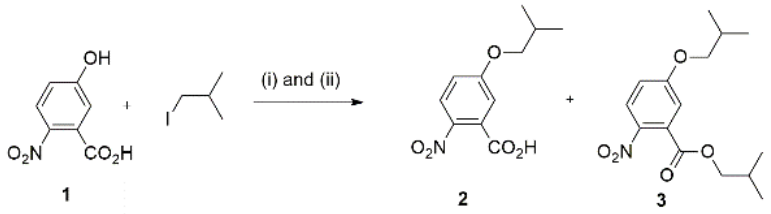

(i) C_4H_9I, Ag_2O, 130°C, 60 sec, 20% **(2),** 20% **(3)**; (ii) C_4H_9I, Ag_2O, 130°C, 18 h, 90% **(3)**.

Scheme 4S-2. Synthesis of anthranilamide oligomers.

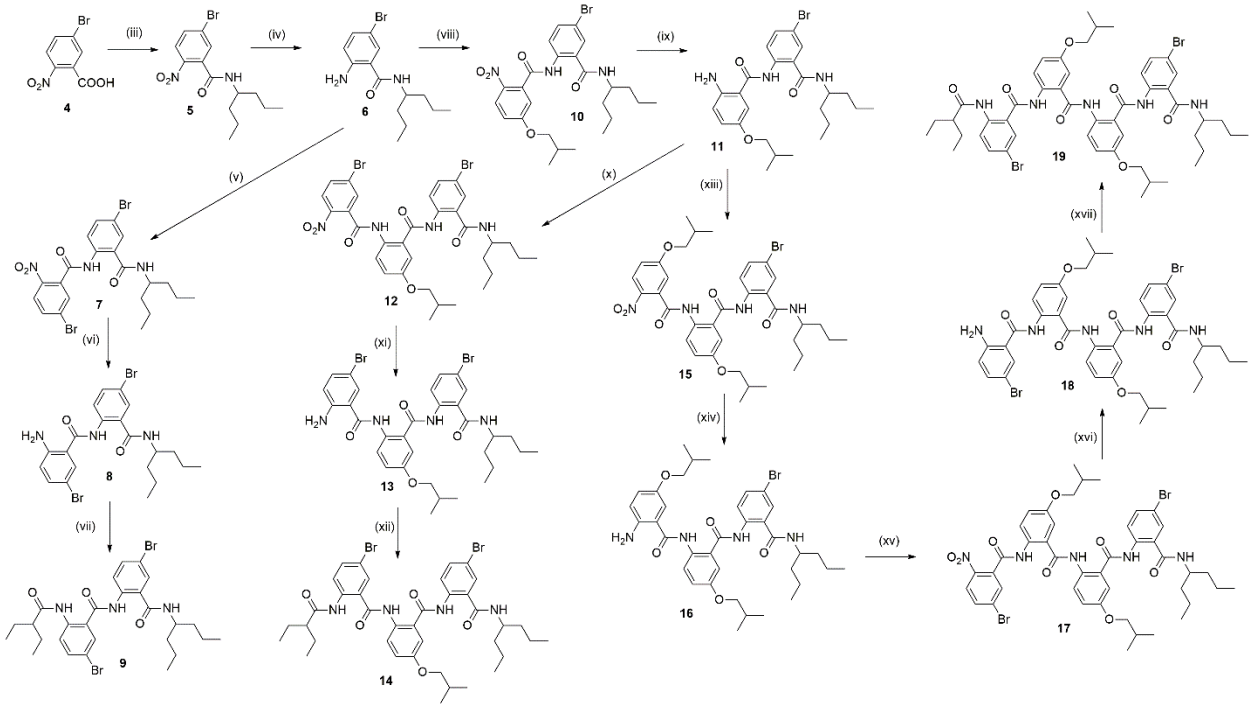

(iii) (1) 5-bromo-2-nitro benzoic acid, $(COCl)_2$, DCM, DMF, -78 °C to r.t., 1 h,; (2) 4-hepylamine, DCM, pyrdine, -78 °C to r.t., overnight, 92%; (iv) $Co_2(CO)_8$, 1,2-Dimethoxyethane, 90°C, 4 h, 72%; (v) (1) 5-bromo-2-nitro benzoic acid, $(COCl)_2$, DCM, DMF, -78 °C to r.t., 1 h,; (2), DCM, pyridine, -78 °C to r.t., overnight, 59%; (vi) $Co_2(CO)_8$, 1,2-Dimethoxyethane, 90°C, 4 h, 75%; (vii) 2-ethylbutyryl chloride, pyridine, THF, r.t., 1 h, 100%; (viii) (1) **(2)**, $(COCl)_2$, DCM, DMF, -78 °C to r.t., 1 h,; (2), DCM, pyridine, -78 °C to r.t., overnight, 0.57%; (ix) $Co_2(CO)_8$, 1,2-Dimethoxyethane, 90°C, 4 h, 33%; (x) 5-bromo-2-nitro benzoic acid, DIC, HOAt, DMAP, pyridine, DMF, r.t., Overnight, 80%; (xi) $Co_2(CO)_8$, 1,2-Dimethoxyethane, 90°C, 4 h, 61%; (xii) 2-ethylbutyryl chloride, pyridine, THF, r.t., 1 h, 85%; (xiii) **(2)**, DIC, HOAt, DMAP, pyridine, DMF, r.t., Overnight, 95%; (xiv) $Co_2(CO)_8$, 1,2-Dimethoxyethane, 90°C, 4 h, 47%; (xv) 5-bromo-2-nitro benzoic acid, DIC, HOAt, DMAP, pyridine, DMF, r.t., Overnight, 56%; (xvi) $Co_2(CO)_8$, 1,2-Dimethoxyethane, 90°C, 4 h, 34%; (xvii) 2-ethylbutyryl chloride, pyridine, THF, r.t., 1 h, 58%

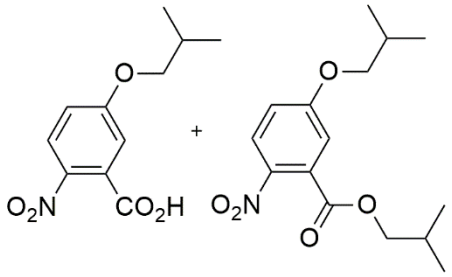

5-isobutoxy-2-nitrobenzoic acid (2) and isobutyl 5-isobutoxy-2-nitrobenzoate (3) (Scheme 4S-1). Ag_2O (463 mg, 2 mmol) was placed in a microwave vial, and purged with argon. Then 5-hydroxy-2-nitrobenzoic acid **(1)** (183 mg, 1 mmol). was added, followed by the 1-iodo-2-methylpropane (1 mL). The microwave vial was capped and put into the microwave. The parameters were set to 130°C, 60 W, 2×30 seconds. After the first interval the reaction mixture was allowed to cool for 5 minutes and then microwaved again at the same exact parameters giving a dark orange solution. The progress of the reaction was monitored via TLC. The mixture was diluted with 5% HCL and extracted with DCM (3×25mL). The organic layer was dried Na_2SO_4 and condensed. The products was purified using flash chromatography (stationary phase: silica gel; eluent gradient: 0:1 (v:v) to 1:1 (v:v) of ethyl acetate and hexanes. The 1:1 elution was mixed with 1% acetic acid. The product was condensed to afford 47 mg (20%) of **(2)** (white crystals) and 60 mg (20%) of **(3)** (brown oil). For **(2)**: ^{1}H NMR (600 MHz, Chloroform-*d*) δ 8.0khggi 2 (d, *J* = 9.1 Hz, 1H), 7.17 (d, *J* = 2.7 Hz, 1H), 7.05 (dd, *J* = 9.1, 2.7 Hz, 1H), 3.84 (d, *J* = 6.5 Hz, 2H), 2.13 (dq, *J* = 13.3, 6.7 Hz, 1H), 1.05 (d, *J* = 6.7 Hz, 6H) ppm. ^{13}C NMR (151 MHz, $CDCl_3$) δ 163.3, 140.1, 130.3, 126.9, 116.9, 115.0, 77.4, 77.2, 77.0, 75.7, 29.9, 28.3, 19.3, 19.1 ppm. HRMS (ESI) m/z calculated for $C_{11}H_{13}NO_5$: $[M-H]^-$ 238.0721, found 238.0827. For **(3)**: ^{1}H NMR (600 MHz, Chloroform-d) δ 7.98 (d, J = 9.0 Hz, 1H), 7.02 (d, J = 2.7 Hz, 1H),

6.98 (dd, J = 9.0, 2.8 Hz, 1H), 4.09 (d, J = 6.6 Hz, 2H), 3.79 (dd, J = 6.5, 3.4 Hz, 2H), 2.14 – 2.05 (m, 1H), 2.01 (m, J = 13.4, 6.7 Hz, 1H), 1.01 (d, J = 6.7 Hz, 6H), 0.94 (d, J = 6.7 Hz, 6H) ppm. ^{13}C NMR (151 MHz, CDCl3) δ 166.4, 163.2, 139.9, 131.6, 126.8, 126.6, 115.9, 114.8, 77.4, 77.2, 77.0, 75.5, 72.8, 28.2, 27.9, 27.7, 19.2, 19.2 ppm. HRMS (ESI) m/z calculated for $C_{15}H_{21}NO_5$: $[M+H]^+$ 295.1420, found 296.1491.

Conventional Heating

5-hydroxy-2-nitrobenzoic acid **(1)** (183 mg, 1 mmol), was placed in in a pressure tube with a stir bar and purged with argon. Two mL of 1-iodo-2-methylpropane was added, followed by the Ag_2O (463 mg, 2 mmol. The mixture was stirred at 130°C overnight. The progress of the reaction was monitored via TLC. The reaction was taken out of the oil bath for 10 minutes to cool and then diluted with 200 mL of 5% HCl and extracted with DCM (3×25mL). Dried over Na_2SO_4 and vacuum filtered. The filtrate was condensed. The product was purified using flash chromatography (stationary phase: silica gel; eluent gradient: 0:1 (v:v) to 1:1 (v:v) of ethyl acetate and hexanes. The 1:1 elution was mixed with 1% acetic acid. The product was condensed to afford 267 mg (90%) of **(3)** as a brown oil.

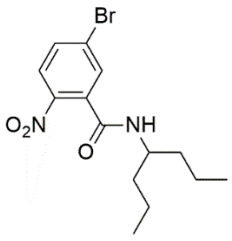

5-bromo-N-(heptan-4-yl)-2-nitrobenzamide (5) (Scheme 4S-2). (4) (500 mg, 2.03 mmol) was transferred to a dry, Ar purged 100 mL round bottom flask, with a stir bar. This was dissolved in 20 mL of DCM, with 3 drops of DMF. The reaction mixture was cooled to -78°C and was stirred for 5 minutes. Then, (270 µL, 3.05 mmol) of oxalyl chloride was added dropwise, the stirred for 1 h. The reaction was monitored via TLC by taking a few drops of reaction mixture and adding it to methanol. This would generate the ester from and move up the TLC plate. The reaction mixture was condensed 3 times, each time adding 20 mL of DCM. The condensed product was dissolved in 20 mL of DCM and cooled to -78°C for 5 min. 4-heptylamine (550 µL, 3.65 mmol) was added dropwise followed by pyridine (250 µL, 3.05 mmol). This was raised to room temperature and reacted overnight. Upon completion of the reaction, the mixture was quenched with 50 mL of 5% HCl. The mixture was extracted with DCM (3×25mL). The organic layer was dried Na_2SO_4 and condensed. The product was purified using flash chromatography (stationary phase: silica gel; eluent gradient: 1:9 (v:v) to 1:4 (v:v) of ethyl acetate and hexanes. The product was condensed to afford 638 mg (92%) of **(5)** as a light yellow powder. ^{1}H NMR (600 MHz, Chloroform-*d*) δ 7.93 (d, *J* = 8.7 Hz, 1H), 7.68 (dd, *J* = 8.7, 2.2 Hz, 1H), 7.59 (d, *J* = 2.1 Hz, 1H), 5.55 (d, *J* = 9.2 Hz, 1H), 4.16 – 4.07 (m, 1H), 1.56 (m, *J* = 13.3, 5.0, 3.1, 1.9 Hz, 4H), 1.51 – 1.38 (m, 4H), 0.97 (t, *J* = 7.1 Hz, 6H) ppm. ^{13}C NMR (151 MHz, $CDCl_3$) δ 164.7, 145.2, 135.2, 133.4, 131.9, 128.8, 126.2, 77.4, 77.2, 77.0, 50.2, 37.2, 19.3, 14.3 ppm. HRMS (ESI) m/z calculated for $C_{14}H_{19}BrN_2O_3$: $[M+H]^+$ 342.0573 found 343.0647.

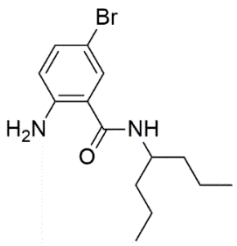

2-amino-5-bromo-N-(heptan-4-yl)benzamide (6) (Scheme 4S-2). (5) (300 mg, 0.88 mmol) and $Co_2(CO)_8$ (600 mg, 1.75 mmol) were placed in a 25-mL pressure tube with a magnetic stir bar in it. While purging with argon, 10 mL of 1,2-dimethoxyethane (DME) and five drops of DI water was added to the tube and tightly closed. While mixing, the pressure tube was immersed in a temperature-controlled oil bath. The mixture was heated to 90 °C and stirred for four hours. It was taken out of the oil bath and allowed to cool to room temperature prior to opening it. The reaction mixture was filtered; the filtrate was collected and condensed then diluted with 20 mL DCM, and washed with water (100 mL). The organic layer was collected, dried over Na_2SO_4, and concentrated in vacuo. The product was purified using flash chromatography (stationary phase: silica gel; eluent gradient: from 1:9 (v:v) to 1:4 ratio of ethyl acetate and hexanes) to afford 198 mg (72%) of **(5)** as a white solid. ^{1}H NMR (600 MHz, Chloroform-*d*) δ 7.37 (d, *J* = 2.2 Hz, 1H), 7.29 (dd, *J* = 8.7, 2.3 Hz, 1H), 6.65 (d, *J* = 8.7 Hz, 1H), 5.96 (s, 2H), 5.65 (d, *J* = 9.1 Hz, 1H), 4.10 (qd, *J* = 8.3, 4.1 Hz, 1H), 1.60 – 1.51 (m, 2H), 1.49 – 1.32 (m, 6H), 0.94 (t, *J* = 7.2 Hz, 6H) ppm. ^{13}C NMR (151 MHz, $CDCl_3$) δ 167.7, 146.7, 134.9, 129.5, 119.6, 119.0, 108.9, 77.4, 77.2, 77.0, 49.3, 37.8, 19.4, 14.3 ppm. HRMS (ESI) m/z calculated for $C_{14}H_{21}BrN_2O$: $[M+H]^+$ 312.0836 found 313.0909.

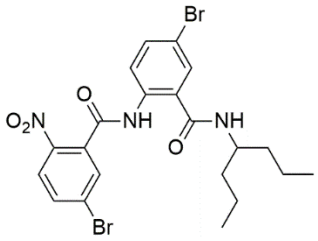

5-bromo-N-(4-bromo-2-(heptan-4-ylcarbamoyl)phenyl)-2-nitrobenzamide (7)

(Scheme 4S-2). 5-Bromo-2-nitrobenzoic acid (244 mg, 0.99 mmol), was transferred to a dry, Ar purged 100 mL round bottom flask, with a stir bar. This was dissolved in 20 mL of DMF. The reaction mixture was cooled to -78°C and was stirred for 5 minutes. Then, (170 µL, 1.99 mmol) of oxalyl chloride was added dropwise, the stirred for 1 h. The reaction was monitored via TLC by taking a few drops of reaction mixture and adding it to methanol. This would generate the ester from and move up the TLC plate. The reaction mixture was condensed 3 times, each time adding 20 mL of DCM. The condensed product was dissolved in 20 mL of DCM and cooled to -78°C for 5 min. **(6)** (465 mg, 1.49 mmol) was added dropwise followed by pyridine (122 µL, 1.49 mmol). This was raised to room temperature and reacted overnight. Upon completion of the reaction, the mixture was quenched with 50 mL of 5% HCl. The mixture was extracted with DCM (3×25mL). The organic layer was dried Na_2SO_4 and condensed. The product was purified using flash chromatography (stationary phase: silica gel; eluent gradient: 0:1 (v:v) to 1:9 (v:v) of ethyl acetate and hexanes. The product was condensed to afford 312 mg (59%) of **(7)** as a yellow oil. HRMS (ESI) m/z calculated for $C_{21}H_{23}Br_2N_3O_4$: $[M+H]^+$ 539.0035 found 542.0092.

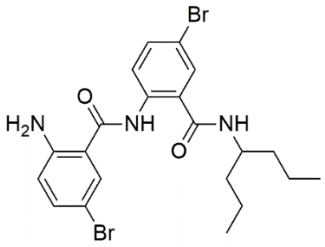

2-amino-5-bromo-N-(4-bromo-2-(heptan-4-ylcarbamoyl)phenyl)benzamide (8) (Scheme 4S-2). (7) (212 mg, 0.39 mmol) and $Co_2(CO)_8$ (267 mg, 0.78 mmol) were placed in a 25-mL pressure tube with a magnetic stir bar in it. While purging with argon, 10 mL of 1,2-dimethoxyethane (DME) and five drops of DI water was added to the tube and tightly closed. While mixing, the pressure tube was immersed in a temperature-controlled oil bath. The mixture was heated to 90 °C and stirred for 4 hours. It was taken out of the oil bath and allowed to cool to room temperature prior to opening it. The reaction mixture was filtered; the filtrate was collected and condensed then diluted with 20 mL DCM, and washed with water (100 mL). The organic layer was collected, dried over Na_2SO_4, and concentrated in vacuo. The product was purified using flash chromatography (stationary phase: silica gel; eluent gradient: from 0:1 (v:v) to 1:9 ratio of ethyl acetate and hexanes) to afford 149 mg (75%) of **(8)** as a yellow oil. ^{1}H NMR (600 MHz, Chloroform-*d*) δ 11.67 (s, 1H), 8.55 (d, *J* = 8.9 Hz, 1H), 7.72 (d, *J* = 2.3 Hz, 1H), 7.60 (dd, *J* = 8.9, 2.3 Hz, 1H), 7.55 (d, *J* = 2.3 Hz, 1H), 7.36 – 7.27 (d, 1H), 6.58 (dd, *J* = 12.1, 8.7 Hz, 1H), 5.83 (d, *J* = 9.2 Hz, 2H), 4.23 – 4.15 (m, 1H), 1.67 – 1.51 (m, 2H), 1.51 – 1.30 (m, 6H), 0.95 (t, *J* = 12.6, 7.2 Hz, 6H) ppm. ^{13}C NMR (151 MHz, $CDCl_3$) δ 167.6, 167.0, 148.8, 138.7, 135.8, 135.2, 130.6, 129.2, 123.7, 123.6, 119.2, 117.3, 115.6, 108.3, 77.4, 77.23, 77.0, 49.8, 37.7,

19.5, 19.4, 14.2, 1.2 ppm. HRMS (ESI) m/z calculated for $C_{21}H_{25}Br_2N_3O_2$: $[M+H]^+$ 509.0313 found 512.0370.

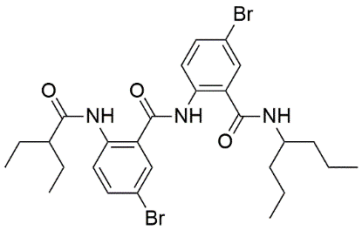

5-bromo-2-(5-bromo-2-(2-ethylbutanamido)benzamido)-N-(heptan-4-yl)benzamide (9) (Scheme 4S-2). (8) (100 mg, 0.196 mmol) was transferred to a dry, Ar purged 100 mL round bottom flask, with a stir bar. This was dissolved in 20 mL of THF. The reaction mixture was cooled to -78°C and was stirred for 5 minutes. Then, (33 µL, 0.24 mmol) of 2-ethylbutyryl chloride was added dropwise followed by pyridine (80 µL, 0.98 mmol) and the stirred for 1 h. Upon completion of the reaction, the mixture was quenched with 50 mL of 5% HCl. The mixture was extracted with DCM (3×25mL). The organic layer was dried Na_2SO_4 and condensed. The product was purified using flash chromatography (stationary phase: silica gel; eluent gradient: 0:1 (v:v) to 1:9 (v:v) of ethyl acetate and hexanes. The product was condensed to afford 127 mg (100%) of **(5)** as a white solid. ^{1}H NMR (600 MHz, Chloroform-*d*) δ 12.08 (s, 1H), 11.12 (s, 1H), 8.67 (d, *J* = 9.0 Hz, 1H), 8.55 (d, *J* = 8.9 Hz, 1H), 7.89 (d, *J* = 2.3 Hz, 1H), 7.64 (dd, *J* = 8.9, 2.3 Hz, 1H), 7.62 – 7.58 (m, 2H), 5.90 (d, *J* = 9.2 Hz, 1H), 4.20 (qt, *J* = 8.9, 5.1 Hz, 1H), 2.19 – 2.11 (m, 1H), 1.77 – 1.64 (m, 2H), 1.64 – 1.54 (m, 4H), 1.53 – 1.34 (m, 6H), 0.95 (t, *J* = 7.2 Hz, 12H) ppm. ^{13}C NMR (151 MHz, $CDCl_3$) δ 181.6, 175.4, 167.4, 166.7, 139.6, 138.1, 136.1, 135.4, 130.3, 129.3, 123.7, 123.3, 122.0, 116.5, 115.6, 77.4, 77.2, 77.0, 53.1, 50.0, 48.7, 37.7, 25.9, 25.0, 19.5,

14.2, 12.2, 12.0 ppm. HRMS (ESI) m/z calculated for $C_{27}H_{35}Br_2N_3O_3$: $[M+Na]^+$ 607.1046 found 632.0932.

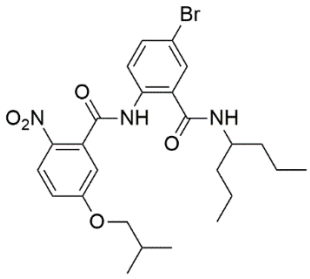

5-bromo-N-(heptan-4-yl)-2-(5-isobutoxy-2-nitrobenzamido)benzamide (10) (Scheme 4S-2). (2) (1271 mg, 5.34 mmol) was transferred to a dry, Ar purged 100 mL round bottom flask, with a stir bar. This was dissolved in 40 mL of DCM, with 5 drops of DMF. The reaction mixture was cooled to -78°C and was stirred for 5 minutes. Then, (916 µL, 10.68 mmol) of oxalyl chloride was added dropwise, the stirred for 1 h. The reaction was monitored via TLC by taking a few drops of reaction mixture and adding it to methanol. This would generate the ester from and move up the TLC plate. The reaction mixture was condensed 3 times, each time adding 20 mL of DCM. The condensed product was dissolved in 20 mL of DCM and cooled to -78°C for 5 min. **(6)** (1834 mg, 5.88 mmol) in 10 mL of DCM was added dropwise followed by pyridine (650 µL, 8.01 mmol). This was raised to room temperature and reacted overnight. Upon completion of the reaction, the mixture was quenched with 50 mL of 5% HCl. The mixture was extracted with DCM (3×25mL). The organic layer was dried Na_2SO_4 and condensed. The product was purified using flash chromatography (stationary phase: silica gel; eluent gradient: 0:1 (v:v) to 1:9 (v:v) of ethyl acetate and hexanes. The product was condensed to afford 161.46 mg (0.57%)

of **(10)** as a light yellow oil. HRMS (ESI) m/z calculated for $C_{25}H_{32}BrN_3O_5$: $[M+Na]^+$ 533.1530 found 558.1409.

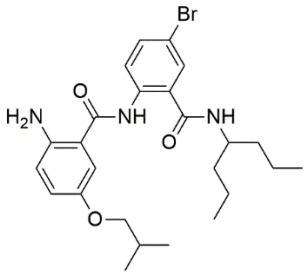

2-amino-N-(4-bromo-2-(heptan-4-ylcarbamoyl)phenyl)-5-isobutoxybenzamide (11) (Scheme 4S-2). (10) (100 mg, 0.188 mmol) and $Co_2(CO)_8$ (128 mg, 0.375 mmol) were placed in a 25-mL pressure tube with a magnetic stir bar in it. While purging with argon, 10 mL of 1,2-dimethoxyethane (DME) and five drops of DI water was added to the tube and tightly closed. While mixing, the pressure tube was immersed in a temperature-controlled oil bath. The mixture was heated to 90 °C and stirred for four hours. It was taken out of the oil bath and allowed to cool to room temperature prior to opening it. The reaction mixture was filtered; the filtrate was collected and condensed then diluted with 20 mL DCM, and washed with water (100 mL). The organic layer was collected, dried over Na_2SO_4, and concentrated in vacuo. The product was purified using flash chromatography (stationary phase: silica gel; eluent gradient: from 0:1 (v:v) to 1:9 ratio of ethyl acetate and hexanes) to afford 31 mg (33%) of **(11)** as a dark yellow solid. ^{1}H NMR (600 MHz, Chloroform-*d*) δ 11.83 (s, 1H), 8.66 (d, *J* = 8.8 Hz, 1H), 7.65 – 7.58 (m, 2H), 7.22 (d, *J* = 2.8 Hz, 1H), 6.96 (dd, *J* = 8.8, 2.7 Hz, 1H), 6.69 (d, *J* = 8.8 Hz, 1H), 5.96 (d, *J* = 9.1 Hz, 1H), 5.15 (s, 2H), 4.21 – 4.14 (m, 1H), 3.78 (d, *J* = 6.6 Hz, 2H), 2.11 (m, *J* = 14.9, 7.5 Hz, 1H), 1.64 – 1.55 (m, 2H), 1.54 – 1.33 (m, 6H), 1.06 (d, *J* = 6.7 Hz, 6H), 0.96 (t, *J* = 7.3 Hz,

6H) ppm. ^{13}C NMR (151 MHz, $CDCl_3$) δ 167.9, 167.6, 151.2, 143.7, 139.1, 135.2, 129.2, 123.4, 123.1, 122.5, 119.4, 116.0, 115.1, 111.8, 77.4, 77.2, 77.0, 75.5, 49.7, 37.6, 28.5, 19.5, 19.5, 14.2 ppm. HRMS (ESI) m/z calculated for $C_{25}H_{34}BrN_3O_3$: $[M-H]^-$ 503.1820 found 502.1749.

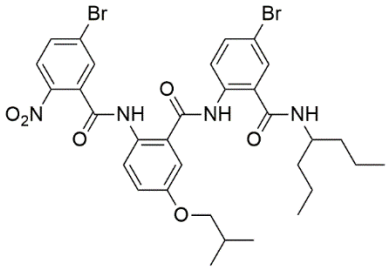

5-bromo-N-(2-((4-bromo-2-(heptan-4-ylcarbamoyl)phenyl)carbamoyl)-4-isobutoxyphenyl)-2-nitrobenzamide (12) (Scheme 4S-2). 5-Bromo-2-nitro benzoic acid (787 mg, 3.2 mmol), 1-Hydroxy-7-azabenzotriazole (HOAt) (490 mg, 3.6 mmol), N,N′-Diisopropylcarbodiimide (DIC) (500 µL, 3.2 mmol), 4-Dimethylaminopyridine (DMAP) (10 mg, 9.47 mmol) and pyridine (460 µL, 5.6 mmol) was dissolved in 20 mL of DMF in a dry, argon purged 100 mL round bottom flask with a stir bar. This was stirred for 15 minutes and then **(11)** (404 mg, 0.802 mmol) in 10 mL of DCM, was transferred and stirred overnight. The progress of the reaction was monitored via TLC. The mixture quenched with 100 mL of 5% HCl then was extracted with DCM (3×25mL). The organic layer was dried Na_2SO_4 and condensed. The product was purified using flash chromatography (stationary phase: silica gel; eluent gradient: 0:1 (v:v) to 1:9 (v:v) of ethyl acetate and hexanes. This afforded 471 mg (80%) of **(12)** as a yellow solid. ^1H NMR (600 MHz, Chloroform-*d*) δ 12.25 (s, 1H), 11.50 (s, 1H), 8.61 (d, J = 9.1 Hz, 1H), 8.52 – 8.47 (d, 1H), 7.97 (d, J = 8.7 Hz, 1H), 7.82 (d, J = 2.3 Hz, 1H), 7.74 (dd, J = 8.7, 2.1 Hz, 1H), 7.59 (d, J

= 7.7 Hz, 2H), 7.39 (d, J = 2.8 Hz, 1H), 7.15 (dd, J = 9.1, 2.8 Hz, 1H), 5.92 (d, J = 9.1 Hz, 1H), 4.20 – 4.10 (m, 1H), 3.84 (d, J = 6.6 Hz, 2H), 2.14 (hept, J = 6.7 Hz, 1H), 1.63 – 1.55 (m, 2H), 1.52 – 1.33 (m, 6H), 1.06 (d, J = 6.7 Hz, 6H), 0.94 (t, J = 7.3 Hz, 6H) ppm. ^{13}C NMR (151 MHz, $CDCl_3$) δ 167.4, 162.7, 155.8, 145.6, 138.3, 135.4, 135.1, 133.8, 133.1, 131.9, 129.3, 129.0, 126.4, 123.7, 123.5, 123.3, 121.8, 120.5, 116.3, 112.5, 77.4, 77.2, 77.0, 75.1, 49.9, 37.5, 29.9, 28.4, 19.5, 19.4, 14.2 ppm. HRMS (ESI) m/z calculated for $C_{32}H_{36}Br_2N_4O_6$: $[M+Na]^+$ 730.0944, found 732.0921.

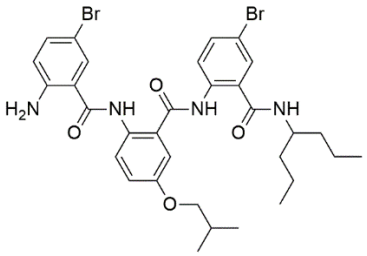

2-amino-5-bromo-N-(2-((4-bromo-2-(heptan-4-ylcarbamoyl)phenyl)carbamoyl)-4-isobutoxyphenyl)benzamide (13) (Scheme 4S-2). (12) (362 mg, 0.496 mmol) and $Co_2(CO)_8$ (339 mg, 0.99 mmol) were placed in a 25-mL pressure tube with a magnetic stir bar in it. While purging with argon, 10 mL of 1,2-dimethoxyethane (DME) and five drops of DI water was added to the tube and tightly closed. While mixing, the pressure tube was immersed in a temperature-controlled oil bath. The mixture was heated to 90 °C and stirred for 4 h. It was taken out of the oil bath and allowed to cool to room temperature prior to opening it. The reaction mixture was filtered; the filtrate was collected and condensed then diluted with 20 mL DCM, and washed with water (100 mL). The organic layer was collected, dried over Na_2SO_4, and concentrated in vacuo. The product was purified using flash chromatography (stationary phase: silica gel; eluent gradient: from 0:1 (v:v) to 1:9

ratio of ethyl acetate and hexanes) to afford 212 mg (61%) of **(13)** as a light yellow solid. ^{1}H NMR (600 MHz, Chloroform-*d*) δ 12.22 (s, 1H), 11.66 (s, 1H), 8.71 (d, *J* = 8.9 Hz, 1H), 8.54 (d, *J* = 9.1 Hz, 1H), 7.83 (d, *J* = 2.2 Hz, 1H), 7.68 (dd, *J* = 9.0, 2.3 Hz, 1H), 7.61 (d, *J* = 2.3 Hz, 1H), 7.40 (d, *J* = 2.8 Hz, 1H), 7.33 (dd, *J* = 8.7, 2.2 Hz, 1H), 7.15 (dd, *J* = 9.1, 2.8 Hz, 1H), 6.61 (d, *J* = 8.7 Hz, 1H), 5.94 (d, *J* = 9.1 Hz, 1H), 5.72 (s, 2H), 4.18 (m, *J* = 23.4, 12.0, 6.1 Hz, 1H), 3.86 (d, *J* = 6.6 Hz, 2H), 2.17 (m, *J* = 13.4, 6.7 Hz, 1H), 1.62 (m, *J* = 14.4, 5.8 Hz, 2H), 1.56 – 1.34 (m, 6H), 1.09 (d, *J* = 6.7 Hz, 6H), 0.97 (t, *J* = 7.3 Hz, 6H) ppm. ^{13}C NMR (151 MHz, $CDCl_3$) δ 167.6, 167.5, 166.7, 155.2, 148.5, 138.5, 135.6, 135.4, 133.5, 130.6, 129.2, 123.7, 123.6, 123.1, 122.3, 120.3, 119.1, 118.1, 116.1, 115.2, 112.4, 108.2, 77.4, 77.2, 77.0, 75.1, 49.9, 37.6, 29.9, 28.4, 19.5, 14.2 ppm. HRMS (ESI) m/z calculated for $C_{32}H_{38}Br_2N_4O_4$: $[M+H]^+$ 700.1260 found 701.1484.

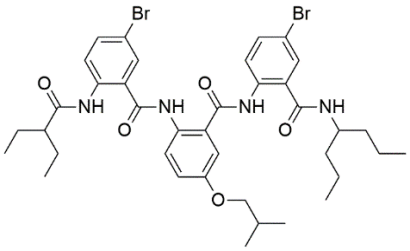

5-bromo-2-(2-(5-bromo-2-(2-ethylbutanamido)benzamido)-5-isobutoxybenzamido)-N-(heptan-4-yl)benzamide (14) (Scheme 4S-2). (13) (50 mg, 0.0714 mmol) was transferred to a dry, Ar purged 25 mL round bottom flask, with a stir bar. This was dissolved in 5 mL of THF. The reaction mixture was cooled to -78°C and was stirred for 5 minutes. Then, (12 µL, 0.086 mmol) of 2-ethylbutyryl chloride was added dropwise followed by pyridine (30 µL, 0.36 mmol) and the stirred for 3 h. Upon completion of the reaction, the mixture was quenched with 50 mL of 5% HCl. The mixture was extracted

with DCM (3×25mL). The organic layer was dried Na_2SO_4 and condensed. The product was purified using flash chromatography (stationary phase: silica gel; eluent gradient: 0:1 (v:v) to 1:9 (v:v) of ethyl acetate and hexanes. The product was condensed to afford 48 mg (85%) of **(13)** as a white solid. ^{1}H NMR (600 MHz, Chloroform-*d*) δ 12.36 (s, 1H), 11.98 (s, 1H), 11.17 (s, 1H), 8.66 (dd, *J* = 17.5, 9.0 Hz, 2H), 8.50 (d, *J* = 9.1 Hz, 1H), 7.97 (d, *J* = 2.3 Hz, 1H), 7.64 (dd, *J* = 8.9, 2.3 Hz, 1H), 7.61 (d, *J* = 2.3 Hz, 1H), 7.57 (dd, *J* = 9.0, 2.2 Hz, 1H), 7.41 (d, *J* = 2.8 Hz, 1H), 7.15 (dd, *J* = 9.1, 2.8 Hz, 1H), 6.12 (d, *J* = 9.1 Hz, 1H), 4.16 (m, *J* = 8.8, 5.0, 4.4 Hz, 1H), 3.84 (d, *J* = 6.6 Hz, 2H), 2.15 (m, *J* = 12.6, 7.9, 4.6 Hz, 2H), 1.74 – 1.66 (m, 2H), 1.64 – 1.52 (m, 4H), 1.49 (m, *J* = 13.7, 9.0, 5.0 Hz, 2H), 1.39 (m, *J* = 16.5, 13.5, 7.2 Hz, 4H), 1.06 (d, *J* = 6.7 Hz, 6H), 0.94 (t, *J* = 7.4 Hz, 12H) ppm. ^{13}C NMR (151 MHz, $CDCl_3$) δ 175.4, 167.6, 167.5, 166.2, 155.7, 139.4, 138.4 135.6, 135.6, 132.9, 130.2, 129.3, 123.7, 123.5, 123.2, 123.0, 122.8, 122.5, 120.3, 116.3, 115.5, 115.2, 112.4, 77.4, 77.2, 77.0, 75.1, 53.0, 49.9, 37.5, 28.4, 25.8, 25.0, 19.5, 19.4, 14.2, 12.2, 12.0 ppm. HRMS (ESI) m/z calculated for $C_{27}H_{35}Br_2N_3O_3$: $[M-H]^-$ 798.2000 found 799.1915.

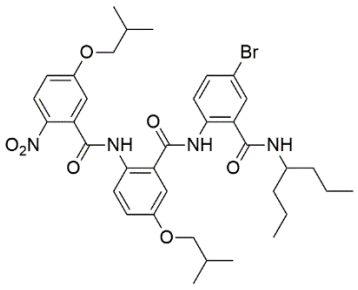

5-bromo-N-(heptan-4-yl)-2-(5-isobutoxy-2-(5-isobutoxy-2-nitrobenzamido)benzamido)benzamide (15) (Scheme 4S-2). (2) (95 mg, 0.40 mmol),

HOAt (61 mg, 0.45 mmol), DIC (62 μL, 0.40 mmol), DMAP (1 mg, 0.001 mmol) and pyridine (60 μL, 0.70 mmol) was dissolved in 10 mL of DMF in a dry, argon purged 100 mL round bottom flask with a stir bar. This was stirred for 15 minutes and then **(11)** (50 mg, 0.099 mmol) in 5 mL of DCM, was transferred and stirred overnight. The progress of the reaction was monitored via TLC. The mixture quenched with 100 mL of 5% HCl then was extracted with DCM (3×25mL). The organic layer was dried Na_2SO_4 and condensed. The product was purified using flash chromatography (stationary phase: silica gel; eluent gradient: 0:1 (v:v) to 2:4 (v:v) of ethyl acetate and hexanes. This afforded 68 mg (95%) of **(15)** as a dark yellow solid. ^{1}H NMR (600 MHz, Chloroform-*d*) δ 12.16 (s, 1H), 11.26 (s, 1H), 8.65 (d, *J* = 9.1 Hz, 1H), 8.50 – 8.46 (m, 1H), 8.14 (d, *J* = 9.1 Hz, 1H), 7.59 – 7.54 (m, 2H), 7.37 (d, *J* = 2.8 Hz, 1H), 7.16 (dd, *J* = 9.1, 2.8 Hz, 1H), 7.08 (d, *J* = 2.7 Hz, 1H), 7.00 (dd, *J* = 9.1, 2.7 Hz, 1H), 5.87 (d, *J* = 9.1 Hz, 1H), 4.20 – 4.10 (m, 1H), 3.83 (d, *J* = 6.5 Hz, 4H), 2.14 (m, *J* = 13.3, 10.1, 6.7 Hz, 2H), 1.64 – 1.53 (m, 2H), 1.53 – 1.44 (m, 2H), 1.39 (m, *J* = 20.8, 9.7, 6.5 Hz, 4H), 1.05 (dd, *J* = 15.5, 6.7 Hz, 12H), 0.95 (t, *J* = 7.3 Hz, 6H). ppm. ^{13}C NMR (151 MHz, $CDCl_3$) δ 167.4, 164.6, 163.7, 155.6, 138.9, 138.4, 136.2, 135.3, 133.3, 129.4, 127.5, 123.7, 123.4, 123.3, 121.9, 120.4, 116.1, 115.6, 115.2, 114.3, 112.4, 77.4, 77.2, 77.0, 75.5, 75.1, 49.9, 37.5, 28.4, 28.3, 19.5, 19.4, 19.3, 14.2 ppm. HRMS (ESI) m/z calculated for $C_{36}H_{45}BrN_4O_7$: $[M+Na]^+$ 724.2472, found 725.2702.

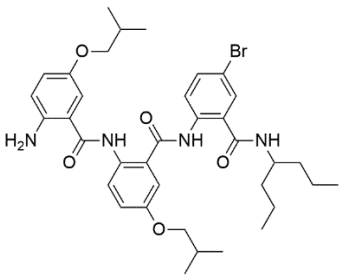

2-amino-N-(2-((4-bromo-2-(heptan-4-ylcarbamoyl)phenyl)carbamoyl)-4-isobutoxyphenyl)-5-isobutoxybenzamide (16) (Scheme 4S-2). (15) (274 mg, 0.379 mmol) and $Co_2(CO)_8$ (259 mg, 0.76 mmol) were placed in a 25-mL pressure tube with a magnetic stir bar in it. While purging with argon, 10 mL of 1,2-dimethoxyethane (DME) and five drops of DI water was added to the tube and tightly closed. While mixing, the pressure tube was immersed in a temperature-controlled oil bath. The mixture was heated to 90 °C and stirred for four hours. It was taken out of the oil bath and allowed to cool to room temperature prior to opening it. The reaction mixture was filtered; the filtrate was collected and condensed then diluted with 20 mL DCM, and washed with water (100 mL). The organic layer was collected, dried over Na_2SO_4, and concentrated in vacuo. The product was purified using flash chromatography (stationary phase: silica gel; eluent gradient: from 0:1 (v:v) to 1:5 ratio of ethyl acetate and hexanes) to afford 123 mg (47%) of **(13)** as a yellow solid. ^{1}H NMR (600 MHz, Chloroform-*d*) δ 12.21 (s, 1H), 11.72 (s, 1H), 8.67 (d, *J* = 8.9 Hz, 1H), 8.63 (d, *J* = 9.1 Hz, 1H), 7.61 – 7.58 (m, 1H), 7.58 – 7.55 (m, 1H), 7.37 (d, *J* = 2.8 Hz, 1H), 7.27 (d, *J* = 2.8 Hz, 1H), 7.13 (dd, *J* = 9.1, 2.8 Hz, 1H), 6.92 (dd, *J* = 8.8, 2.7 Hz, 1H), 6.66 (d, *J* = 8.8 Hz, 1H), 5.93 (d, *J* = 9.1 Hz, 1H), 5.40 – 5.37 (m, 2H), 4.16 (m, *J* = 8.7, 4.9, 4.3 Hz, 1H), 3.83 (d, *J* = 6.6 Hz, 2H), 3.78 (d, *J* = 6.6 Hz, 2H), 2.18 – 2.06 (m, 2H), 1.58 (m, *J* = 11.4, 9.6, 5.8 Hz, 2H), 1.51 – 1.33 (m, 6H), 1.06 (d, *J* = 6.7 Hz, 12H), 0.94 (t, *J* = 7.3 Hz, 6H) ppm. ^{13}C NMR (151 MHz, $CDCl_3$) δ 167.8, 167.6, 167.5, 155.0, 151.0, 143.8, 138.7, 135.3, 134.1, 129.3, 123.4, 123.1, 122.0, 121.8, 120.4, 119.2, 116.7, 115.9, 112.3, 112.1, 77.4, 77.2, 77.0, 75.7, 75.1, 49.9, 37.6, 28.5, 28.4,

19.6, 19.5, 14.2 ppm. HRMS (ESI) m/z calculated for $C_{36}H_{47}BrN_4O_5$: $[M+H]^+$ 694.2709 found 697.2772.

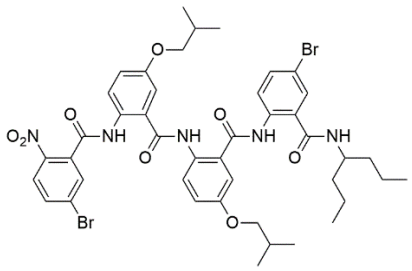

5-bromo-N-(2-((2-((4-bromo-2-(heptan-4-ylcarbamoyl)phenyl)carbamoyl)-4-isobutoxyphenyl)carbamoyl)-4-isobutoxyphenyl)-2-nitrobenzamide (17) (Scheme 4S-2). 5-Bromo-2-nitro benzoic acid (172 mg, 0.70 mmol), HOAt (108 mg, 0.79 mmol), DIC (109 µL, 0.70 mmol), DMAP (3 mg, 0.02 mmol) and pyridine (100 µL, 1.23 mmol) was dissolved in 15 mL of DMF in a dry, argon purged 100 mL round bottom flask with a stir bar. This was stirred for 15 minutes and then **(16)** (122 mg, 0.176 mmol) in 5 mL of DCM, was transferred and stirred overnight. The progress of the reaction was monitored via TLC. The mixture quenched with 100 mL of 5% HCl then was extracted with DCM (3×25mL). The organic layer was dried Na_2SO_4 and condensed. The product was purified using flash chromatography (stationary phase: silica gel; eluent gradient: 0:1 (v:v) to 1:4 (v:v) of ethyl acetate and hexanes. This afforded 91 mg (56%) of **(17)** as a yellow solid. ^{1}H NMR (600 MHz, Chloroform-*d*) δ 12.36 (s, 1H), 12.10 (s, 1H), 11.60 (s, 1H), 8.69 – 8.65 (m, 1H), 8.63 (d, *J* = 9.1 Hz, 1H), 8.47 (d, *J* = 9.1 Hz, 1H), 7.96 (d, *J* = 8.7 Hz, 1H), 7.82 (d, *J* = 2.1 Hz, 1H), 7.72 (dd, *J* = 8.7, 2.1 Hz, 1H), 7.62 – 7.56 (m, 2H), 7.45 (d, *J* = 2.8 Hz, 1H), 7.40 (d, *J* = 2.8 Hz, 1H), 7.13 (ddd, *J* = 20.8, 9.1, 2.8 Hz, 2H), 5.93 (d, *J* = 9.1 Hz, 1H), 4.16 (m, *J* = 8.6, 3.6 Hz, 1H), 3.86 (d, *J* = 6.6 Hz, 2H), 3.83 (d, *J* = 6.6 Hz, 2H), 2.15

(m, J = 19.9, 6.7 Hz, 2H), 1.63 – 1.55 (m, 2H), 1.53 – 1.31 (m, 6H), 1.07 (dd, J = 21.5, 6.7 Hz, 12H), 0.94 (t, J = 7.3 Hz, 6H) ppm. ^{13}C NMR (151 MHz, $CDCl_3$) δ 167.6, 167.5, 167.0, 162.7, 155.7, 145.6, 138.6, 135.5, 135.2, 133.8, 133.1, 133.0, 131.9, 129.3, 129.0, 126.4, 123.6, 123.4, 123.0, 122.3, 120.4, 120.1, 116.2, 115.2, 112.5, 77.4, 77.2, 77.0, 75.2, 75.1, 49.9, 37.6, 28.5, 28.4, 19.5, 19.5, 19.4, 14.2. HRMS (ESI) m/z calculated for $C_{43}H_{49}Br_2N_5O_8$: $[M+Na]^+$ 921.1911, found 946.1795.

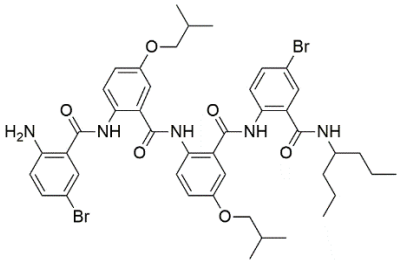

2-amino-5-bromo-N-(2-((2-((4-bromo-2-(heptan-4-ylcarbamoyl)phenyl)carbamoyl)-4-isobutoxyphenyl)carbamoyl)-4-isobutoxyphenyl)benzamide (18) (Scheme 4S-2). **(17)** (48 mg, 0.0521 mmol) and $Co_2(CO)_8$ (36 mg, 0.10 mmol) were placed in a 25-mL pressure tube with a magnetic stir bar in it. While purging with argon, 10 mL of 1,2-dimethoxyethane (DME) and five drops of DI water was added to the tube and tightly closed. While mixing, the pressure tube was immersed in a temperature-controlled oil bath. The mixture was heated to 90 °C and stirred for four hours. It was taken out of the oil bath and allowed to cool to room temperature prior to opening it. The reaction mixture was filtered; the filtrate was collected and condensed then diluted with 20 mL DCM, and washed with water (100 mL). The organic layer was collected, dried over Na_2SO_4, and concentrated in vacuo. The product was purified using flash chromatography (stationary phase: silica gel; eluent gradient: from 0:1 (v:v) to 1:4 ratio of ethyl acetate and hexanes)

to afford crude of **(17)** as a yellow solid. HRMS (ESI) m/z calculated for $C_{43}H_{51}Br_2N_5O_6$: $[M-H]^-$ 891.2197 found 892.2111.

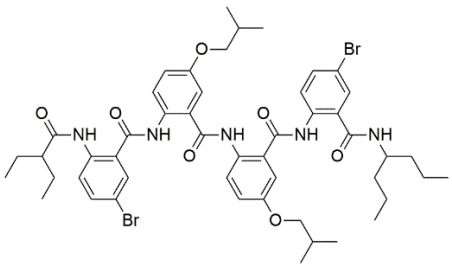

5-bromo-2-(2-(2-(5-bromo-2-(2-ethylbutanamido)benzamido)-5-isobutoxybenzamido)-5-isobutoxybenzamido)-N-(heptan-4-yl)benzamide (19) (Scheme 4S-2). The crude mixture of **(18)** (0.0521 mmol) was transferred to a dry, Ar purged 25 mL round bottom flask, with a stir bar. This was dissolved in 5 mL of THF. The reaction mixture was cooled to -78°C and was stirred for 5 minutes. Then, (3 µL, 0.021 mmol) of 2-ethylbutyryl chloride was added dropwise followed by pyridine (7 µL, 0.36 mmol) and the stirred for 3 h. Upon completion of the reaction, the mixture was quenched with 50 mL of 5% HCl. The mixture was extracted with DCM (3×25mL). The organic layer was dried Na_2SO_4 and condensed. The product was purified using flash chromatography (stationary phase: silica gel; eluent gradient: 0:1 (v:v) to 1:9 (v:v) of ethyl acetate and hexanes. The product was condensed to afford 10 mg (19%) of **(13)** as a white solid. ^{1}H NMR (600 MHz, Chloroform-*d*) δ 12.38 (s, 1H), 12.21 (s, 1H), 12.08 (s, 1H), 11.20 (s, 1H), 8.71 – 8.65 (m, 3H), 8.51 (d, *J* = 9.1 Hz, 1H), 7.99 (d, *J* = 2.3 Hz, 1H), 7.61 – 7.56 (m, 3H), 7.48 (d, *J* = 2.8 Hz, 1H), 7.42 (d, *J* = 2.8 Hz, 1H), 7.16 (ddd, *J* = 21.7, 9.1, 2.8 Hz, 2H), 5.91 (d, *J* = 9.1 Hz, 1H), 4.17 (m, *J* = 13.2, 4.5, 3.9 Hz, 1H), 3.87 (d, *J* = 6.6 Hz, 2H), 3.84 (d, *J* = 6.6 Hz, 2H), 2.16 (m, *J* = 17.7, 13.2, 6.9 Hz, 2H), 1.75 – 1.67 (m,

2H), 1.65 – 1.53 (m, 4H), 1.52 – 1.33 (m, 6H), 1.08 (dd, *J* = 17.8, 6.7 Hz, 12H), 0.94 (t, *J* = 7.4, 4.1 Hz, 12H) ppm. ^{13}C NMR (151 MHz, $CDCl_3$) δ 175.3, 167.8, 167.5, 167.1, 166.2, 155.7, 139.5, 138.6, 135.6, 135.4, 133.3, 132.9, 130.3, 129.3, 123.7, 123.5, 123.3, 123.1, 122.8, 121.9, 120.6, 120.0, 116.2, 115.5, 112.6, 112.4, 77.4, 77.2, 77.0, 75.2, 75.1, 53.1, 49.9, 37.6, 29.9, 28.5, 28.4, 25.9, 19.6, 19.5, 14.2, 12.2 ppm. HRMS (ESI) m/z calculated for $C_{49}H_{61}Br_2N_5O_7$: $[M-H]^-$ 989.2934 found 990.2853.

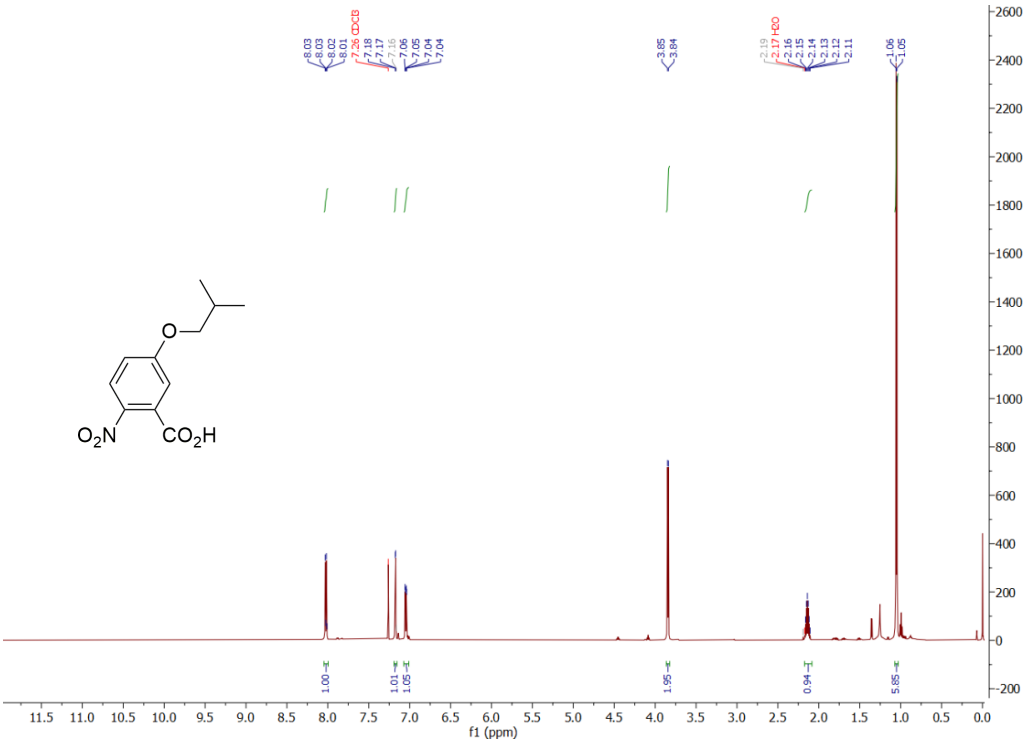

a

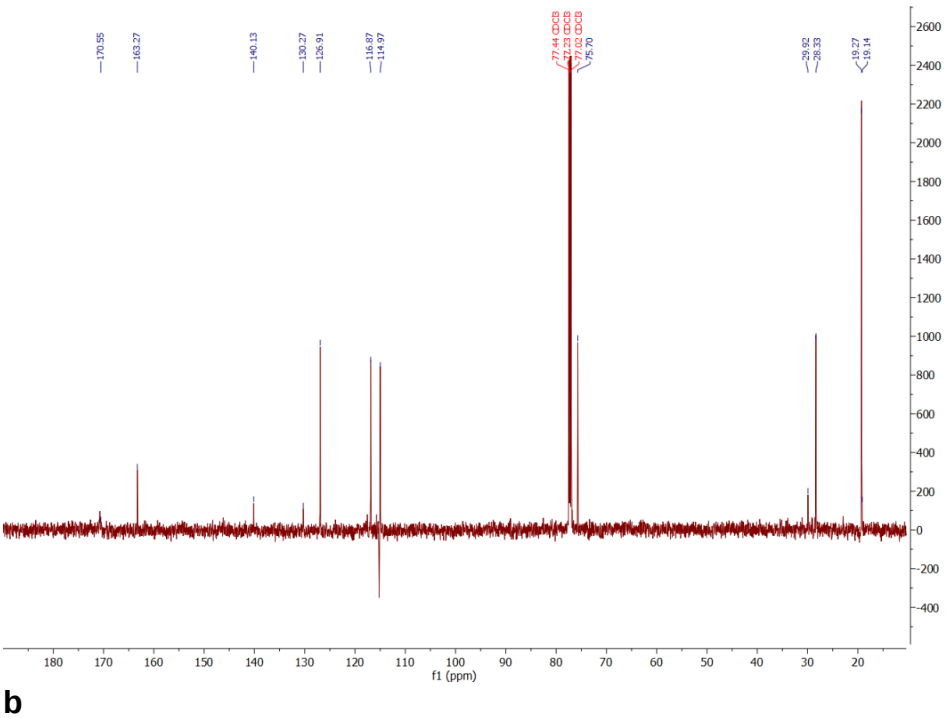

b

Figure 4S-1. (a) ^{1}H NMR of **(2)** (600 MHz, $CDCl_3$); (b) ^{13}C NMR of **(2)** (151 MHz, $CDCl_3$).

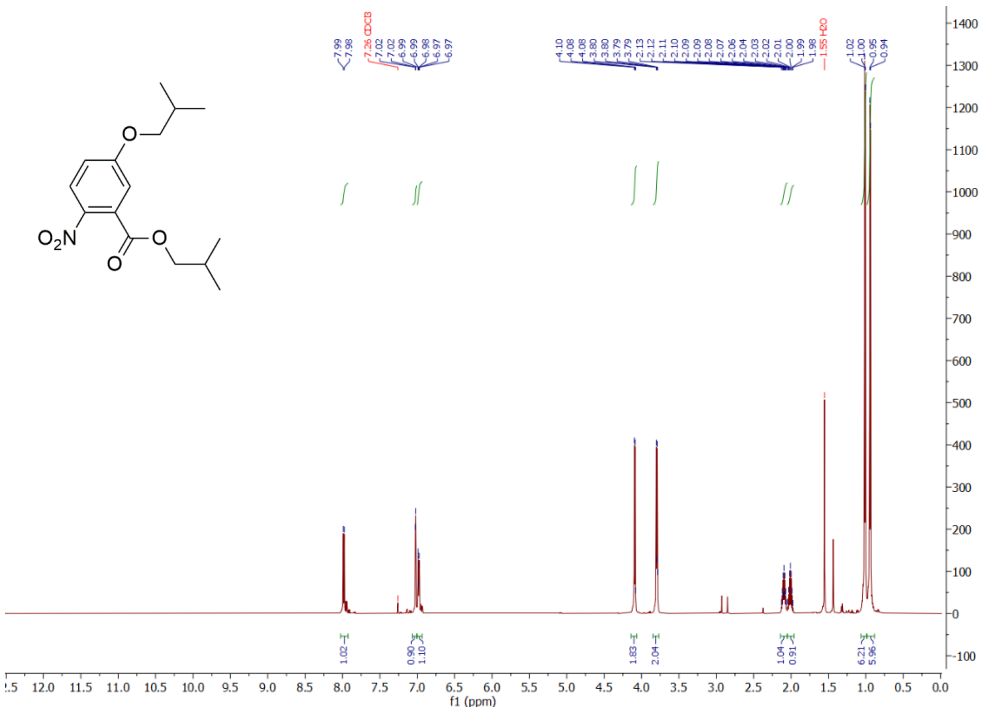

a

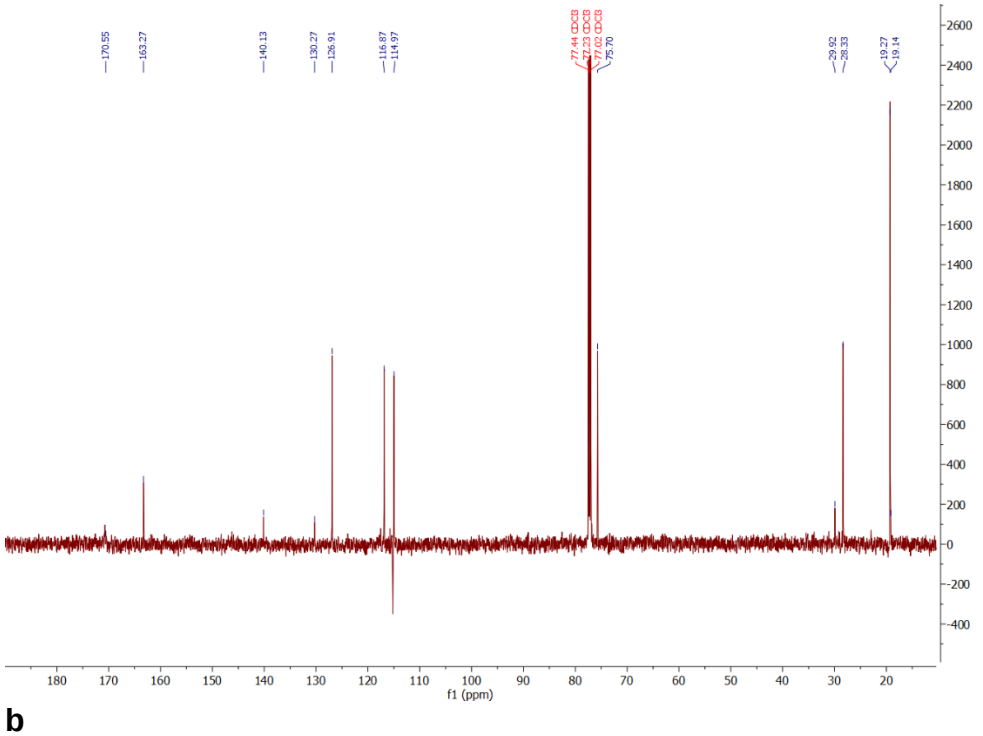

b

Figure 4S-2. (a) ^{1}H NMR of **(3)** (600 MHz, $CDCl_3$); (b) ^{13}C NMR of **(3)** (151 MHz, $CDCl_3$).

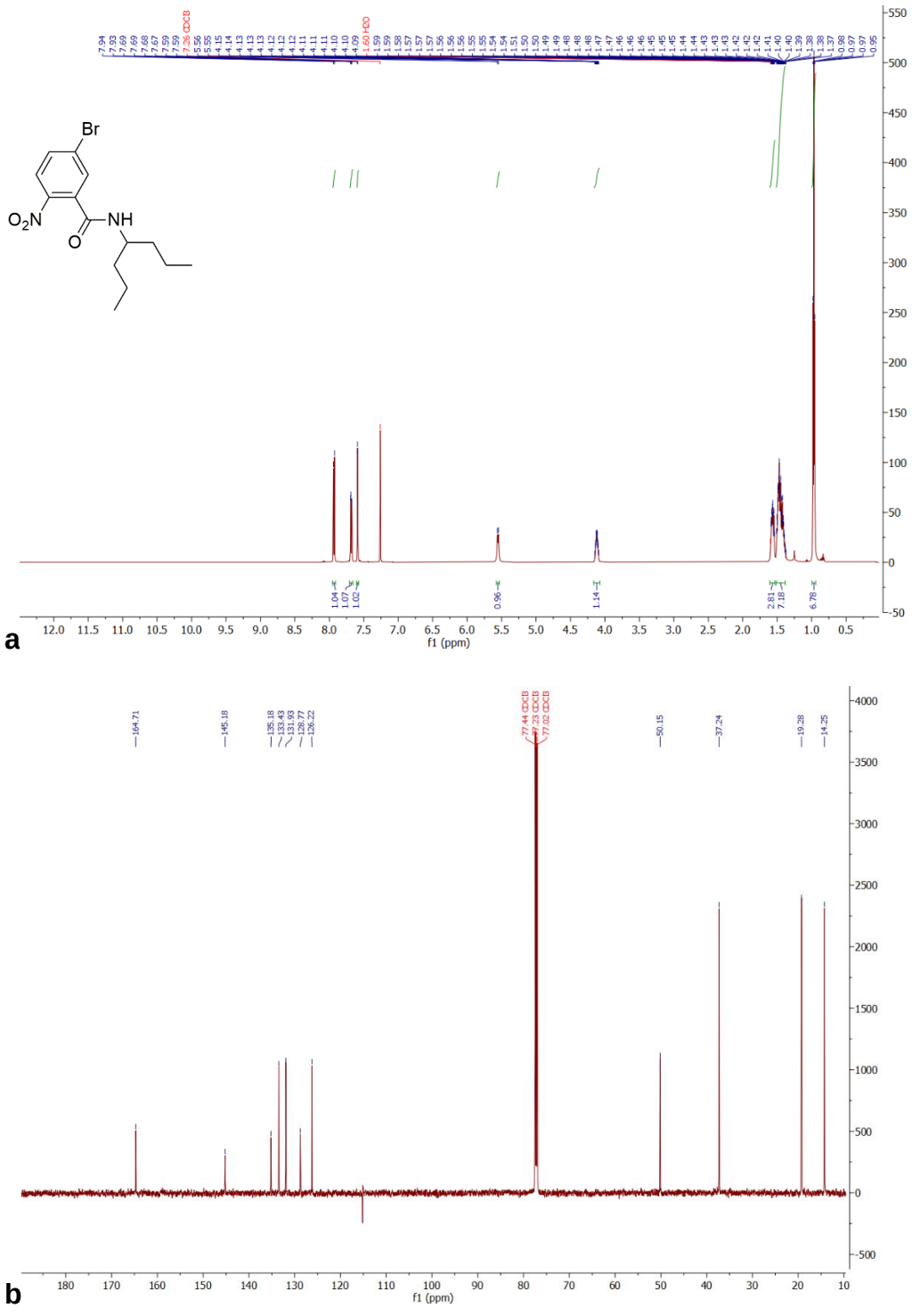

Figure 4S-3. (a) ^{1}H NMR of **(5)** (600 MHz, $CDCl_3$); (b) ^{13}C NMR of **(5)** (151 MHz, $CDCl_3$).

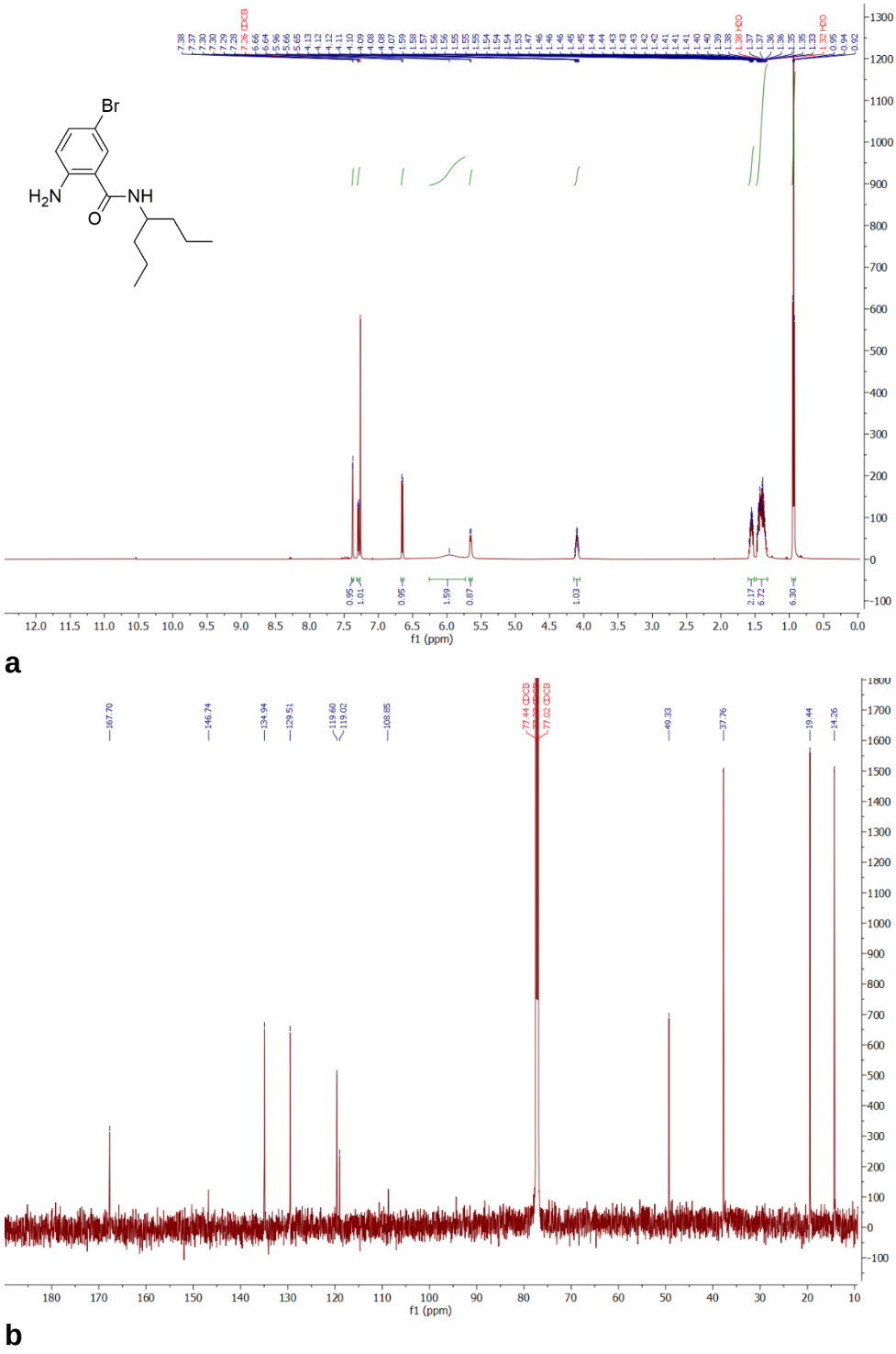

Figure 4S-4. (a) ^{1}H NMR of **(6)** (600 MHz, $CDCl_3$); (b) ^{13}C NMR of **(6)** (151 MHz, $CDCl_3$).

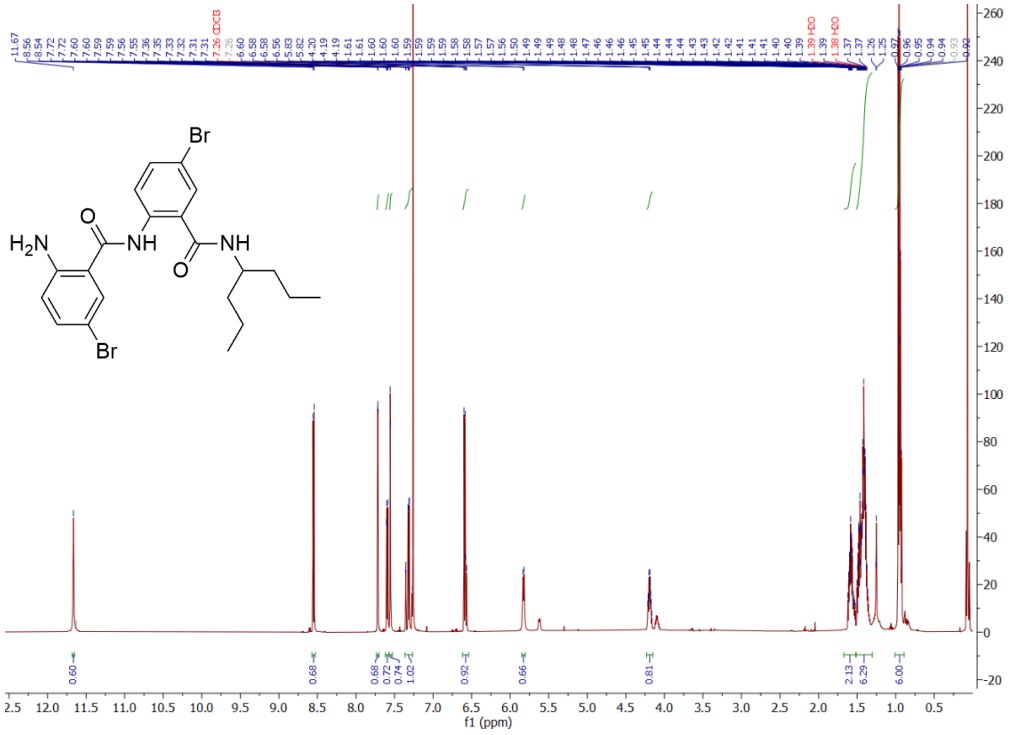

a

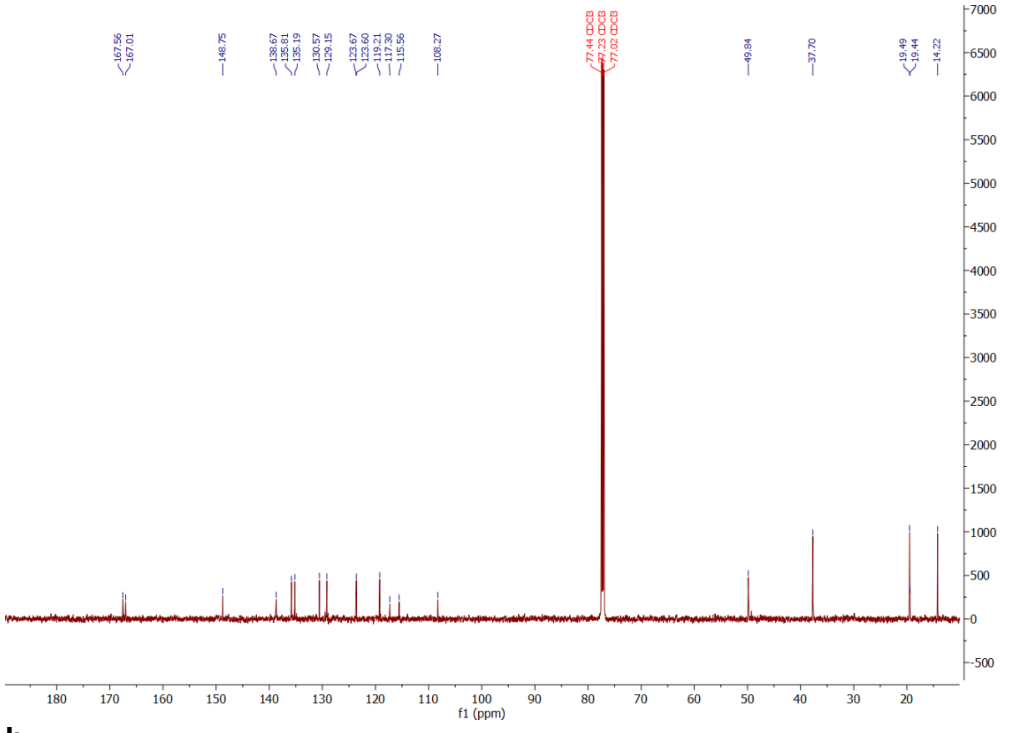

b

Figure 4S-5. (a) ^{1}H NMR of **(8)** (600 MHz, $CDCl_3$); (b) ^{13}C NMR of **(8)** (151 MHz, $CDCl_3$).

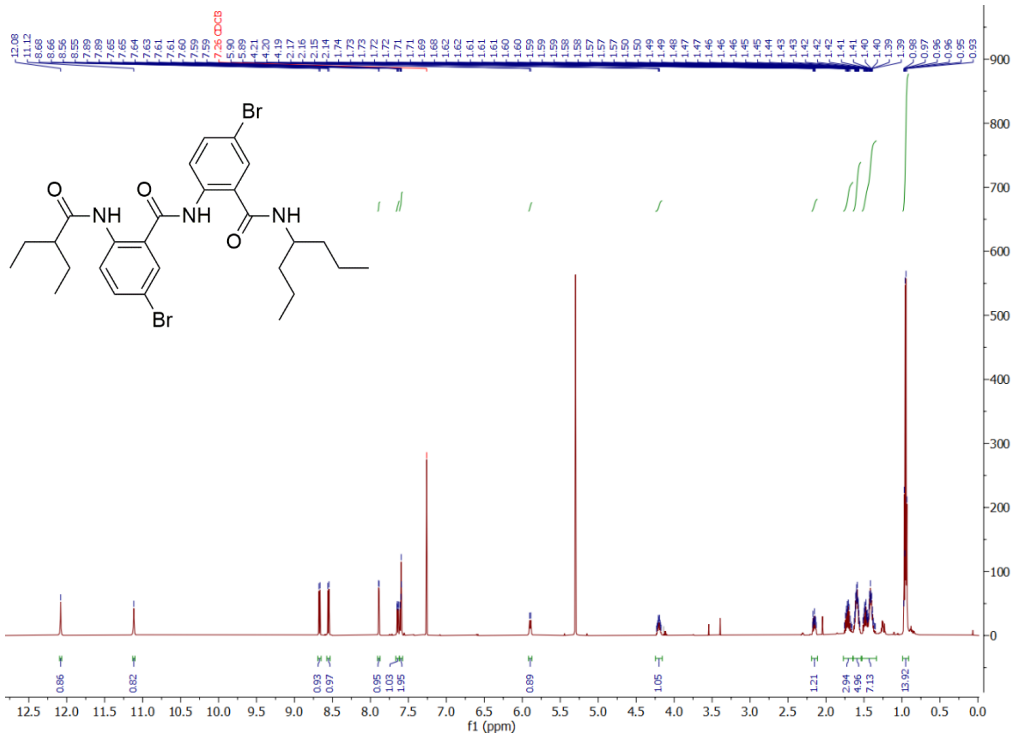

a

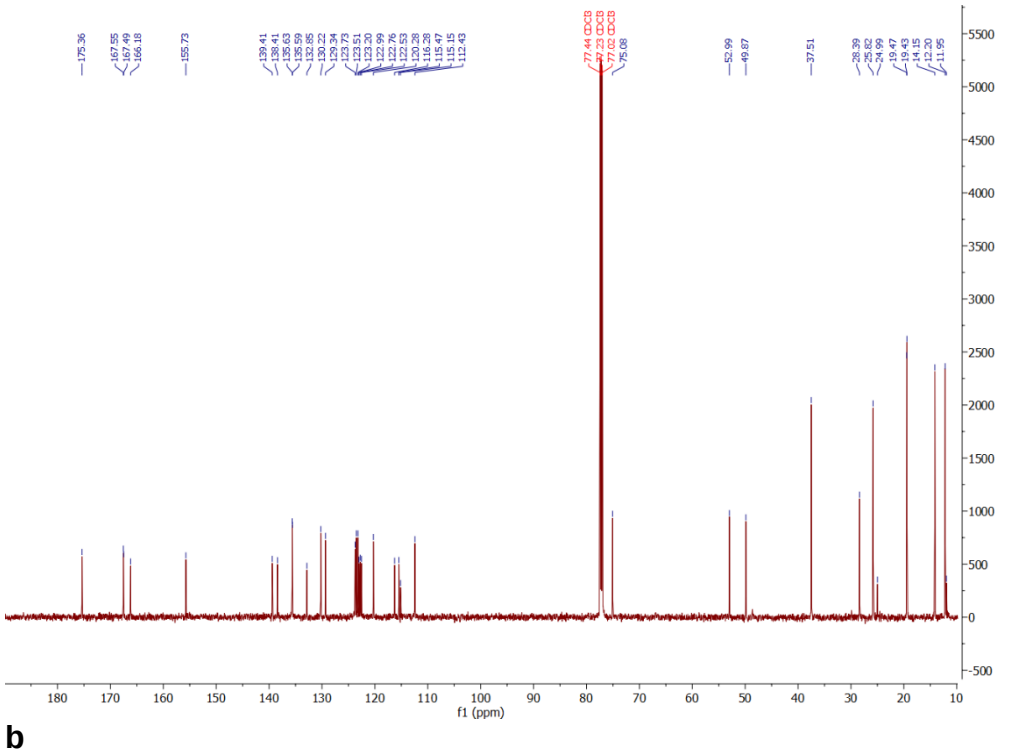

b

Figure 4S-6. (a) ^{1}H NMR of **(9)** (600 MHz, $CDCl_3$); (b) ^{13}C NMR of **(9)** (151 MHz, $CDCl_3$).

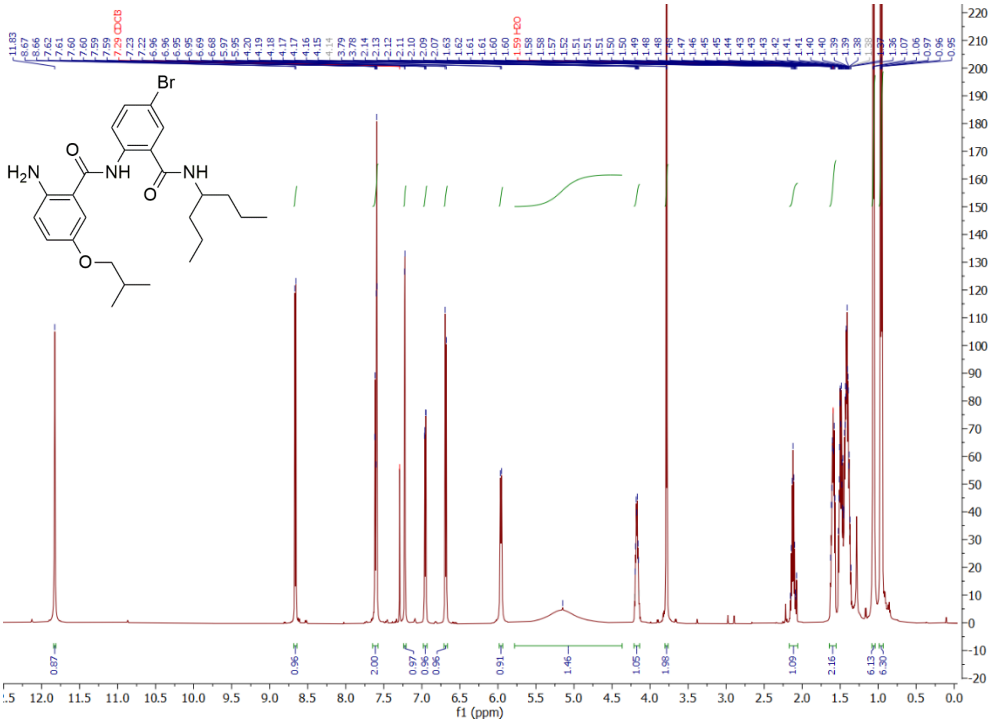

a

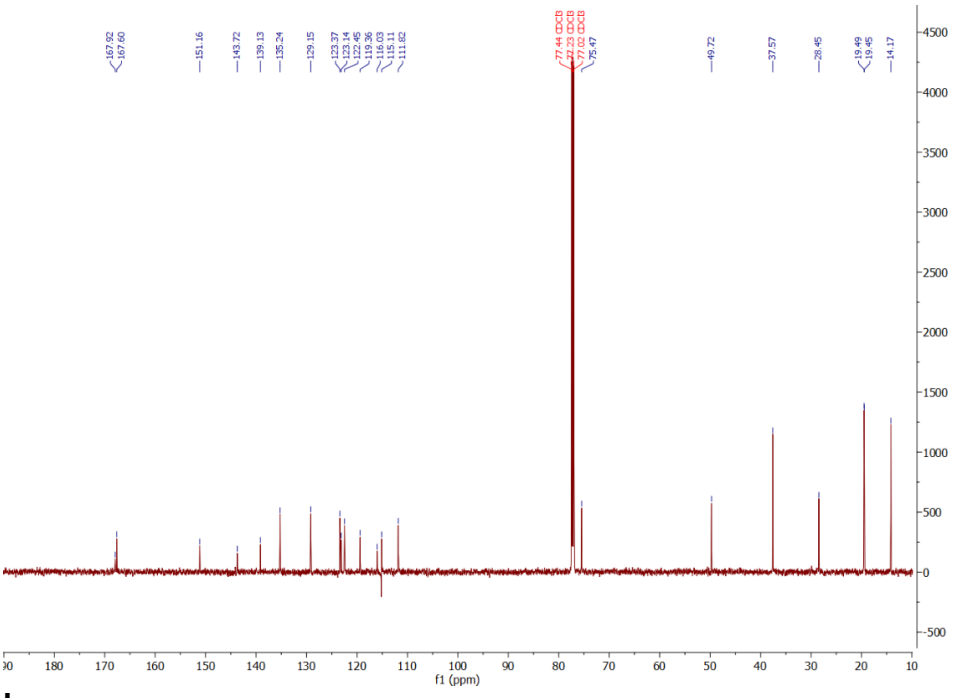

b

Figure 4S-7. (a) ^{1}H NMR of **(11)** (600 MHz, $CDCl_3$); (b) ^{13}C NMR of **(11)** (151 MHz, $CDCl_3$).

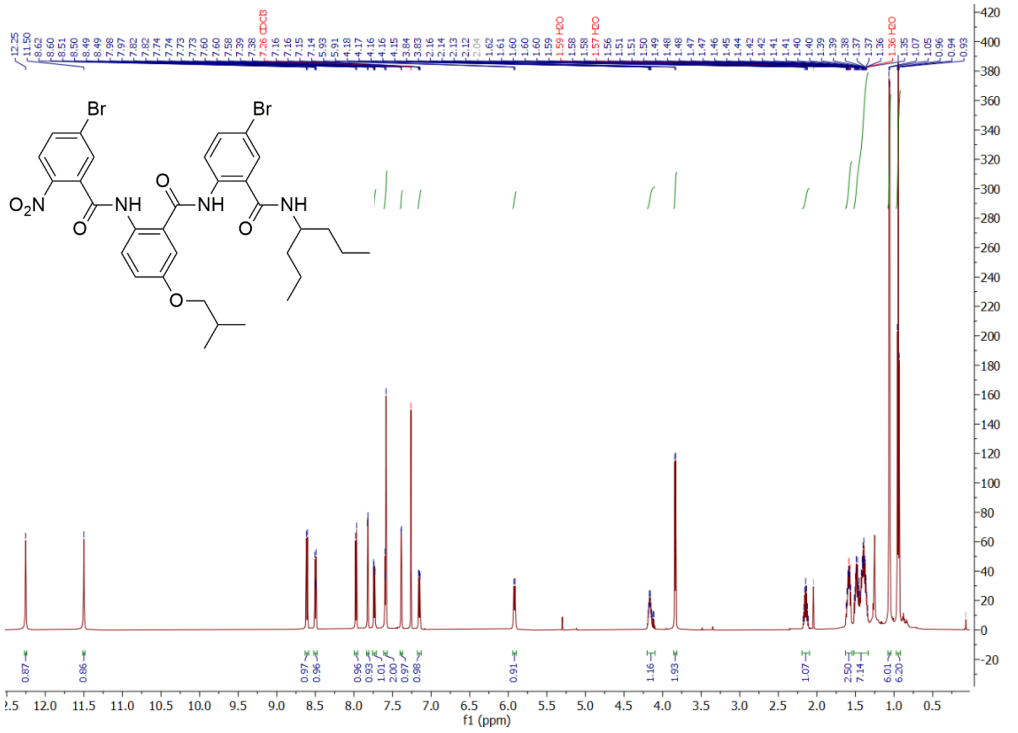

a

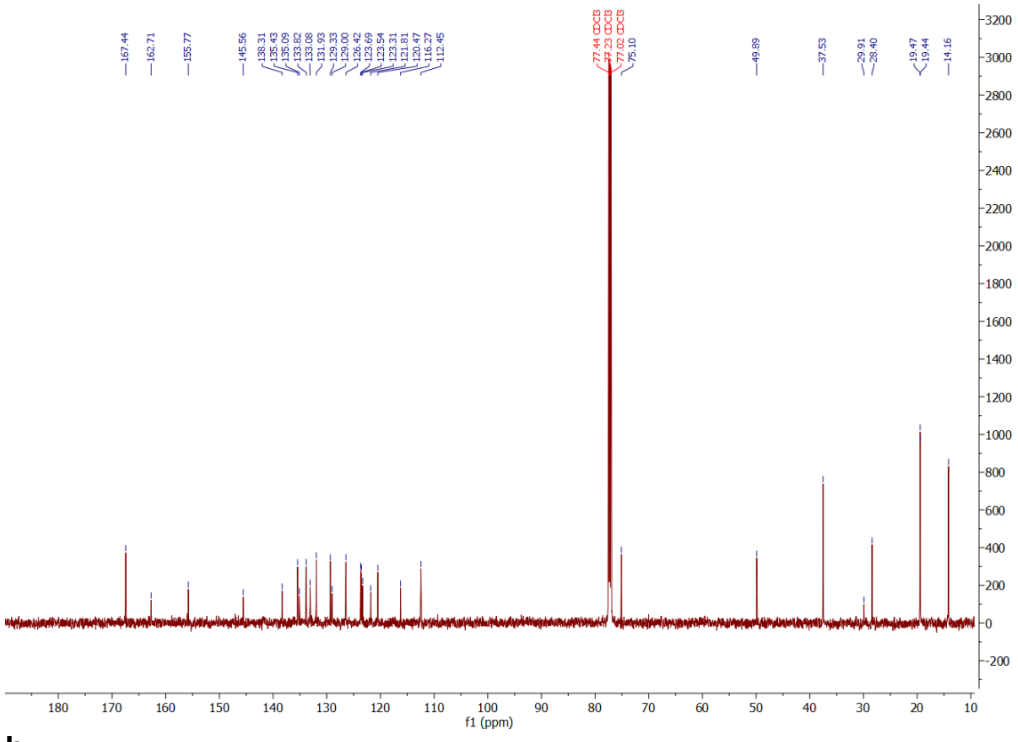

b

Figure 4S-8. (a) ^{1}H NMR of **(12)** (600 MHz, $CDCl_3$); (b) ^{13}C NMR of **(12)** (151 MHz, $CDCl_3$).

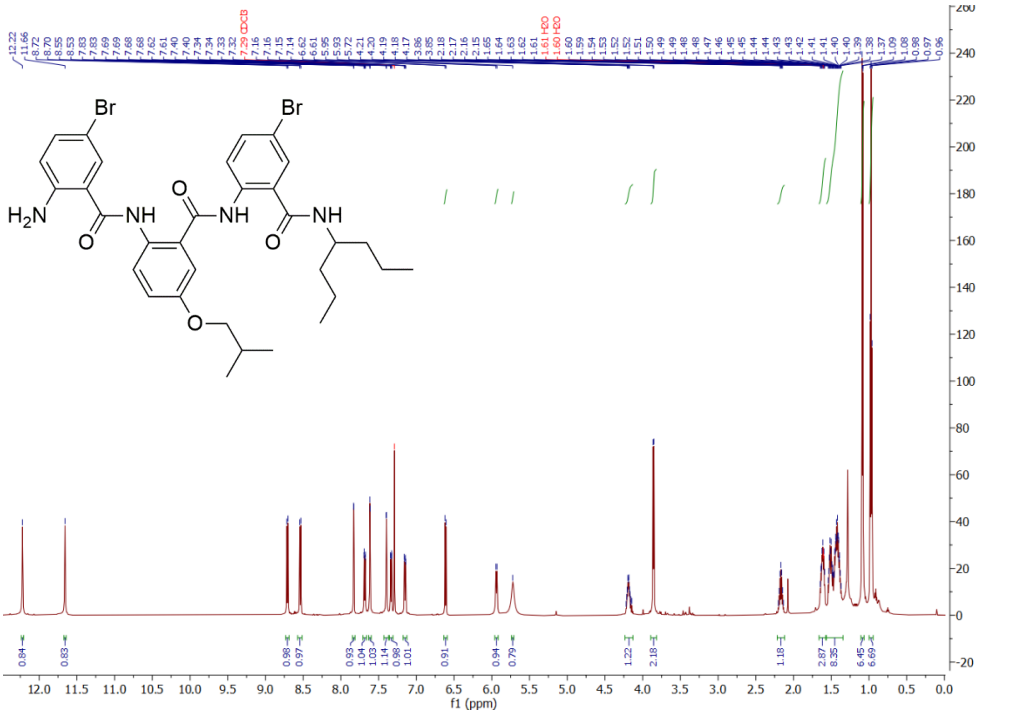

a

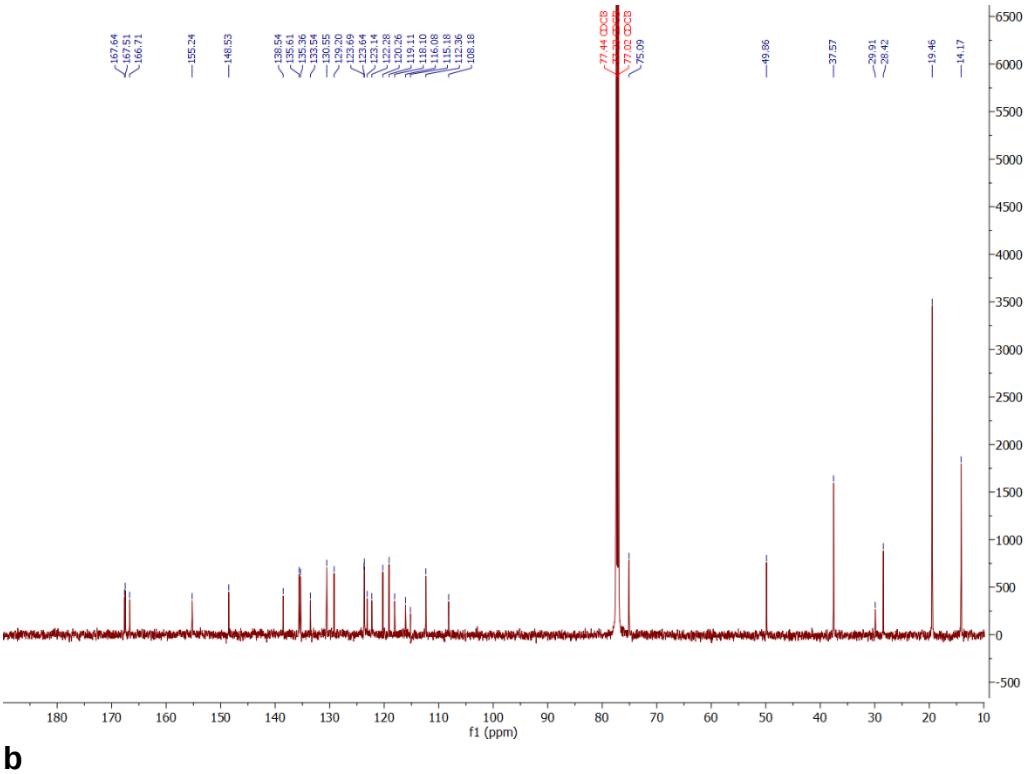

b

Figure 4S-9. (a) ^{1}H NMR of **(13)** (600 MHz, $CDCl_3$); (b) ^{13}C NMR of **(13)** (151 MHz, $CDCl_3$).

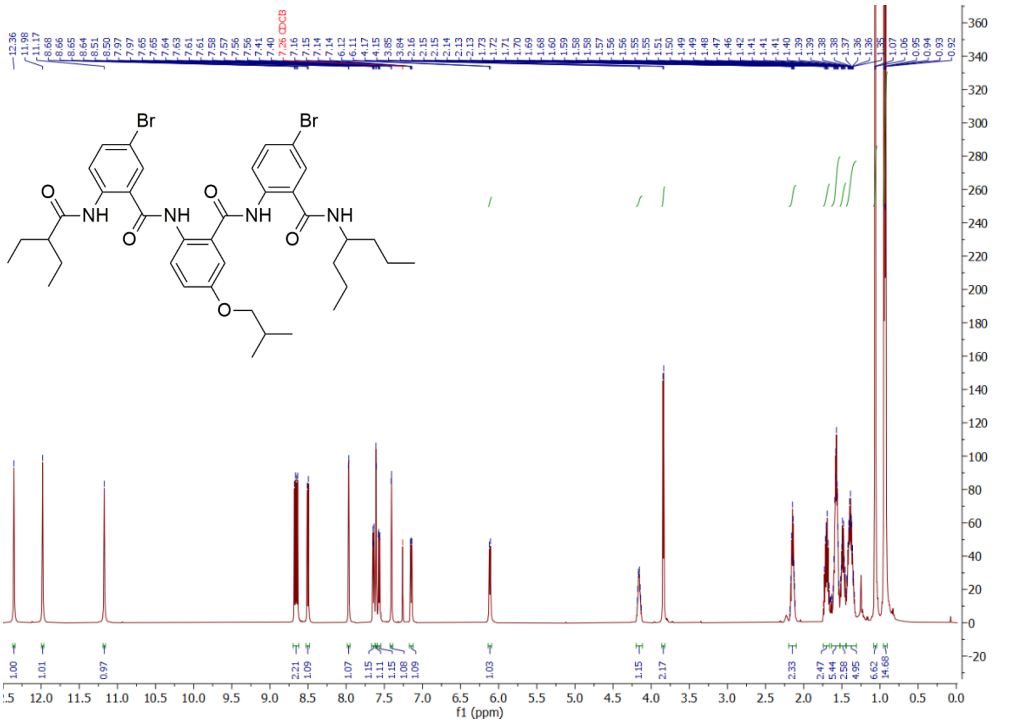

a

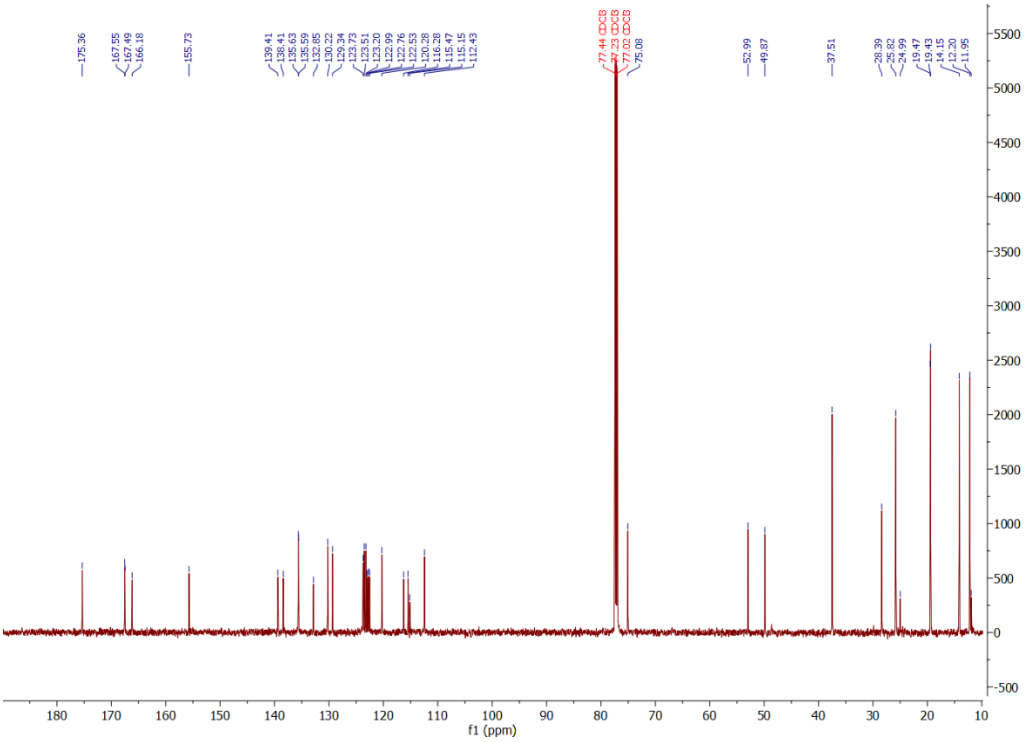

b

Figure 4S-10. (a) ^{1}H NMR of **(14)** (600 MHz, $CDCl_3$); (b) ^{13}C NMR of **(14)** (151 MHz, $CDCl_3$).

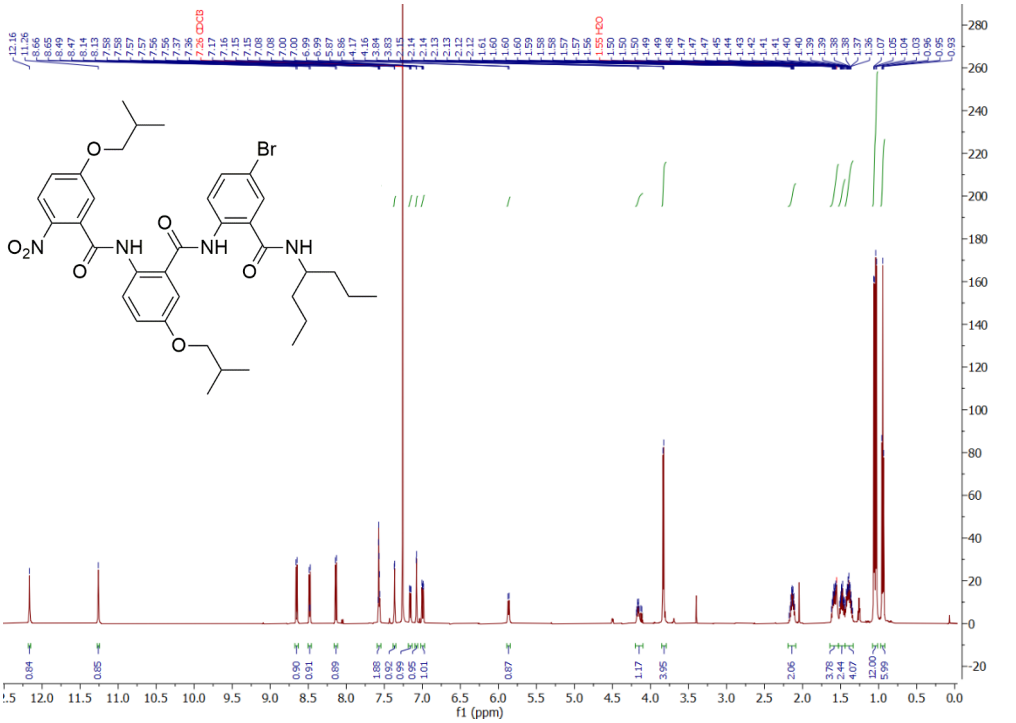

a

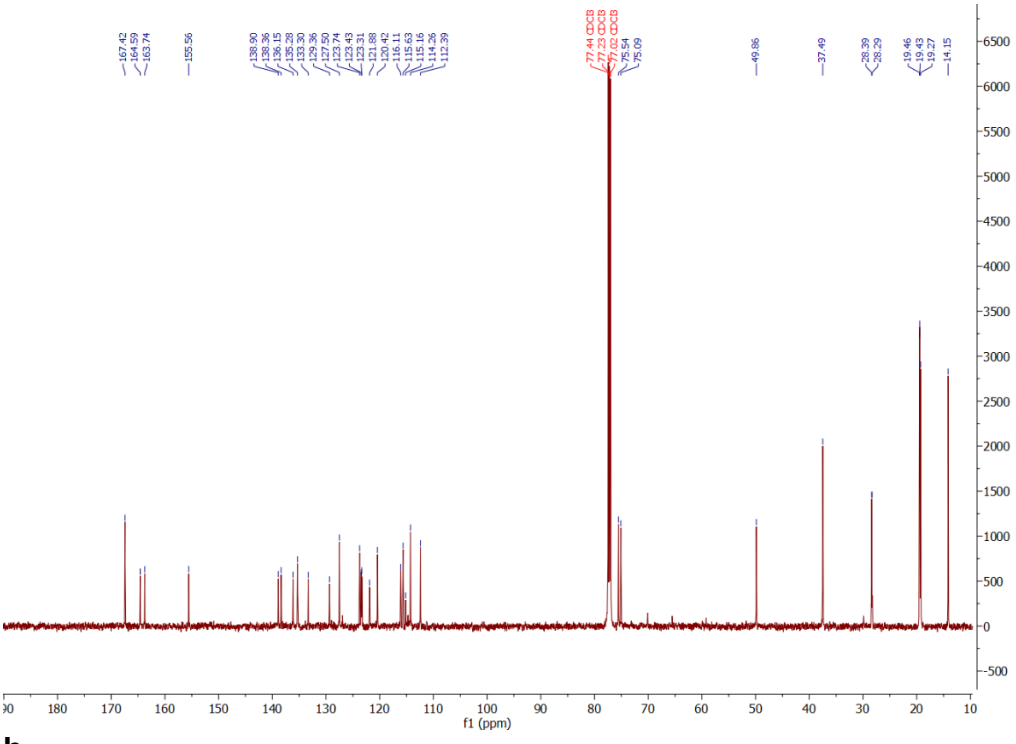

b

Figure 4S-11. (a) ^{1}H NMR of **(15)** (600 MHz, $CDCl_3$); (b) ^{13}C NMR of **(15)** (151 MHz, $CDCl_3$).

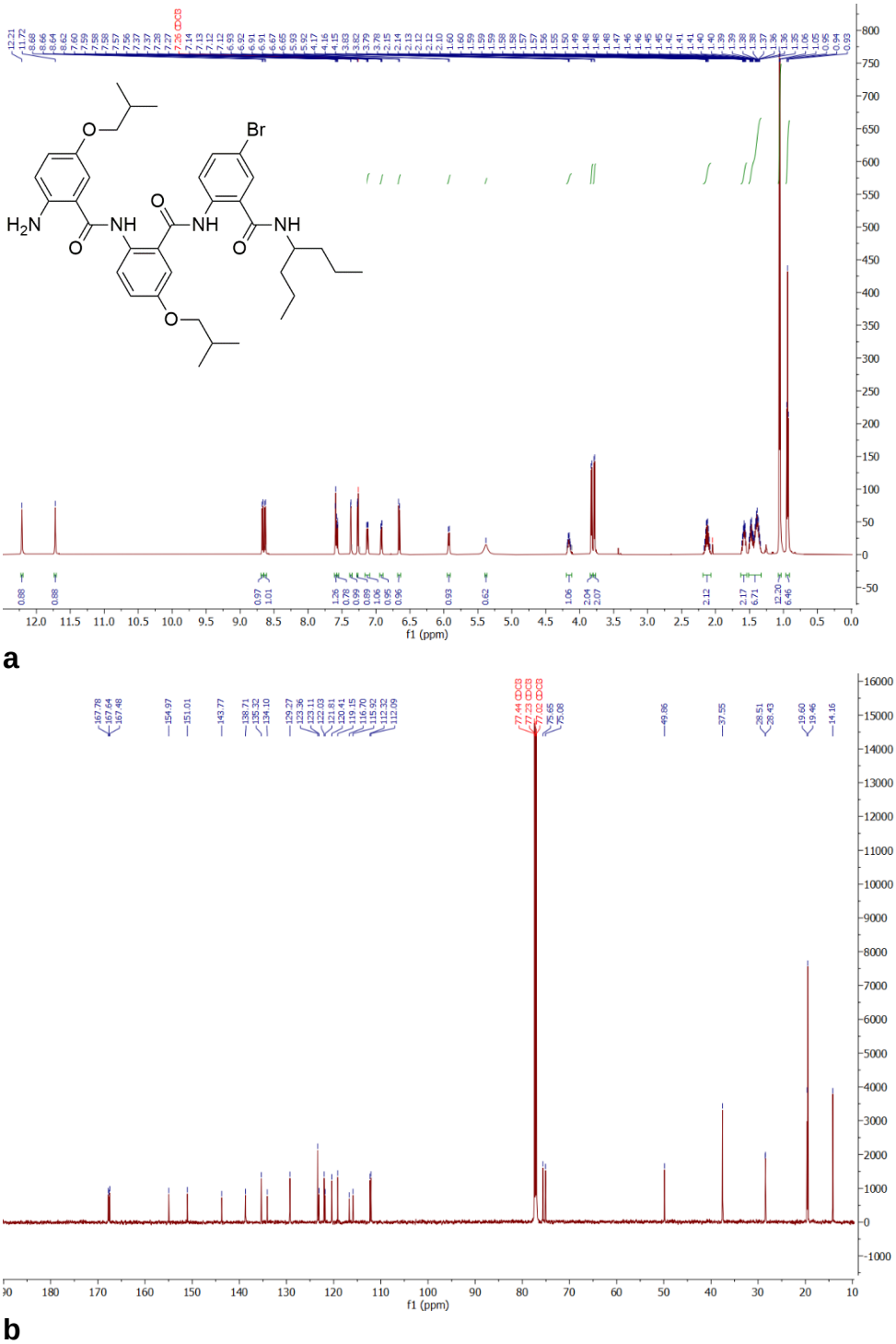

Figure 4S-12. (a) ^{1}H NMR of **(16)** (600 MHz, $CDCl_3$); (b) ^{13}C NMR of **(16)** (151 MHz, $CDCl_3$).

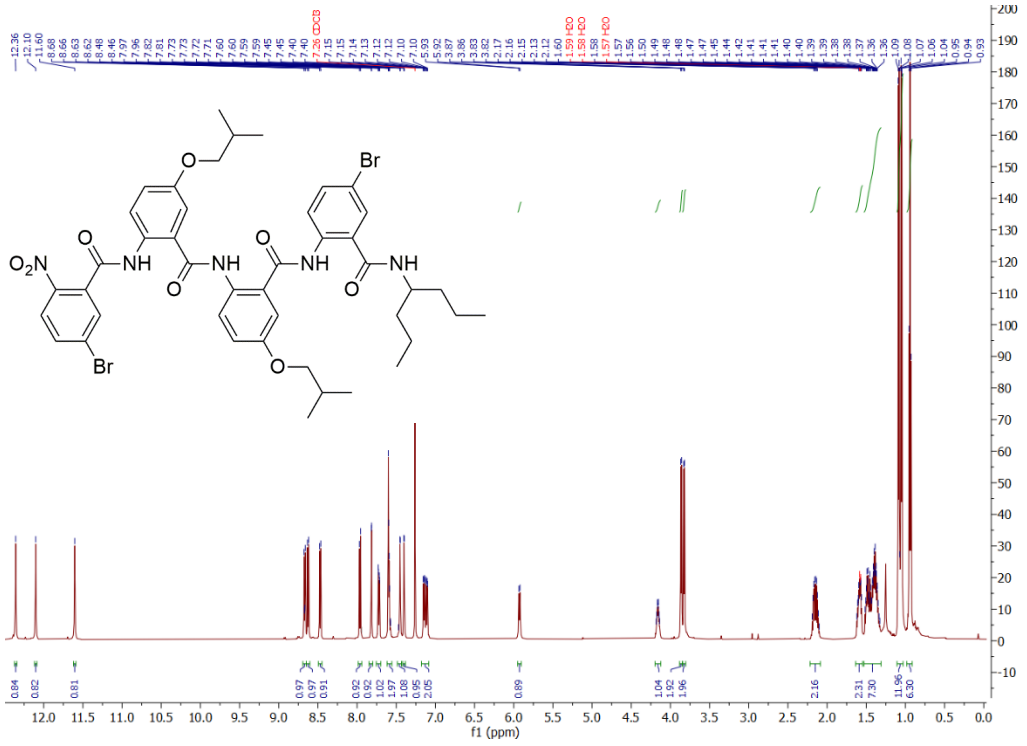

a

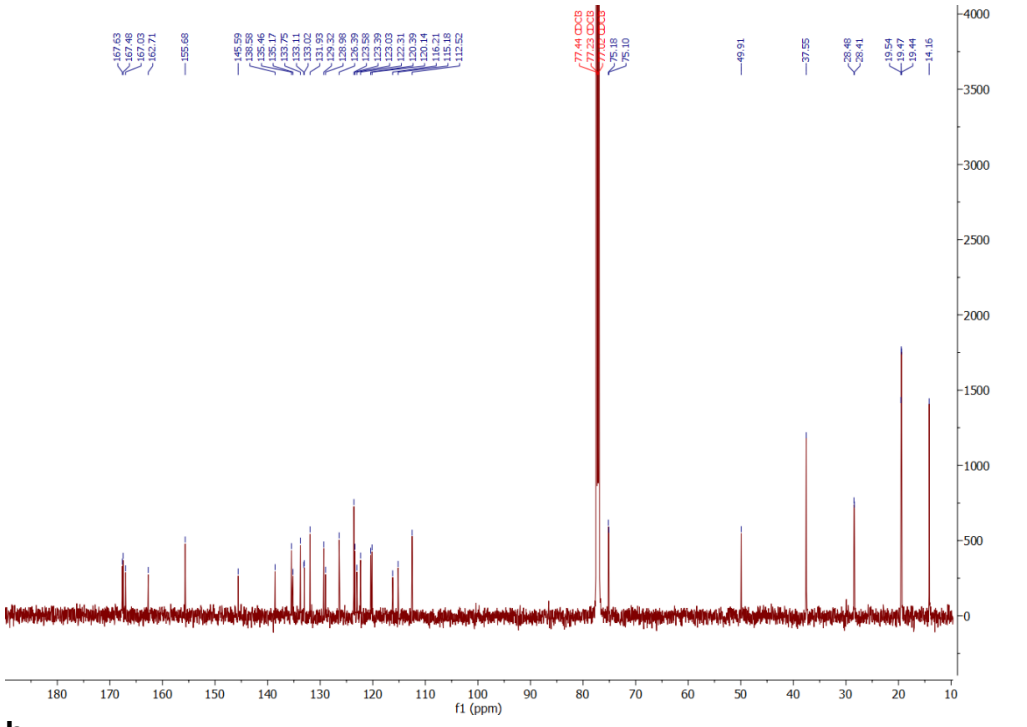

b

Figure 4S-13. (a) ^{1}H NMR of **(17)** (600 MHz, $CDCl_3$); (b) ^{13}C NMR of **(17)** (151 MHz, $CDCl_3$).

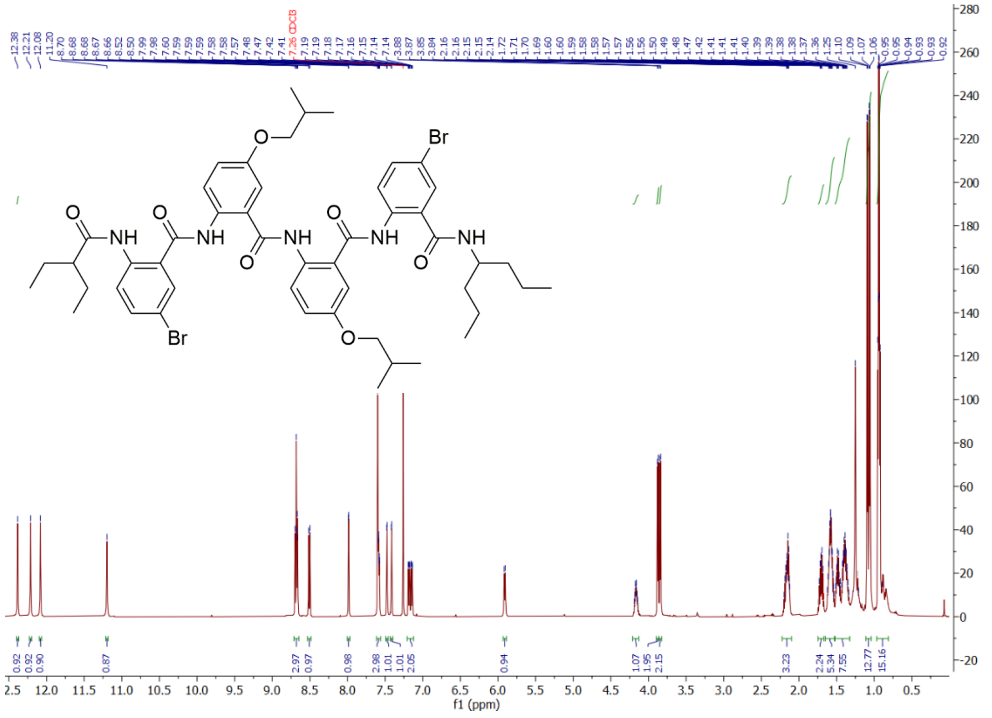

a

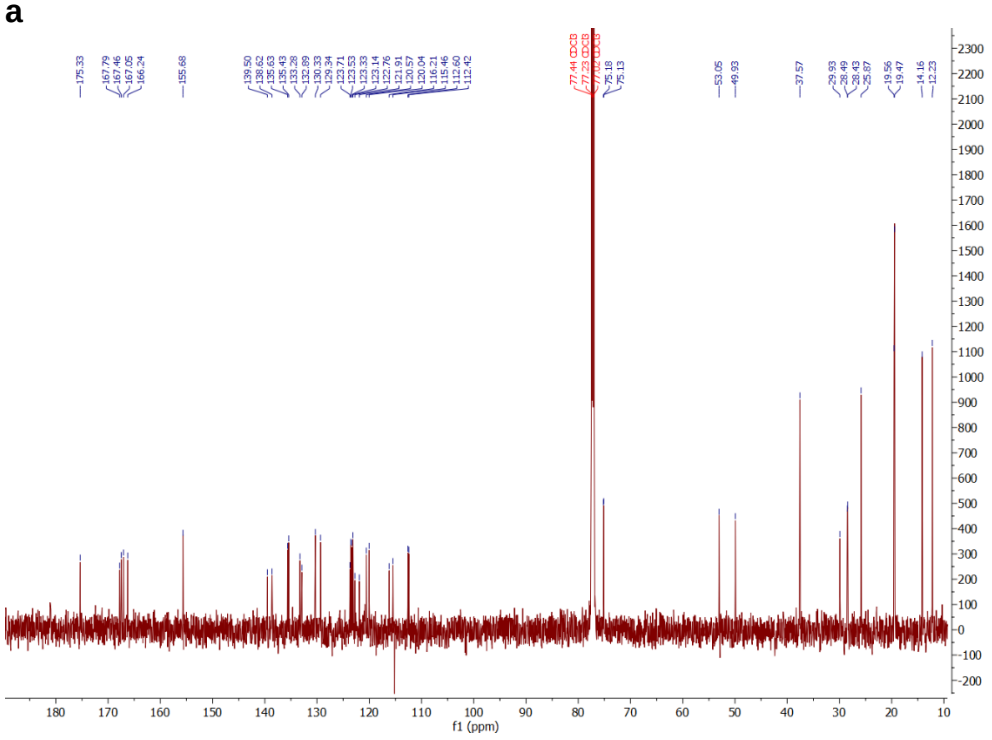

b

Figure 4S-14. (a) ^{1}H NMR of **(19)** (600 MHz, $CDCl_3$); (b) ^{13}C NMR of **(19)** (151 MHz, $CDCl_3$).